# INFORMATION TO USERS

This manuscript has been reproduced from the microfilm master. UMI films the text directly from the original or copy submitted. Thus, some thesis and dissertation copies are in typewriter face, while others may be from any type of computer printer.

**The quality of this reproduction is dependent upon the quality of the copy submitted.** Broken or indistinct print, colored or poor quality illustrations and photographs, print bleedthrough, substandard margins, and improper alignment can adversely affect reproduction.

In the unlikely event that the author did not send UMI a complete manuscript and there are missing pages, these will be noted. Also, if unauthorized copyright material had to be removed, a note will indicate the deletion.

Oversize materials (e.g., maps, drawings, charts) are reproduced by sectioning the original, beginning at the upper left-hand corner and continuing from left to right in equal sections with small overlaps.

Photographs included in the original manuscript have been reproduced xerographically in this copy. Higher quality 6" x 9" black and white photographic prints are available for any photographs or illustrations appearing in this copy for an additional charge. Contact UMI directly to order.

Bell & Howell Information and Learning
300 North Zeeb Road, Ann Arbor, MI 48106-1346 USA

UMI®
800-521-0600

# CONTROL OF
# ROBOTIC FIXTURELESS ASSEMBLY

By

KA MING (TIMBER) YUEN, B.ENG., M.ENG.

A Thesis
Submitted to the School of Graduate Studies
in Partial Fulfilment of the Requirements
for the Degree
Doctorate of Philosophy

McMaster University

# CONTROL OF
# ROBOTIC FIXTURELESS ASSEMBLY

DOCTORATE OF PHILOSOPHY
(Mechanical Engineering)

McMASTER UNIVERSITY
Hamilton, Ontario

| | |
|---|---|
| TITLE: | Control of Robotic Fixtureless Assembly |
| AUTHOR: | Ka Ming (Timber) Yuen, B. Eng. (McMaster University), M. Eng. (McMaster University) |
| SUPERVISORS: | Drs. G. M. Bone and M. A. Elbestawi |
| NUMBER OF PAGES: | xvi, 206 |

*This thesis is dedicated to*

*my loving wife and best friend, Carman,*

*and my dear son, Avian*

# Abstract

Robotic Fixtureless Assembly (RFA) refers to the performance of assembly tasks by robots without the aid of jigs and fixtures. Two control problems encountered in RFA of sheet metal parts assembly are addressed in this thesis. They are the control of vibration when handling the sheet metal parts and the control of the contact state between the parts during assembly. Both 2-D parts and 3-D parts will be considered when the two problems are addressed. A unique sensor, termed a Strain Gauge equipped Finger (SGF), was first developed which can measure the part's vibration during handling and the contact state during assembly. For the vibration control problem, a novel Learning Extremum Control (LEC) algorithm is proposed. Using SGFs mounted on the robot gripper for vibration feedback, the orientation of the part in 3-D space relative to its path is controlled to reduce vibration. Furthermore, as an alternate approach, a feedforward Input Command Shaping Method (ICSM) is employed to reduce the vibration. Experimental results confirmed the effectiveness of both control algorithms. The LEC and the ICSM reduced the vibration amplitude by up to 71% and 78%, respectively.

In order to solve the contact state control problem, the contact state measurement problem in 2-D parts assembly is first considered. Measurement methods are developed based on the use of a Force/Moment Sensor (FMS) alone, SGFs alone and the sensor fusion

of the FMS and SGFs information. The methods are verified in 160 robotic assembly trials. The success rate for the FMS method increased from 28% to 88% when the sheet thickness was increased from 0.32 mm to 1.88 mm. Under the same conditions, the success rate for the SGF method decreased from 100% tc 55%. The sensor fusion method surpassed the best individual performances of the other methods by achieving a 100% success rate for the complete set of sheet thicknesses and contact states tested.

After the contact state measurement problem is considered, the contact state control problem is examined. The SGFs and a Force/Moment Sensor (FMS) are used to provide feedback about the contact condition between two sheet metal parts. An Integral Contact Controller (ICC) is used to correct angular error between the parts to ensure full contact along the joints for subsequent welding. Experimental results confirmed the effectiveness of the ICC algorithms. For 2-D parts, using the fusion of the FMS and SGF sensory information, the ICC reduced the Yaw joint angular error from 0.5° to 0.025° within 1.7 seconds. For 3-D parts, the ICC reduced the angular error in both the Pitch and Yaw angles from 0.5° to 0.05° within 2.4 and 3.6 seconds using the FMS alone and SGFs alone, respectively. Finally, an investigation is performed to determine the effectiveness of applying the Input Command Shaping Method in the contact state control experiments. This method's limitations are discussed.

# Acknowledgements

I would like to express my special, heartfelt thanks to Dr. G. M. Bone, my main research supervisor since the second year of this research, for his valuable guidance and endless support. His help in debugging the control software and designing the hardware for the experiments facilitated my work tremendously. Furthermore, his help in proof reading the manuscript of this thesis is gratefully acknowledged.

Gratitude is also expressed to Dr. M. A. Elbestawi, my other research supervisor, for his suggestion of the research topic, and for his guidance, especially during the first year of this research. I would like to thank the other members of my supervisory committee: Drs. D.W. Capson and M. Sklad for their suggestions throughout this work.

I would like to thank the Mechanical Engineering Technical Staff, Dave Schick, Ron Lodewyks, Jim McLaren and Joe Verhaeghe, for their technical assistance and friendship.

The financial support provided by McMaster University, and Ontario Graduate Scholarship program is gratefully acknowledged.

Finally, I would like to thank my wife, Carman, and my son, Avian, for being so patient and supportive while I was working long hours in the laboratory and writing this thesis at home. Without your love, encouragement and support, this work would not have been possible.

# Table of Contents

# List of Figures

# List of Tables

# Chapter 1

# Introduction

In recent years, due to rapidly changing customer tastes and market demand, the environment surrounding the automobile industry has changed drastically. In the past, automobile manufacturers used to be able to maintain their product models relatively unchanged for a few years. Nowadays, due to stiff competition, it is sometimes necessary to make major changes in vehicle body shape and structure ahead of schedule to accommodate customers' expectations and meet market demand. The sudden demand for a second sliding door on a mini-van in recent years is a good example. In order to accommodate changes like this, major modification in the car body design is required. The automakers are challenged to come up with methods to allow modifications to be introduced on their products easily, and to allow their products to be built with high quality, on a timely basis and at a reasonable cost.

Currently, automobile assembly consists of four major processes [ 3 ]. They are stamping, body assembly, painting, and final assembly. Among these processes, the body

assembly process is the most complex to change in the event of model change over. In this process, a vehicle body is assembled from 300 to 350 stamped sheet metal parts [ 24 ]. These parts have to go through many sub-assembly lines and a main assembly line undergoing thousands of spot welds. In each main and sub assembly line, the sheet metal parts have to go through two processes. The first process is positioning and preliminary welding, and the second is re-spot welding [ 3 ].

In the process of re-spot welding, car bodies that have been put together in the previous process are spot welded again to achieve the required structural stiffness and integrity. Since the sheet metal parts have already been put together with some preliminary spot welds, only relatively simple positioning devices are required to hold the basically assembled parts in place for welding. On the other hand, in the process of positioning and preliminary welding, flexible sheet metal parts are being put together. In order to position, support and fix the flexible and geometrically complicated sheet metal parts, mechanically rigid and complex positioning fixtures are required. On these fixtures, there are locating pins, clamps and spot welding guns. The locating pins are there to locate the part through the precision holes on each of the parts. Once the parts are located properly, the clamps are actuated to hold the parts in place. This is to ensure that when spot welding is performed by the welding guns or the welding robots, the parts will not be deformed or dislocated. After the parts are fixtured securely, a few preliminary spot welds are applied to put the parts together into a sub-assembly. Then smaller sub-assemblies are put together into larger sub-assemblies by following the same procedure. Since the sheet metal parts are flexible, to allow sheet metal parts to be assembled accurately, fixtures have to be exclusively designed for

each sub-assembly of each car model. As mentioned before, the number of sheet metal parts involved is large, and the number of fixtures required is therefore substantial.

In the event of model changeover new fixtures must be designed and fabricated, and finally installed in the plant. This retooling process normally requires a period of 9-12 months [ 3 ]. Due to the long lead time associated with the design and manufacture of the fixtures, and the loss of production during their installation, this retooling operation is very costly. In order to avoid shortage of product, automakers have to build up a huge inventory to account for the loss of production during the period of retooling. Also, due to the factory down time, workers in the factory may lose employment during the introduction of a new model. Besides, most fixture design is performed before production parts and real production processes become available, and only after these are available can the fixtures be adequately tested. Since successful introduction of a new model requires the support and involvement of skilled workers, it is difficult for workers who have been off the job for 12 months during the retooling process to be able to get up to speed to operate the production line and make the necessary adjustments required. It is because of the high costs and retooling complexity associated with the fixtures that there is a great desire to develop a new technology to replace them.

Traditionally, robots are used to carry weld guns to perform welding on a part held by a fixture; or sometimes robots are employed to carry a sheet metal sub-assembly that has been preliminary welded for re-spot welding. A possible solution to the problems with fixtures is the use of two robots to assemble and join the workpieces in the preliminary welding stage without fixtures as illustrated in Figure 1.1. This approach is referred to as

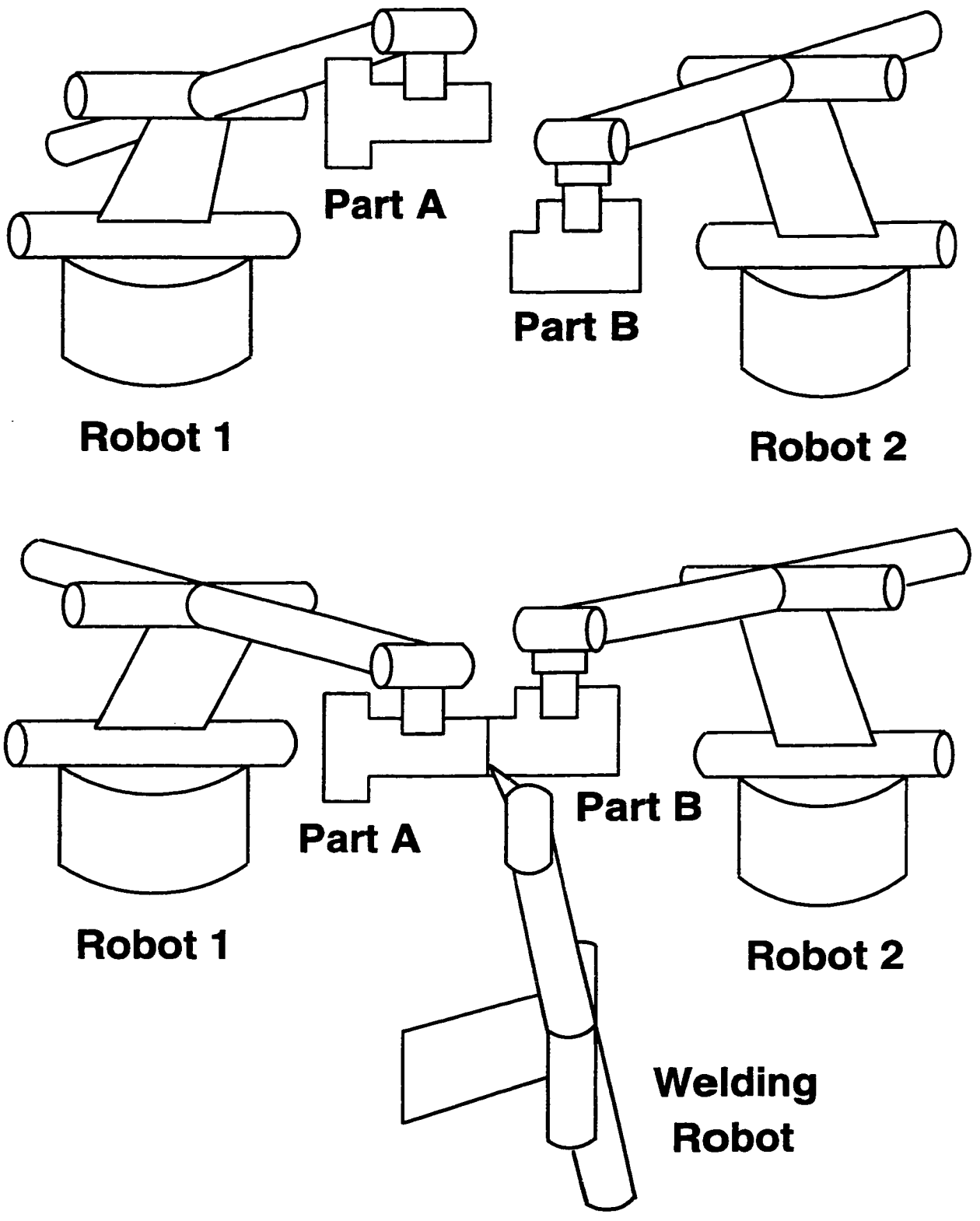


Figure 1.1 The Idea of Robotic Fixtureless Assembly

Robotic Fixtureless Assembly (RFA).

A fully developed RFA system will have the following advantages over a conventional robotic sheet metal assembly system using fixtures:

(1) Elimination of expensive fixtures. This will reduce cost and lead time. It is expected that the use of RFA in the automotive industry can reduce retooling costs by 80% [3].

(2) Reduce or totally eliminate the workers needed for loading and unloading the fixtures. This cuts cost and reduces the possibility of injury when heavy sheet metal parts with sharp edges are carried manually.

(3) When sheet metal parts are changed for a new model, the parts' CAD model software file can be used to generate the robot's new motion trajectories with little or no manual programming.

(4) Automatically reconfigurable robot end effector/gripper can be used to pick-up a wide range of parts.

(5) No bulky fixtures are required, which reduces overall facility space. This in turn cuts cost further.

(6) Changes between different versions of a product, such as 4 door and 2 door, can be done quickly.

(7) Even switching the production line over to produce a few vehicles for trials and then back to the old model can be done relatively quickly.

The structure of a RFA system is shown in Figure 1.2. The system involves five main stages. The first is the Trajectory Planning Stage. In this stage, the robots' trajectories are planned based on the CAD models of the sheet metal parts and the environment of the

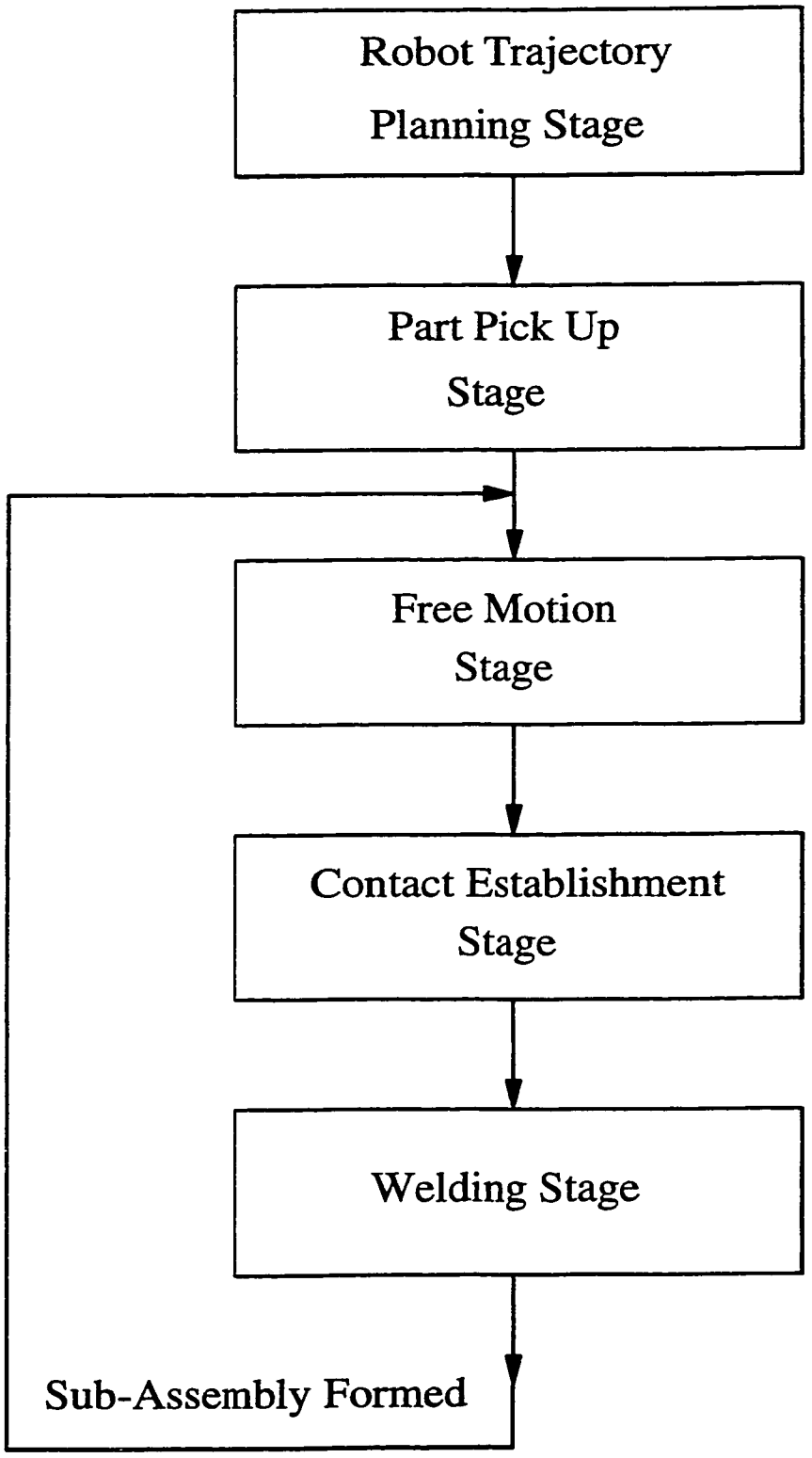


Figure 1.2 The Structure of a Robotic Fixtureless Assembly System

assembly work cell. The second stage is the Part Pick Up Stage. This involves the locating, grasping and picking up of the sheet metal parts by the robots. This may be performed based on the planned trajectories obtained from the first stage, with or without additional sensory feedback. The third stage is the Free Motion Stage. At this stage, the sheet metal parts are transported by the robots. The problem encountered at this stage is the measurement and control of the vibration of the sheet metal parts. The fourth stage is the Contact Establishment Stage. At this stage, the sheet metal parts are brought together and assembled by the robots. During assembly, the contact state between the sheet metal parts to be assembled has to be measured and controlled. The fifth stage involves the welding of the parts. The welding may be done by a third robot or by performing the assembly at the opening of a spot welding gun so that when the assembly is finished, the welding can be performed right at the spot. After the welding process, a sheet metal sub-assembly is formed. This sub-assembly may be carried by one of the robots, and the RFA process is repeated starting from stage three to form larger sub-assemblies with other sheet metal parts.

In this thesis, two control problems encountered in the development of RFA are addressed. They are:

1. The control of the vibration of the sheet metal parts in the Free Motion stage, and
2. The control of contact state between the parts in the Contact Establishment stage and Welding Stage.

Regarding the first control problem, in order to maximize the production rate, it is desirable to move the sheet metal parts as fast as possible. However, at the same time, it is important to control the vibration of the part when it is being handled to avoid damage and to achieve

a high assembly accuracy. The greater the speed, the more the part's structural vibration modes will be excited. The usual way of dealing with this problem is to dwell for a period of time to let the vibration damp out by itself. However, this dwelling period could be very long. For a sheet metal part having a 10 Hz natural frequency and 0.5% damping, typical for sheet metal parts, it takes 7.3 seconds to achieve a 90% reduction in vibration amplitude. In order to reduce the dwelling period, the speed of the part handling may have to be sacrificed.

Large car body panels, because of their flexibility, currently require specially designed grippers to control vibration when handled by a robot. These are typically large devices which use several widely spaced vacuum pickups to support the part in order to reduce vibration. Each gripper must be designed and manufactured for a particular part's size and shape to provide proper support to the part when it is picked up, and to avoid interference with the subsequent welding operation. A much more flexible and cost effective alternative is the use of a reconfigurable robotic gripper. Such a gripper, which has multi-degrees of freedom and is capable of handling a wide range of sheet metal parts, has been developed by Van Varseveld [ 4 ]. However, since this gripper will only grasp the center of the parts, for relatively large parts' vibration control during part handling is a problem which must be tackled.

The second problem encountered in the development of RFA is the control of the contact state between the sheet metal parts. Under ideal conditions, when two robots are used to assemble two sheet metal parts, full contact along the joint to be welded will be achieved. However, in reality, the parts may not be aligned properly. This misalignment could be due to the parts own dimensional error or the handling robots' positioning error. If the two parts

are misaligned, an inaccurate sub-assembly and a poor weld joint may be produced. Thus, it is important to control the contact state between the parts.

In the following chapters of this thesis, the control problems mentioned above for the development of RFA will be addressed. In chapter 2, the state of current research in related areas is first reviewed. Then in chapter 3, the selection and development of the sensors employed in this thesis are presented. The sensors employed include an industrial Force/Moment Sensor (FMS) and novel Strain Gauge-equipped Fingers (SGFs). In Chapter 4, vibration control strategies are developed for controlling sheet metal vibration when handled by robot. These strategies are first simulated and then verified experimentally for 2-D and 3-D parts, respectively. Chapter 5 deals with the contact state measurement problem. Strategies are developed for measuring the contact state between 2-D and 3-D sheet metal parts. Experiments are performed and results presented to prove the effectiveness of these strategies. In Chapter 6, the contact state control problem is addressed. Algorithms are developed for the contact state control of sheet metal parts assembly for 2-D and 3-D parts. The effectiveness of these control algorithms is then tested experimentally. Results are presented and discussed. The thesis is concluded in Chapter 7. The major contributions of the current study and some recommendations for further research are outlined.

# Chapter 2

# Literature Survey

## 2.1 INTRODUCTION

In order to control vibration of sheet metal parts effectively, it is important to measure the vibration accurately. This applies to the control of contact state as well. If one wants to control the contact state between two parts, it is essential to measure the present contact state. A literature survey has been conducted on the control of fixtureless assembly of sheet metal parts. It should be noted that as this is a relatively new field, the body of relevant literature is quite small. This chapter presents the results of the survey in three sections. Section 2.2 is on the vibration measurement and control problem when flexible parts are being handled. Section 2.3 is on the contact state measurement and control problem in sheet metal parts assembly. Lastly, section 2.4 is on all the other aspects of the fixtureless assembly problem.

## 2.2 VIBRATION MEASUREMENT AND CONTROL WHEN HANDLING FLEXIBLE PARTS

Various sensors and control strategies have been proposed and developed in the literature to measure and control the vibration and/or tip position in flexible structures. Kotnik et. al. [ 5 ] studied the control of a flexible manipulator arm. Two independent methods of identifying the poles and zeros of the transfer function from motor input current to endpoint position were used, and the results were averaged to form the empirical model. The first method was to determine the open loop frequency response of the system. From this, the frequencies at which the endpoint deflections occur were found. The second method was to take the Fast Fourier Transform of the step response for a given step input command. Three control designs were tested for endpoint position control. The first was endpoint position feedback. An incandescent lamp was mounted at the tip of a flexible robot arm, and a linear array line scan camera which detected the relative position of the lamp with a resolution of one tenth of a degree, was used to detect the end point position of the robot. Based on the endpoint position feedback from the camera, classical root locus techniques were used for the control of the endpoint position. The block diagram for this control scheme is shown in Figure 2.1 [ 5 ]. The second control design involved an observer with full state feedback to place the poles. A predictor type observer, making use of the current input and output to predict the next state, was employed. The state feedback gains were computed using discrete Linear Quadratic Regulator theory. The third control design employed an accelerometer for endpoint acceleration feedback. A static feedback gain was used to control the end point position. The shaft position was also used in feedback for the control of the rigid body motion of the robot. The block diagram of the acceleration feedback control scheme is shown in Figure 2.2 [ 5 ]. Experimental results demonstrated that the responses

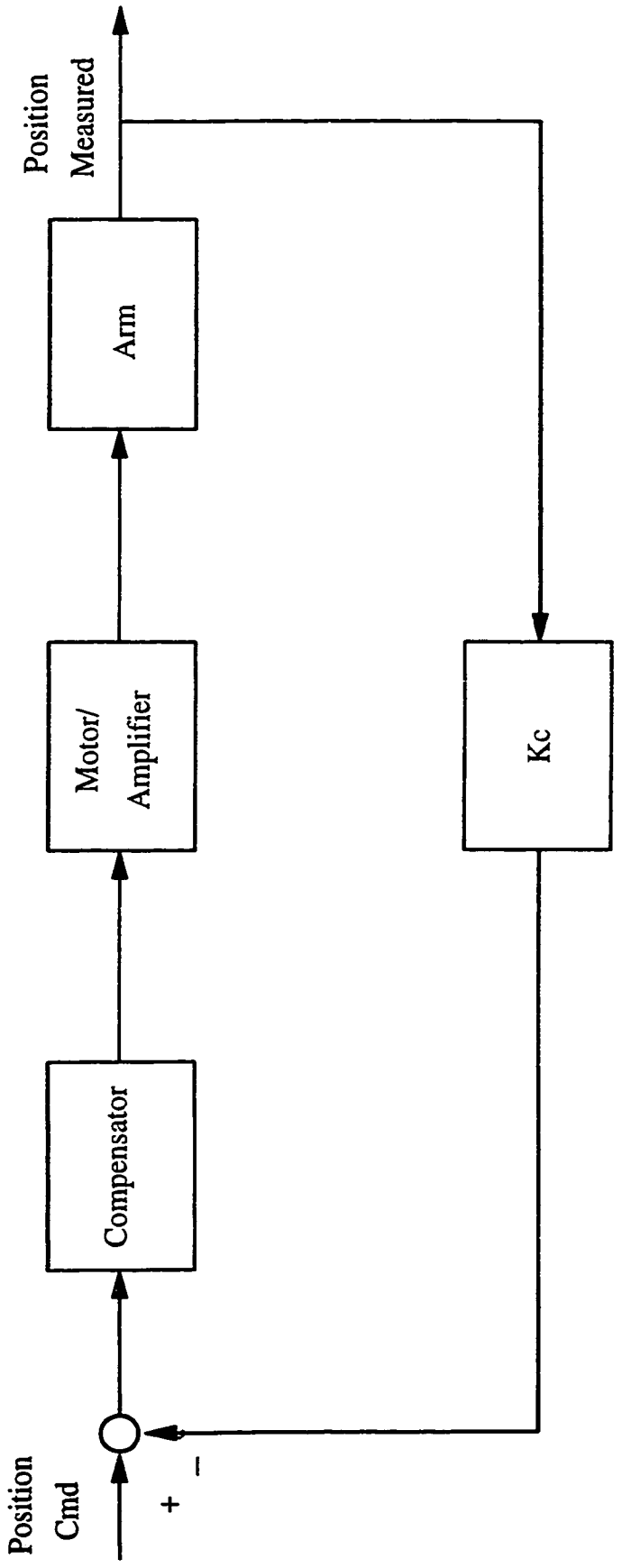


Figure 2.1 Block Diagram for Endpoint Position Control Using Vision Sensor [ 5 ]

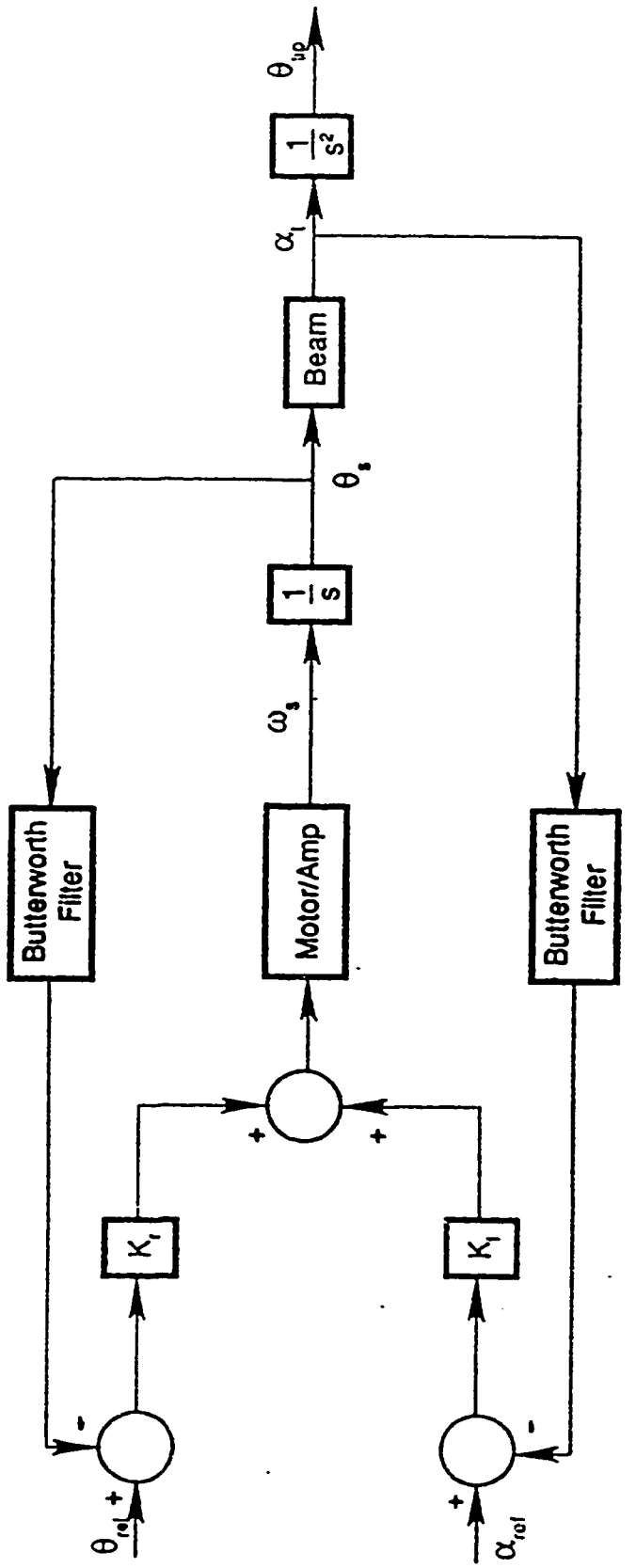


Figure 2.2 Block Diagram for Acceleration Feedback Using an Accelerometer [ 5 ]

from the first controller were smoother than those from the second controller. However, the control with acceleration feedback was found to be the fastest and smoothest of the three controller designs.

Hastings and Book [ 7 ] developed a method to generate a linear model for use in controlling flexible manipulators. The method employed to generate the model utilizes a separable formulation of assumed modes to represent the transverse displacement due to bending. Lagrangian dynamics were applied to determine the kinetic and potential energies for the system. The resultant dynamic equations were then organized into a state-space model. In order to verify the model, two strain gauges were bonded onto the single joint robot arm, one near the joint and one near the middle to determine the frequency response of the flexible robot. It was found that the model agreed favourably with the measured response for a selection of lumped-mass assumed modes, and the dominant parts of the transient response could be characterized by inclusion of as few as two flexible modes.

Instead of mounting the sensor at the tip of the flexible robot, Jain and Khorrami [8] made use of a wrist mounted Force/Torque Sensor to detect the end point vibration of an unknown flexible payload. Since motion of the arm was restricted to the horizontal plane, only the torque signal along the vertical axis was used for feedback of the payload dynamics. A controller utilizing the wrist torque feedback was designed based on the payload dynamics. The objective of the control design was high-speed positioning of payloads with structural flexibility by damping out the vibrational modes of the payload. The control scheme involves a two-stage design. The first stage involves positioning of the manipulator in the workspace and utilizes feedback from joint mounted encoders and tachometers. A PD controller was

designed assuming that the payload has no internal dynamics. The controller for the second stage was designed utilizing feedback from the force/moment sensor mounted at the wrist to damp out the payload vibrations while maintaining the desired final configuration. An adaptive scheme for online identification of the payload dynamic parameters and controller parameters was employed. A model including the first two vibration modes was found to be adequate. The controller was found to be effective for a 60 degree slew. The performance of the torque feedback is questionable with smaller slew angles since the resulting torque value is difficult to measure.

Zheng et al. [ 9 ] & [ 10 ] studied the deflection behaviour of a deformable beam when inserting the beam into a hole. The deformation of the beam was detected by a vision sensor. A model to describe the deformation was determined using cubic spline functions to approximate the contour of the deformed beam. To estimate the deformation of the beam, a numerical differential method was used to solve the nonlinear equation involved. The error of the numerical method was controlled with the aid of the vision sensor. To search for the free end of the beam using the vision sensor, the length of the beam was assumed known. The background of the workplace was set up to be dark and uniform, and the illumination of the workplace was so designed that the brightness of the beam is much higher than that of the background. Only certain evenly distributed edge points of the beam were detected, and spline functions were applied to represent the contour of the deformed beam. A successful experiment was reported. However, only static deformation of the beam was considered.

Chen and Zheng [ 20 ] have studied the effect of the relative orientation of a flexible

beam to the direction of motion on the vibration of the beam. Various motion patterns have been studied (Figure 2.3) to carry a sheet metal beam by a robot. It is demonstrated that by proper motion planning, it is possible to reduce the vibration of the beam when it is being moved. The advantage of this open-loop method is its simplicity in comparison to other approaches. In the paper, dynamic equations of a flexible beam handled by a robot end effector were first formulated and analysed. From the analysis, it was revealed that the inertia forces caused by the beam's motion should affect the vibration of the beam in certain motion patterns. The motion trajectory of the end effector that leads to minimum vibration of the beam could then be specified. However, for the handling of a more complicated 3-D object, like a pre-formed sheet metal part, no suggestion was given as to how to determine the relative orientation of the part to the direction of motion. Detailed investigation of an extension of this-open loop method will be given in Chapter 4 of this thesis.

In the same paper [ 20 ], another passive vibration control method was also suggested. The approach employs a rubber pad in parallel with a spring installed on the robot grippers. The model of this passive damping device is shown in Figure 2.4. Theoretical studies indicated that the passive damping device was equivalent to a negative feedback in the active control approach, and could eliminate the vibration if optimal damping parameters were selected. The optimal damping parameter was derived from the "Most Favourable Amplitude Curve". Its effectiveness was confirmed in simulation only.

Singer and Seering [ 28 ] proposed a method to generate shaped command inputs to reduce end-point vibration of a flexible structure. There are three steps involved in shaping input commands. First, the transient residual vibration amplitude of a system is directly

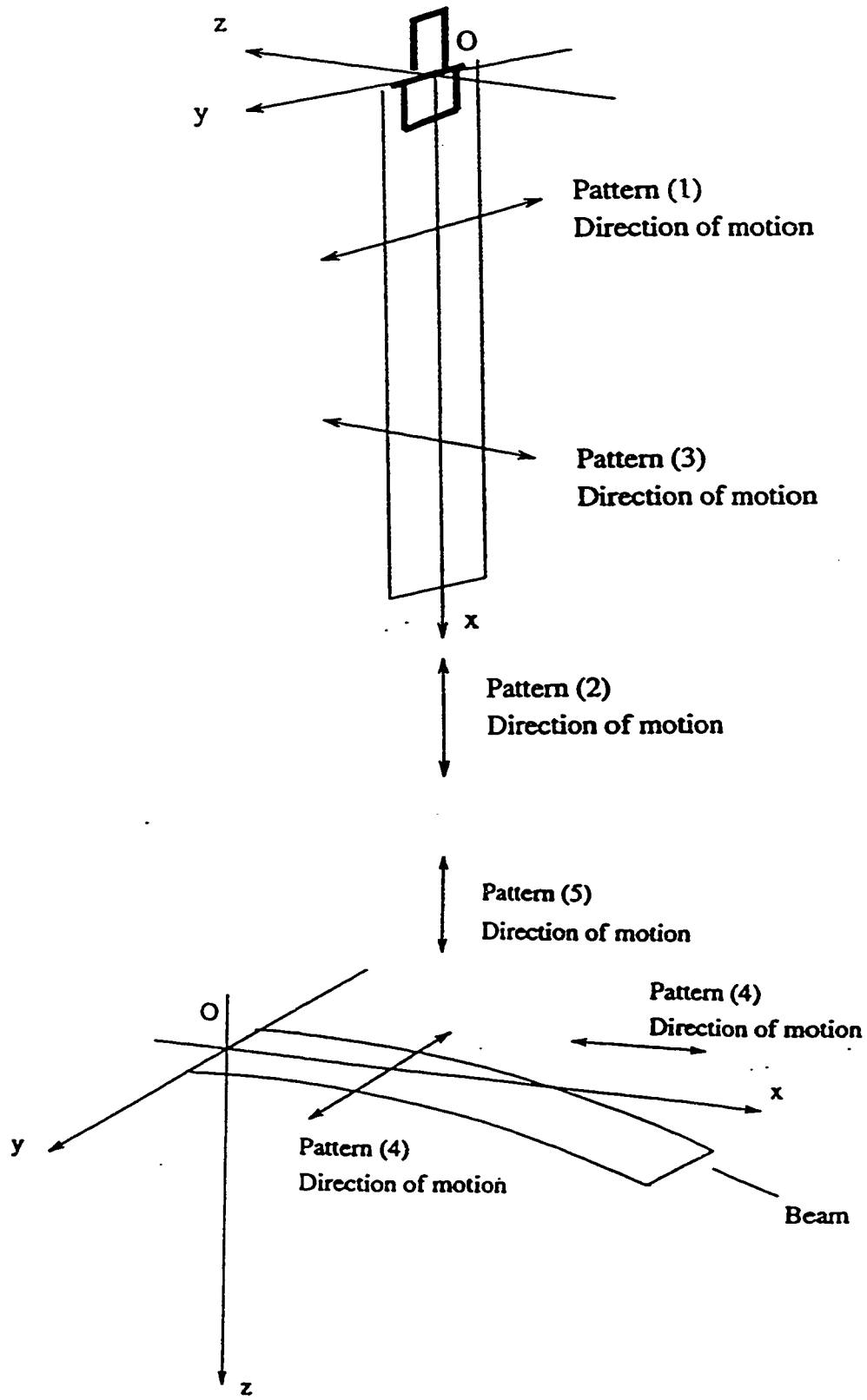


Figure 2.3 Motion Patterns Studied by Chen and Zheng for Vibration Control [20]

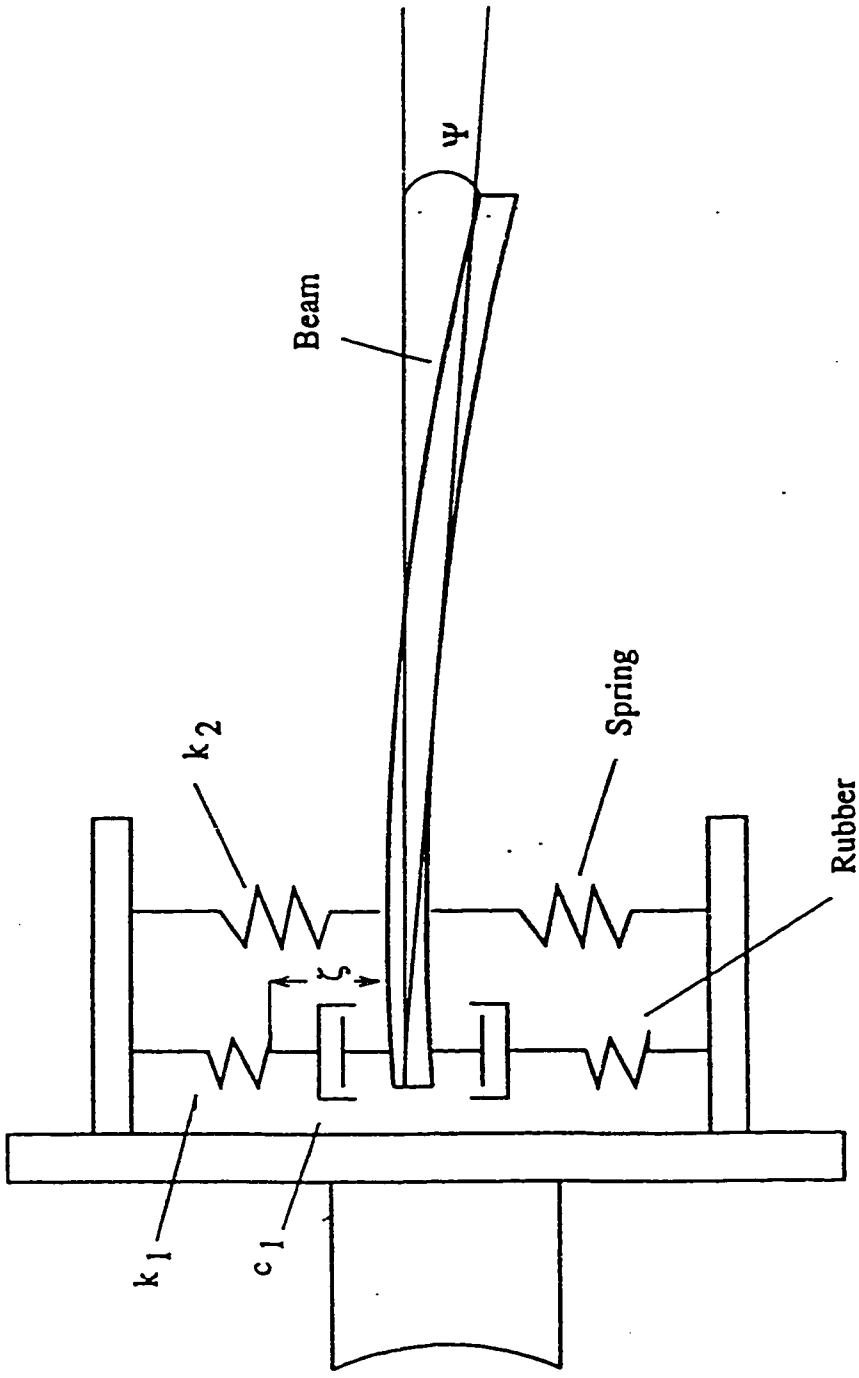


Figure 2.4 The Model of the Passive Damping Device Employed by Chen & Zheng [ 20 ]

expressed as a function of its transient input. Second, the input is specified so that the system's natural tendency to vibrate is used to cancel its own residual vibration. Third, the input commands are specified to include insensitivity to uncertainties. Simulation results demonstrated a factor of 25 reduction in end point residual vibration. Detailed investigation of this vibration control method will be given in Chapter 4 of this thesis. Additional references regarding the control of end-point position of flexible structure include [39]&[40].

## 2.3 MEASUREMENT AND CONTROL OF THE CONTACT STATE BETWEEN TWO PARTS

Several methods have been developed by researchers to measure and control the contact state between two parts during assembly. Suehiro and Takase [ 6 ] estimated the contact state between two objects by observing the instantaneous motion centre of the actual motion. Based on this principle, the constrained motion in contact can be analysed. A motion control method for keeping, getting into and detaching from contact, and a method for detecting contact state were obtained. Motion to keep contact is obtained by rotating about the intersection of two contact normals. A contact normal is the line perpendicular to the common tangent through the contact point between two objects. Motion for detaching from multi-point contact to non-contact is realized by gradually decreasing the number of contacts. To achieve this, a motion centre should be placed on the boundary of the detach centre area so the motion will detach from one contact while maintaining the other contacts. A detach centre is defined as the centre of a motion which has its velocity directed to the moving object side of the common tangent. As an example, consider a detach motion which changes

the state from three point contact to non-contact. As illustrated in Figure 2.5 (a), the centre of motion which eliminates one contact while maintaining contact at two points will be point X, Y or Z. If a rotation is made in the clockwise direction about point Z, contact will be maintained at points A and B, but contact will be lost at point C. A state shown in Figure 2.5 (b) will be attained. To go from state (b) to state (c), a centre of motion which will be in the left detach centre area for point E and on the contact normal for point D is selected to make a counterclockwise rotation. Contact at point E will be detached with contact at point D maintained, and a state as shown in Figure 2.5 ( c ) can be obtained. By reversing the above procedure from state (c ) to (b) then to (a), a sequence of motion which can attain three point contact is obtained. The contact state is detected by observing the motion centre of the actual motion. When a contact is made, the actual motion is constrained. Therefore, the centre of motion will be limited on the constraint normal. Where and what kind of contact is made can be estimated to a certain degree by observing the motion centre of the actual motion. Hybrid control of force and position is proposed to implement the algorithm to achieve various contact states. However, no details were given on actual implementation, and this algorithm would probably only work for rigid workpieces.

Kitagaki, et al. [ 22 ] developed a method to estimate the position of the contact point, and another method to detect the transition of the contact state between two parts using a force/moment sensor. The contact position was estimated with two sets of observed relative forces and moments, and the forces to be applied for the estimation were determined based on the singular value decomposition method. Detection of contact state transition was achieved by monitoring the relation between observed force and moment (Figure 2.6). The

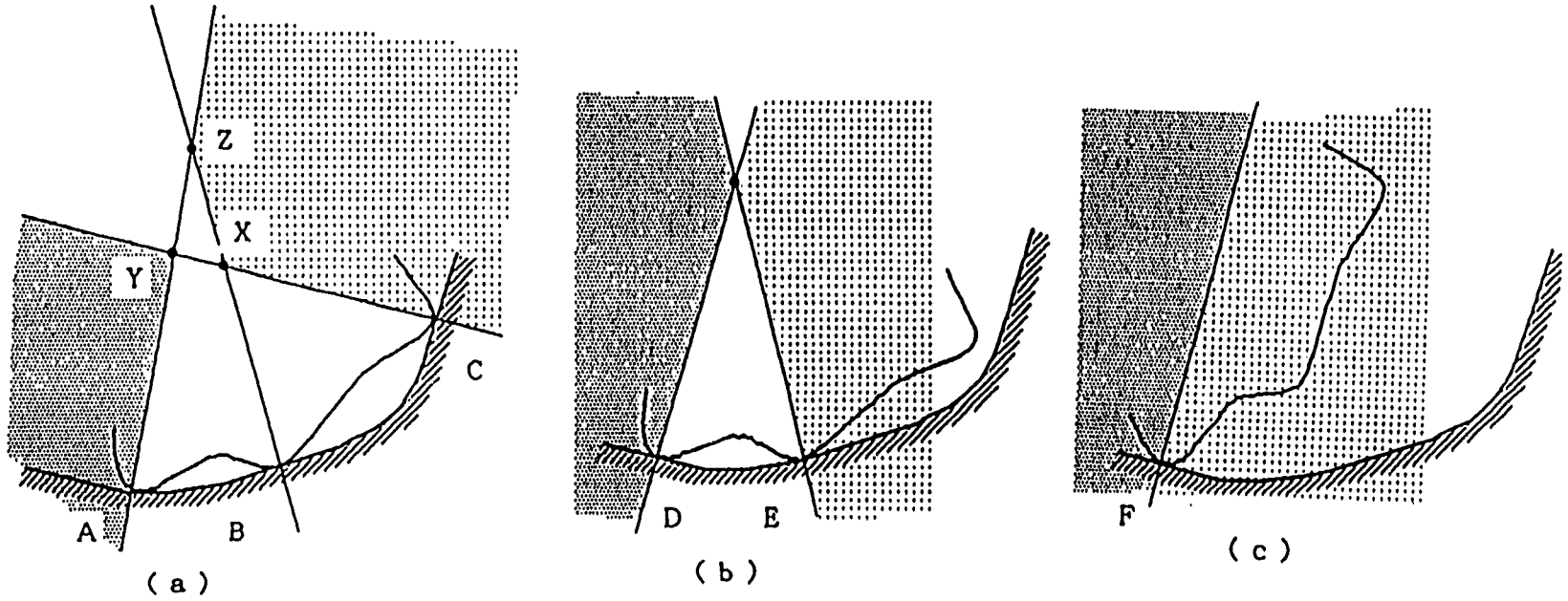


Figure 2.5 Sequential Detach Motion from Three-Point Contact State [ 6 ]

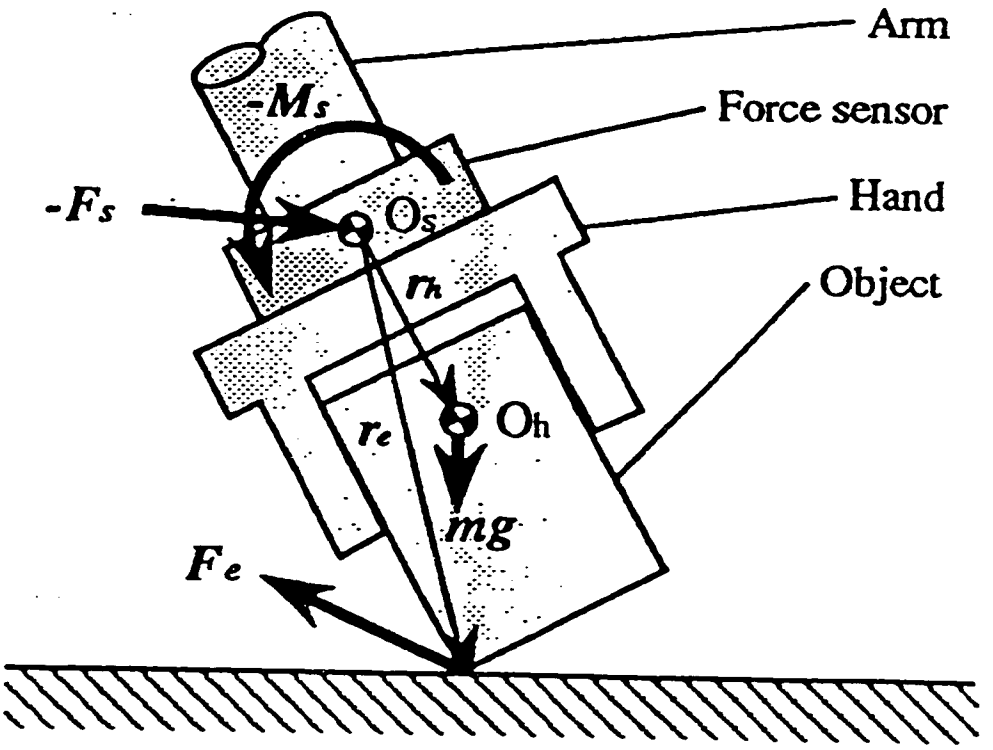


Figure 2.6 Detection of Contact State Transition Using Force/Moment Sensor [ 22 ]

expected moment when the contact point does not change may be calculated using the observed force. However, at the time of contact state transition, the difference between the expected moment and the observed moment may significantly increase. Experiments to estimate the position of a contact point and to detect the transition of the contact state during an edge mating were performed using a direct-drive robot. A rigid metal block was directly attached to the force/moment sensor which was in turn attached to the robot arm. Experimental results demonstrated that the technique was robust against noise in the force signal.

Hirai and Iwata [ 21 ] used a geometric model of a part for contact state recognition (Figure 2.7). First, the process of part mating was modelled as a set of transitions of contact states. Second, static forces were analysed and formulated by applying the theory of polyhedral convex cones in order to derive the ranges of possible force signals that can be measured at each contact state. The face vectors of the polyhedral convex cones directly provide the discriminant functions to determine the contact state from measured force signals. To test the algorithm, a 6 Degree-Of-Freedom (DOF) force sensor was mounted on the wrist of a 6 DOF manipulator so that the reaction forces acting on the robot wrist could be measured. Contact states were identified successfully in an experiment involving two rigid workpieces, one held by the robot, the other fixed onto a table.

Inspired by insect antennae, Ueno and Kaneko [ 11 ] developed the Dynamic Active Antenna system (Figure 2.8) capable of detecting the contact point along a flexible beam and an object. In the searching phase, the flexible beam is actuated by the joint motor to move freely on the horizontal plane. An encoder is implemented to detect the angular displacement

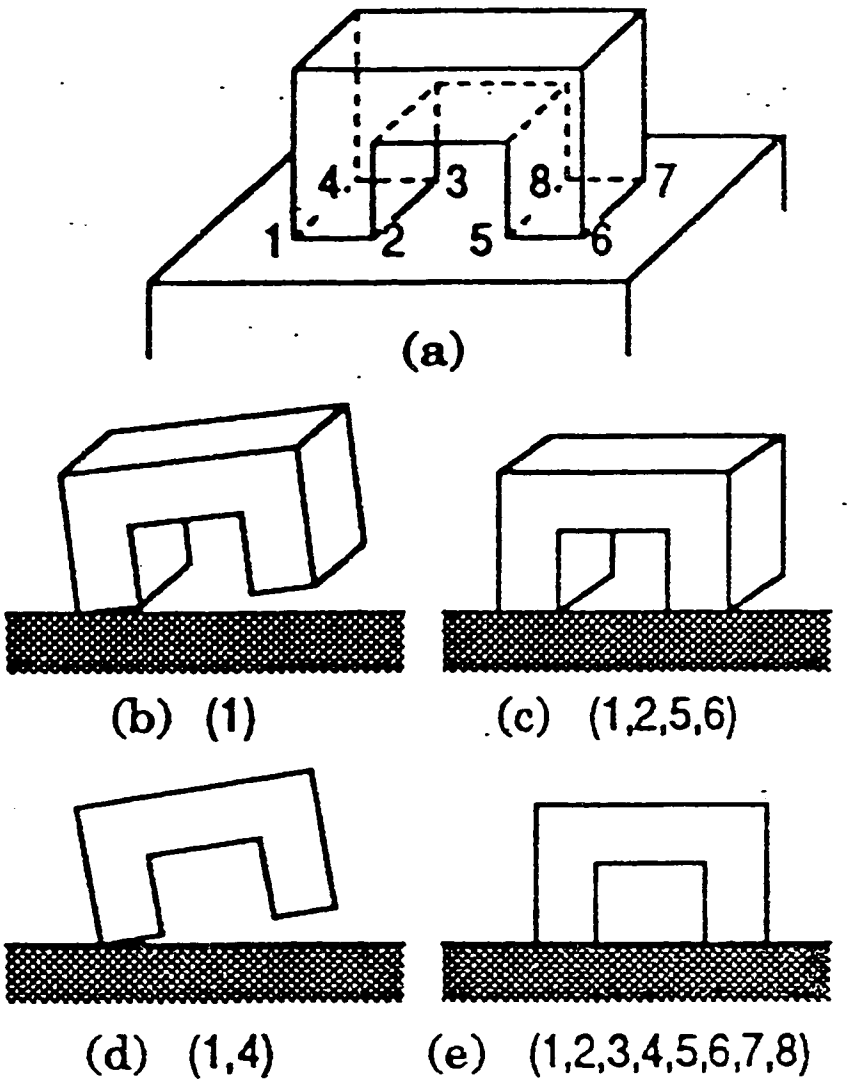


Figure 2.7 Detection of Contact State Based on Geometric Model [ 21 ]

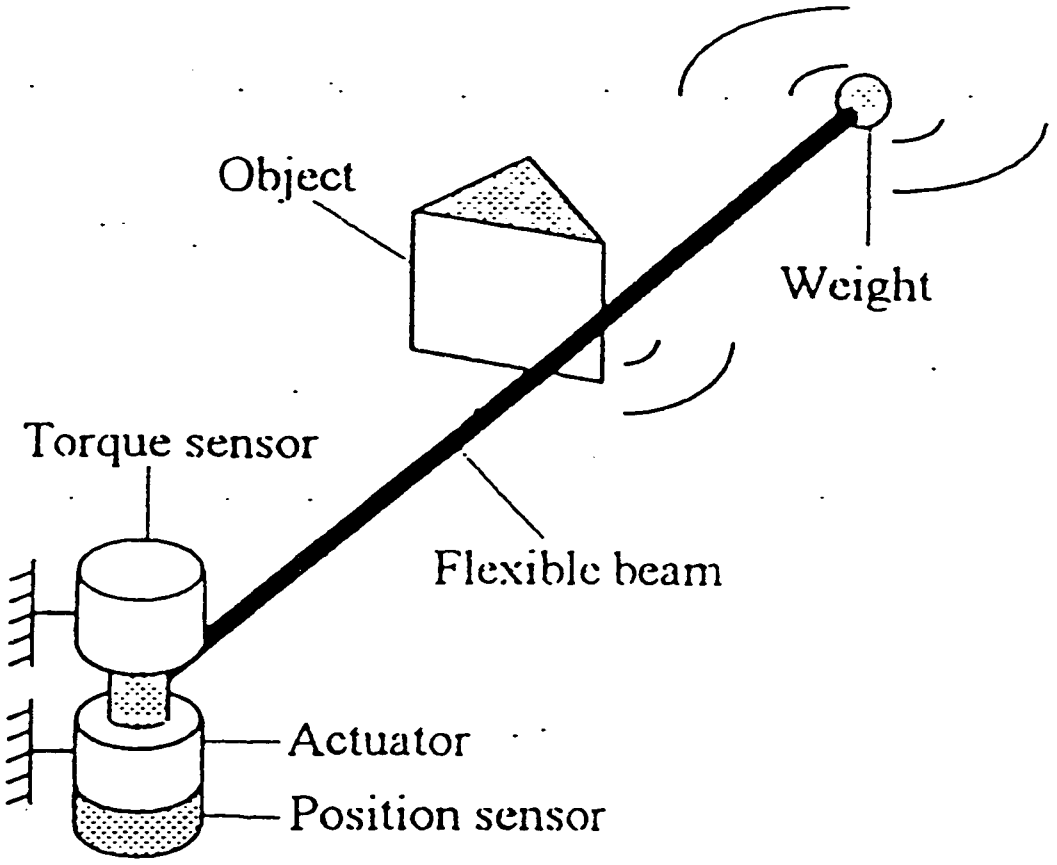


Figure 2.8 The Dynamic Active Antenna [ 11 ]

of the flexible beam. At the moment the beam hits an object, the strain gauge bonded near the fixed end of the flexible beam will detect a change in the joint torque. Then a signal is sent to stop the actuator, and the beam will start to oscillate at its natural frequency. Since the natural frequency of the beam's vibration depends on the beam length, by detecting the vibration frequency and comparing with a previously determined calibration curve, the contact location along the beam can be determined. It was found that adding a single mass to the free end of the beam (essentially changing the infinite degree of freedom system into a single degree of freedom system) could improve the performance of the sensing system. The attached mass causes two important effects: first, to open up the gap between the fundamental frequency and its harmonics, which allows the fundamental frequency to be detected more easily, and second, to shift the peak of frequency curve to the free end of the beam. Experimental results confirmed the effectiveness of the system.

Wasfy [ 12 ] modelled the contact/impact interactions of flexible manipulators with a fixed rigid surface using a finite-element based technique. The conservation of energy and momentum equations or the Newton's collision rule and conservation of momentum equations are used as a velocity constraint on the nodes in contact with the rigid surface to obtain the post-impact velocities of those nodes. Simulation results were presented to demonstrate the effectiveness of the technique; however, no experimental results were presented. This technique may be useful in predicting the post-contact/impact behaviour of a part in RFA.

## 2.4 OTHER LITERATURE RELATED TO THE CONTROL OF FIXTURELESS ASSEMBLY OF SHEET METAL PARTS

Kosuge et. al. [ 14 ] proposed a control algorithm for the bending of a piece of sheet metal supported by two manipulators. A relation between the static deformation of the sheet and bending moments exerted on the sheet was derived using Lagrange's equation based on a finite element model of the sheet. Then a control algorithm was designed using the resultant force applied to the sheet as feedback to control the deformation of the sheet. In the experiments, two 6 DOF robots were employed. A force moment sensor was mounted on the wrist of each of the robots to bend an aluminium sheet. It took about 5 seconds for the robots to bend the sheet from 0 to 13 degrees.

In the same paper, the problem of pressing down a deformed piece of sheet metal while one corner of the sheet is in contact with the environment is considered as well. The contact state of the sheet metal part with respect to a work table needs to be changed from point contact to edge contact. Since the stiffness of the deformed sheet depends on the direction along which the external force is applied, the compliance of the sheet metal could not be used for tasks having interaction between the sheet and the environment. In order to handle such a problem, the control algorithm was designed so that the apparent impedance of the sheet metal was specified. In the experiment, the sheet was rotated by the external force applied to the sheet and completely complied with the surface in about 4 seconds.

To replace conventional car body assembly lines, Nissan has developed the Intelligent Body Assembly System [ 3 ]. The core part of this system is a programmable fixture which consists of 35 positioning robots and 16 welding robots. Under this system, the assembly of

sheet metal parts is achieved by forcing the workpieces to their desired locations. As there is no feedback of the actual position of the workpieces, robots with high rigidity and very accurate calibration are required. Since the clamping and mating forces are not monitored, large forces, resulting in damage to the workpieces, could occur if the workpieces' dimensional tolerances are not high.

A discontinuous control approach was proposed by Mills [ 23 ] for robotic sheet metal assembly to handle the transition from noncontact to contact motion. A closed kinematic chain was assumed during the motion control, and force control was used to maintain a constant contact force in between two sheet metal parts. However, the control of vibration of the parts before assembly and the problem of measuring and control of the contact state were not addressed.

Mills and Ing [ 13 ] modelled the dynamics of a system consisting of two manipulators bringing sheet metal components of a car body into contact. A sheet metal mock-up of a car door was first discretized into finite shell elements. The flexible payload dynamics were derived using the Lagrangian formulation and combined with the robot dynamics to form one system model. The system model was simplified by applying Guyan reduction. The resulting model was employed to simulate the mating of two halves of a car door. Three control methods were considered: PD control with gravity compensation, computed torque control, and master and slave hybrid position/force control. Results of the simulations indicated that all three controllers were able to achieve stable contact and accurate positioning within about 0.5 seconds following initial contact, when the approach speed was set at 0.25m/s.

Nguyen and Mills [ 24 ] developed and tested experimentally a novel control approach

to robotic sheet metal assembly. Since measurement of flexible modes of the payloads was not feasible, a "rigid" control law was implemented. The "rigid" control law constructed the feedback from the robot joint states and the forces measured with wrist-mounted force sensors. Experiments were performed with two 6 DOF robots, each equipped with a 6 DOF force/moment sensor at the wrist. A pneumatic gripper with three vacuum suction cups was used to grasp the sheet metal parts. The test reported involved three phases. In phase I, the robots approached each other to bring the sheet metal parts together under position control. In phase II, the robots pushed the sheet metal into contact, following a prescribed trajectory. In phase III, the robots held the parts without any motion. The robots were under position and force control in phases II and III. Force errors of +/- 5 N and position error of about 0.01 m were observed during the robots' coordinated motion. It was concluded that with a faster control update rate the position errors could be reduced to within the limit set by the automobile manufacturers.

## 2.5 CONCLUSIONS

From the literature survey, it was found that there is a lack of an effective and practical sensor for the measurement of both the vibration and contact state of flexible sheet metal parts. In order to carry out RFA successfully, a suitable sensing device is badly needed. In the literature, vibration control strategies were mainly developed for flexible robot arms and flexible beams. Little attention was paid to the vibration control of complicated 3-D sheet metal parts. In the area of control of contact state, effort was concentrated on strategies for use with rigid parts. Much more work is required to develop methods for the control of contact state for flexible sheet metal parts.

# Chapter 3

# Development of a Novel Sensor for Part Vibration and Contact State Measurement

## 3.1 INTRODUCTION

In the conclusions of the previous chapter, the lack of an effective and practical sensor in the literature for the measurement of both the vibration and contact state of flexible parts was identified. In this chapter, the development of a novel sensor suitable for part vibration and contact state measurement in RFA is described.

## 3.2 SENSOR DESIGN FOR VIBRATION MEASUREMENT

In this section, the design of the sensor for vibration measurement is described. The issues concerning the sensor design is discussed first. Then sets of criteria and constraints are obtained from the discussion. Based on these criteria and constraints the sensor is designed.

### 3.2.1 Issues Concerning the Sensor Design for Vibration Measurement

#### 3.2.1.1 Sensor Characteristics

From some preliminary experiments, the typical vibration amplitude of a sheet metal part when handled by a robot is a few millimetres. However, in order to position the parts accurately for spot welding, an alignment accuracy of +/- 0.1 mm [3] is required.

Since the sheet metal parts to be assembled are freshly stamped, and not painted, there is often a layer of oil put on the metal surface to protect the parts from rusting. This makes the parts' surface very shinny and reflective. Since the sheet metal parts are also light gray in colour, and the manufacturing shop area usually has poor lighting and is often full of smoke and sparks generated from welding the parts together, the application of a vision system to the desired task becomes very difficult. Tactile sensors such as force/moment sensors and strain gauges are the most promising candidates.

#### 3.2.1.2 Sensor Mounting Location

The sensor mounting location is one of the most important factors for the final success of the sensor application. In selecting a sensor mounting location, there are usually two choices: structure mounted and field mounted. A structure mounted sensor is mounted directly on the structure from which measurements are to be taken, while a field mounted sensor is mounted somewhere on the field which takes measurements of the structure from a distance. From an application point of view, for an RFA system, a structure mounted sensor has several advantages over a field mounted sensor. First of all, the robot arm can be moved

through large angles without having to be concerned about the sensitivity range of the sensor. Secondly, a field mounted sensor requires an extra fixture for mounting which often increases production cost. Thirdly, a field mounted sensor may take up extra floor space and become an obstacle for the robots' movement.

When mounting the sensor on the structure itself, care must be taken in selecting a good mounting location. For the sheet metal vibration measurement problem, mounting the sensor at the edge of the flexible sheet metal part is not feasible. One of the reasons is that welding usually occurs along the edges of a sheet metal part. The presence of a sensor there may interfere with the assembly operation. Also the sensor cannot be mounted permanently onto the part because this may deface the part. Besides, attaching and removing of a sensor from the part will inevitably increase the cycle time; therefore, it is not advisable to mount the sensor directly onto the sheet metal part itself.

#### 3.2.1.3 Sensor Cost

Cost is a very important factor in selecting a sensor for RFA. One of the reasons why it is desirable to eliminate the fixtures from the assembly process is the high cost associated with the fixtures. Therefore, in selecting a sensor for RFA, it is important not to bring the cost up again. Also, in order to convince the automotive manufacturers to switch to a new technology, both the initial cost and the maintenance cost must be low enough to make RFA an attractive idea.

In general, the cost of a vision sensor is higher than that of a force/moment sensor. The higher cost is associated with the cost of the sensor itself, the high speed computer

required to process the large volume of image information, and the higher cost for maintenance. Compared to a vision sensor and a force/moment sensor, the cost of strain gauges is the lowest of all (in general less than C$10 each). This makes the strain gauge a very attractive choice for RFA.

Since both the vibration control problem and the contact state control problem have to be dealt with, one of the best ways to cut the sensor cost is to be able to use the same sensor for both measurements. By doing so, both the initial sensor cost and the maintenance cost will be reduced.

### 3.2.2 Sensor Design Criteria and Constraints

From the above discussion of the issues concerning the sensor design, some criteria and constraints were obtained for the sensor selection/development. They are listed below in descending order of importance:

1. The sensor precision must be higher than 0.1 mm
2. Must be portable
3. Cannot be mounted onto the part permanently
4. Preferably able to be mounted onto the robot gripper
5. Suitable for oily, shiny, unpainted sheet metal parts
6. Suitable for an automobile assembly plant environment, which means poor lighting with lots of sparks and smoke generated from welding being performed in the surrounding area

7. Preferably able to measure both the vibration and the contact state between the parts
8. Easy to maintain
9. Low cost

### 3.2.3 The Use of Strain Gauge-equipped Fingers for Vibration Monitoring

#### 3.2.3.1 The Strain Gauge-equipped Finger Design

Based on the design criteria and constraints listed above, the Strain Gauge-equipped Fingers (SGFs) were developed. The SGF is a strain gauge based sensing device. The SGF avoids the impractical approach of installing a strain gauge directly onto a part to measure its vibration. Instead, a strain gauge is mounted onto a finger shaped piece of spring steel, which is in turn mounted onto the robot gripper. From the discussion above on sensor mounting location selection, it was concluded that the best place to mount the sensor is on the robot gripper. When the part is picked up by the gripper, the sensor will be able to come into contact with the part automatically, and start measuring its vibration. And after the assembly process, when the part is released from the gripper, the sensor will come off the part without defacing the part. Mounting the sensor onto the gripper in this way makes the sensor portable and eliminates the extra processes of attaching and removing the sensor. This will reduce cycle time and eliminate any possibility of measurement errors due to inaccurate mounting of the sensor.

Each of the SGFs is made from a piece of 0.4 x 10 x 95 mm spring steel. As shown in Figure 3.1, the steel pieces are bent into L shaped fingers. A photograph of a SGF is

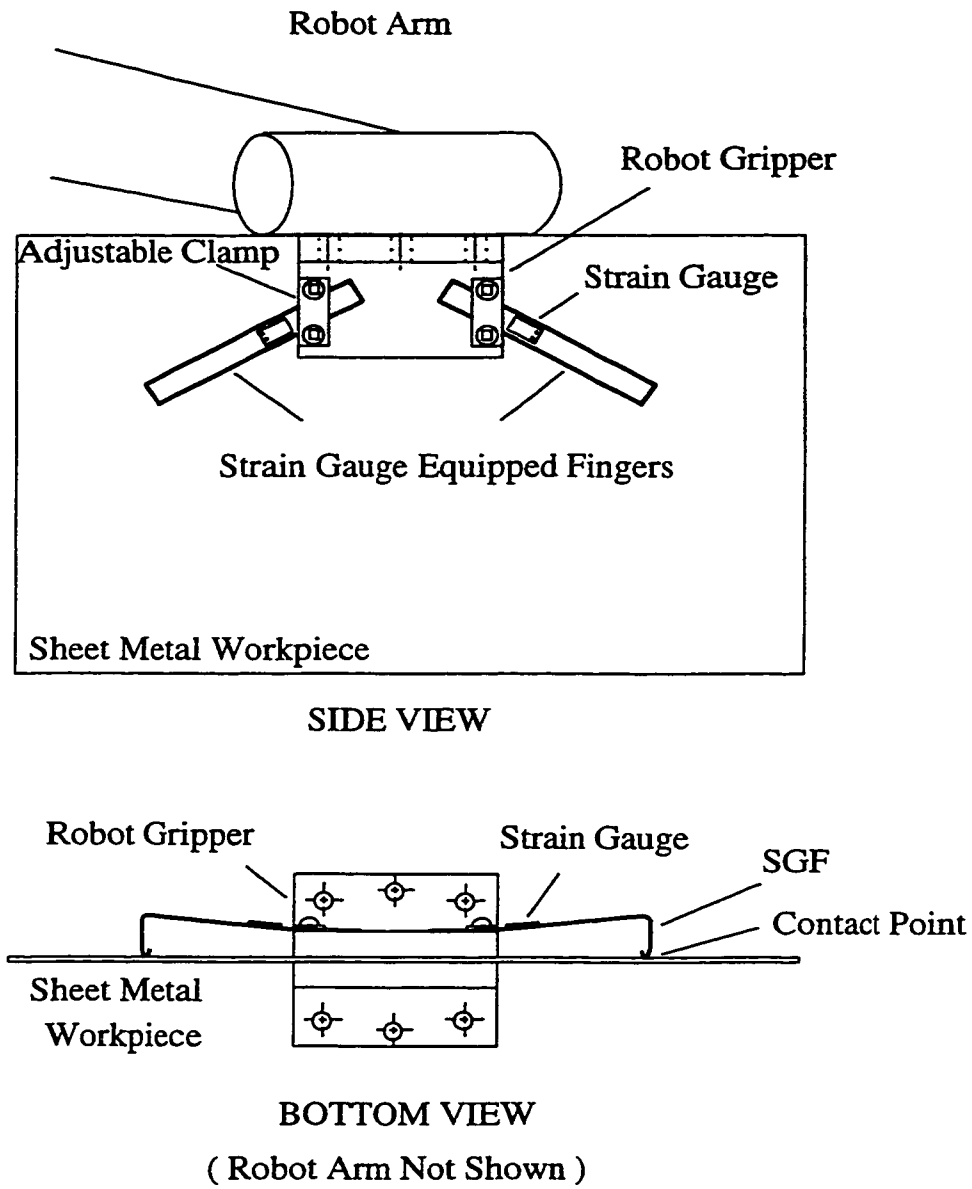


Figure 3.1 Design of the Strain Gauge-equipped Fingers (SGFs)

shown in Figure 3.2. A small 8mm x 5mm 350 ohms general purpose strain gauge ( part number: CEA-06-062UW-350 ) manufactured by Measurements Group Inc. was selected. This gauge was selected primarily because of its compact size, self-temperature compensation feature, and low cost (less than C$10 each). One strain gauge is bonded onto the top side of the L shaped finger to form a SGF. Since the strain gauge selected has self-temperature compensation feature, there is no need to put an extra strain gauge on the back side of the SGF for temperature compensation. This will not only cut down the cost in material and labour to put in an extra strain gauge, but will also eliminate any sensor error due to misalignment of the top and bottom strain gauges.

The SGFs are held onto the gripper by adjustable clamps. The clamps allow the orientation and cantilever length of the fingers to be varied. In the present model, the SGF length and physical location can only be adjusted manually. In the future, these adjustment can certainly be done automatically to optimize the performance of the SGF. For maximum sensitivity, the strain gauge should be located very close to the clamp, as shown in Figure 3.2. The height of the finger at the tip was designed to be greater than that at the base to ensure that contact is maintained with the sheet metal part. As the part deflects during vibration, the SGF will also deflect. This SGF deflection will generate strain, which is measured by the strain gauge. Note that the contact point of the SGF is rounded to avoid scratching the part and to allow the tip of the SGF to slide freely on the part's surface.

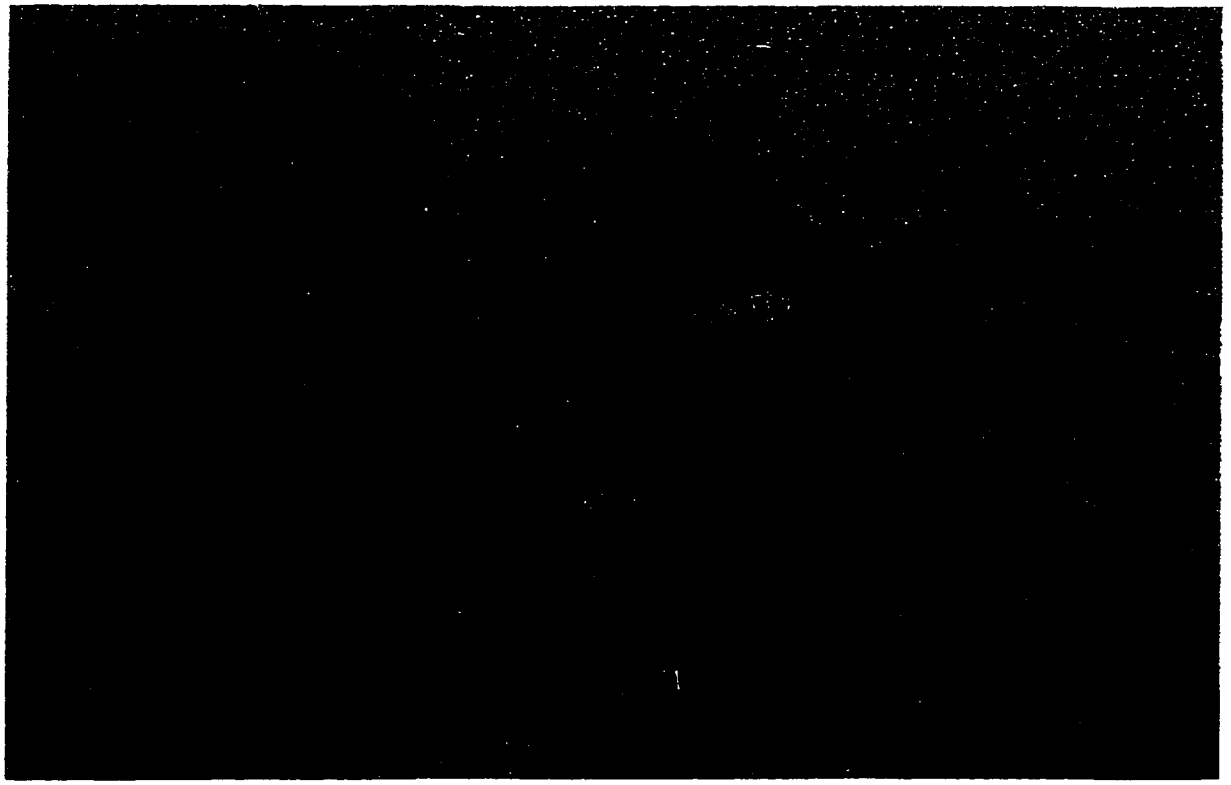

Figure 3.2 A Photograph of a Strain Gauge-equipped Finger (SGF)

### 3.2.3.2 Comparison of a SGF to a Workpiece Mounted Strain Gauge

Since many researchers have used strain gauges bonded onto a flexible structure to monitor its vibration successfully [ 27 ], there is no doubt that a strain gauge mounted onto a sheet metal workpiece will be able to monitor its vibration as well. In order to determine how well a SGF compared with a strain gauge mounted directly onto a sheet metal part, tests were performed to compare the output of the two devices. A 0.69 mm thick (gauge 23) galvanized steel sheet workpiece was used. The sheet was deflected to produce compressive and tensile strains as shown at the top of Figure 3.3. The voltage outputs for identical amplifier gains are shown at the bottom of Figure 3.3. It can be seen that the two outputs have a linear relationship, proving that the SGF is effective in measuring the strain on the sheet metal workpiece. Note that the SGF produces a higher voltage output than the workpiece mounted strain gauge, and should have a better signal to noise ratio as a result. The higher output is due to the lower stiffness of the spring steel from which the SGF is made. This lower stiffness results in a greater localized strain which makes the strain gauge on the SGF deform more than the gauge on the sheet metal part.

### 3.2.3.3 Calibration of the SGF

In order to determine the actual vibration amplitude at the edge of a sheet metal part, it is necessary to calibrate the strain gauge voltage output against a known deflection in millimetres. To perform a calibration process, a sheet is bolted onto a robot gripper which has a SGF installed as shown in Figure 3.4. The robot is commanded to move normal to the

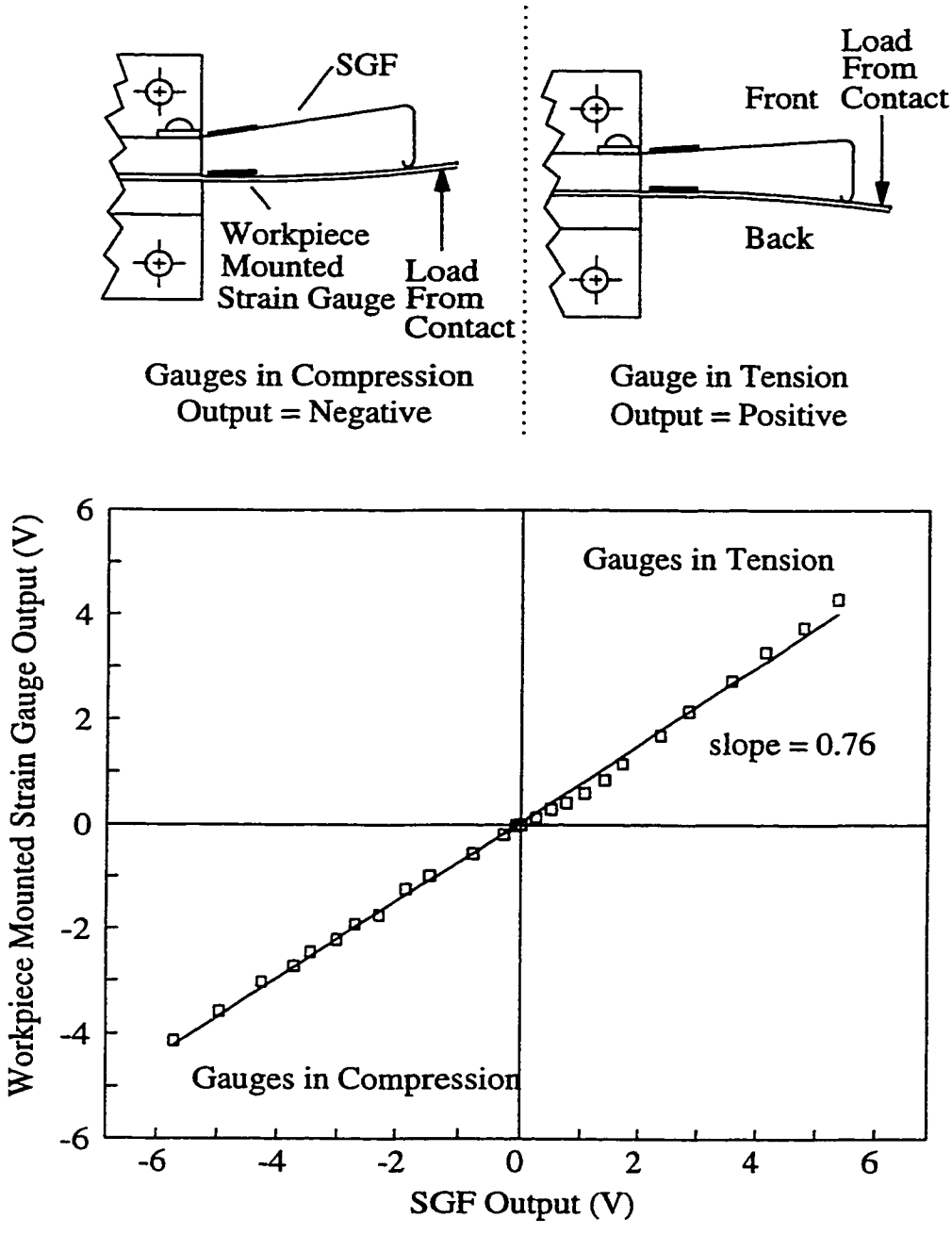


Figure 3.3 Comparison of the Outputs of a SGF and a Workpiece Mounted Strain Gauge

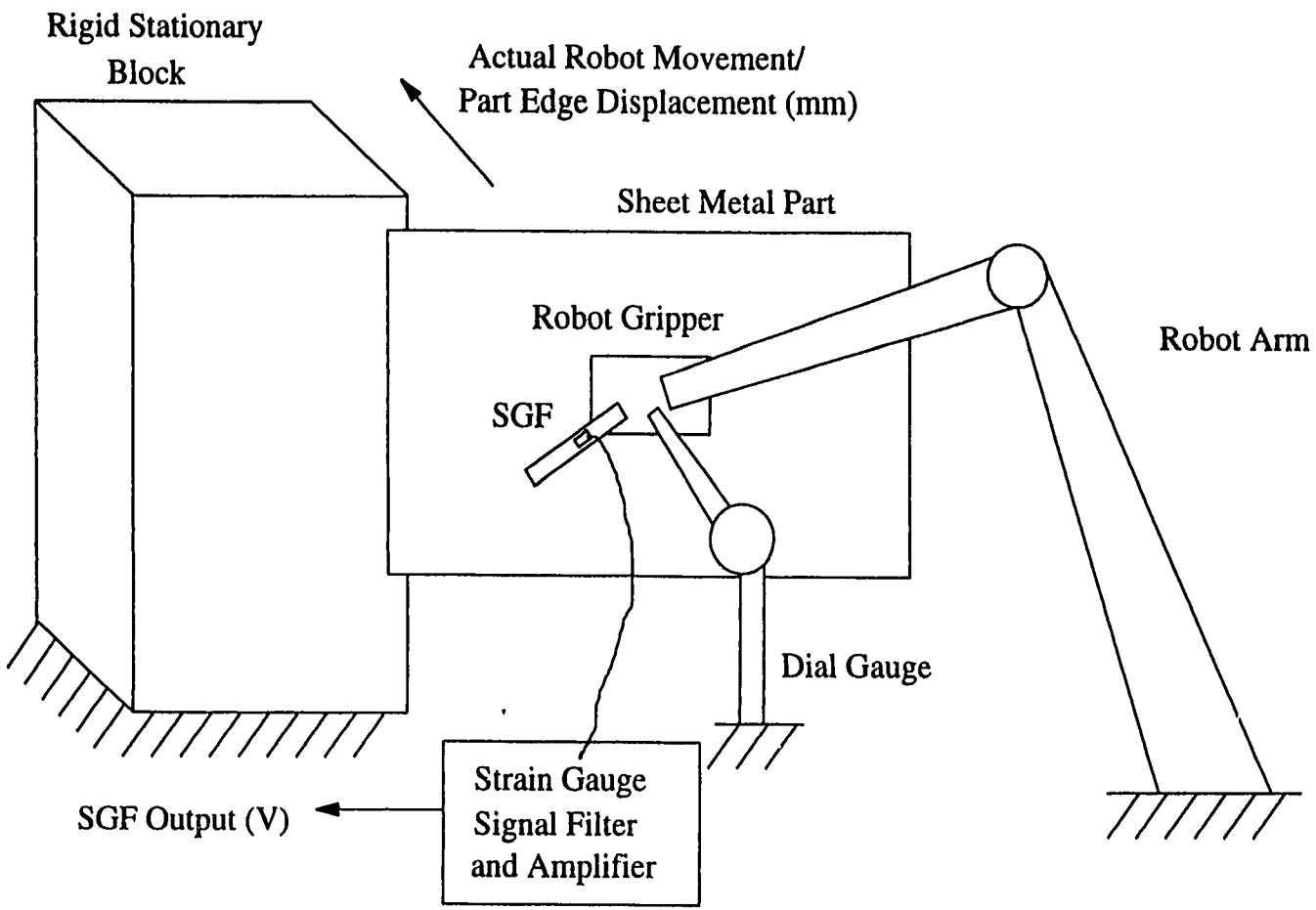


Figure 3.4 Calibration of the Strain Gauge-equipped Finger (SGF)

surface of the sheet in steps of 0.5 mm, to push an edge of the sheet against a rigid stationery block bolted onto a work table. As shown in the figure, a dial gauge mounted rigidly on the work table is needed to verify the actual movement of the robot gripper. If the calibration process is started with the sheet metal part just touching the rigid block bolted onto the table, the amount of deflection at the edge of the sheet metal part should be equal to the actual robot gripper movement. Plotting the output of the SGF in Volts against the actual robot movement in millimetres, a calibration curve for the SGF used on this particular sheet metal part can be obtained. Since the amount of strain generated depends on the cantilever length and stiffness of the sheet metal part in use, in order to determine the actual amount of vibration on the part, calibration is required for each part with different characteristics to be assembled. In practice, if there is no need to know what the absolute vibration amplitude is as long as the relative vibration amplitude is known, then this calibration process would not be necessary. The calibration curve for a SGF applied on a sheet steel 560 mm x 460 mm x 0.92 mm is shown in Figure 3.5 as an example. The slope of the curve is 2.5 mm/V which is also the calibration constant for the SGF for this workpiece. Using a 12 bit resolution A/D board with maximum input range of +/- 5.0 V, a resolution of 0.0024 V can be achieved. Using the calibration constant of 2.5 mm/V, gives a theoretical resolution of 0.006 mm for the SGF with this part.

## 3.3 SENSOR DESIGN FOR CONTACT STATE MEASUREMENT

### 3.3.1 Issues Concerning the Sensor Design for Contact State Measurement

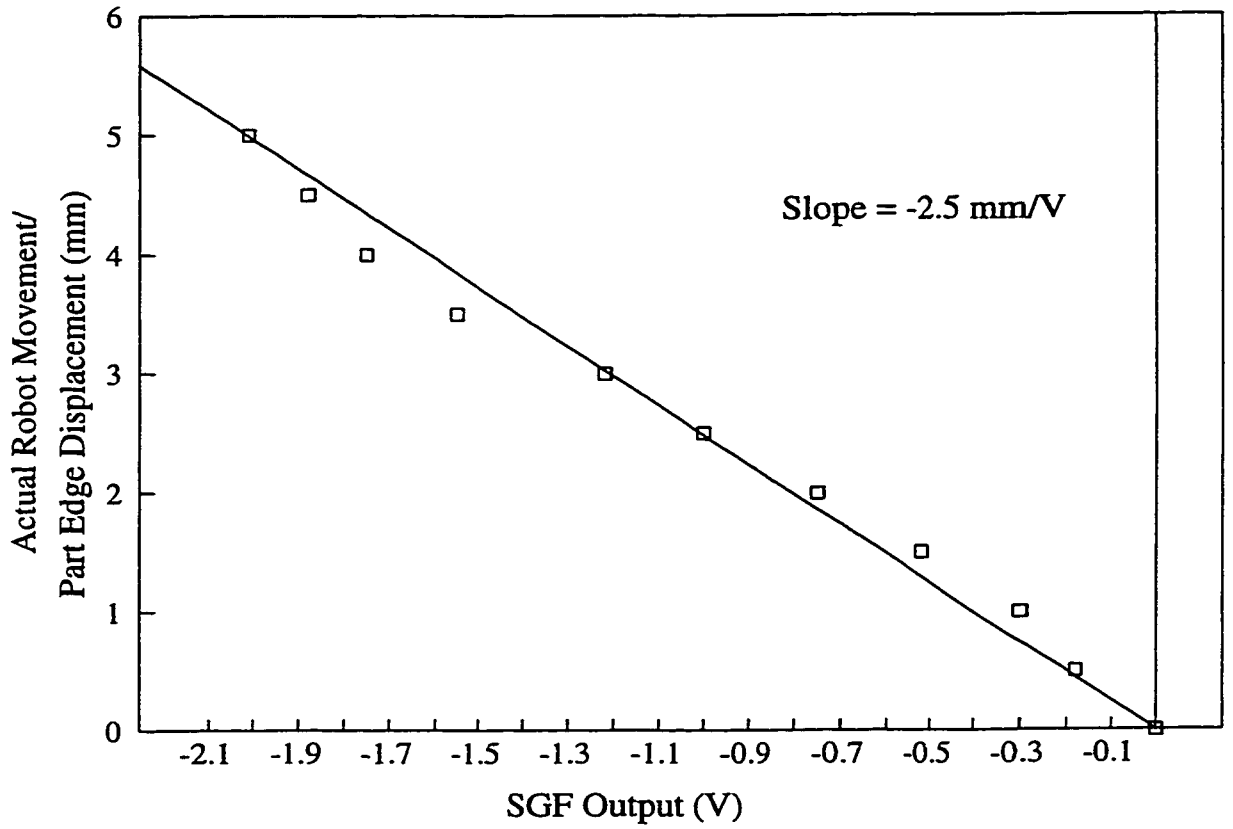


Figure 3.5 Calibration Curve for a SGF

#### 3.3.1.1 Sensor Characteristics

When two parts are being assembled, there are four possible contact states between them. The parts can either be in point contact, edge contact, plane contact or no contact. In general, when two sheet metal parts are in contact, due to robot positioning error and part dimensional error, there will be contact force generated, and the parts may be deformed as well. The amount of deformation is dependent on the parts' stiffness and the magnitude of the contact force. For parts with high stiffness, the contact force tends to be relatively high even with a small robot positioning error. In this case, a standard force/moment sensor may be used. On the other hand, for parts with low stiffness, the contact force is usually very small even with relatively large deflection on the parts. In this situation, a force/moment sensor is unlikely to be successful and a sensor based on part deflection is a better option.

### 3.3.2 The Use of Strain Gauge-equipped Fingers for Contact State Measurement

When two sheet metal parts are in contact, the contact force generated will deform the parts elastically. The SGF developed in section 3.2 can be used to detect this deformation. By strategically positioning several SGFs around the robot gripper, the deformation of the part can be detected and hence the state of the contact between the parts can be identified. The use of the SGFs for contact state measurement, along with force/moment sensing and a sensor fusion approach are described fully in Chapter 5.

## 3.4 CONCLUSIONS

The development of the novel SGF was described in this chapter. The SGF met all the design criteria and constraints for RFA, and it allowed the measurement of both the vibration and contact state of flexible parts. An experiment was performed to compare the output of a SGF and a workpiece mounted strain gauge. The voltage outputs of the two had a linear relationship proving that the SGF is as effective as a workpiece mounted strain gauge. A typical sensitivity of 0.4 V per mm of part edge displacement was obtained for the SGF. The application of the SGFs in vibration control is presented in the next chapter.

# Chapter 4

# Vibration Control

## 4. 1 INTRODUCTION

In this chapter, the vibration control problem encountered when a sheet metal part is handled by a robot at high speed is examined. The control objective is to reduce the vibration of the sheet metal part as much as possible. In order to control the sheet metal part's vibration, two feedforward control algorithms are investigated. The first is a novel Learning Extremum Control algorithm [ 30 ]. The performance of this algorithm is studied based on vibration control experiments using 2-D and 3-D parts. (In this thesis, a 2-D part is defined as one whose thickness is much smaller than its remaining two dimensions.) The second control algorithm investigated is the Input Command Shaping Method [ 28 ]. The performance of this algorithm is studied based on simulated and experimental results.

## 4.2 CONTROL OF VIBRATION IN SHEET METAL PART HANDLING

In order to maximize the production rate, it is desirable to move the sheet metal parts as fast as possible. However, at the same time, it is important to control the vibration of the

part when it is being handled to avoid damage and to achieve a high assembly accuracy. In general, the greater the speed, the more the part's structural vibration modes will be excited. In today's car body assembly plant, the usual way of dealing with this problem is to dwell for a period of time to let the vibration damp out by itself. However, this dwelling period could be very long. For a sheet metal part having 10 Hz natural frequency and 0.5 % damping (typical for sheet metal parts) it takes 7.3 seconds to achieve a 90 % reduction in vibration amplitude.

## 4.3 LEARNING EXTREMUM CONTROL (LEC) OF VIBRATION

In iterative learning control schemes, the system inputs are modified over a sequence of repetitions or trials with the objective that the system outputs converge to a predetermined reference trajectory. This differs from conventional adaptive control in that the learning is performed off-line between trials, and the controller parameters are typically fixed. Learning control schemes are applicable to processes which are repetitive in nature and operate over a fixed time interval. The robotic sheet metal assembly process is a good candidate for learning control since the same kind of sheet metal part will be handled repeatedly. However, as stated earlier, to apply learning control to the control of vibration, it is necessary to have a predetermined reference trajectory for the output (ie. the vibration) to follow. Although ideally the vibration should be zero, in reality this will never happen. Therefore, it is necessary to search for the trajectory to produce minimum vibration. This introduces the need for extremum control.

The objective of an extremum controller is to locate the steady state maximum or minimum of a process and then continuously keep the process operating at its optimum if it is varying [ 31 ]. In order to apply extremum control, the static response curve relating the inputs and the outputs has to be concave/convex. In the problem at hand, the inputs are the various part orientations, and the outputs are the resulting vibration amplitudes. It is expected that the vibration amplitude versus the part orientation curve contains at least one minimum point. The tracking of the part orientation for minimum vibration should be achievable by a combination of learning and extremum control. A Learning Extremum Control scheme is described below which can automatically determine the best orientation for a sheet metal part to be transported by a robot for minimum vibration.

### 4.3.1 The LEC Algorithm

The block diagram of the Learning Extremum Control (LEC) system employed is shown in Figure 4.1. The learning is achieved through an optimization search, and it is performed off-line between trials. The objective of the optimization search is to find the part orientation angle relative to the path that will create the minimum amount of vibration. The amount of vibration is quantified by the average vibration amplitude within a fixed period of time immediately after the motion.

Figure 4.2 shows a response curve relating the input, the part orientation angle, and the output, the vibration amplitude. The minimum point on the curve is the optimal operation point which is unknown at the beginning. The optimization search starts with best guess for

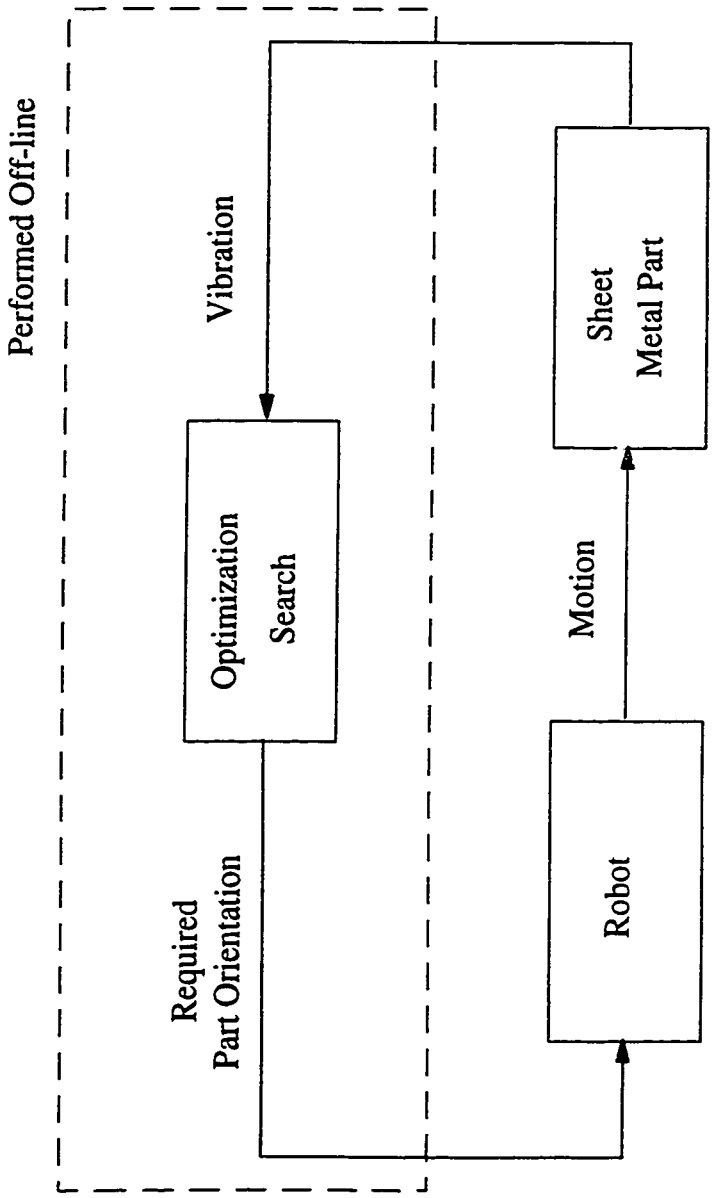


Figure 4.1 Block Diagram of the Learning Extremum Controller

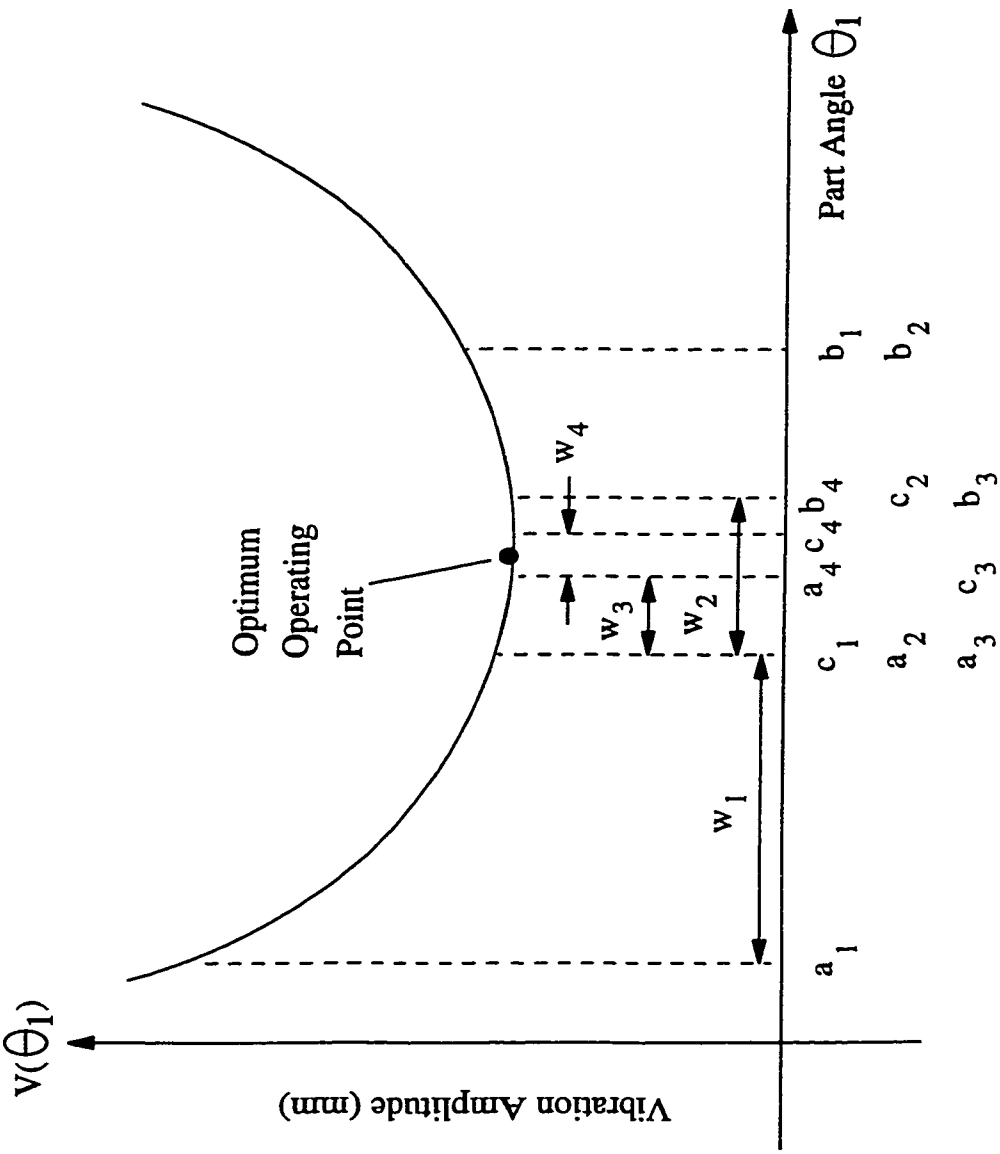


Figure 4.2 Vibration Amplitude Vs. Workpiece Orientation Angle Graph

the part orientation angle, for example point $c_1$. After the robot has transported the part to where the subsequent assembly is going to take place, the resulting vibration is recorded. As the operation repeats, more vibration data is recorded and an average vibration amplitude associated with the current part orientation angle can be established. The same procedure is then repeated at two more positions along the response curve, one at angle $a_1$ and another at angle $b_1$, obtained by rotating the part for $+w_1$ and $-w_1$ degrees respectively from its original orientation. The interval between $a_1$ and $b_1$ is the uncertainty interval within which the optimal operation point is expected to be located. This operation completes the first trial. The remaining trials start by performing an optimization search using the following algorithm:

```
0     Procedure LEARNING
1     IF  ( V(a_i) < V(b_i) )
2         a_{i+1} = a_i
3         b_{i+1} = c_i
4     ELSE
5         a_{i+1} = c_i
6         b_{i+1} = b_i
7     ENDIF
8     w_{i+1} = w_i * 0.5
9     c_{i+1} = a_{i+1} + w_{i+1}
10    i = i + 1
11    RETURN
```

The uncertainty interval between the part orientation angles $a_i$ and $b_i$ is first divided into two halves, with the angle $c_i$ at the centre. The algorithm then compares the average

vibration amplitude, V, associated with each of part orientation angles, $a_i$ and $b_i$. The half of the uncertainty interval in which the average vibration is lower will be preserved. The angle $c_i$ and the angle $a_i$ or $b_i$ which gives the smaller vibration amplitude will form the new uncertainty interval. Therefore, each time this algorithm is executed, the uncertainty interval is halved. The number of times this algorithm should be repeated depends on the size of the initial uncertainty interval and the desired accuracy of the estimated optimal orientation angle of the part. Finally, after n trials, the estimated optimal orientation angle can be determined by comparing the three vibration amplitudes associated with the angles $a_{i+n}$, $b_{i+n}$ and $c_{i+n}$. Since a change in the part's Pitch, Yaw and Roll angle may reduce the part's vibration while it is being handled, such an optimization search should be carried out by changing respectively each of the three angles mentioned above . The part orientation that gives the minimum average vibration amplitude should be chosen as the optimal orientation for the transportation of that particular part. The accuracy of the part orientation angle with respect to the optimal angle is represented by $w_j$, where j is the number of orientation angles tested for one part. $w_j$ is related to the initial $w_1$ and j by:

$$w_j = \frac{w_1}{2^{j-2}}, \qquad j > 1 \qquad (4.1)$$

Figure 4.2 also depicts the uncertainty intervals for four consecutive learning trials. The three orientation angles associated with each trial are shown as well. Note that only one new orientation angle is tested for each new trial. The other two angles are carried over from the previous trial.

### 4.3.2 Experimental Verification of LEC of Vibration in 2-D Parts Handling

The Learning Extremum Control (LEC) algorithm was tested experimentally to determine its effectiveness. To start with, the LEC algorithm was employed for vibration control 2-D parts handling. The part was assumed to be held by a robot gripper at the centre of one of the part's edge. In order to measure the vibration of the sheet metal part, two Strain Gauge equipped Fingers (SGFs) were installed onto the robot gripper, as shown in Figure 4.3.

Other than the SGFs and the strain gauge signal conditioning devices, the equipment consisted of a 5 Degree-Of-Freedom (DOF) GMF-A1 industrial robot with gripper and an IBM PC. The GMF robot had been retrofitted and was controlled by a Delta Tau PMAC motion control board equipped with an A/D convertor. The sheet metal part selected was a gauge 23 flat galvanized steel sheet. Its dimensions are 370 x 290 x 0.69 mm. A flat sheet was chosen so that the optimal orientation angle of the part relative to the motion path was known ahead of time. Therefore, the experimental result could be compared with the expected value of zero degrees.

#### 4.3.2.1 Experimental Procedure for LEC of Vibration in 2-D Parts Handling

The setup for the vibration control experiments is shown in Figure 4.4. The sheet metal part is clamped by the robot gripper at the centre of its top edge. This is an approximation to holding a larger sheet at its centre with a single vacuum pickup. The experimental procedure described in section 4.3.1 was then followed. A 300 mm straight horizontal path, and an average velocity of 1 m/s were used. At each orientation angle the

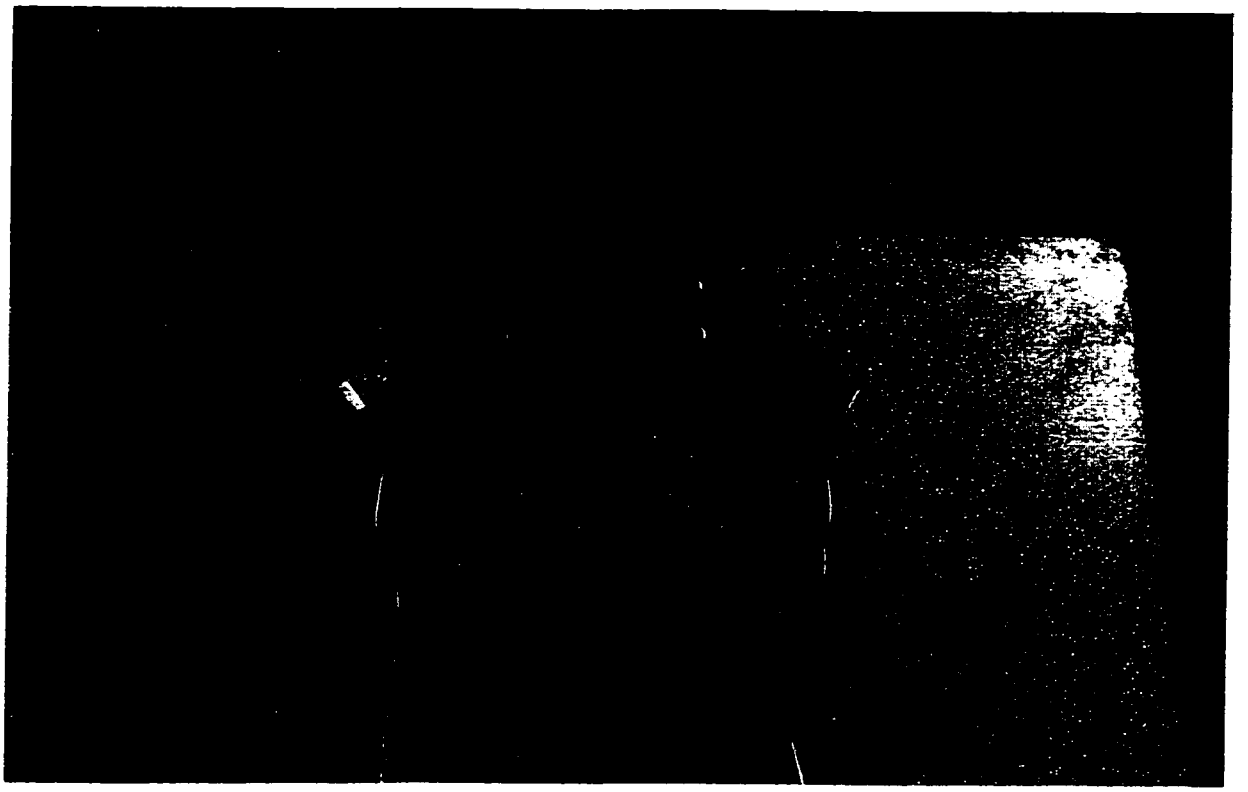

Figure 4.3 The Use of Two SGFs to Measure

the Vibration of a Sheet Metal Part

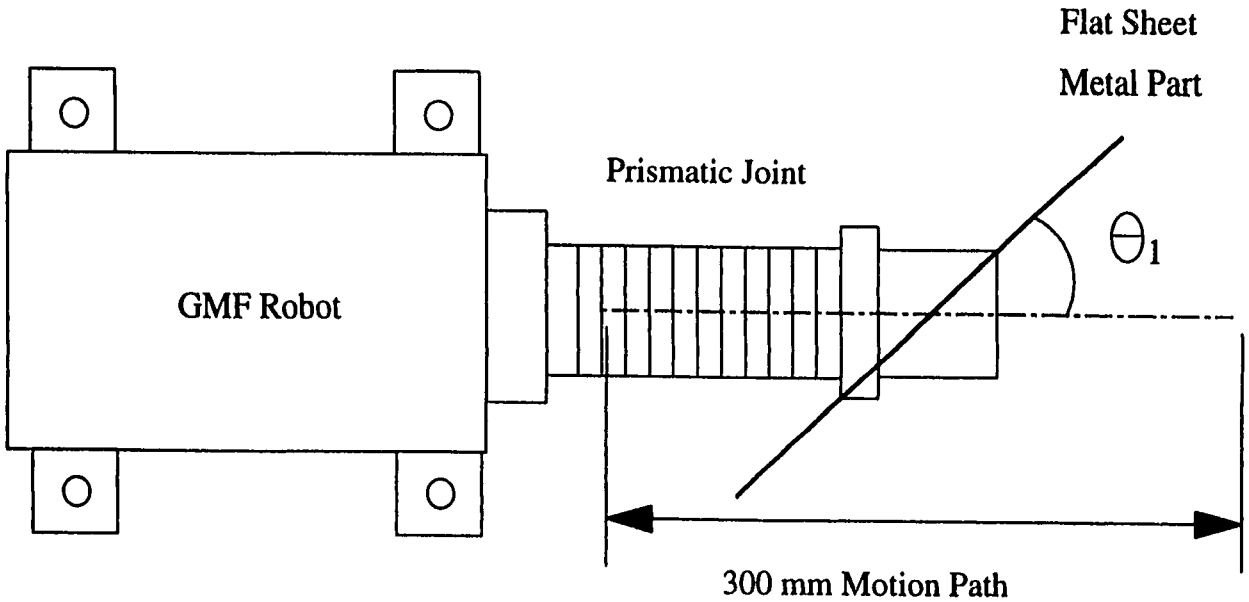


Figure 4.4 Setup for the Vibration Control Experiment (Top View)

motion and vibration measurement were repeated ten times and the amplitude averaged to calculate V. The signals from the SGFs were sampled at 200 Hz (over 20 times the 6.5 Hz natural frequency of the part). The robot was dwelled between motions until the vibration had completely damped out. Values of 8 ° and 4 were used for $w_t$ and n, respectively, which allowed the optimal part orientation to be determined to within 1° precision.

#### 4.3.2.2 Experimental Results for LEC of Vibration in 2-D Parts Handling

Figure 4.5a shows a graph of the part orientation angle versus the number of trials for a part with $\theta_1 = 5°$ initially. The corresponding vibration amplitude versus number of trials graph is shown in Figure 4.5b. In Figure 4.5a, the centre angle $c_i$ is connected by a line to highlight its change. As the iterative learning operated, the vibration amplitude decreased rapidly as the orientation angle of the part was optimized. Figure 4.6 shows a summary of results of vibration control experiments when LEC was applied for 8 different initial part orientation angles. In all cases, the estimated optimal orientation agreed with the expected value of zero degrees. With an initial orientation angle of 6.5°, the vibration amplitude without LEC was 2.34 mm. With LEC the vibration amplitude dropped down to 1.28 mm. There was a reduction in vibration amplitude of more than 45%. Smaller reductions were obtained with smaller initial angles.

### 4.3.3 Experimental Verification of LEC of Vibration in 3-D Parts Handling

The LEC algorithm was also tested experimentally for vibration control in 3-D parts

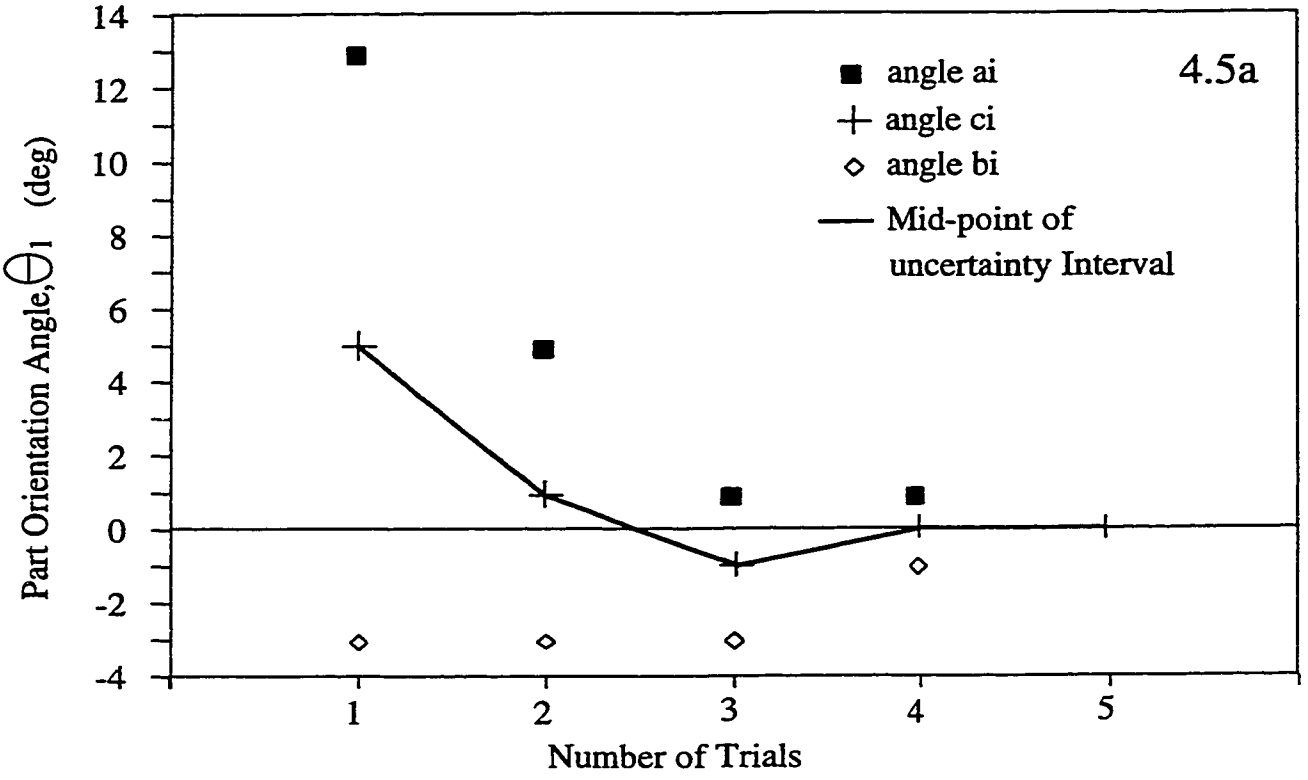


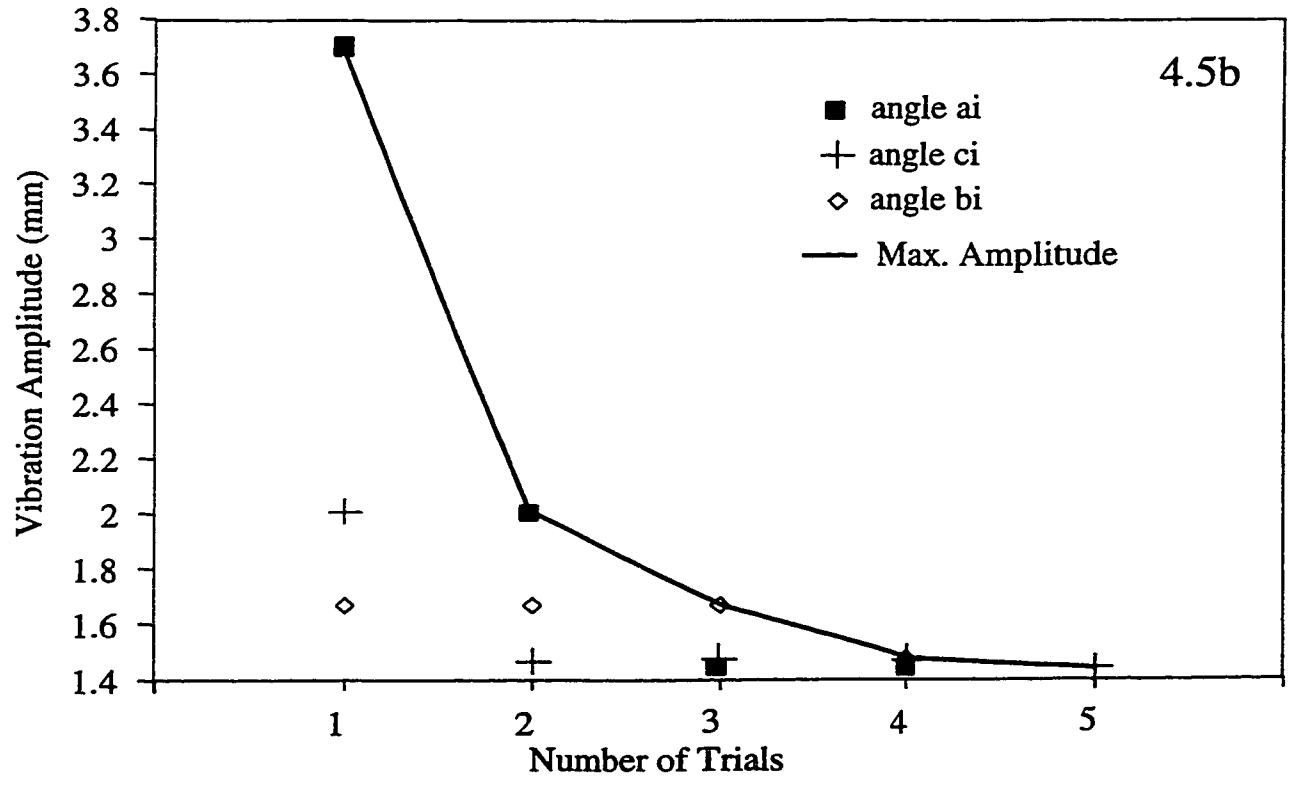


Figure 4.5 Part Orientation Angle and Vibration Amplitude Versus Number of Trials ( 2-D Parts Experiment )

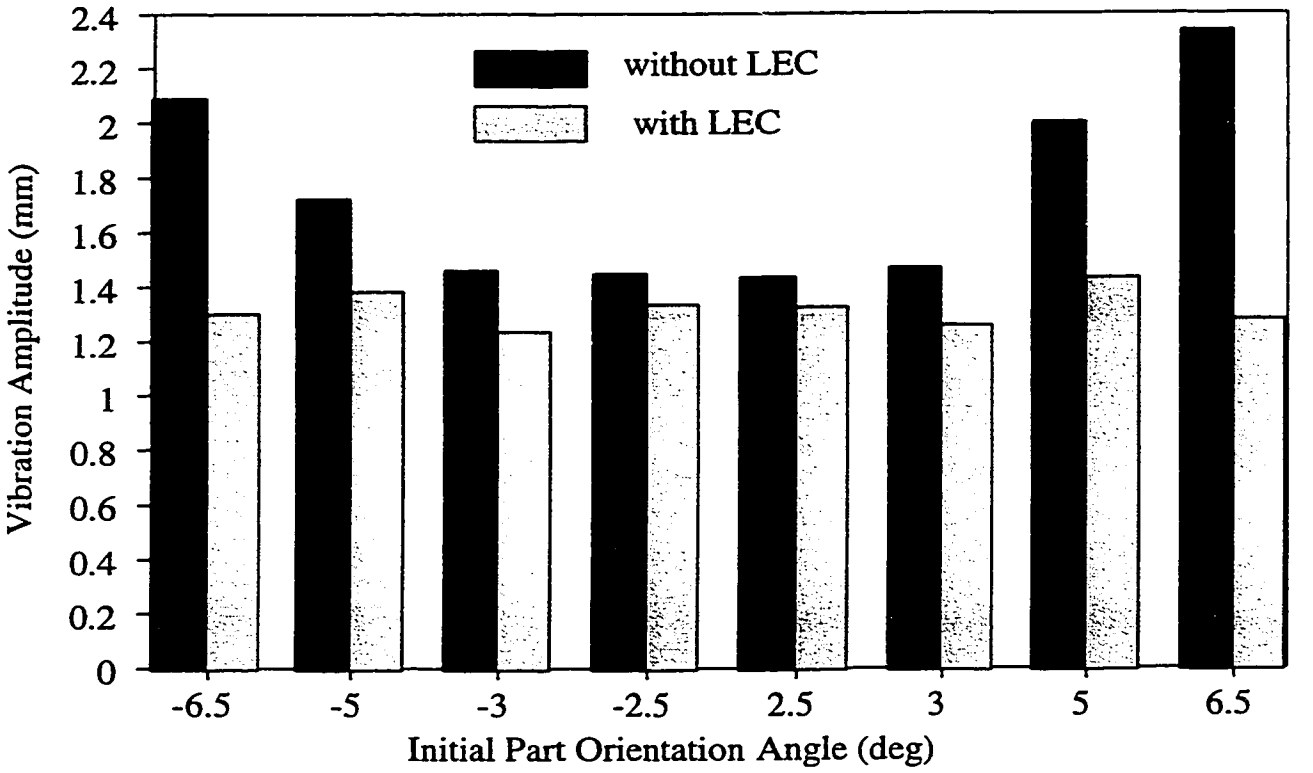


Figure 4.6 Comparison of Vibration Amplitude with and without LEC at Various Initial Orientation Angles ( 2-D Parts Experiment )

handling. In order to measure the vibration of the sheet metal part, four Strain Gauge equipped Fingers (SGFs) were installed onto the robot gripper, as shown in Figure 4.7. At the time that the experiments were performed, the robot employed had only 5 DOF. Therefore, the tests were limited to changing of either of the part's Pitch, Yaw or Roll angles individually. The definition of these angles is shown in Figure 4.8. The effect of the change of these angles in combination was not tested.

Figure 4.9 shows the experimental set up for the vibration control tests. The 3-D sheet metal part selected was made of a gauge 20 galvanized steel sheet. The steel sheet was folded into a 508 x 406.4 x 76.2 mm rectangular box with one end open. There is a 12.7 mm wide flange folded over around its opening for joining with other parts by spot welding. A gauge 20 sheet was chosen since it is the one of typical thicknesses used for car body panels.

#### 4.3.3.1 Experimental Procedure for LEC of Vibration in 3-D Parts Handling

As shown in Figure 4.9, during the experiments, the 3-D sheet metal part was clamped by the robot gripper at the centre. Similar to the tests performed with the 2-D parts, the procedure described in section 4.3.2.1 was followed. A 300 mm straight horizontal path, and an average speed of 1 m/s were used. At each orientation angle the motion and vibration measurement were repeated ten times. During each time, the maximum of the four SGFs readings obtained was recorded and later averaged to calculate V. The signals from the SGFs were sampled at 200 Hz. The robot was dwelled between motions until the vibration had completely damped out.

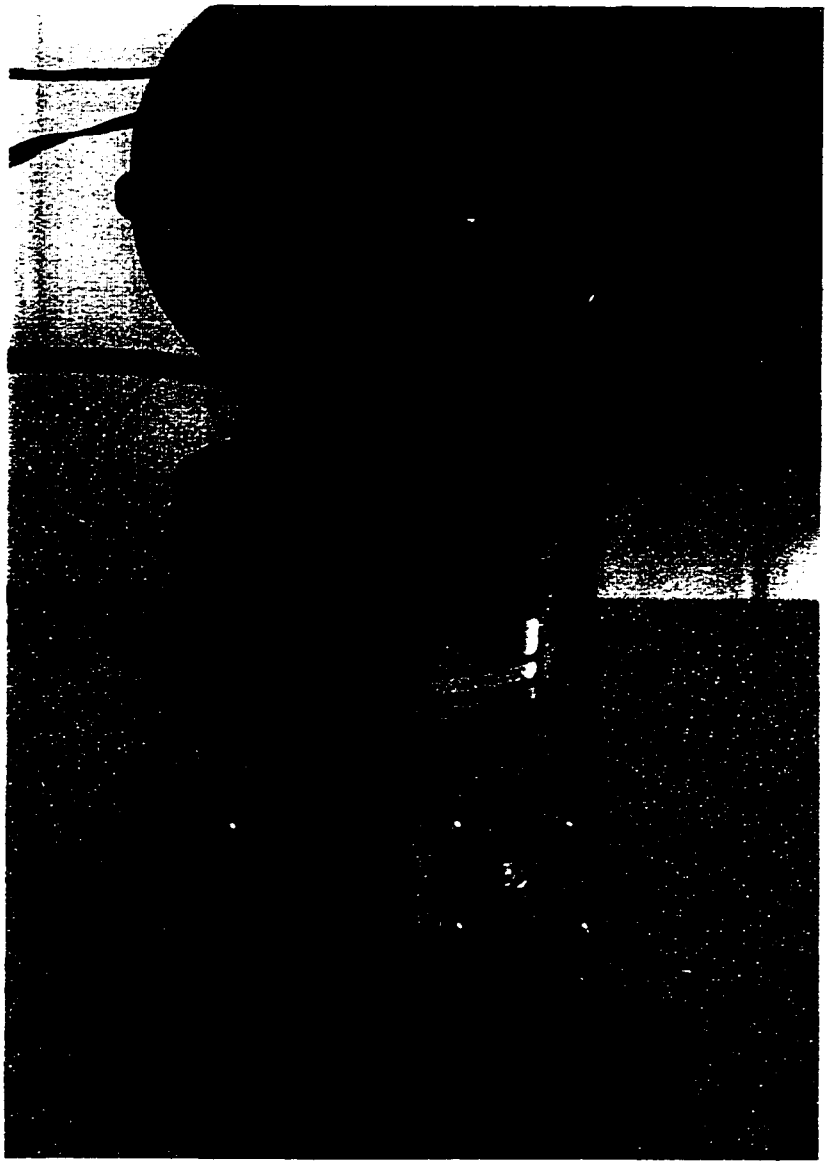

Figure 4.7 Strain Gauge-equipped Fingers (SGFs) Mounted on a Gripper
To Measure Vibration of a 3-D Part

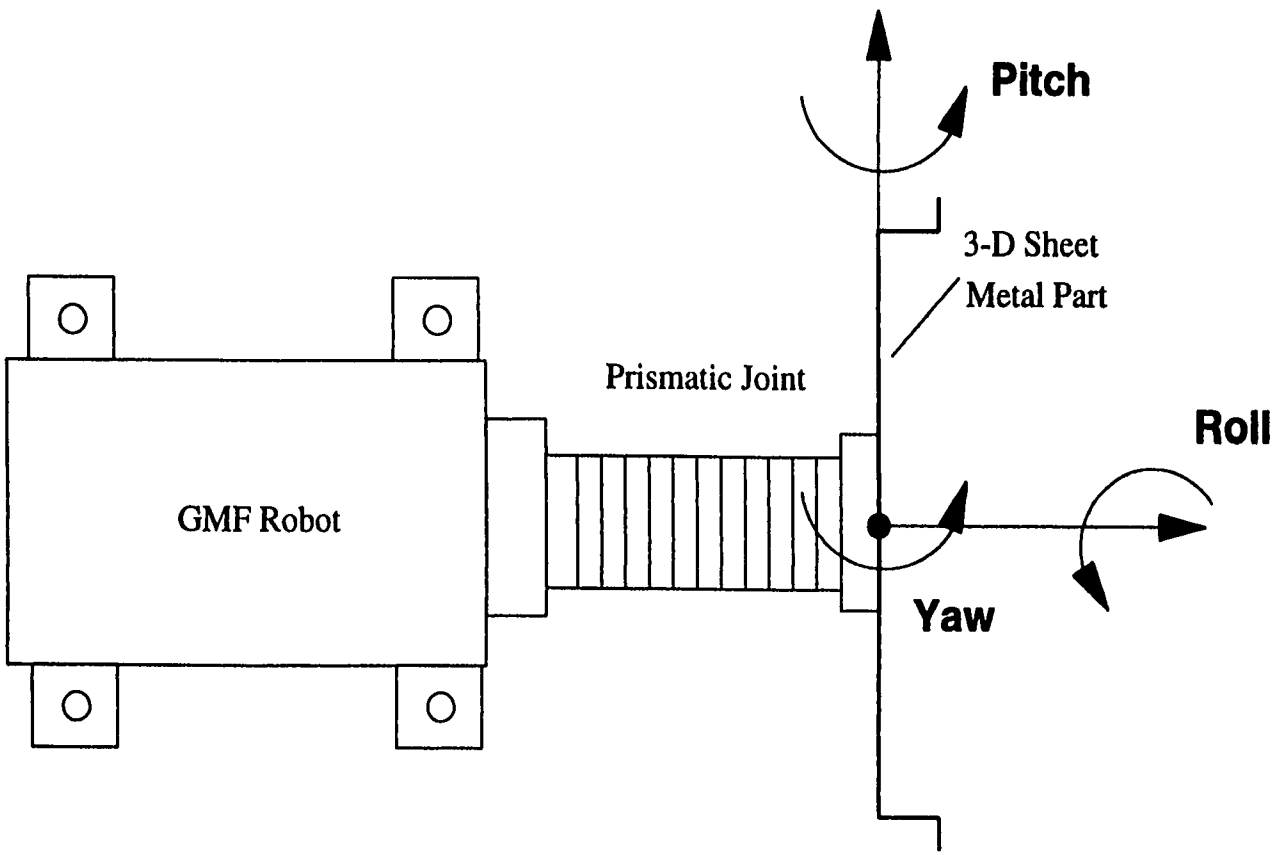


Figure 4.8 Definition of the Pitch, Yaw and Roll Angles

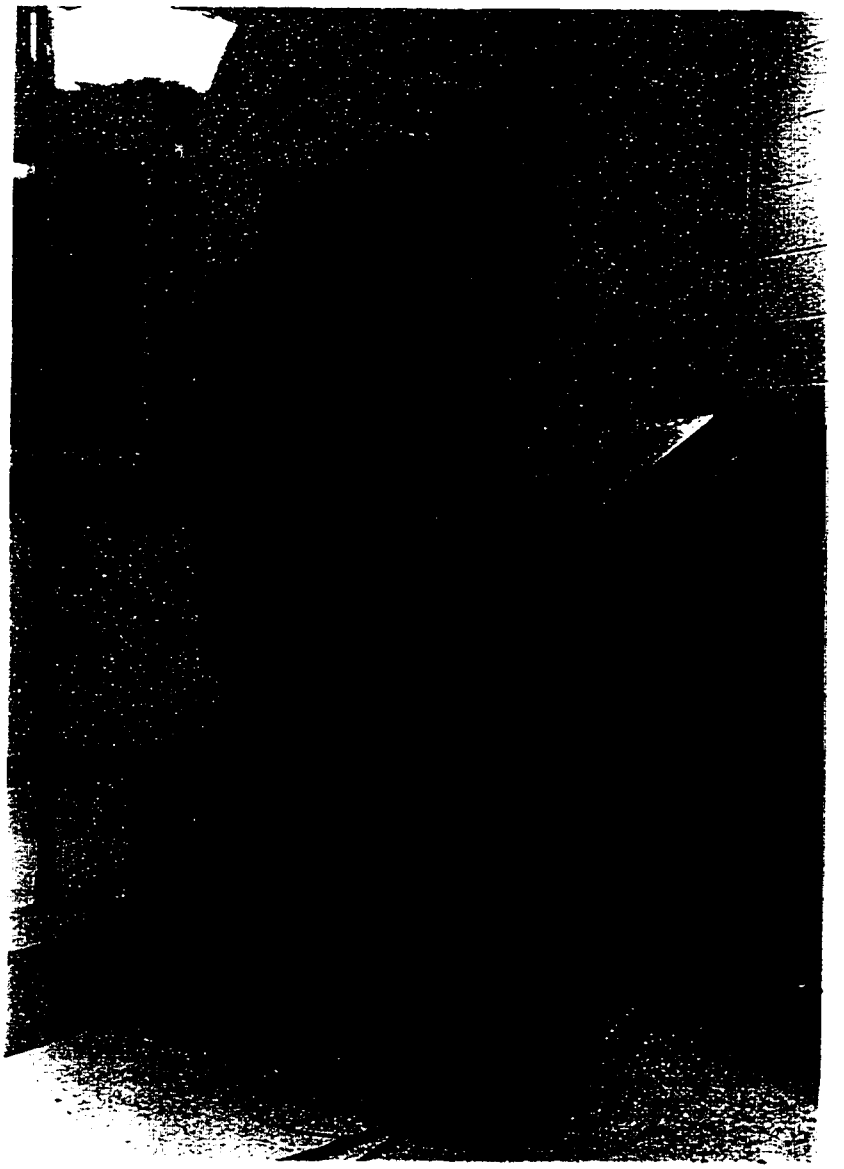

Figure 4.9 Experimental Setup for Learning Extermum Control for Vibration

### 4.3.3.2 Experimental Results for LEC of Vibration in 3-D Parts Handling

Figure 4.10 shows the vibration amplitude versus the part Pitch angle graph. The robot's Pitch angle was changed from -50° to +50°. Two graphs are shown respectively for the part Yaw angle = 0° and 90°. Over the range tested, there is one global minimum point for Yaw angle = 0° and two local minimum points for Yaw angle = 90°. If the optimization algorithm is applied over the entire range tested with Yaw angle = 90° (for example with $\theta_1 = 0°$ and $w_1 = 50°$) it is possible that the final answer could fall into a local minimum point. In order to reduce the chance of occurrence of this problem, the algorithm can be applied with a smaller value for $w_1$ and repeated several times to cover the whole range of interest. Then the local optimal points can be compared to determine the global optimal point for minimum vibration.

Figures 4.11 and 4.12 depict the vibration amplitudes versus the part's Yaw and Roll angles, respectively. In Figure 4.12, the robot Pitch joint was set = 90° to allow the part's Roll angle to be changed. Again, more than one minimum point appeared on the graph for Yaw angle = 0° and 90°. The LEC algorithm should be applied several times over the whole 90° range to avoid falling into a local minimum point.

From these figures it is clear that the factors affecting the vibration amplitude of a part being transported by a robot include the orientation of the robot, and the orientation of the part relative to the robot. Other factors could include the effect of gravity, air resistance (damping from air) and the part's inertial force. Without the help of the Learning Extremum Controller, it is very difficult to predict ahead of time what is the best orientation to transport

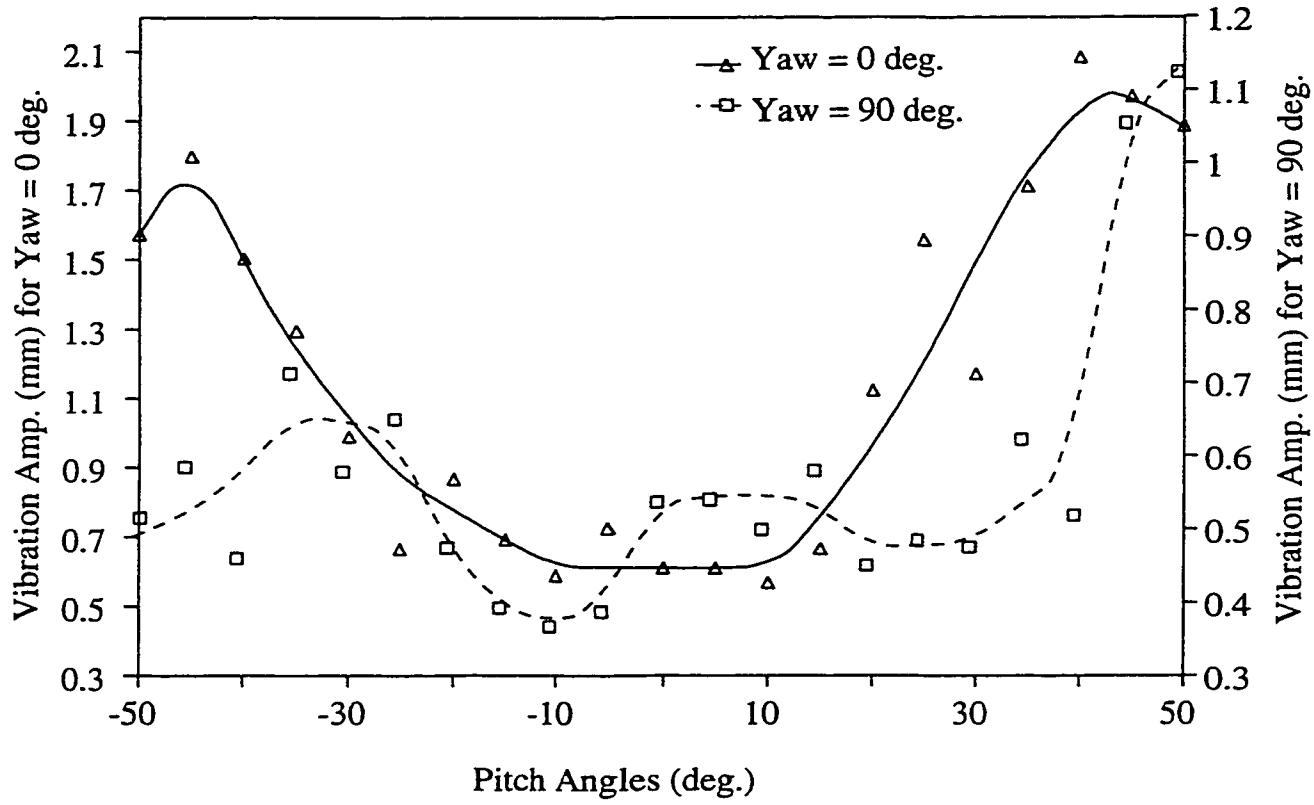


Figure 4.10 Vibration Amplitude Vs. Part Pitch Angles

( 3-D Parts Experiment )

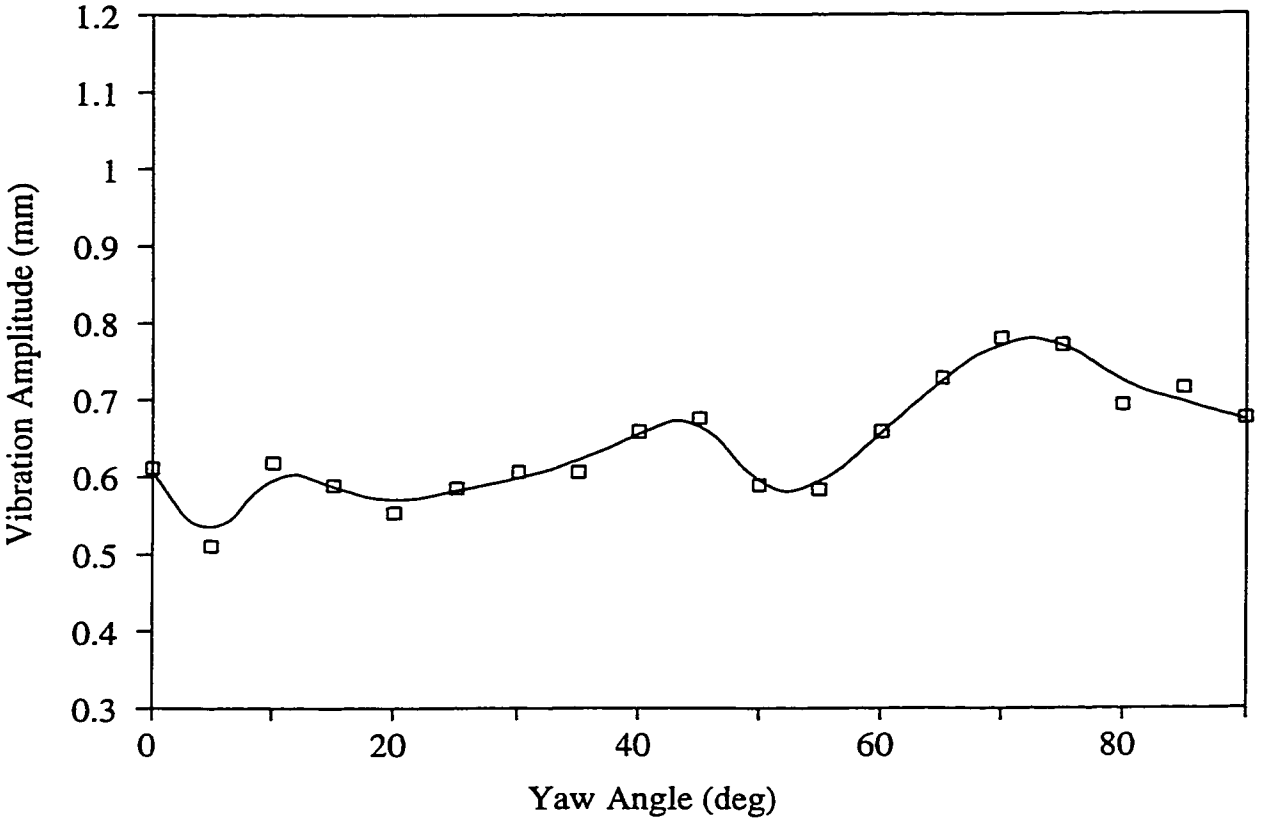


Figure 4.11 Vibration Amplitude Vs. Part Yaw Angles

( 3-D Parts Experiment )

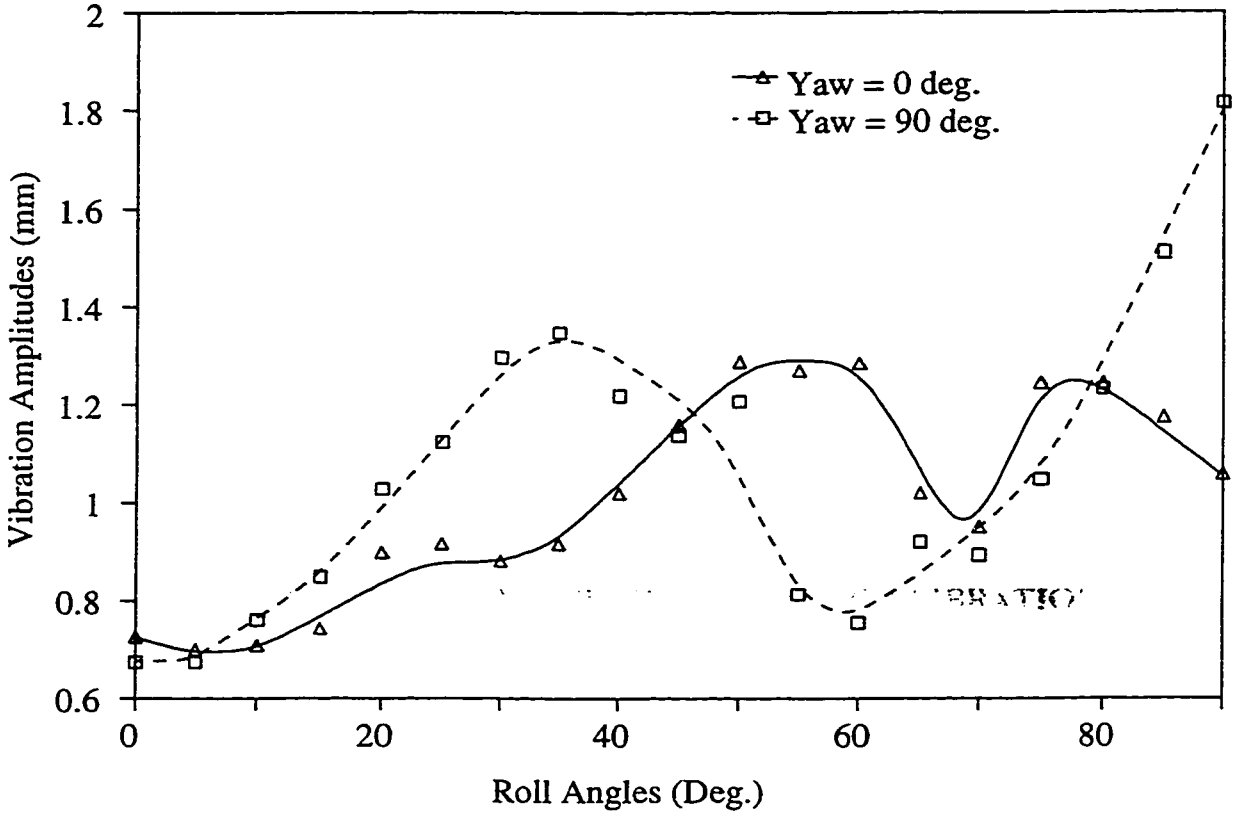


Figure 4.12 Vibration Amplitude Vs. Part Roll Angles

( 3-D Parts Experiment )

the part for minimum vibration.

Figure 4.13a shows a graph of the part pitch angle versus the number of trials for a part with $\theta_1 = 0°$ initially and Yaw angle = 0°. Values of 45° and 4 where used for $w_1$ and n, respectively, which allowed the optimal part orientation to be determined within 5.625°. The corresponding vibration amplitude versus number of trials graph is shown in Figure 4.13b. In Figure 4.13a, the centre angle $c_i$ is connected by a line to highlight its change. The vibration amplitude decreased rapidly as the pitch angle of the part was optimized by the LEC. From a pitch angle of 45° changed to the optimized angle of -5.625 , the vibration amplitude was reduced from 1.97 mm to 0.57 mm. This indicates a reduction in vibration amplitude of 71%.

## 4.4 INPUT COMMAND SHAPING METHOD (ICSM) FOR VIBRATION CONTROL

Command Shaping involves altering the shape of either actuator commands or setpoints so that system oscillations are reduced. The Input Command Shaping Method (ICSM) developed by Singer and Seering [ 28 ] is considered here to control the vibration of the sheet metal workpiece when it is handled by a robot. To the author's knowledge, this is the first time ICSM has been applied to this problem.

### 4.4.1 The ICSM Algorithm

Singer and Seering [ 28 ] demonstrated that two or more impulse responses can be superimposed so that the system can proceed without vibration after the input has ended.

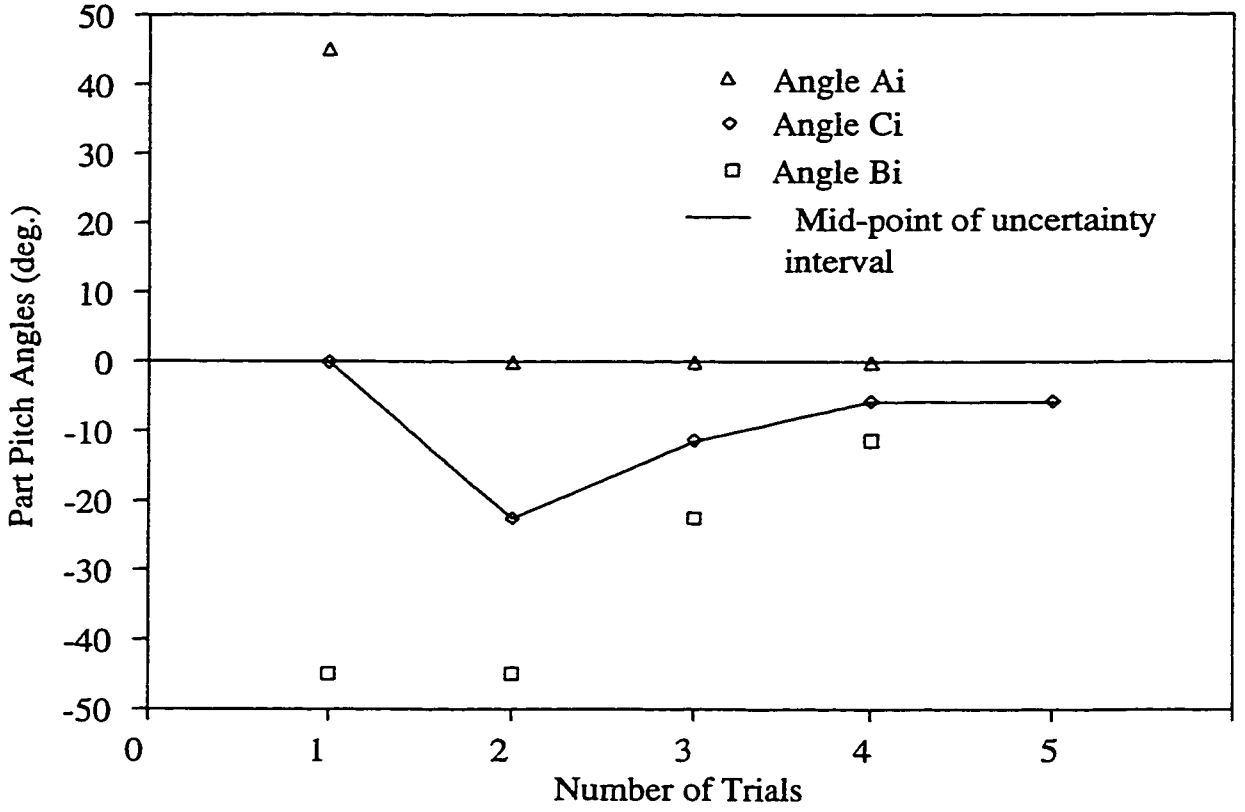


Figure 4.13a Part Pitch Angle Vs. Number of Trials (3-D Part)

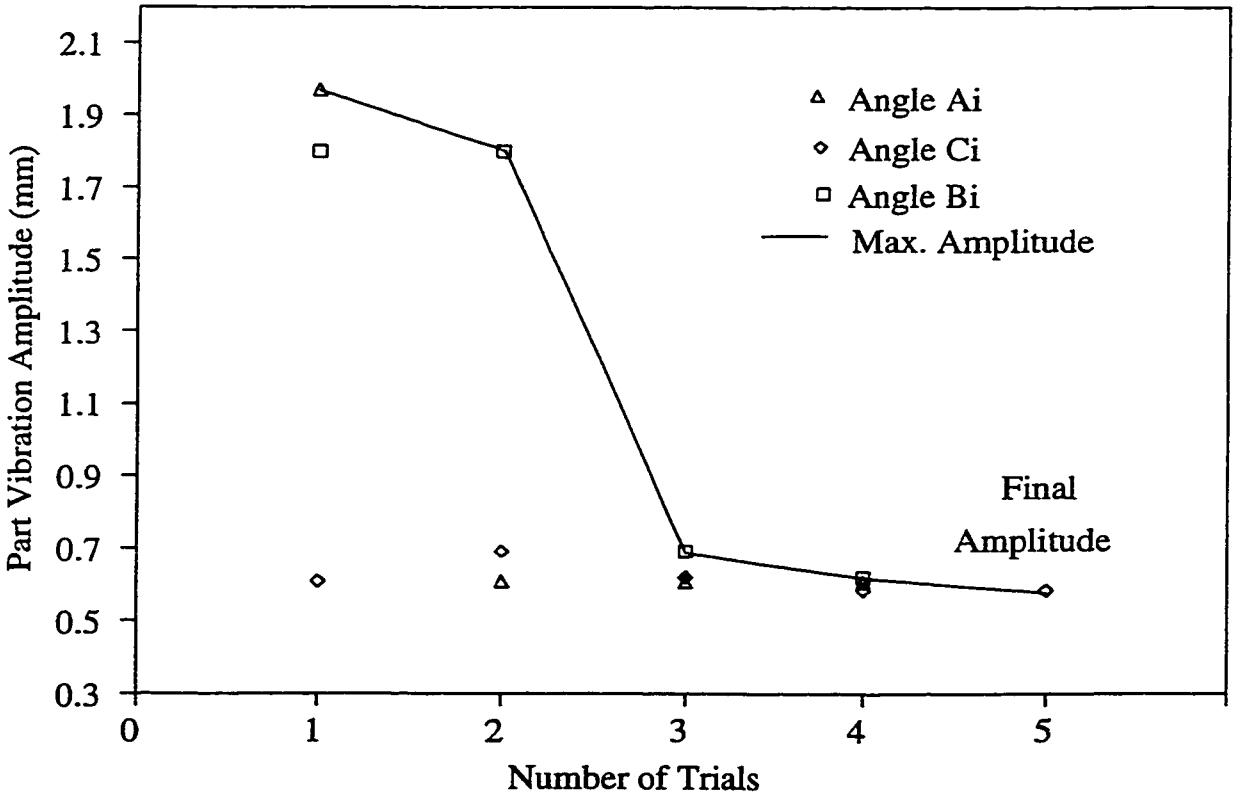


Figure 4.13b Part Vibration Amplitude Vs. Number of Trials (3-D Part)

Figure 4.14 was used as an example. In this case, the input consists of two impulses; the duration of the input is the time of the second impulse. If the magnitude and time of application of these two impulses are calculated carefully, it is possible to make the vibrations generated by the two impulses cancel each other. The calculation is based on the system natural frequencies and damping ratios. The formulas for the calculation of the input magnitude and time of application for the two-impulse case are shown in Figure 4.15. However, it was shown that the system response of the two- impulse input technique is extremely sensitive to variation in the natural frequency and damping ratio of the system. The three-impulse input design is less sensitive to system parameter variation and more robust than the two-impulse input design. The formulas for the calculation of the input magnitude and time of application for the three-impulse design are shown in Figure 4.16. The magnitudes of the three impulses are :

$$A1 = \frac{1}{1+2K+K^2} \qquad (4.2)$$

$$A2 = \frac{2K}{1+2K+K^2} \qquad (4.3)$$

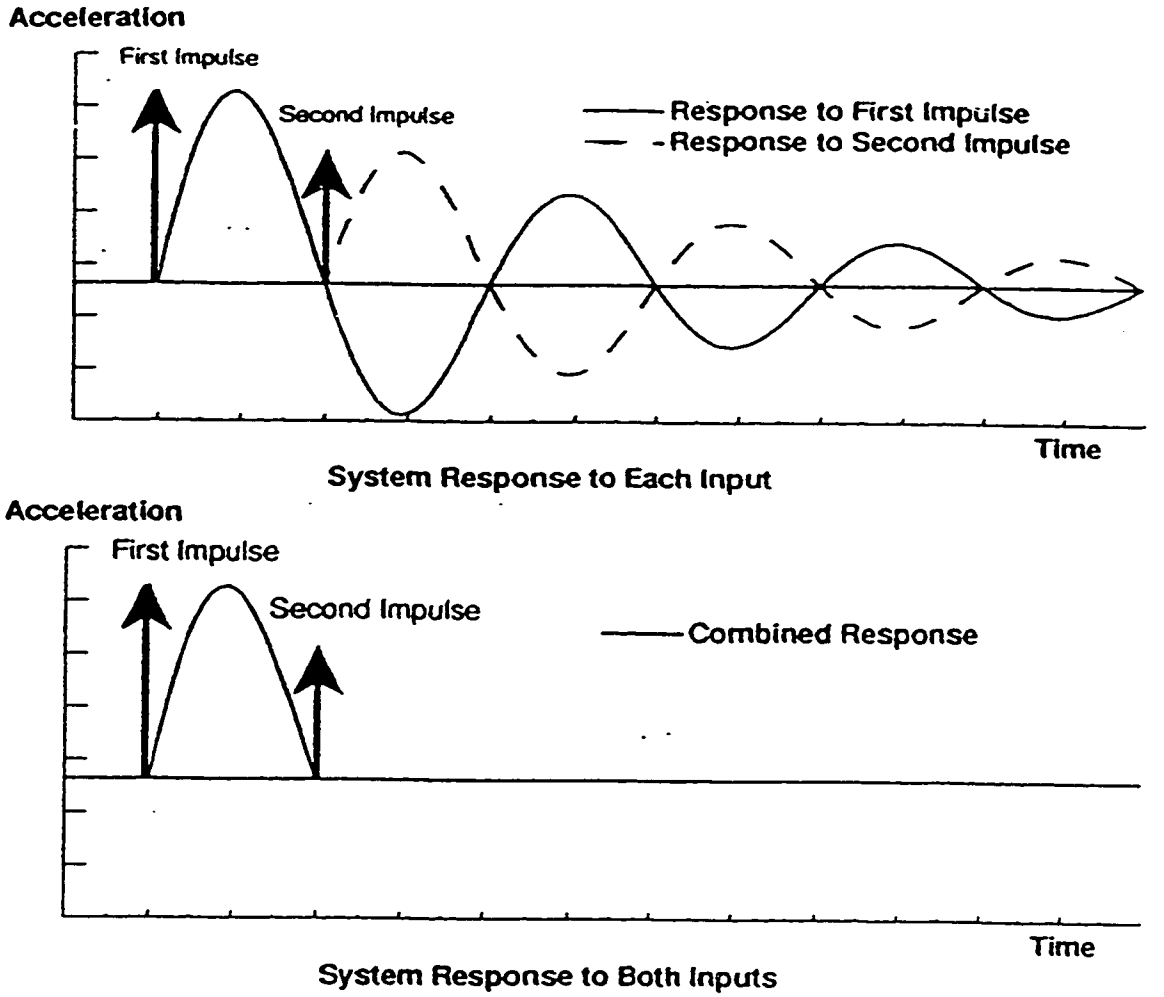


Figure 4.14 The Two Input Responses Shown in [ 28 ] to Demonstrate the ICSM Algorithm

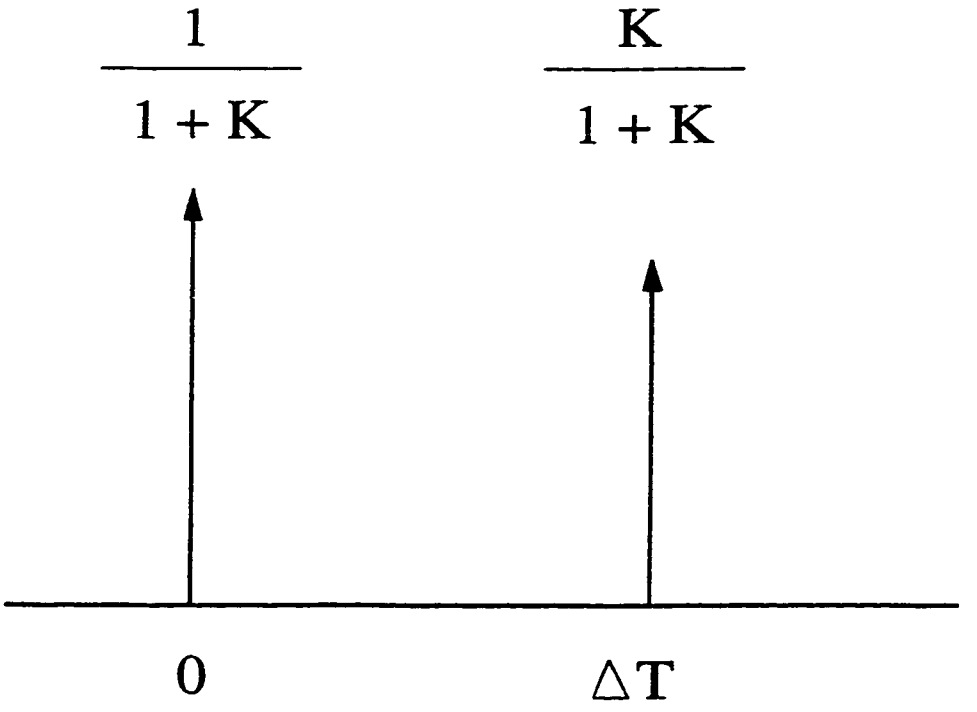


$$K = e^{-\frac{\xi\pi}{\sqrt{1-\xi^2}}} \qquad \Delta T = \frac{\pi}{\omega_o \sqrt{1-\xi^2}}$$

Figure 4.15 The Two-impulse Input for ICSM [28]

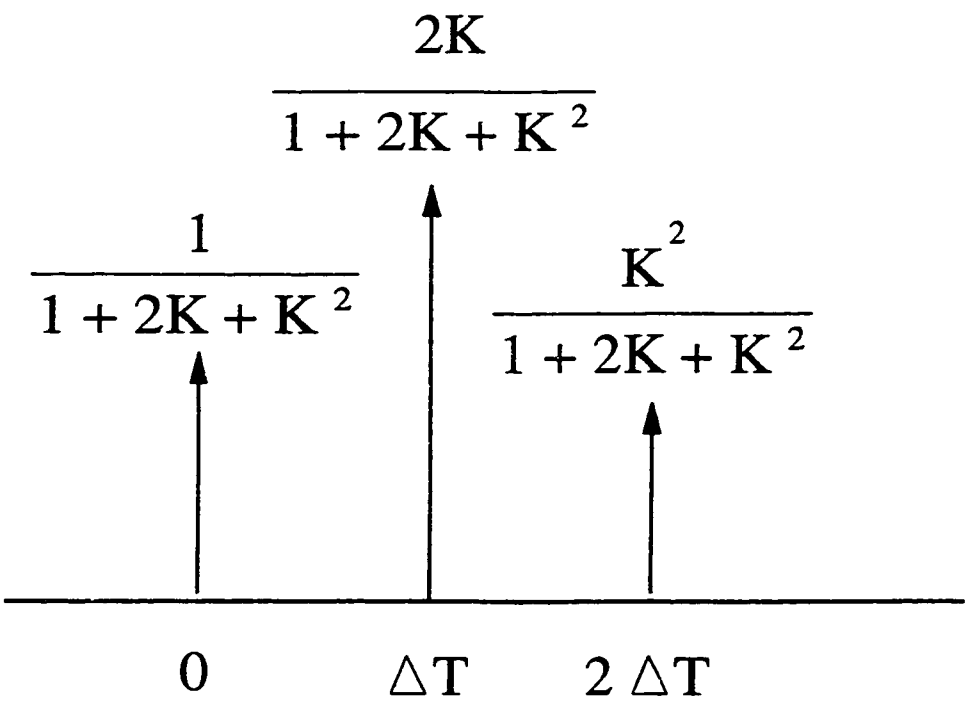


$$K = e^{-\frac{\xi\pi}{\sqrt{1-\xi^2}}} \qquad \Delta T = \frac{\pi}{\omega_o \sqrt{1-\xi^2}}$$

Figure 4.16 The Three-impulse Input for ICSM [28]

$$A3 = \frac{K^2}{1+2K+K^2} \qquad (4.4)$$

and A1, A2 and A3 are applied respectively at time 0, $\Delta T$ and $2\Delta T$, where

$$K = e^{\frac{\xi\pi}{\sqrt{1-\xi^2}}} \qquad (4.5)$$

and

$$\Delta T = \frac{\pi}{\omega_o \sqrt{1-\xi^2}} \qquad (4.6)$$

The symbols $\xi$ and $\omega_o$ are the damping ratio and the natural frequency of the system respectively.

To implement the ICSM for vibration reduction, the impulse sequences mentioned above are applied by convolving them with the desired input to the system. Since the impulse sequences from Figures 4.15 and 4.16 have been normalized to sum to one, the convolved system input will never exceed the maximum value of the original commanded input. The sequence becomes a prefilter for any input to the system [ 28 ]. Figure 4.17 shows a schematic diagram for implementation of the ICSM.

In the next section a model describing the vibration of the workpiece due to the

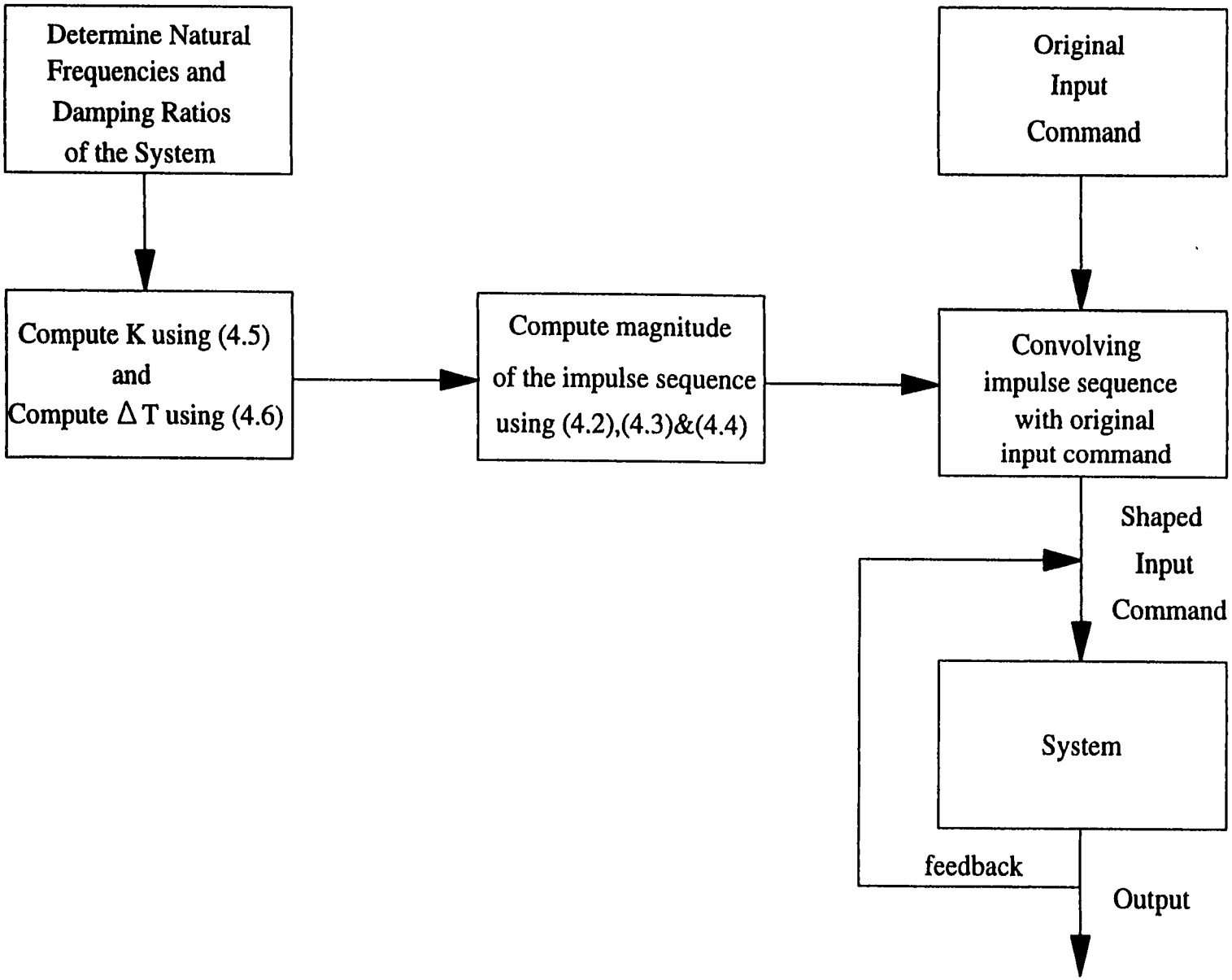


Figure 4.17 Schematic Diagram for the Implementation of ICSM

motion of the robot is identified for use in the computer simulation. The damping factors and natural frequency of the vibration modes are also determined.

### 4.4.2 System Model Identification

In order to perform the simulation studies, two models were developed to describe the vibration of the workpiece due to the robot's translational and rotational motion from joints 3 and 4, respectively (Joint 3 is a prismatic joint , and joint 4 is a revolute joint). Four SGFs were used to collect the vibration data at a rate of 225 Hz. A total of 744 data points were collected from each of the four SGFs. Since there is one input ( motion in joint 3 or joint 4 ) and 4 outputs ( vibration measured by the 4 SGFs ), a single-input-multi-output model was required. The system model identification was performed using MATLAB, and the function ARX. For the modelling of the vibration due to motion in joint 3, a forward translational motion of 10 mm was used as an input. The average velocity for the motion was 40 mm/s. Since the model was not intended for real time application, a relatively high model order could be used to give a more accurate representation of the true system. An ARX model structure with order 30 and dead time 2 was found to be adequate to describe the response due to the translational motion. Similarly, an ARX model with order 25 and dead time 2 was identified for the vibrations due to rotational motion in joint 4 using an 1° input. The average velocity for the motion was 6 degrees per second. Comparisons of the actual response measured by a SGF and the simulated response generated by the model for joint 3 and joint 4's motion are shown in Figures 4.18 and 4.19, respectively.

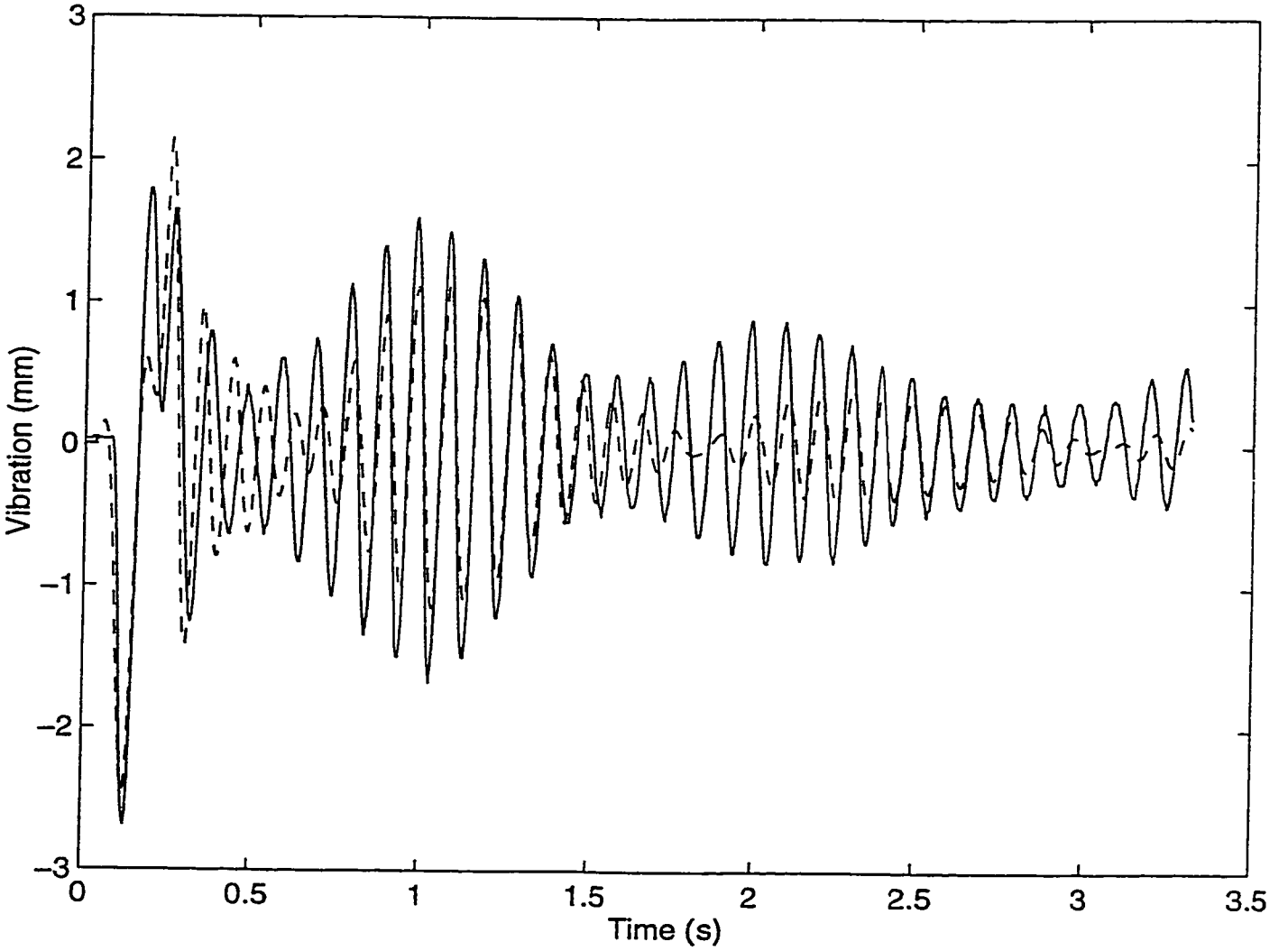


Figure 4.18 Comparison of the Actual Response and the Simulated Response Generated by the Model for Joint 3's Motion

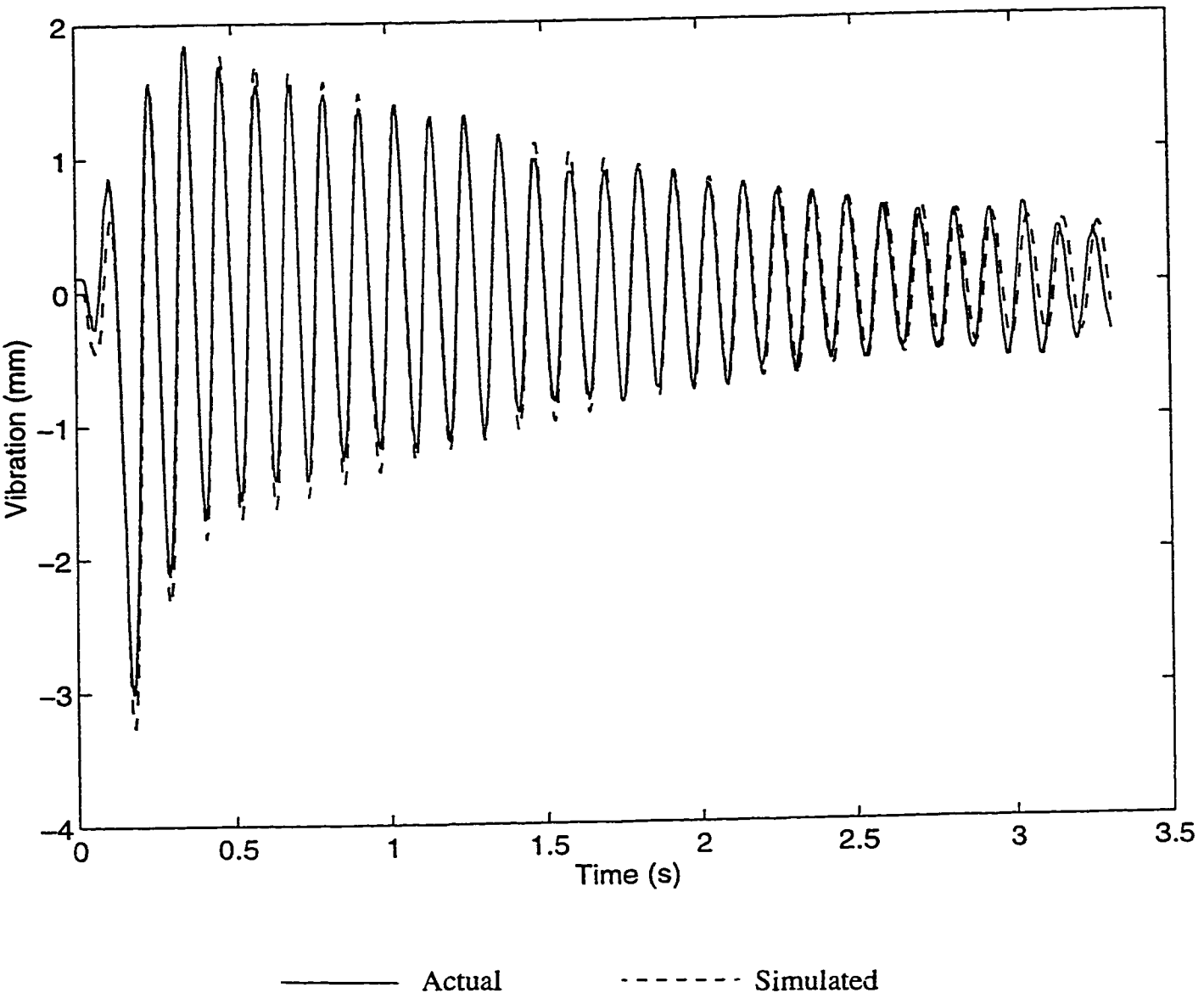


Figure 4.19 Comparison of the Actual Response and the Simulated Response Generated by the Model for Joint 4's Motion

### 4.4.3 Shaping of the Input Commands

All the computation required to implement the command shaping method was performed using MATLAB. In order to shape the input commands, the natural frequency and the damping factor of the first two vibration modes were extracted from the model parameters using the MATLAB DDAMP function. In order to use this function, it was necessary to convert the model parameters from the MATLAB theta format to the MATLAB state space format. Note that when the model is in the state space format, it is much easier to perform simulation using the DLSIM function as well. The model format conversion was achieved using the TH2SS function. A listing of the MATLAB programs for the ICSM simulation is given in Appendix A.

### 4.4.4 Simulation Studies for ICSM

#### 4.4.4.1 Simulation Studies with Single Vibration Mode Suppressed

To test the effectiveness of the ICSM in handling small input motions, the inputs used to generate the data for modelling in the last section were shaped to suppress the first and second mode of vibration, respectively. The original input for a 10 mm motion in joint 3 and the shaped input for controlling the first mode of vibration are shown in Figure 4.20 as an example. When only the first mode is suppressed, the delay between the shaped input and the original input is $2\Delta T$ seconds, where $\Delta T$ is calculated as shown in equation (4.6). The damping ratio, the natural frequency and the time delay between the original and the shaped input for joint 3 are shown in Table 4.1 for the first and second modes of vibration. The time

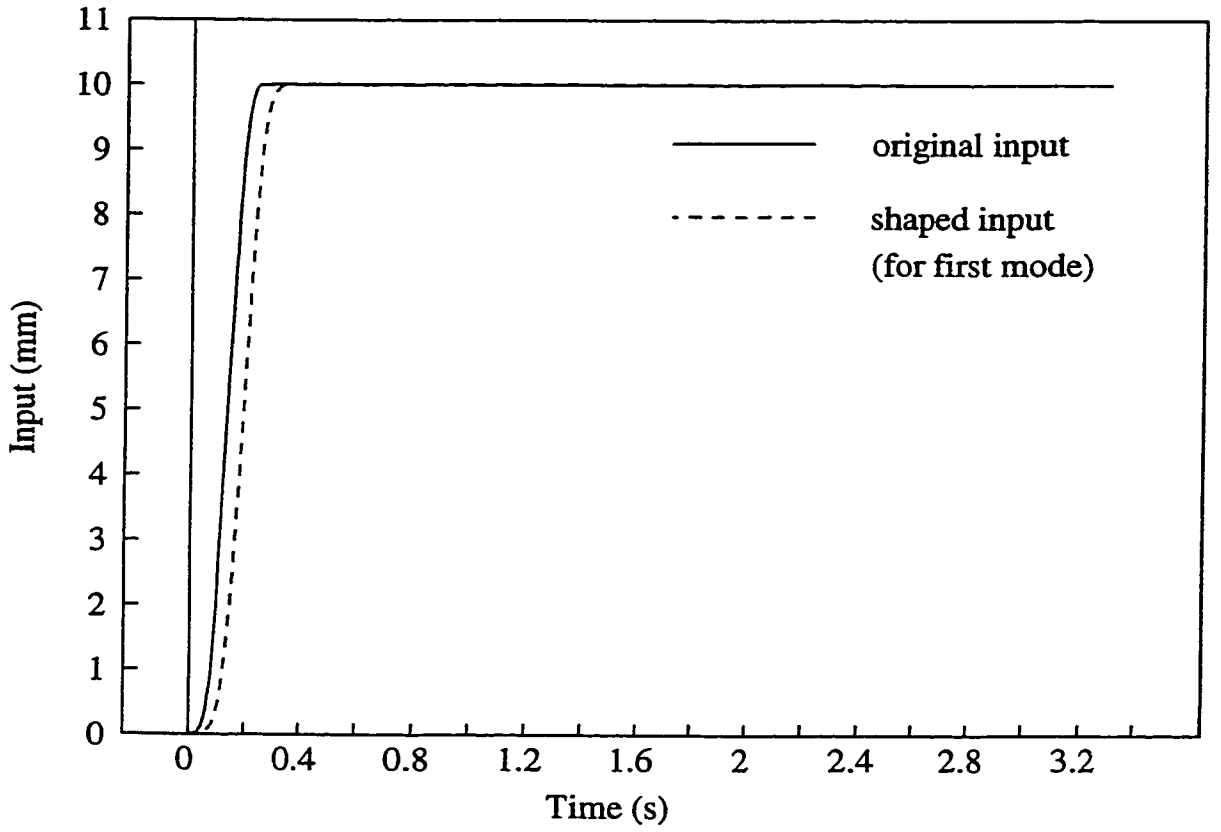


FIgure 4.20 Comparison of Original Input and Shaped Input for Joint 3

for the application of the impulses are shown in column 4 of Table 4.1 in controller periods. Since the Delta Tau motion controller was updated every 4.4 ms, the impulses should be applied at the first, the tenth and the nineteenth controller periods for suppressing the first mode of vibration. Similarly, for suppressing the second mode of vibration, the impulses should be applied at the first, the eleventh and the twenty first periods. Table 4.2 shows the same information for joint 4.

| Joint 3 modes | Damping Ratio | Natural Frequency (rad/s) | Time for the Application of Impulses (controller periods) | Input Time Delay Due to Shaping (i.e.2ΔT) (ms) |
|---|---|---|---|---|
| 1 | 0.0068 | 70.023 | 1, 10, 19 | 80.17 |
| 2 | 0.0111 | 62.43 | 1, 11, 21 | 89.08 |

Table 4.1. Information Required for the Application of ICSM in Joint 3

| Joint 4 modes | Damping Ratio | Natural Frequency (rad/s) | Time for the Application of Impulses (controller periods) | Input Time Delay Due to Shaping (i.e.2ΔT) (ms) |
|---|---|---|---|---|
| 1 | 0.0097 | 55.861 | 1, 13, 25 | 106.90 |
| 2 | 0.0483 | 68.927 | 1, 10, 19 | 80.17 |

Table 4.2. Information Required for the Application of ICSM in Joint 4

Figures 4.21 and 4.22 show the simulation results when the first and second most significant modes were suppressed respectively for 10 mm input in joint 3. The resulting vibration from the shaped input is plotted as a dotted line. The original vibration when no shaping control is applied is plotted in the same figure as a solid line for comparison. Similarly, the plots for 1° input in joint 4 with first and second modes suppressed are shown in Figures 4.23 and 4.24, respectively. From these results, it is clear that even when only one mode of vibration is suppressed, the ICSM is effective in controlling the system vibration. In the next section, simulations will be performed to test the effectiveness of suppressing two modes of vibration.

#### 4.4.4.2. Simulation Studies with the Two Most Significant Vibration Modes Suppressed

When the two most significant modes are suppressed, the impulses are to be applied

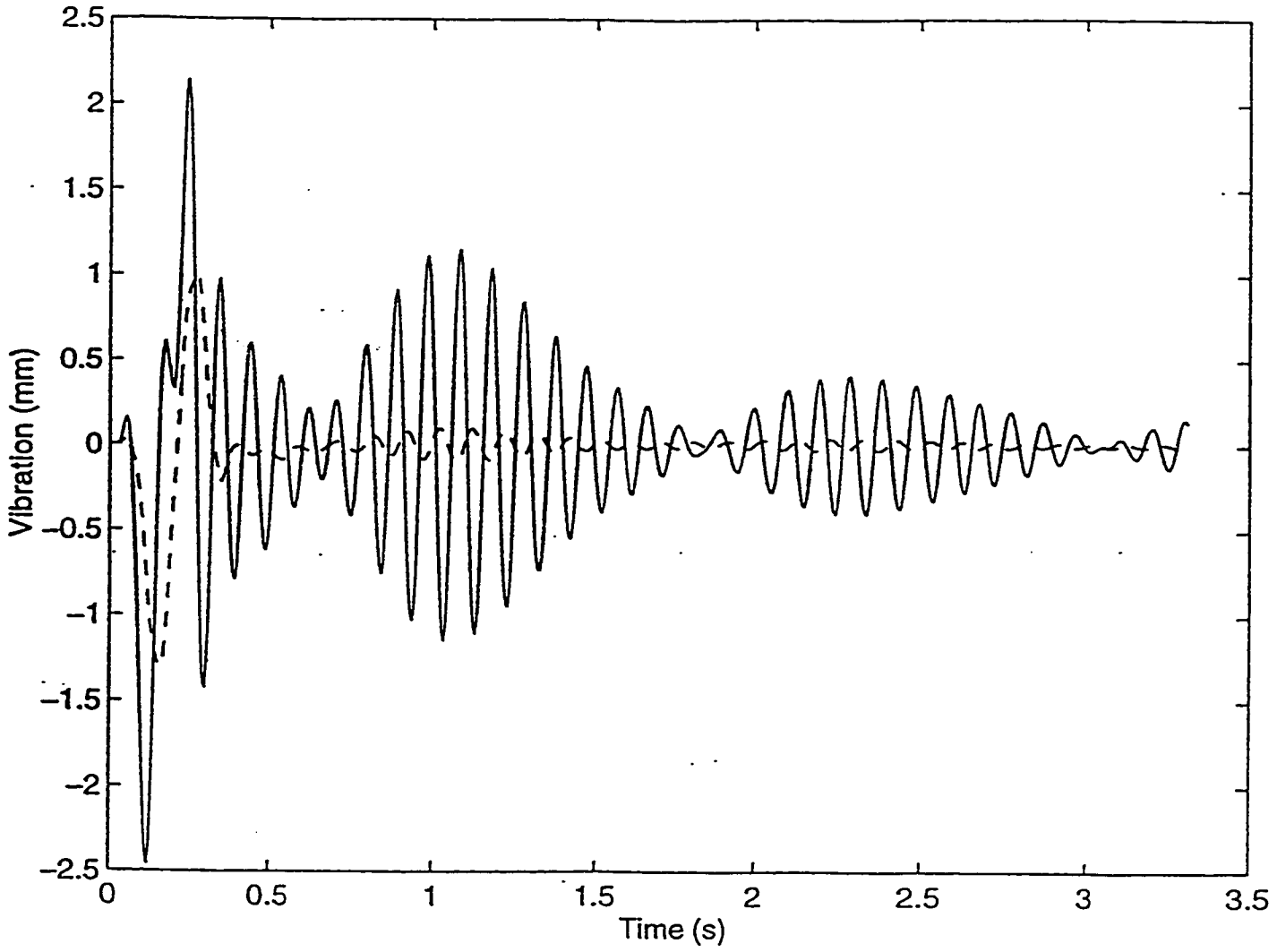


Figure 4.21 Simulated Response from Moving Joint 3 by 10 mm with ICSM Applied to suppress the First Mode of Vibration

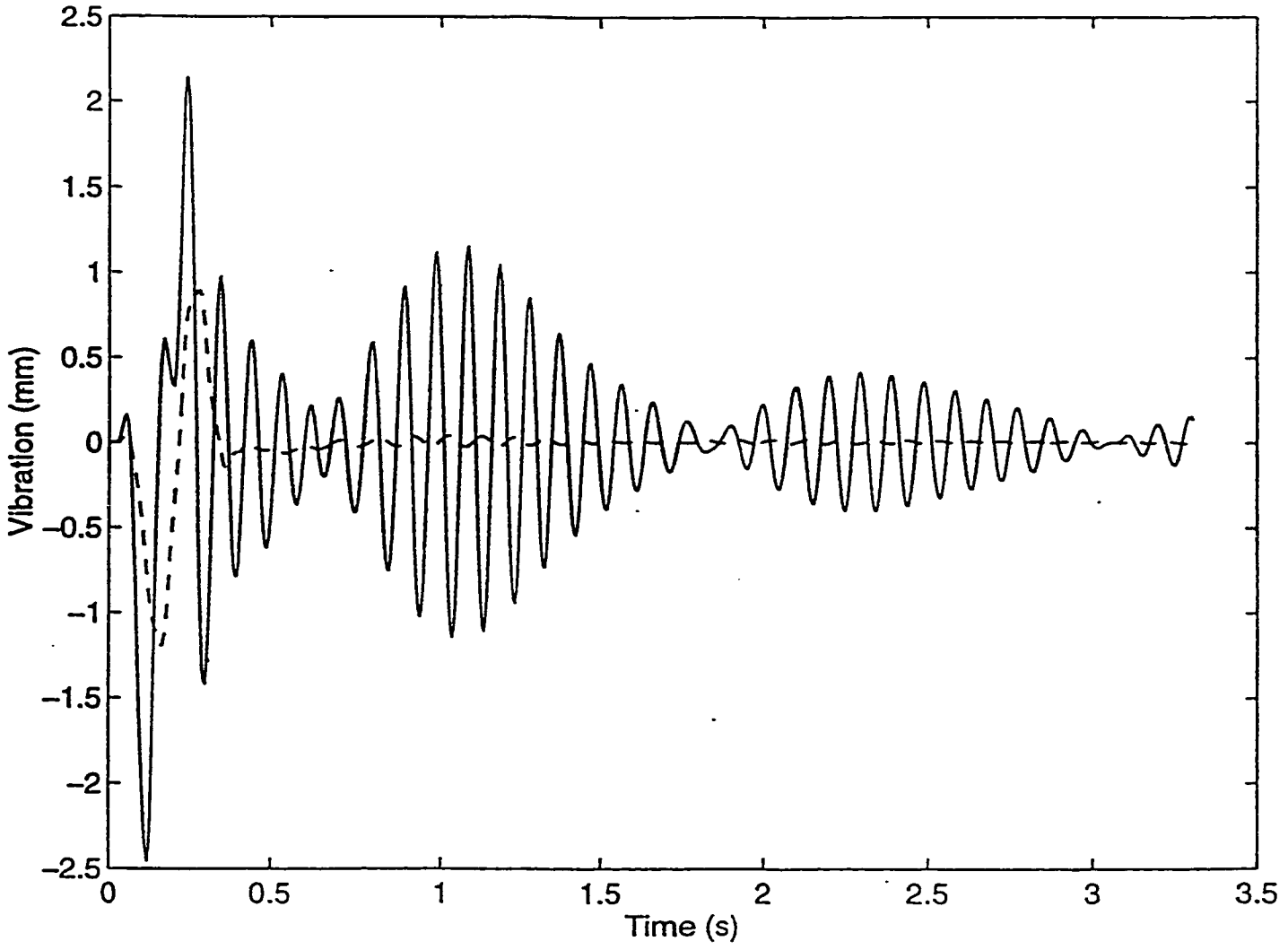


Figure 4.22 Simulated Response from Moving Joint 3 by 10 mm with ICSM Applied to Suppress the Second Mode of Vibration

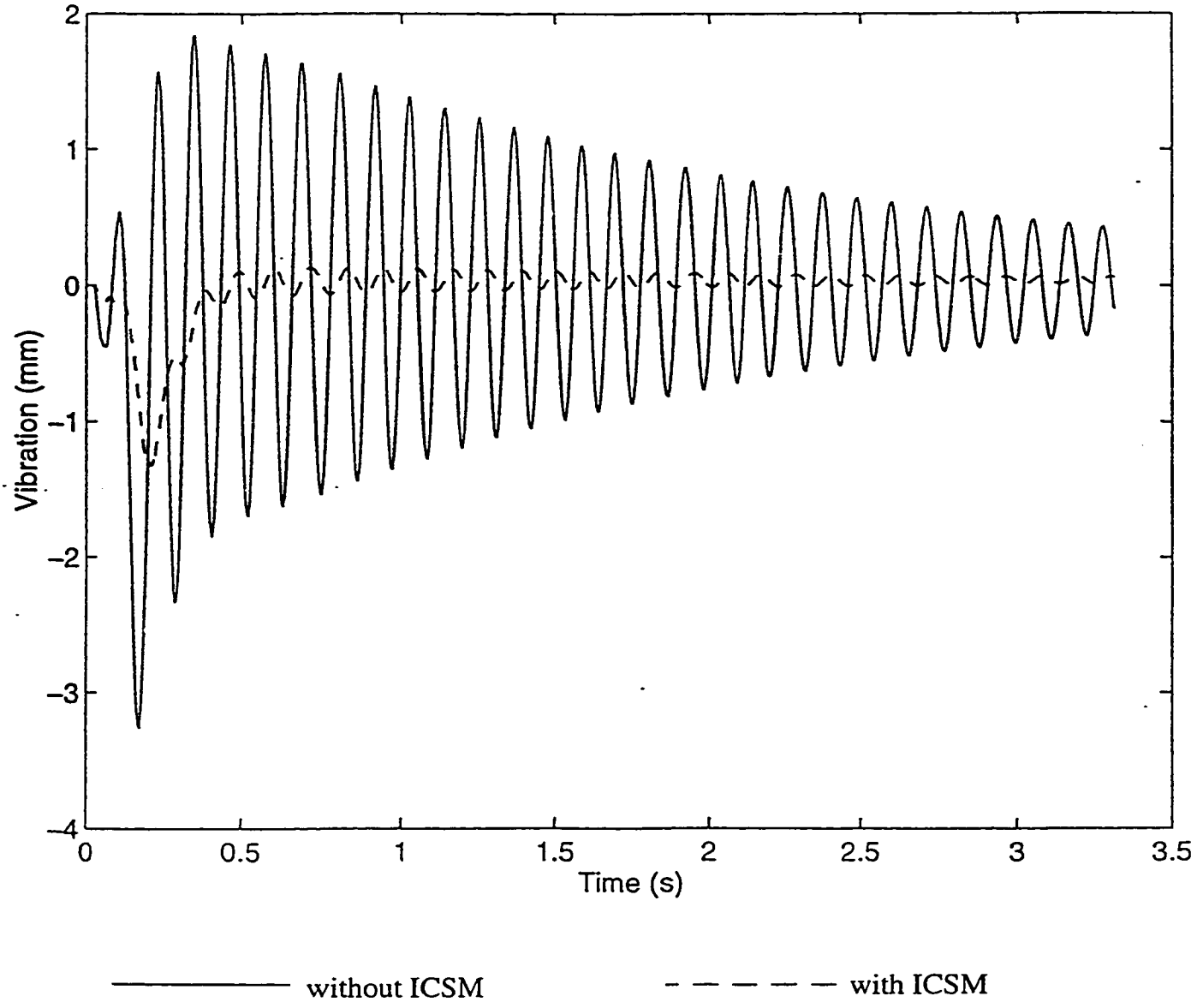


Figure 4.23 Simulated Response from Moving Joint 4 by 1 Degree with ICSM Applied to Suppress the First Mode of Vibration

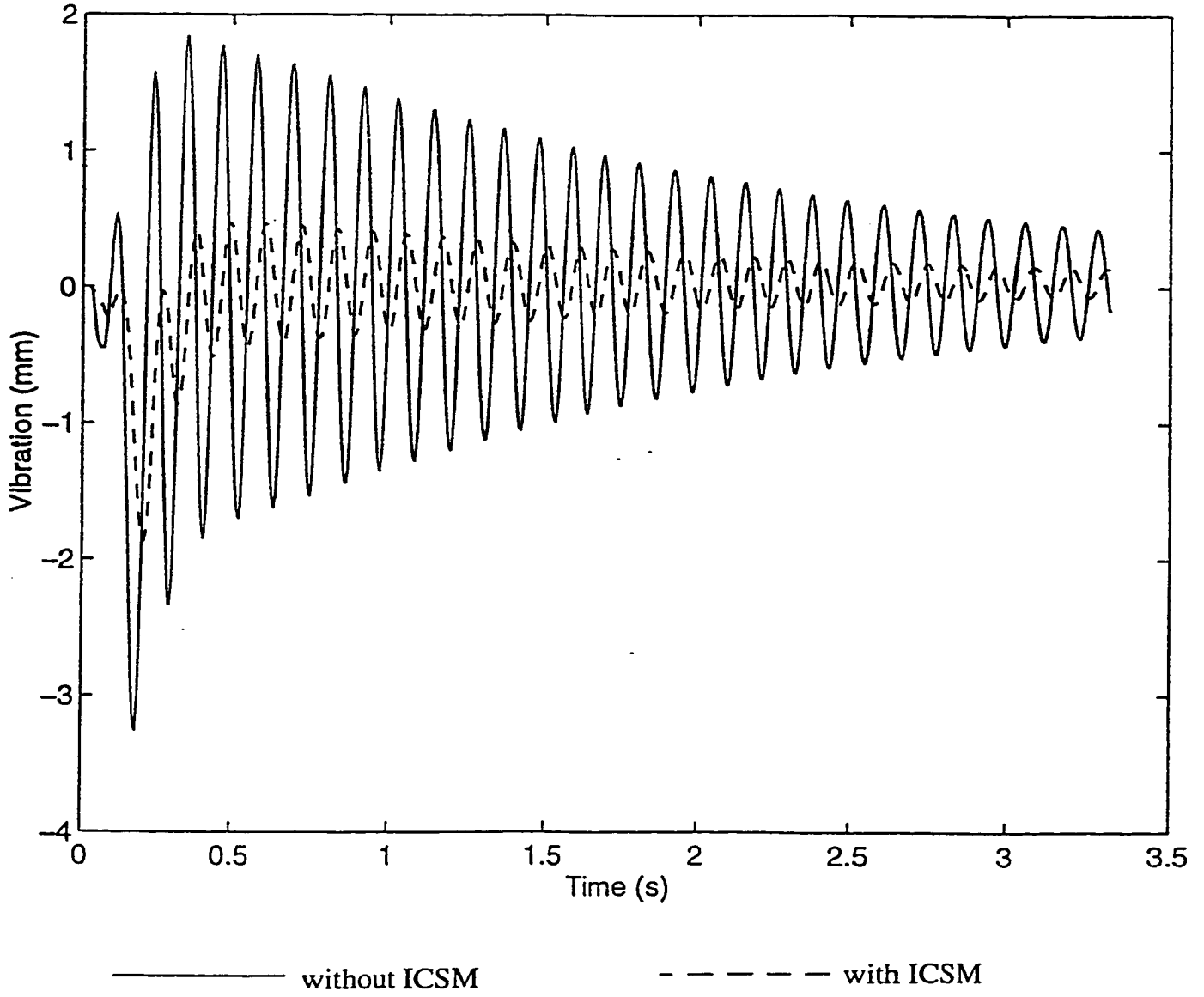


Figure 4.24 Simulated Response from Moving Joint 4 by 1 degree with ICSM Applied to Suppress the Second Mode of Vibration

at nine locations. The time for the application of these impulses are shown in Table 4.3 below in controller periods. Since there are nine impulses to be applied here instead of three as in the case of single mode vibration suppression, the time required to complete the input command is longer. The time delay between the original input and the shaped input is $2(\Delta T1+\Delta T2)$ seconds when two modes are suppressed, and $2\Delta Ti$ seconds when only the ith mode is suppressed. Figure 4.25 and Figure 4.26 depict the simulation results from applying the 10 mm and 1° input shaped for the two most significant modes in joints 3 and 4, respectively. The output from SGF 1 is plotted as a dotted line as an example. The original output with no control applied is plotted as a solid line in the same plot for easy comparison. As shown in these simulation results, when two vibration modes are suppressed, the vibrations are almost totally eliminated.

| Motion Joint | Damping Ratio for Modes 1 & 2 | Natural Frequency for Modes 1 & 2 (rad/s) | Time for the Application of Impulses (controller periods) | Input Time Delay Due to Shaping: $2(\Delta T1+\Delta T2)$ (ms) |
|---|---|---|---|---|
| 3 | 0.0068, 0.0111 | 70.023, 62.430 | 1, 10, 11, 19, 20, 21, 29, 30, 39 | 169.25 |
| 4 | 0.0059, 0.0083 | 55.861, 68.927 | 1, 10, 13, 19, 22, 25, 31, 34, 43 | 187.07 |

Table 4.3. Information Required for the Application of ICSM for Suppressing Two Modes of Vibration for Motions in Joints 3 and 4

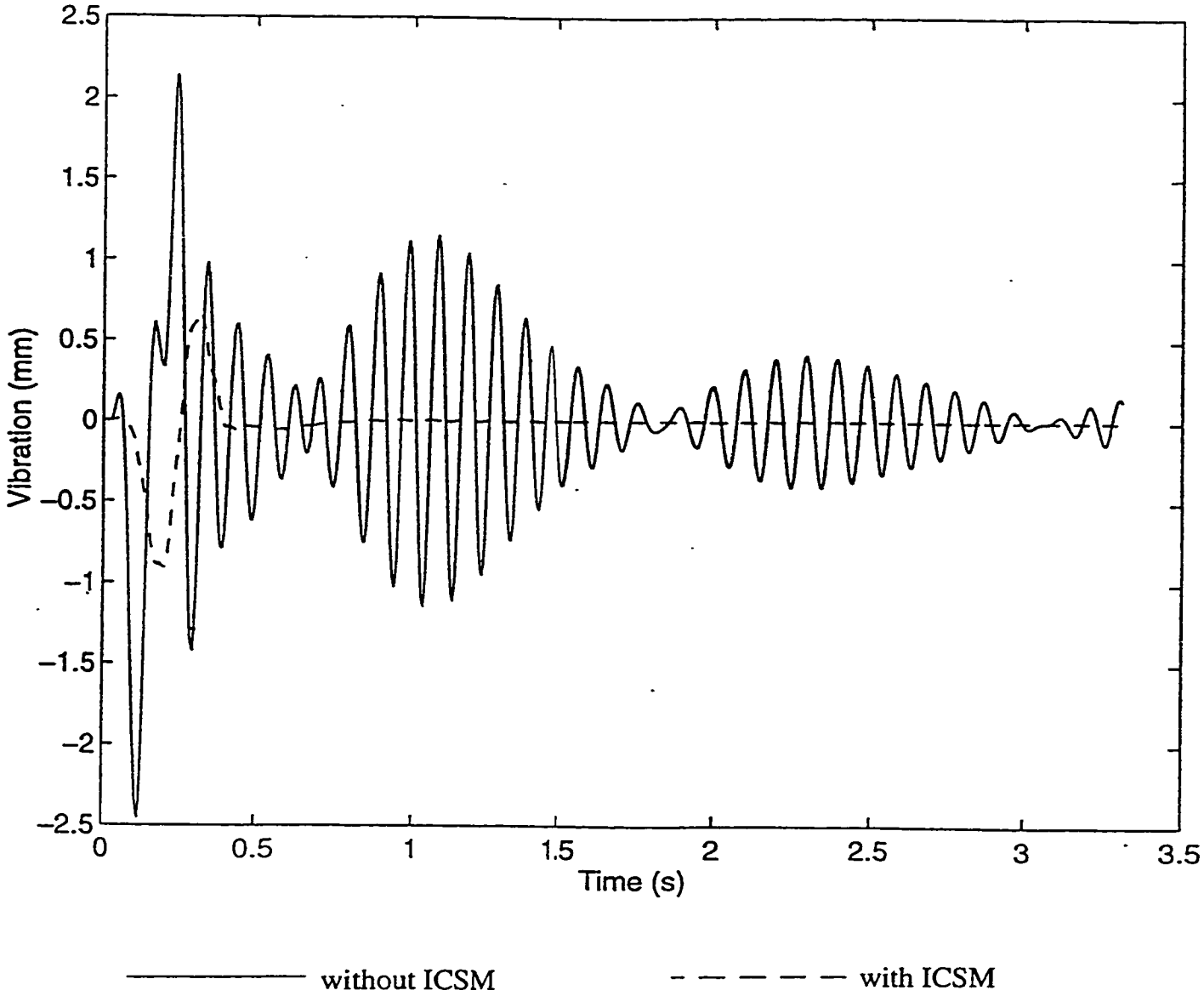


Figure 4.25 Simulated Response from Moving Joint 3 by 10 mm

with ICSM Applied to Suppress the First and Second Modes of Vibration

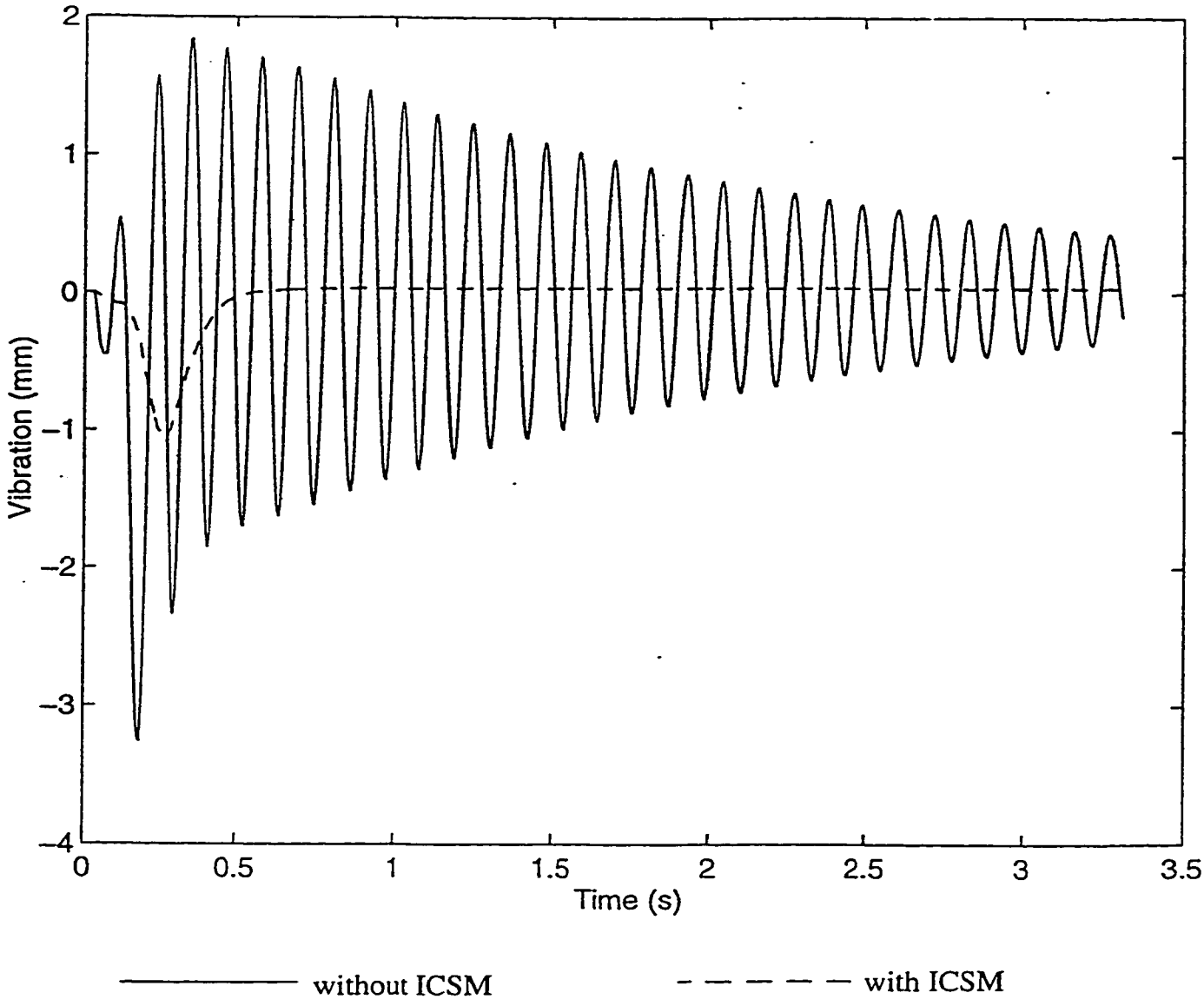


Figure 4.26 Simulated Response from Moving Joint 4 by 1 Degree with ICSM Applied to Suppress the First and Second Modes of Vibration

### 4.4.5 Experimental Verification of the ICSM for Vibration Control

In the last section simulation studies were performed to investigate the effectiveness of the ICSM in handing the workpiece vibration when the robot is in motion. It was determined that although the time delay induced was slightly longer, it was much more effective when the first two modes of the vibrations were suppressed. In fact, in the simulations the vibrations were reduced to almost zero. It is the objective of this section to verify the algorithm experimentally. Only tests with the first two modes suppressed were performed.

#### 4.4.5.1 Implementation of the ICSM

To implement the ICSM effectively, it is important to apply the shaped input sequence precisely. The Delta Tau PMAC controller employed to control the GMF robot for the experiment allows the programmer to select the desired Position, Velocity and Time to follow the trajectory of a motion segment with the "PVT" command. This command puts the motion program into Position-Velocity-Time move mode, and specifies the time for each segment of the move. In this mode, each move segment in the program must specify the ending position and velocity for the axis. Taking the starting position and velocity from the previous segment, the ending position and velocity, and segment time, the Delta Tau PMAC controller computes the unique cubic position profile and parabolic velocity profile to meet these constraints.

The procedure for the implementation of the ICSM is as follows:

1. Use the MATLAB simulation program 2 listed in Appendix A to generate the shaped input command trajectory, x4.
2. Discretize x4 into small segments. The time for each move segment is specified as multiples of the command update period of 4.4 ms.
3. For each of these segments of the input command, determine the incremental position traveled, ( $d_k$ - $d_o$ ), the move time, ( $t_k$ - $t_o$ ), and the ending velocity, $V = (d_k - d_{k-1}) / ( t_k - t_{k-1})$, where k is the duration of the segment in command update periods.
4. Construct the PMAC motion control program for PVT mode according to the PMAC Software Reference [38].

An example PMAC motion control program used to implement ICSM is given in Appendix B.

#### 4.4.5.2 Experimental Setup

The same setup employed to collect data for modelling was utilized again here for the experiments. The sheet metal workpiece was bolted right at its centre to the wrist of the GMF robot. The orientation of the robot and the workpiece is depicted in Figure 4.27.

#### 4.4.5.3 Experimental Results of the ICSM for Vibration Control

Experiments were performed to verify the effectiveness of the ICSM for vibration control. Tests were performed with and without the ICSM for comparison purposes. When

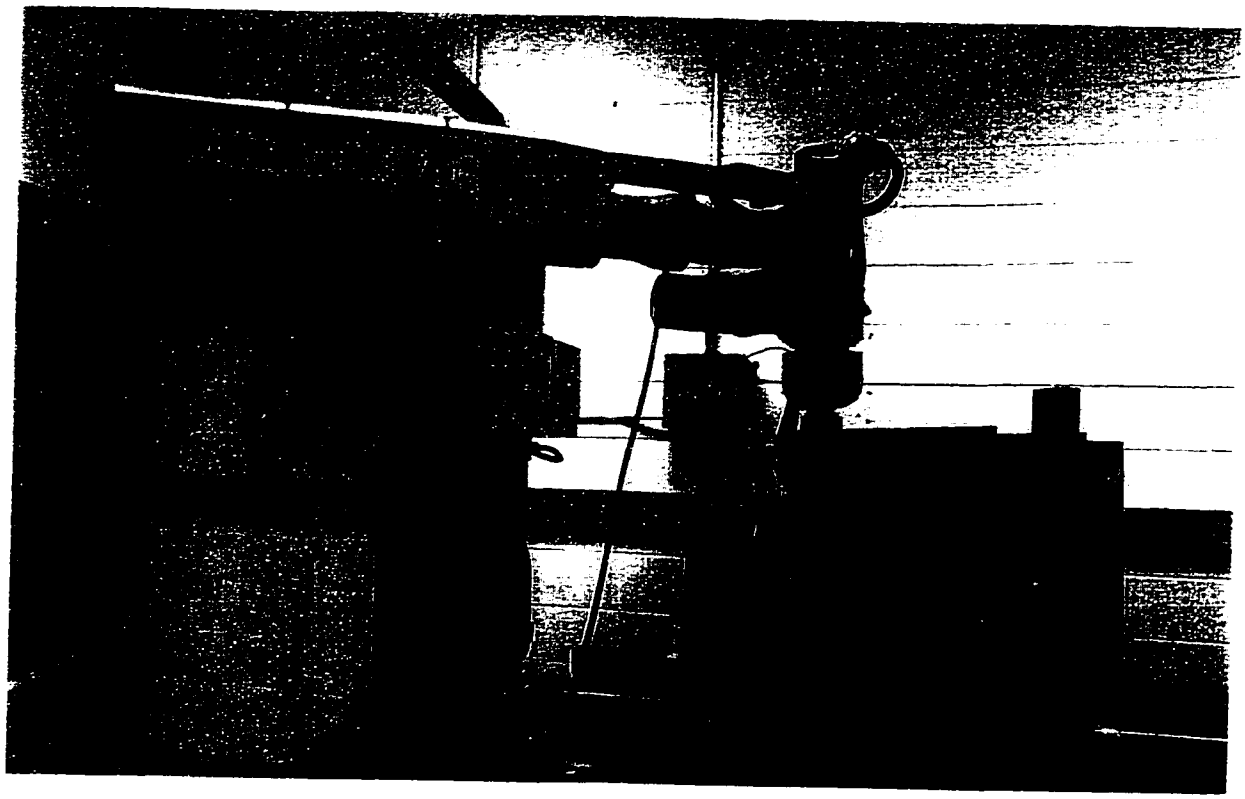

Figure 4.27 Experimental Setup for Input Command Shaping Method

ICSM was implemented, the first two modes of vibrations were suppressed in the controller design. The following five test cases were performed:

(a) 10 mm forward motion in joint 3 at 40 mm/s average velocity

(b) 1 deg. clockwise motion in joint 4 at 6 deg/s average velocity

(c) 300 mm forward motion in joint 3 at 480 mm/s average velocity

(d) 20 deg. clockwise motion in joint 4 at 29 deg/s average velocity

(e) Coordinated motion, performing (c ) & (d) with joints 3 and 4 simultaneously

The input command trajectory and the corresponding response measured by SGF 1 for the cases (a) and (b) without ICSM are shown in Figure 4.28a and Figure 4.29a, respectively. The results obtained when ICSM was applied in test cases (a) and (b) are plotted in Figure 4.28b and 4.29b, respectively. Although vibrations were monitored by four SGFs, the measurement from SGF 1 were chosen arbitrarily to represent the vibration of the workpiece during each test run.

Figures 4.30a and 4.31a show the results obtained with no ICSM applied for test cases ( c ) and (d), respectively. Similarly, the corresponding graphs with ICSM applied for test cases ( c ) and (d) are shown in Figures 4.30b and 4.31b. The average vibration amplitude in the first 3 seconds immediately after the robot motion started is used here to access the amount of vibration reduction using the ICSM. The results obtained from experiments with and without using the ICSM are summarized in Table 4.4 in the next section. The details on the implementation of test case (e) are discussed in the next section as well.

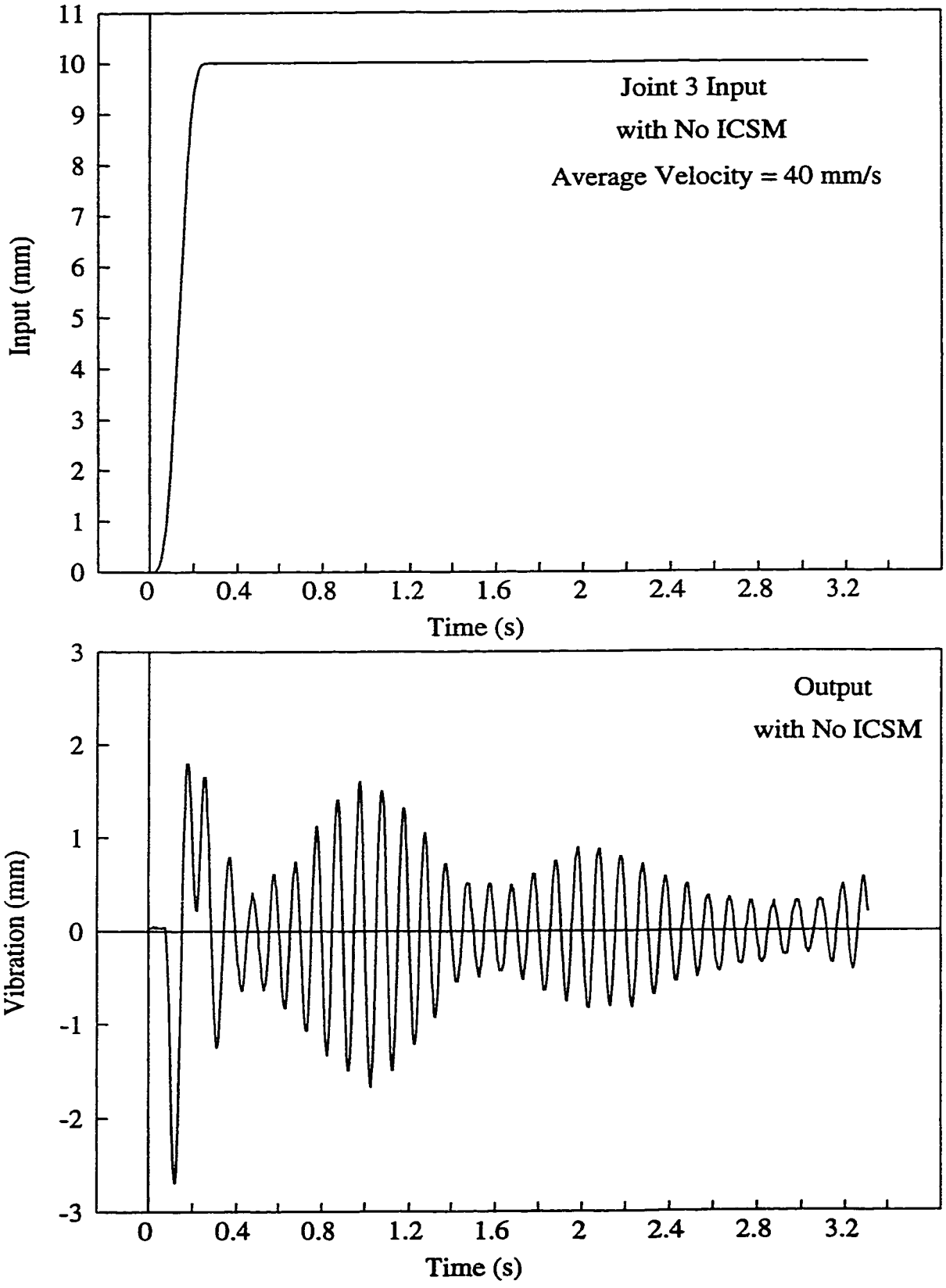


Figure 4.28a Real Time Test Result from Moving Joint 3 by 10 mm (with No ICSM Applied)

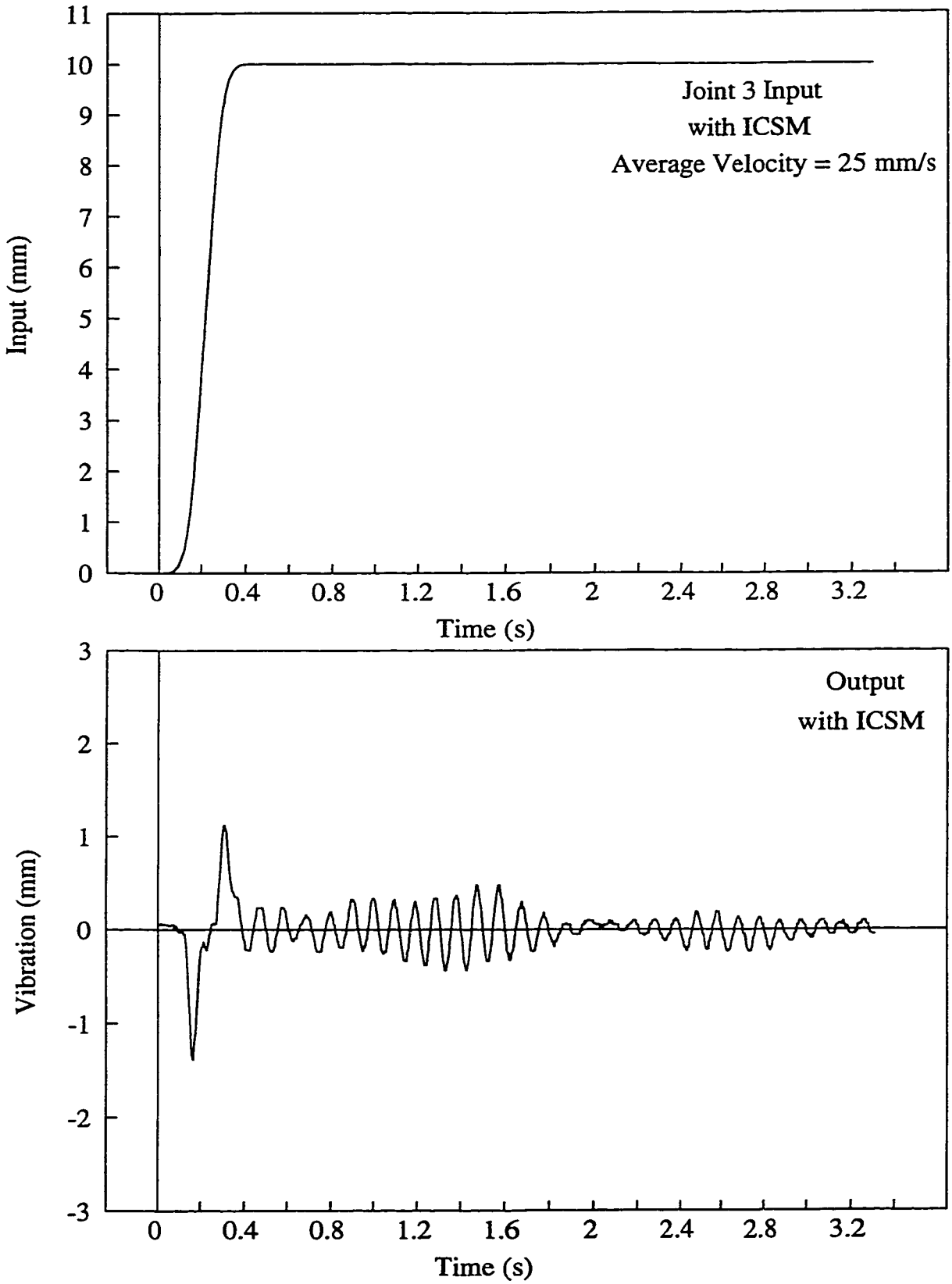


Figure 4.28b Real Time Test Result from Moving Joint 3 by 10 mm
(with first 2 modes of vibration controlled by ICSM)

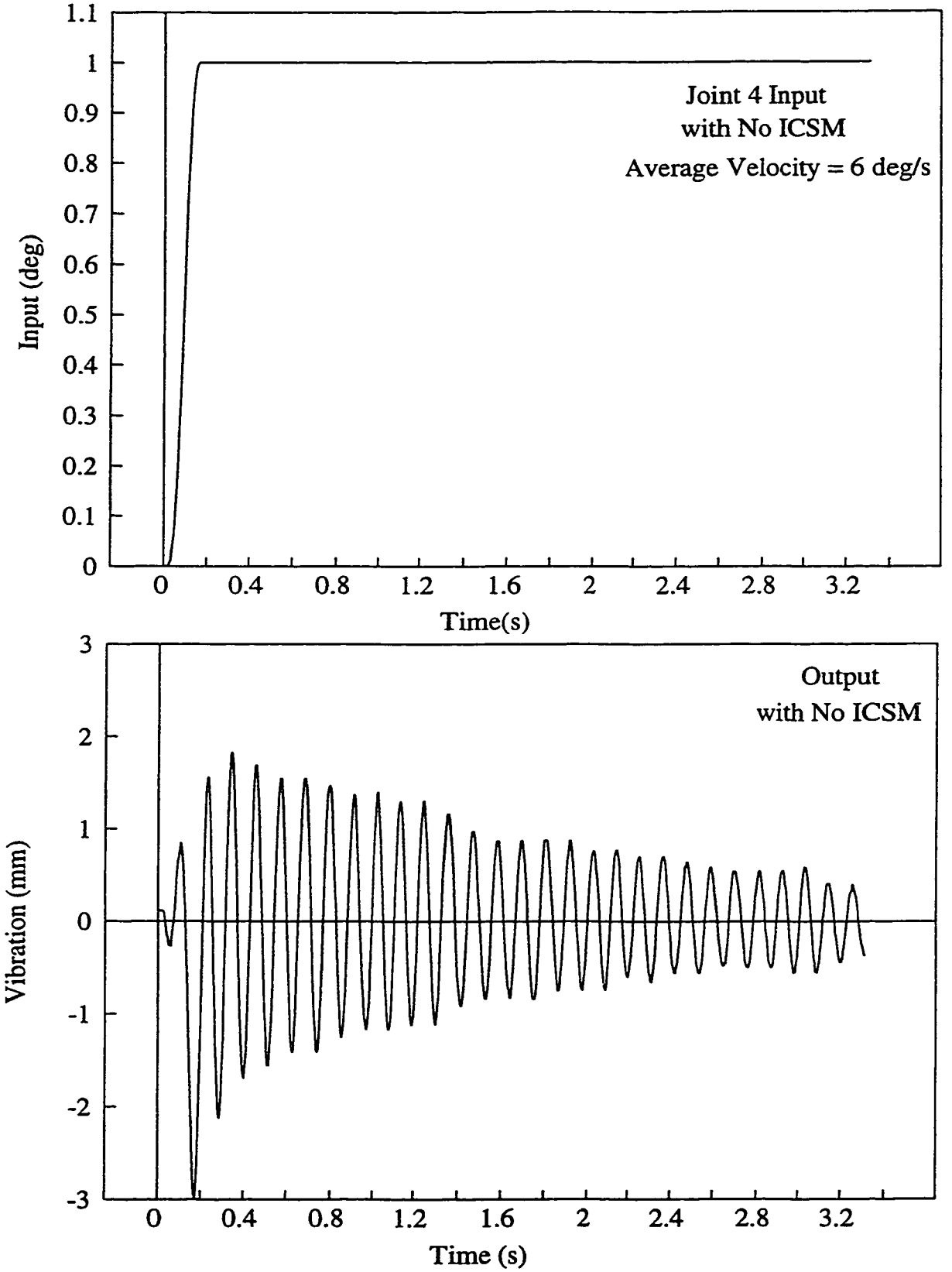


Figure 4.29a Real Time Test Result from Moving Joint 4 by 1 Degree (with No ICSM Applied)

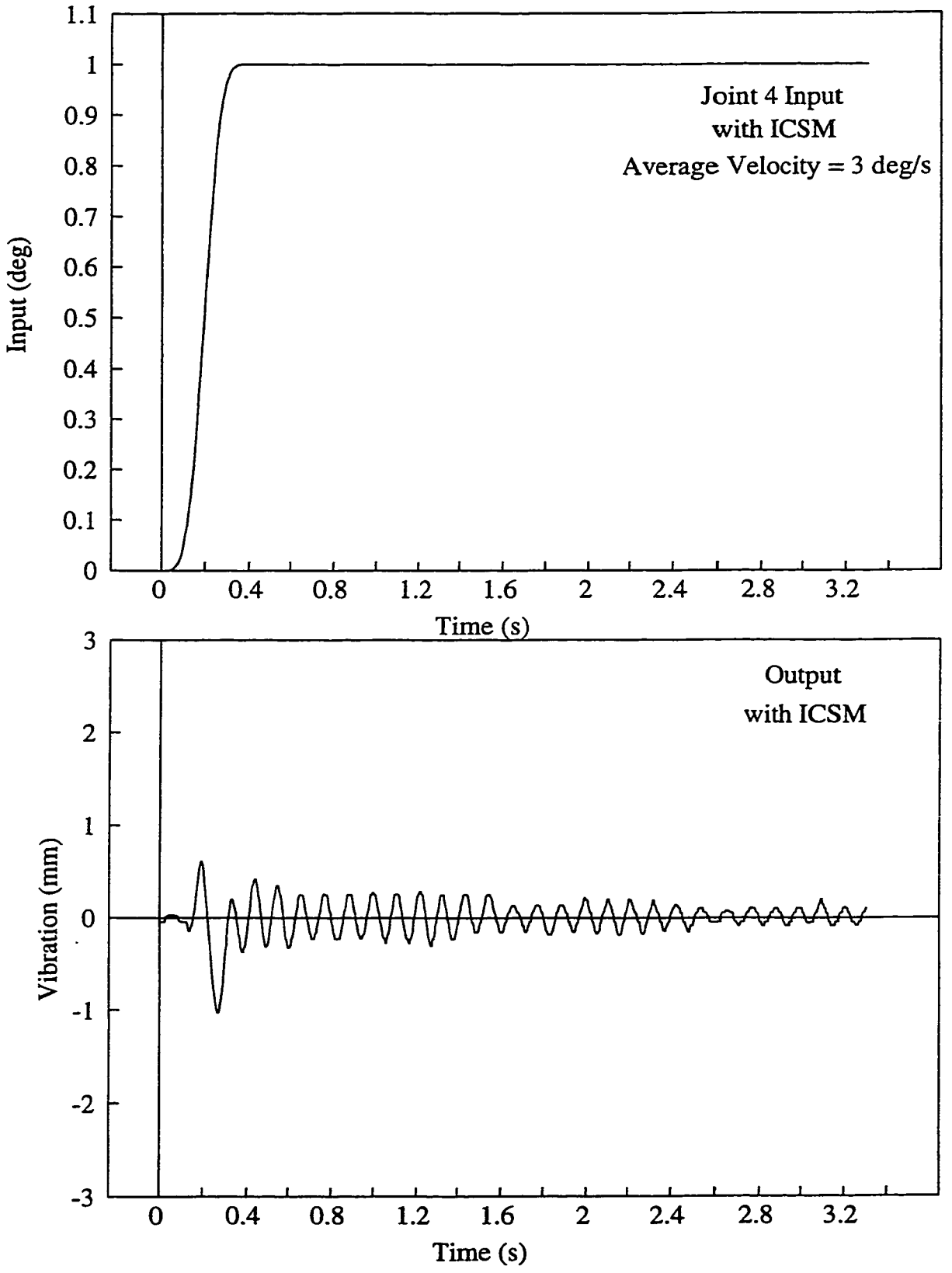


Figure 4.29b Real Time Test Result from Moving Joint 4 by 1 Degree
(with first 2 modes of vibration controlled by ICSM)

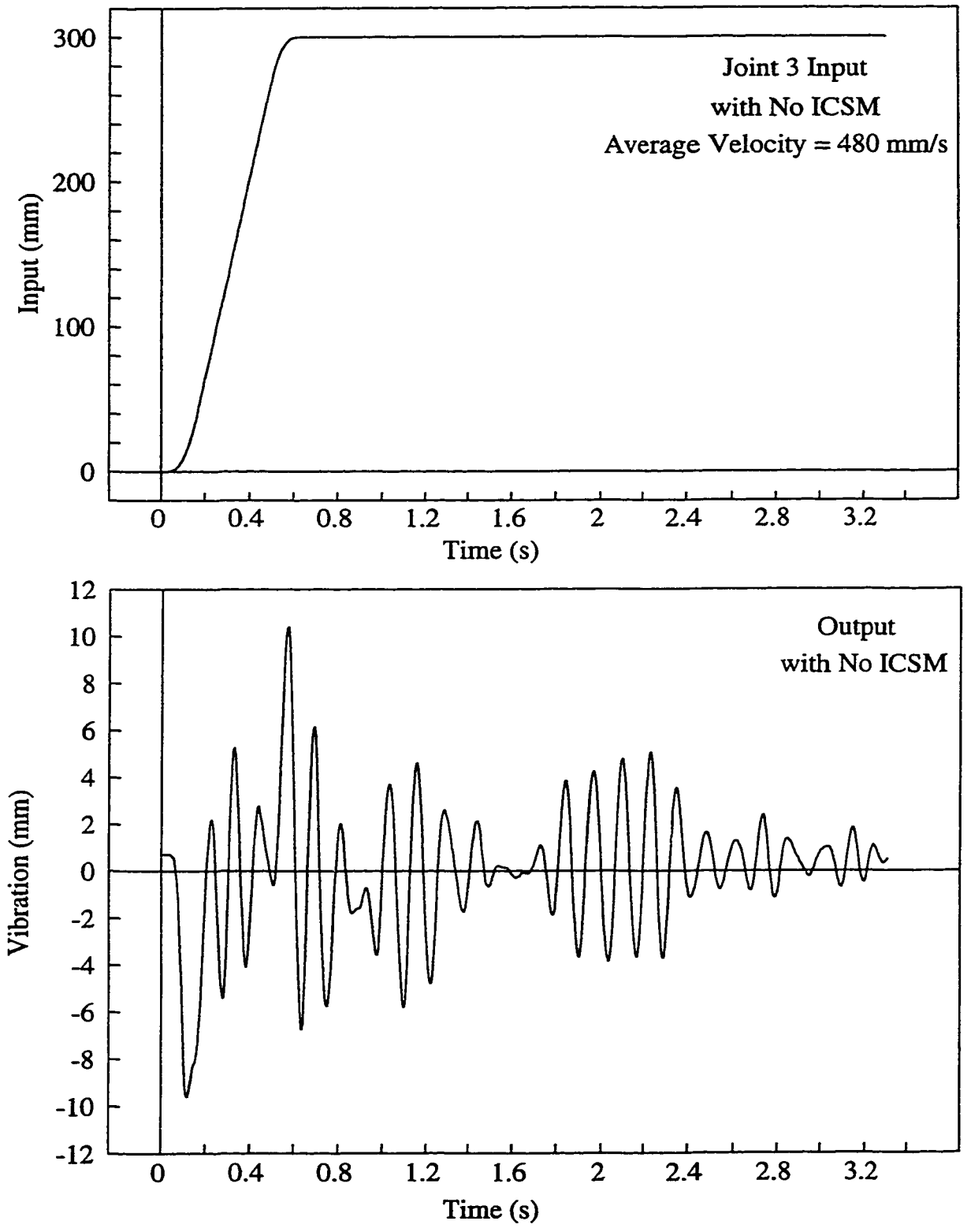


Figure 4.30a Real Time Test Result from Moving Joint 3 by 300 mm

(with No ICSM Applied)

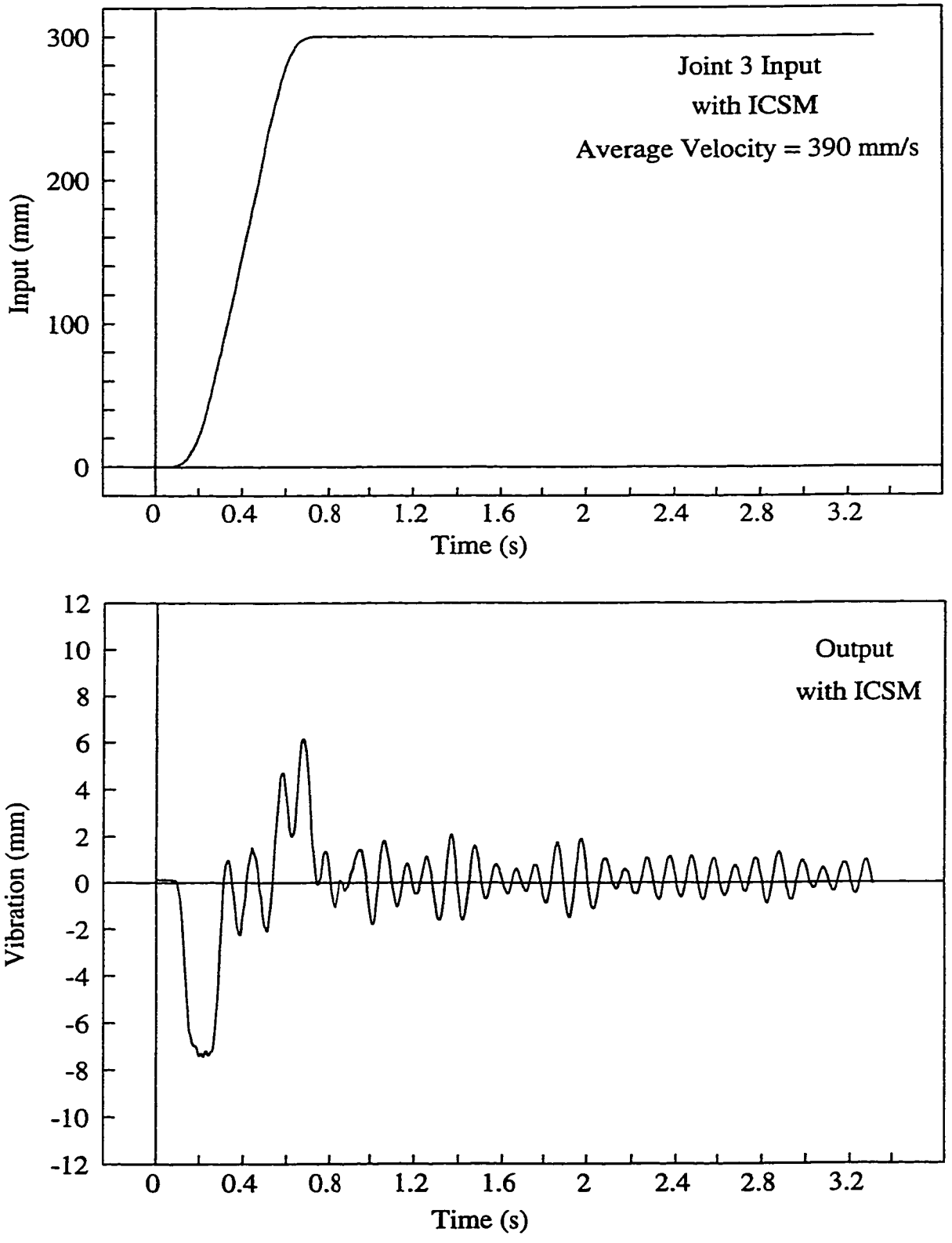


Figure 4.30b Real Time Test Result from Moving Joint 3 by 300 mm
(with first 2 modes of vibration controlled by ICSM)

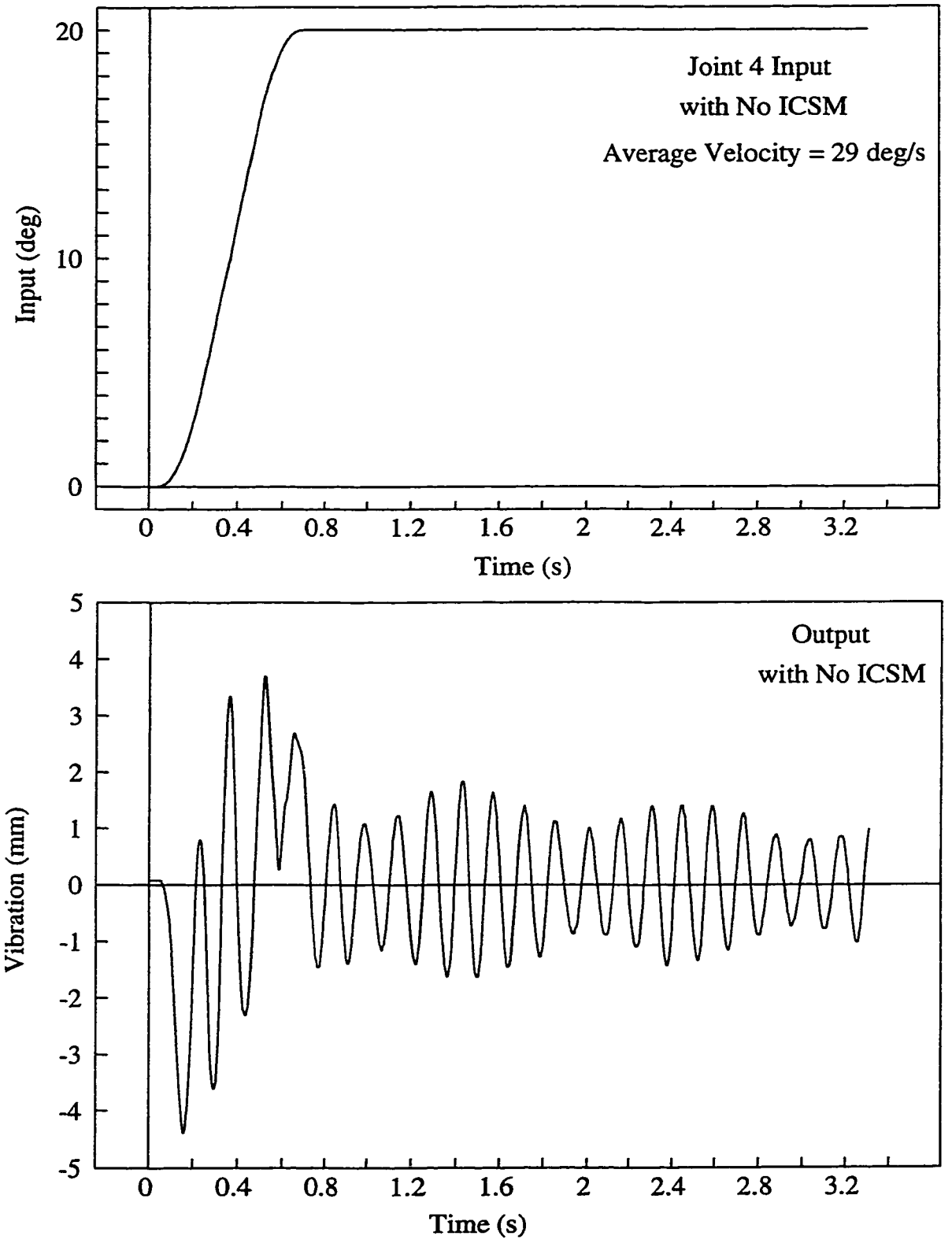


Figure 4.31a Real Time Test Result from Moving Joint 4 by 20 Degrees (with No ICSM Applied)

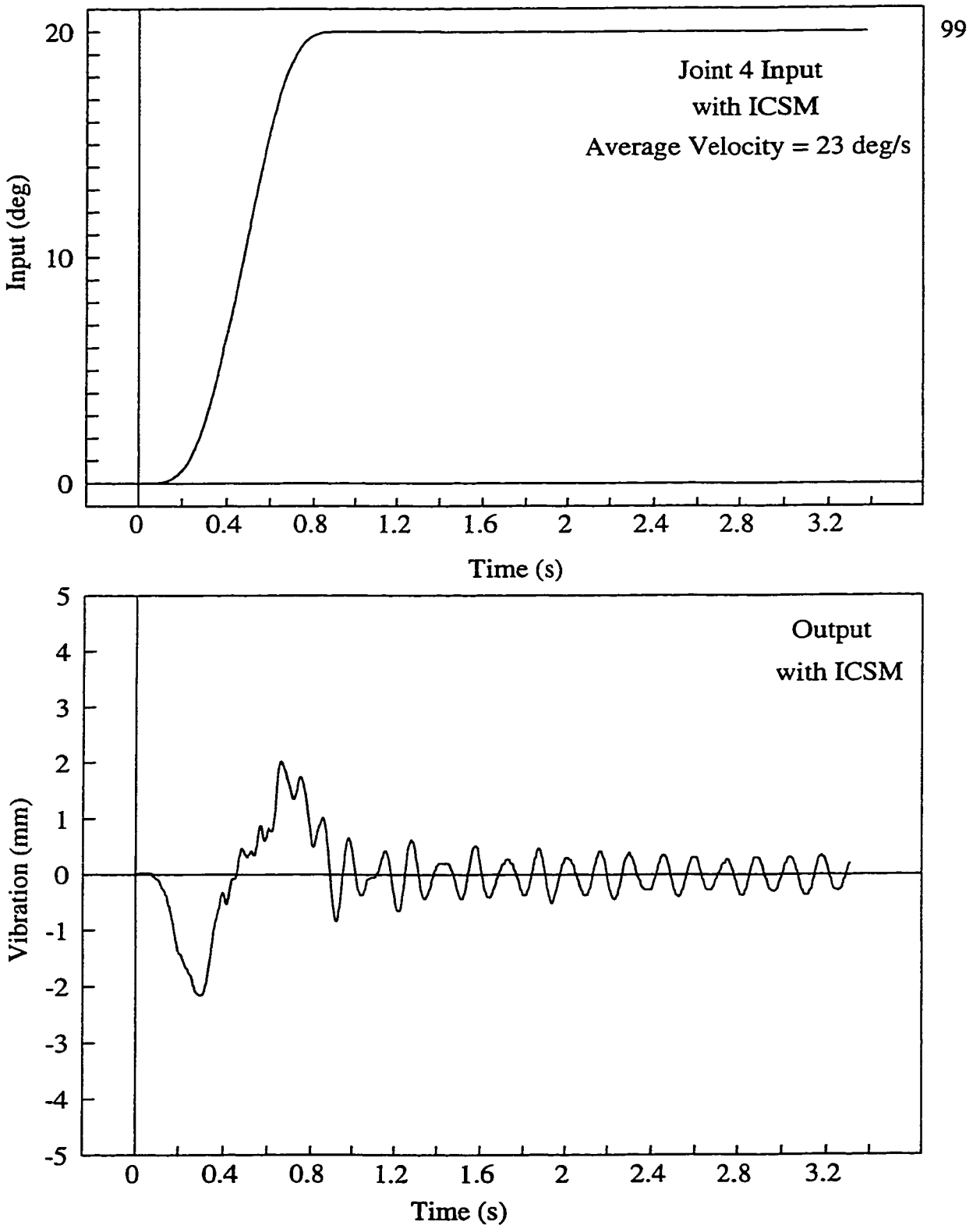


Figure 4.31b Real Time Test Result from Moving Joint 4 by 20 Degrees

(with first 2 modes of vibration controlled by ICSM)

#### 4.4.5.4 Experimental Results of the ICSM for Coordinated Motion in Two Joints

In the last section, experiments were performed using the ICSM with motion in a single joint. In the real life situation it is much more common to move the robot in coordinated motion. A coordinated motion is a robot motion in which all the joints involved in the motion are started and stopped at the same time. Since all joints move together to accomplish the required motion, it usually takes much less time to complete the motion than when moving the joints one at a time.

The ICSM has been applied by other researchers to control the vibration of a two-link flexible robot [ 29 ]. In that case, the same impulse sequence was applied to both of the links. However, in the situation at hand, the two most significant vibration modes in joints 3 and 4 are different so that two different impulse sequences are needed here for the two joints' motion.

As shown in Table 4.3, since the vibration modes to be suppressed in joints 3 and 4 are different, the amount of time required to complete the input sequences is different. If joints 3 and 4 are to be programmed for coordinated motion, the inputs to the joints should start and stop at the same time. However, when the shaped command sequences shown in Table 4.3 are applied to joints 3 and 4 for coordinated motion, it will take joint 4 more time (to be exact 187.07-169.25 = 17.82 ms) to complete its motion than joint 3. Therefore, a true coordinated motion will not result. This is a limitation of the ICSM algorithm. Figures 4.32a and 4.32b show the results obtained with no ICSM and with ICSM applied for motion (e), respectively.

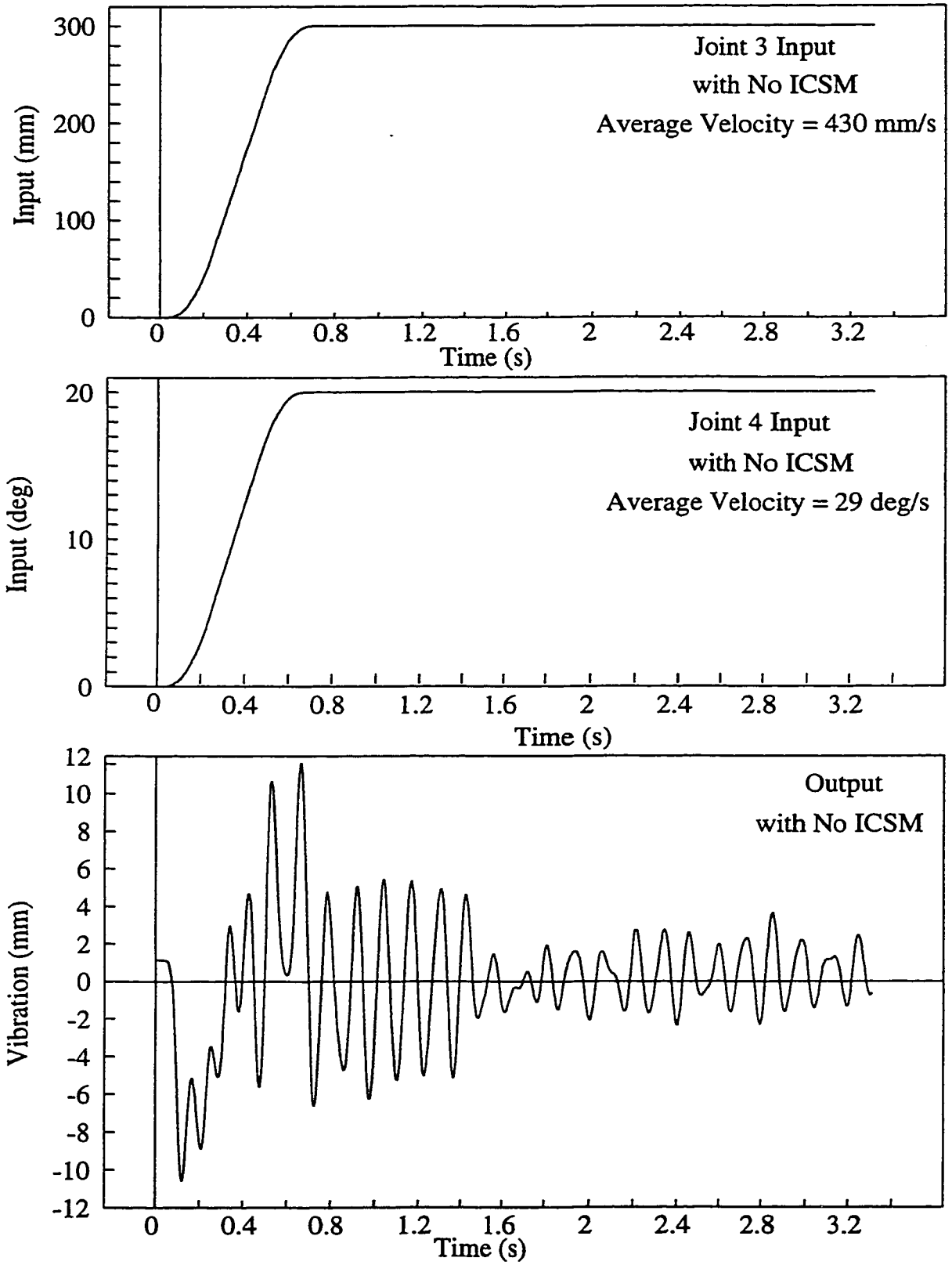


Figure 4.32a Real Time Test Result from Moving Joint 3 by 300 mm and Joint 4 by 20 Degrees simultaneously (with No ICSM Applied)

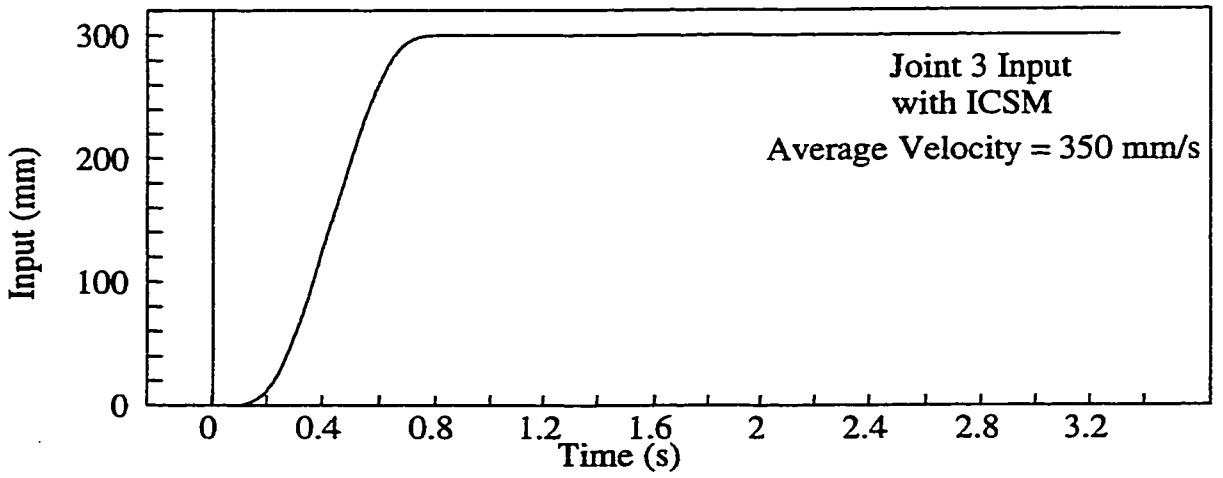


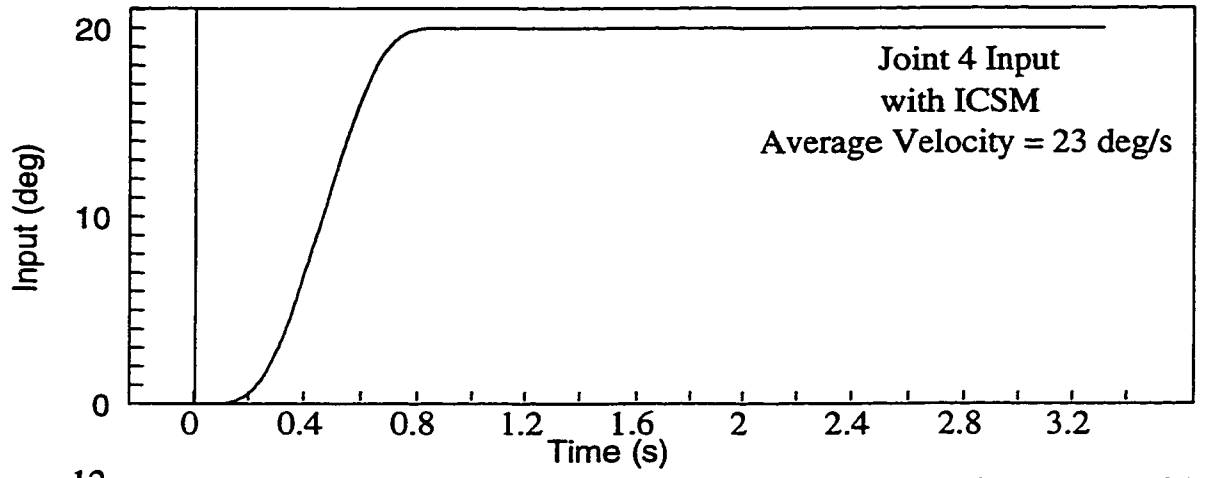


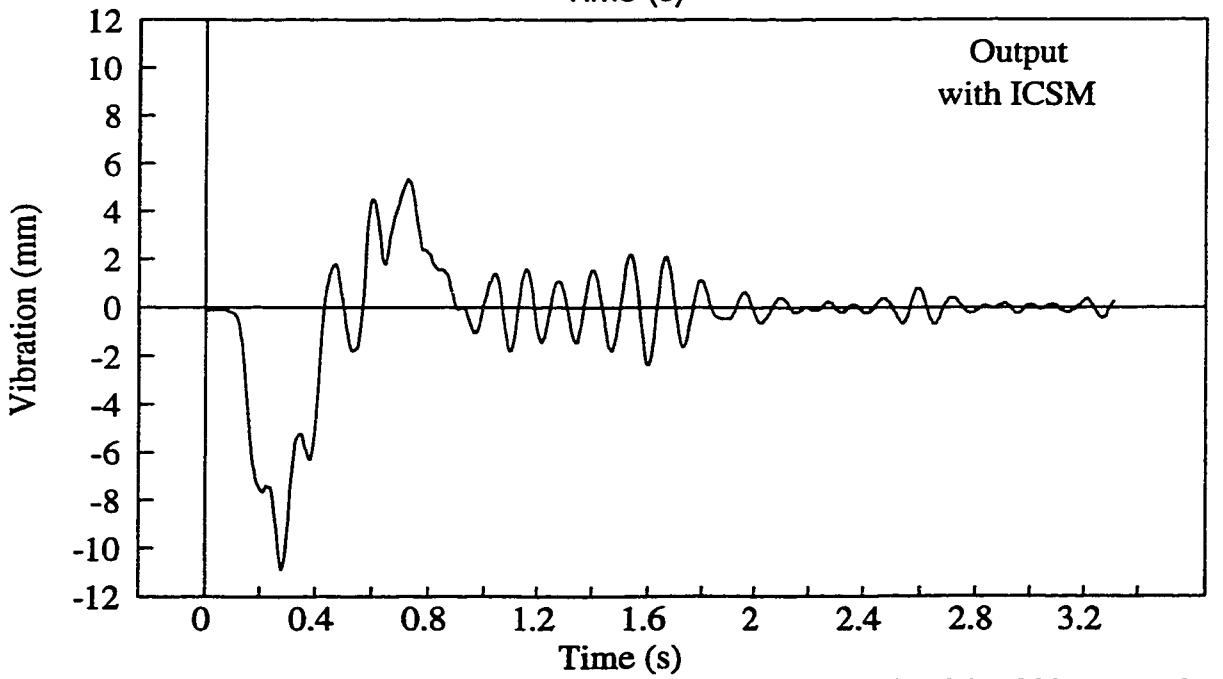


Figure 4.32b Real Time Test Result from Moving Joint 3 by 300 mm and Joint 4 by 20 degrees simultaneously
(with first 2 modes of vibration controlled by ICSM)

Table 4.4 summarizes the experimental results of the five test cases performed. The peak-to-peak vibration amplitude measured from SGF 1 in the first 3 seconds immediately after the motion started was averaged. It is very clear that the ICSM is very effective in controlling the vibration of the sheet metal part. In the five tests performed, the reduction in vibration amplitude ranges from 60 % to 78 %. In the next section the effect of the ICSM on the input command trajectory is examined.

| Test Motion | Average Vibration Amplitude Without ICSM (mm) | Average Vibration Amplitude With ICSM (mm) | % Reduction in Vibration Amplitude |
|---|---|---|---|
| a : (J3, 10 mm) | 1.64 | 0.52 | 68 % |
| b : (J4, 1°) | 1.98 | 0.44 | 78 % |
| c : (J3, 300 mm) | 6.04 | 2.40 | 60 % |
| d : (J4, 20°) | 2.96 | 1.05 | 65 % |
| e : ( J3, 300mm & J4, 20°) | 6.48 | 2.26 | 65 % |

Table 4.4. Summary of Average Vibration Amplitudes for Motions with and without ICSM

#### 4.4.5.5 Effect of ICSM on the Input Command Trajectory

The ICSM was found to be very effective in controlling vibration for sheet metal

handling; however, the input command trajectory was altered by the shaping algorithm. In general, a delay is introduced by the ICSM algorithm. Table 4.5 summarizes the average velocity of the input command trajectory of the five test cases before and after the ICSM was implemented. The percent reduction in the average velocity is also listed. One can see that for test cases (a) and (b), the percent reduction in the average velocity is relatively high. This is due to the fact that a fixed delay, which is equal to $2(\Delta T1+\Delta T2)$, is added onto the time required for the input command to finish. As listed before in Table 4.3, for Joint 3 and Joint 4 this delay is 169.25 ms and 187.07 ms respectively. Therefore, for shorter moves, as in test cases (a) and (b), the percent reduction in the average velocity was relatively higher.

| Test Motion | Average Velocity Without ICSM | Average Velocity With ICSM (2 modes suppressed) | % Reduction in Velocity due to ICSM |
|---|---|---|---|
| a : (J3, 10 mm) | 40 mm/s | 25 mm/s | 37.5 % |
| b : (J4, 1°) | 6 deg/s | 3 deg/s | 50 % |
| c : (J3, 300 mm) | 480 mm/s | 390 mm/s | 18.9 % |
| d : (J4, 20°) | 29 deg/s | 23 deg/s | 20.7% |
| e : ( J3, 300mm & J4, 20°) | 430 mm/s<br>29 deg/s | 350 mm/s<br>23 deg/s | 18.6%<br>20.7 % |

Table 4.5 Effect of ICSM on the Average Velocity of the Test Motions

In any case, the ICSM does slow the system down somewhat. In section 6.5 of Chapter 6, a study is carried out to determine whether the vibration reduction resulting from ICSM is mainly due to the reduction in motion velocity for the case of small moves.

## 4.5 CONCLUSIONS

The LEC algorithm was developed and implemented successfully with SGFs to control the vibration in sheet metal parts for RFA. The performance of this algorithm was studied based on vibration control experiments using 2-D and 3-D parts. Experimental results demonstrated that LEC could effectively reduce the residual vibration of the parts when they were handled by a robot. The vibration amplitude was reduced by up to 45% in 2-D parts and 71% in 3-D parts.

The effectiveness of ICSM for the flexible payload application was examined. The 3-impulse ICSM was studied in computer simulations to control the vibration of a sheet metal part by suppressing the first mode, the second mode and both the first and second mode of vibration, respectively. The ICSM performed the best when both the first and second modes were suppressed. The performance of ICSM was then examined experimentally. It was found to be very effective in suppressing the sheet metal part's vibration when moving at high speed in large motions. The vibration amplitude was reduced by up to 78%. However, a time delay was introduced into the input command trajectory by the ICSM algorithm.

# Chapter 5

# Contact State Measurement

## 5.1 INTRODUCTION

In order to control the contact state, it is first necessary to measure the contact state between the two workpieces. In this chapter, the contact state measurement problem is investigated using two 2-D flat sheet metal workpieces. The objective is to develop a method for measuring the contact state of a lap joint for a range of sheet metal thicknesses. The contact states detected were: left end, right end, full contact, and no contact. Methods based on the use of a Force/Moment Sensor (FMS), Strain Gauge equipped Fingers (SGFs), and sensor fusion of the FMS and SGFs information are developed [ 36 ]. Experiments are performed using several aluminum and steel sheet metal workpieces to determine the effectiveness of each of the methods for a range of sheet thicknesses. Furthermore, the contact state measurement algorithms developed for 2-D parts are extended to allow the contact state of 3-D parts to be measured.

## 5.2 CONTACT STATE MEASUREMENT METHODS FOR 2-D PARTS ASSEMBLY

The assembly of a lap joint using two robots is shown in Figure 5.1. In this work it is assumed that the robots hold the workpieces rigidly, and that the grasping locations are known. The analysis is confined to the static case. The robots' motions therefore must be planned so as not to excite the dynamic vibrations of the workpieces, or time must be given to allow the vibrations to dampen out. Figure 5.2 illustrates the four states which are to be measured: no contact, left end, right end and full contact. The measurement will utilize a normalized decision index. Values of -1, 0, and +1 will indicate left end, full and right end contact, respectively. In the following sections the methods for determining this index using the FMS, SGFs and sensor fusion of the two will be described.

### 5.2.1 Using a Force/Moment Sensor (FMS) for Contact State Measurement

The choice of a FMS was based on its successful application to the measurement of contact state for rigid workpieces by other researchers [ 33 ], [ 21 ] & [ 22 ] . A six degree-of-freedom FMS manufactured by JR3 Inc. was employed. The location of the FMS and its coordinate system are shown in Figure 5.3. As the contact is made on the bottom edge of the workpiece, only the force $F_y$ and the moment $M_z$ are necessary to determine the contact state. Figure 5.4 illustrates the case of right end contact. The moment and force are related by:

$$M_z = F_y \cdot R \qquad (5.1)$$

where R is the coordinate of the point of contact along the FMS's x-axis. Therefore, it is

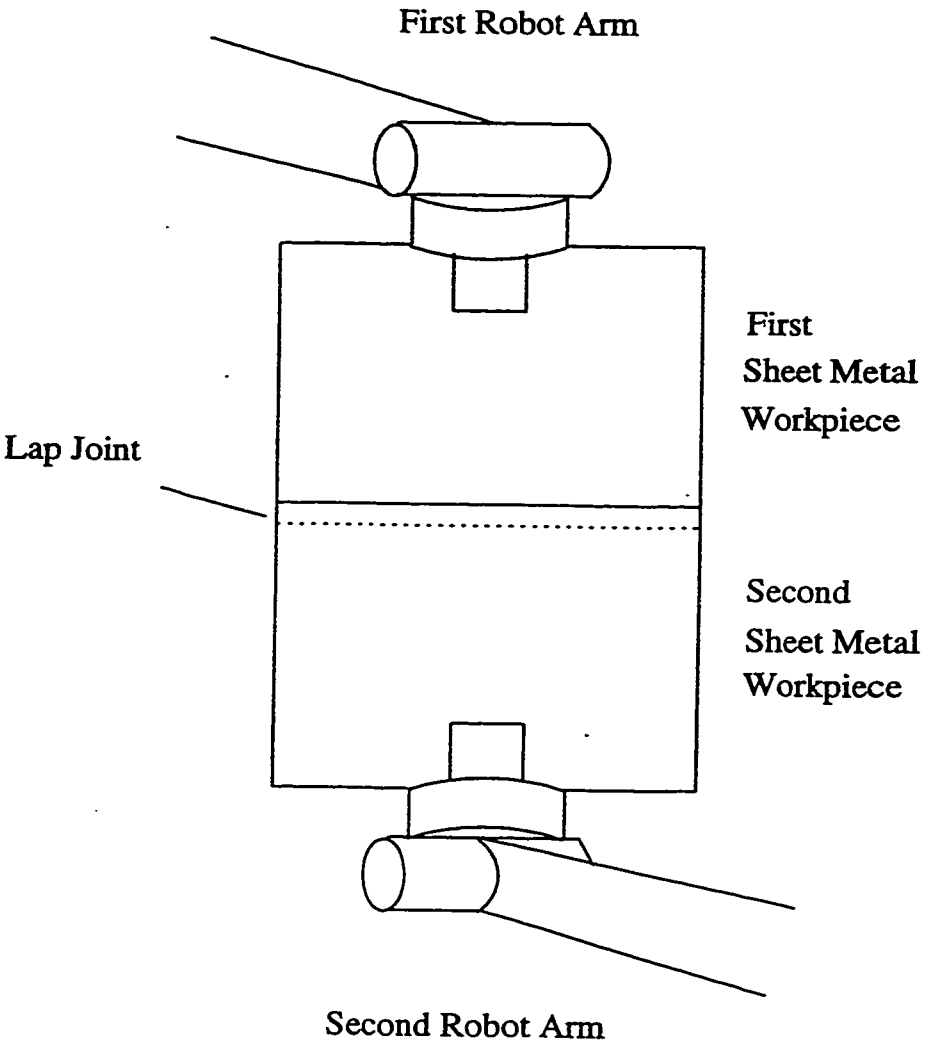


Figure 5.1 Robotic Fixtureless Assembly of Sheet Metal Parts

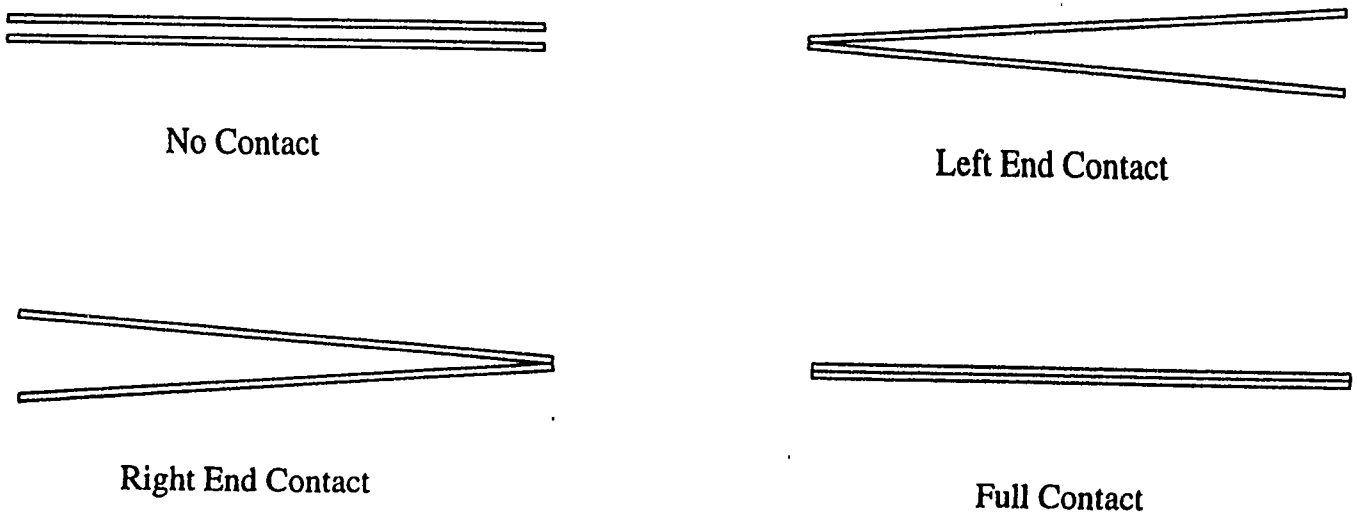


Figure 5.2 The Four Contact States to be Detected

( TOP VIEW. NOT TO SCALE )

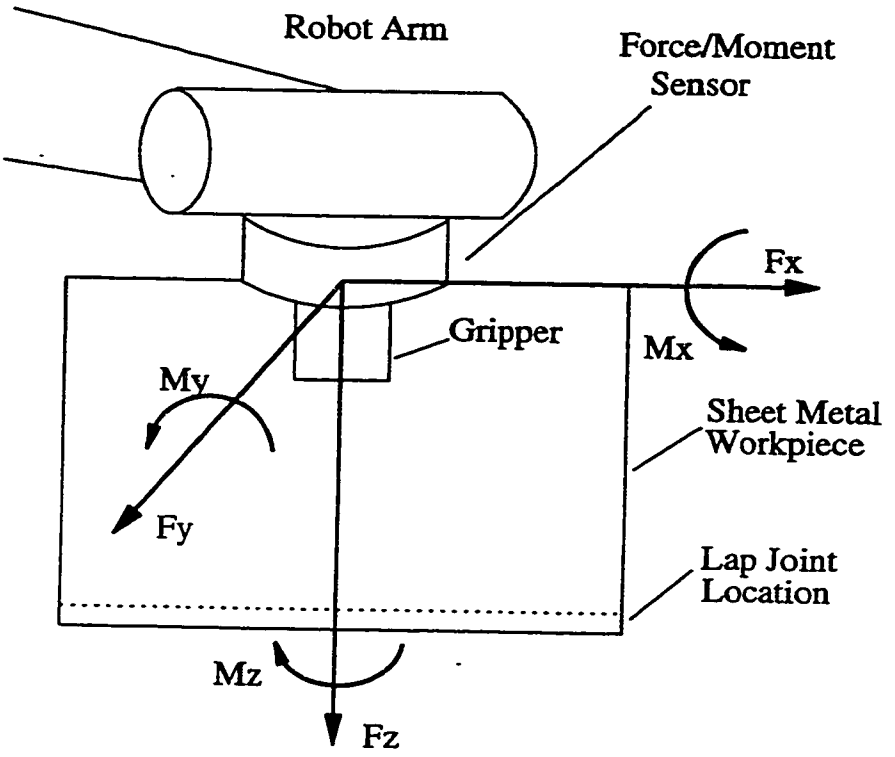


Figure 5.3 The Mounting Location and Coordinate System
of the Force/Moment Sensor

possible to estimate the location of the point of contact by checking the ratio:

$$R = \frac{M_z}{F_y} \qquad (5.2)$$

Note that R will be negative for left end contact and positive for right end contact. Assuming that the distances, D1 and D2, (as shown in Figure 5.4) are known, the normalized decision index, X1, may be produced as follows:

$$XI = \begin{cases} \frac{R}{DI}, & R<0 \\ \frac{R}{D2}, & R>0 \end{cases} \qquad (5.3)$$

By substituting equation (5.2) into (5.3) the final equation for the calculation of the decision index is obtained:

$$XI = \frac{Mz}{Fy \cdot D} \qquad (5.4)$$

where D equals D1 or D2 as given by equation (5.3). In this thesis, only the case where R=D is considered. Therefore X1 should be -1 for left end and +1 for right end contact. When there is full contact along the joint the net moment should be zero, and a decision index of zero will result.

### 5.2.2. Using Strain Gauge Equipped Fingers (SGFs) for Contact State Measurement

For thin sheets, because of their low stiffness, it was expected that the contact

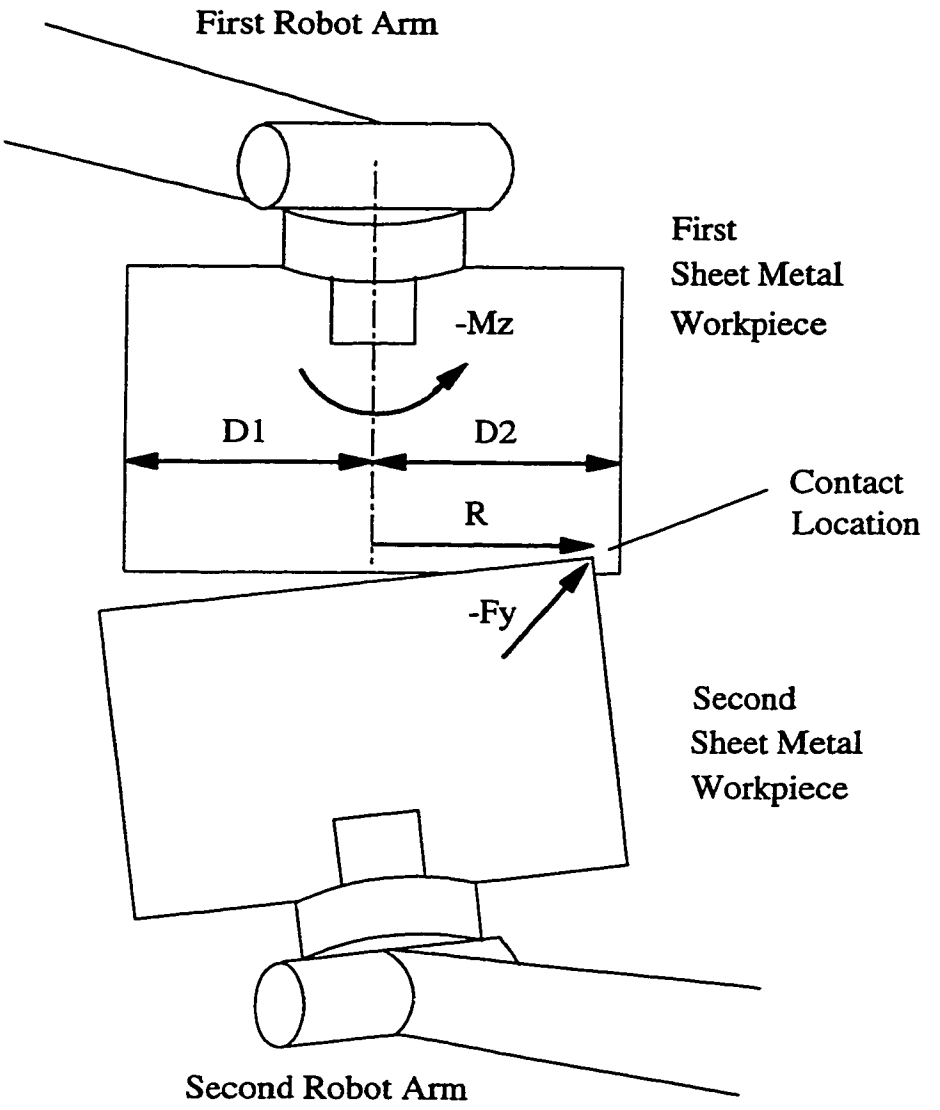


Figure 5.4 Using FMS for Contact State Measurement

force/moment may be too small for the FMS to be used successfully. Since the deflections due to contact will be significant, contact state measurement based on strain measurement was selected as an alternative method. Installation of strain gauges on the workpieces would be ideal from a theoretical viewpoint, but not as a practical solution. The gauges could not be installed on the gripper directly either, since its rigidity would result in very poor sensitivity. The SGFs employed before for vibration measurement were used here again to circumvent these problems.

In order to detect contact at either end of the workpiece, two SGFs were mounted to the gripper as shown in Figure 3.1. As illustrated in Figure 3.3, when there is contact from the front, the voltage output will be positive. The voltage outputs from the left and right SGFs are termed VL and VR, respectively. Ideally, when there is left end contact from the front, VL will be positive and VR will be zero. The opposite is true for right end contact. When there is full contact, both fingers should experience the same deflection, so VL should equal VR. Therefore the decision index:

$$X2 = \frac{VR - VL}{VR + VL} \qquad (5.5)$$

should produce the desired values of -1, 0 and +1 for left end, full and right end contact, respectively.

### 5.2.3. Using Sensor Fusion of FMS and SGFs for Contact State Measurement

Sensor fusion involves combining the output from two or more sensors to reduce the measurement uncertainty. This uncertainty is due to sensor errors, signal noise, or in the

extreme case, sensor failure. A multi-sensor approach is particularly beneficial if the sensors are selected such that at least one sensor's measurement uncertainty is low when the others' are high. The combined output will therefore be more reliable over a wider range of conditions. For the contact state measurement problem, the aim of fusion is to increase the range of sheet thickness which may be used. As previously mentioned, the FMS measurement uncertainty is expected to be low for thick sheets and high for thin sheets. Since the opposite is expected for the SGFs, the two sensors are good candidates for sensor fusion.

The first step in sensor fusion is to transform the unrelated raw sensor data into a common form. Data in the common form may then be combined. The first step was achieved by transforming the raw data from the FMS and SGFs into the decision indices X1 and X2. X1 and X2 are assumed to be independent scalar observations of the environment, each derived from a Gaussian distribution. The outputs may be combined to give the maximum likelihood estimate [ 34 ]:

$$X3 = \frac{\sigma_1^{-2}}{\sigma_1^{-2} + \sigma_2^{-2}} \cdot X1 + \frac{\sigma_2^{-2}}{\sigma_1^{-2} + \sigma_2^{-2}} \cdot X2 \qquad (5.6)$$

where X3 is the decision index for the sensor fusion method, $\sigma_1^2$ is the estimated variance of X1 and $\sigma_2^2$ is the estimated variance of X2. This is simply the weighted average of the two indices, where each weight is approximately inversely proportional to the variance of each index. Therefore, when the uncertainty of one index is high, its contribution to X3 will be small. Note that X3 should also produce the desired values of -1, 0, and 1 for left end,

full, and right end contact, respectively.

## 5.3 DECISION BOUNDARIES FOR CONTACT STATE MEASUREMENT

When two parts are in contact, under ideal conditions, the decision indices should equal -1, 0 or 1 depending on the contact state. In reality, due to measurement uncertainty, other values will be produced. In order to detect the contact state, these uncertain values will be mapped into the final decision $X \in \{-1, 0, 1\}$. A simple approach is to map Xn to X according to:

$$X = \begin{cases} -1, & Xn \le B1 \\ Indeterminate, & B1 < Xn \le B2 \\ 0, & B2 < Xn < B3 \\ Indeterminate, & B3 \le Xn < B4 \\ 1, & Xn \ge B4 \end{cases} \qquad (5.7)$$

$$B1 \le B2 < B3 \le B4 \qquad (5.8)$$

where n=1, 2 and 3 for the FMS, SGFs and sensor fusion methods respectively, and B1 to B4 are the decision boundaries. In this relation, there are no extreme bounds for X=1 or -1 since there are no values of X beyond -1 and 1. Note that as the size of the indeterminate regions is decreased, the probability of an incorrect decision is increased. If the decision is indeterminate, the measurement must be repeated. However, if the uncertainty of Xn exceeds the decision boundaries the time to obtain a correct decision may be impractically

long (since most of the decisions will be indeterminate). A trade-off will exist between the measurement time and the success rate. A systematic approach for selecting the decision boundaries will now be described.

It has been previously assumed that the decision indices X1 and X2 were each derived from Gaussian distributions, and from equation (5.6) the distribution of X3 will also be Gaussian. Since Xn follows a Gaussian distribution, 99.7% of the values of Xn should lie in the interval $\bar{X}n \pm 3\sigma_n$, where $\sigma_n$ is an estimate of the standard deviation of Xn, and $\bar{X}n$ is the sample mean of Xn [ 35 ]. Assuming $Xn \in \{-1, 0, 1\}$, an indeterminate decision should occur only 0.3% of the time when:

$$B1 = -1 + 3 \cdot \sigma_n \qquad (5.9)$$

$$B2 = -3 \cdot \sigma_n \qquad (5.10)$$

$$B3 = 3 \cdot \sigma_n \qquad (5.11)$$

$$B4 = -1 + 3 \cdot \sigma_n \qquad (5.12)$$

If $\sigma_n$ underestimates the true standard deviation then indeterminate decisions will occur more than 0.3% of the time, and conversely they will occur less frequently. Since $B1 \leq B2$ and $B3 \leq B4$, incorrect decisions will occur less than 0.3% of the time. The limiting case occurs when B1=B2 and B3=B4. This choice eliminates the indeterminate regions which act as protection against incorrect decisions. From equations (5.9) to (5.12), for incorrect decisions

not to occur greater than 0.3% of the time with this limiting case:

$$\sigma_n \leq \frac{1}{6}, \tag{5.13}$$

$$B1 = B2 = -\frac{1}{2} \tag{5.14}$$

$$B3 = B4 = \frac{1}{2} \tag{5.15}$$

In practice, if equations (5.14) and (5.15) are implemented and equation (5.13) is violated, then X should be considered indeterminate. This reduces the probability of incorrect decisions.

## 5.4 DETECTION OF "NO CONTACT" STATE

When there is no contact between the two workpieces, the outputs of the FMS ($F_y$ and $M_z$) and the SGFs (VL and VR) should theoretically be zero. In practice, due to sensor error and signal noise, the outputs are expected to be close to zero and highly oscillatory. Equations (5.4) and (5.5) will involve division by these small changing values resulting in large standard deviations for X1 and X2. A threshold T could then be used to detect the state of no contact (NC). For the FMS and SGF then:

$$X = NC, \ \sigma_n > T \qquad n = 1, 2 \tag{5.16}$$

With the sensor fusion method, X1 and X2 should be tested prior to calculating X3 as follows:

$$X = NC,\ \sigma_1 > T \wedge \sigma_2 > T \qquad (5.17)$$

If only one of $\sigma_1$ and $\sigma_2$ exceeds T, then X3 and X are calculated in the normal manner. This means that as long as one sensor's uncertainty is small, the contact state will still be detected.

To help select T, its effect on the frequency of indeterminate decisions should be considered. If equation (5.13) is implemented in combination with equation (5.17) then:

$$X = Indeterminate,\ \frac{1}{6} < \sigma_n \leq T \qquad (5.18)$$

Once again there is a trade-off between minimizing the probability of incorrect decisions and doing likewise for indeterminate decisions. If T » $\frac{1}{6}$ there will be a high probability for indeterminate decisions and a low probability for incorrect ones. If T = $\frac{1}{6}$ there will be no indeterminate decisions, but the probability for incorrect decisions will be increased.

## 5.5 EXPERIMENTAL VERIFICATION OF THE CONTACT MEASUREMENT METHODS

### 5.5.1 Experimental Setup

Experiments were performed to determine the effectiveness of each of the measurement methods for a range of sheet thicknesses. The equipment used for vibration control experiments was employed here again. The setup was as shown in Figure 5.1, except that the one workpiece was clamped onto a worktable. The other workpiece was gripped by the GMF robot at the centre of its top edge, so D1 = D2 = width/2. For the workpiece held

by the robot, three flat galvanized steel sheets and one aluminium sheet were used in turn. The dimensions of these sheet metal workpieces are given in Table 5.1. The workpiece clamped on the worktable had the same dimensions as workpiece #3 in Table 5.1. The FMS was mounted between the robot's wrist and the gripper (as shown in Figure 5.3). The SGFs were clamped to the gripper as shown in Figure 3.1.

| Workpiece # | Length (mm) | Width (mm) | Thickness (mm) | Thickness (Gauge) |
|---|---|---|---|---|
| 1 | 370 | 290 | 0.32 | (aluminum) |
| 2 | 370 | 290 | 0.69 | 23 |
| 3 | 370 | 200 | 0.89 | 20 |
| 4 | 370 | 200 | 1.88 | 15 |

Table 5.1. Dimensions of the Sheet Metal Workpieces Employed in the Experiments

### 5.5.2 Experimental Procedure

The experiments consisted of first moving the robot under manual control until one of the four contact states (as illustrated in Figure 5.2) was achieved. Initial contact was proceeded by a forward move of approximately 3 mm. Time was then allowed for any vibrations to dampen out. The FMS and SGFs outputs ($F_y$, $M_z$, VL and VR) were then sampled 50 times using the IBM PC. A 100 Hz sampling rate was used. Decision indices

were calculated from each set of outputs. The robot was then moved back to its original position. This procedure was repeated ten times for each of the four workpieces and the four contact states, giving a total of 160 trials.

The final decision indices were calculated with B1 = B2 = -½, B3 = B4 = ½ and T = $\frac{1}{6}$. As discussed in section 5.2, this setting will result in no indeterminate decisions so repeated measurements were not required to detect the contact state. This benefit occurred at the cost of a higher probability for incorrect measurements.

### 5.5.3 Experimental Results

Sample experimental results for each of the workpieces are given in Tables 5.2 to 5.4. For these results, the correctness of the FMS, SGFs and sensor fusion methods may be obtained by comparing the expected X values to those given by each method. The success rate for each of the measurement methods by workpiece is given in Figure 5.5. These rates are based on the 40 tests performed with each of the 4 workpieces.

From Table 5.2 for the 0.32 mm Aluminum workpiece (#1), the FMS detected all contact states as no contact (i.e. NC). The overall summary of measurement results shown in Figure 5.5 shows that the FMS correctly measured only 28 % of the time for this workpiece. This result was due to the fact that the aluminum workpiece was too flexible to produce any force significant enough for the FMS to detect the contact state properly. While the FMS did not do well for this workpiece, the SGFs and sensor fusion correctly detected all contact states. Clearly, this demonstrates the effectiveness of the SGFs in working with flexible workpieces, and the performance of the sensor fusion algorithm.

| Contact State | Expected X | FMS | | | SGFs | | | Fusion | |
|---|---|---|---|---|---|---|---|---|---|
| | | X1 | $\sigma_1^2$ | X | X2 | $\sigma_2^2$ | X | X3 | X |
| No Contact | NC | -0.195 | 7.9 | NC | 1.072 | 134.5 | NC | NC | NC |
| Left End | -1 | 0.548 | 40.9 | NC | -1.96 | 0.0021 | -1 | -1.96 | -1 |
| Right End | 1 | 2.42 | 20.5 | NC | 2.72 | 0.0014 | 1 | 2.72 | 1 |
| Full | 0 | 0.354 | 1.3E-2 | NC | 0.093 | 2.1E-4 | 0 | 0.093 | 0 |

Table 5.2 Sample Contact State Measurement Results for Workpiece #1

(Aluminum, 0.32 mm thick)

| Contact State | Expected X | FMS | | | SGFs | | | Fusion | |
|---|---|---|---|---|---|---|---|---|---|
| | | X1 | $\sigma_1^2$ | X | X2 | $\sigma_2^2$ | X | X3 | X |
| No Contact | NC | -0.87 | 45 | NC | 0.29 | 97 | NC | NC | NC |
| Left End | -1 | 3.2 | 0.56 | NC | -2.1 | 6.8E-4 | -1 | -2.1 | -1 |
| Right End | 1 | 0.29 | 5.3E-3 | 0 | 2.0 | 5.3E-3 | 1 | 1.1 | 1 |
| Full | 0 | -0.40 | 1.0E-2 | 0 | 0.27 | 3.5E-3 | 0 | 0.10 | 0 |

Table 5.3 Sample Contact State Measurement Results for Workpiece #2

(Galvanized Steel, 0.69 mm thick)

| Contact State | Expected X | FMS | | | SGFs | | | Fusion | |
|---|---|---|---|---|---|---|---|---|---|
| | | X1 | $\sigma_1^2$ | X | X2 | $\sigma_2^2$ | X | X3 | X |
| No Contact | NC | 0.11 | 61 | NC | -2.6 | 350 | NC | NC | NC |
| Left End | -1 | -0.81 | 3.3E-3 | -1 | -1.5 | 2.9E-3 | -1 | -1.2 | -1 |
| Right End | 1 | 0.68 | 1.2E-2 | 1 | 1.1 | 8.0E-4 | 1 | 1.0 | 1 |
| Full | 0 | 0.17 | 2.1E-4 | 0 | -0.07 | 1.8E-4 | 0 | 0.04 | 0 |

Table 5.4 Sample Contact State Measurement Results for Workpiece #3

(Galvanized Steel, 0.89 mm thick)

| Contact State | Expected X | FMS | | | SGFs | | | Fusion | |
|---|---|---|---|---|---|---|---|---|---|
| | | X1 | $\sigma_1^2$ | X | X2 | $\sigma_2^2$ | X | X3 | X |
| No Contact | NC | 0.80 | 174 | NC | 2.7 | 31 | NC | NC | NC |
| Left End | -1 | -1.3 | 5.4E-2 | -1 | 0.58 | 191 | NC | -1.3 | -1 |
| Right End | 1 | 0.24 | 2.2E-3 | 0 | 1.1 | 1.3E-4 | 1 | 1.1 | 1 |
| Full | 0 | -0.10 | 1.3E-2 | 0 | 0.70 | 2.6E-2 | 1 | 0.17 | 0 |

Table 5.5 Sample Contact State Measurement Results for Workpiece #4

(Galvanized Steel, 1.88 mm thick)

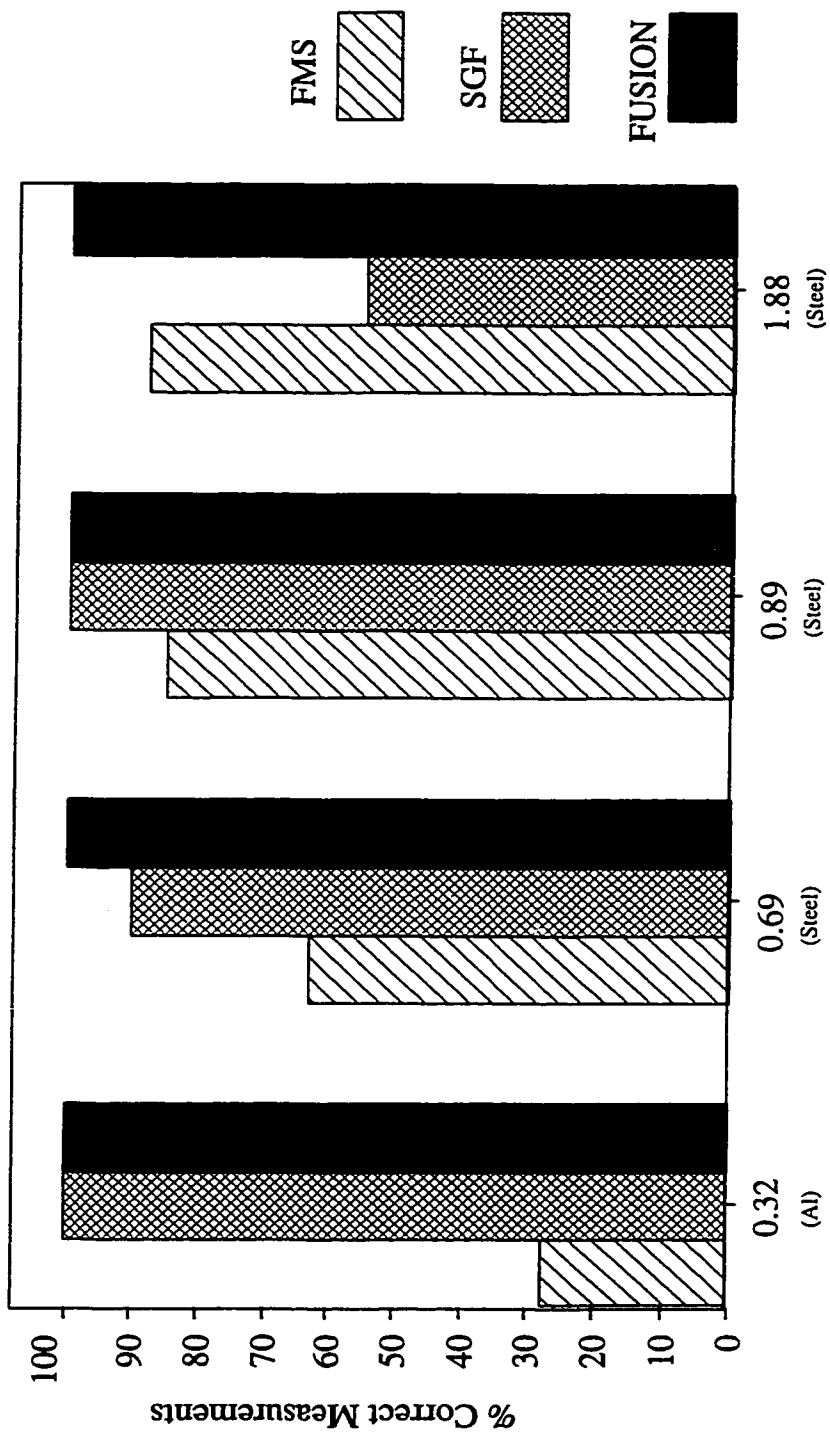


Figure 5.5 Summary of Results of 160 Contact State Measurement Tests

From Table 5.3 for the 0.69 mm steel workpiece (#2), the FMS incorrectly detected left end contact as no contact and right end contact as full contact. The SGFs and sensor fusion again produced no incorrect measurements. Note that the magnitude of X2 for either end contact is much greater than the expected value of unity. When the experiments were performed, the workpiece was observed deflecting forwards on the end opposite to where the contact occurred. In developing the SGFs method it was assumed that the deflection only occurred at the contact end. Although this assumption was incorrect for this workpiece, the larger magnitudes of the experimental results only helped to distinguish between the end and full contact states. From Figure 5.5, it can be seen that with this workpiece the FMS had a success rate of 63%, and the SGFs 90%. This pattern was expected since the relatively high flexibility of the workpiece made it poorly suited to FMS and well suited to the SGFs. An 100% success rate was achieved for sensor fusion. It was expected that sensor fusion would only match the best individual sensor. The improved success may be understood by comparing the X1, X2 and X3 values in Table 5.3 to the expected X values. In two of the three contact cases, sensor fusion tended to cancel out the errors in X1 and X2, bringing X3 much closer to the expected values. This may also be observed in some of the sample results given in Tables 5.4 and 5.5.

For the 0.89 mm thick steel workpiece (#3) all three methods produced correct measurements for the sample results given in Table 5.4. The overall success rates for the FMS, SGFs and sensor fusion were 85%, 100% and 100%, respectively. The decreased workpiece flexibility should have increased the success rate of the FMS and decreased the SGFs success rate. Although the rate for the SGFs did not decrease in the absolute sense,

it did decrease relative to the FMS by 12%.

The expected trend of increasing the FMS success rate relative to SGFs with increasing sheet thickness continued with the 1.88 mm thick steel workpiece (#4). In comparison to workpiece #3 the FMS rate increased by 3% while for the SGFs it decreased by 45%. For the sample results given in Table 5.5, the SGFs produced two incorrect measurements and the FMS produced one. Once again, sensor fusion produced no incorrect measurements.

The frequency distributions of the sensor fusion decision index, X3, for each of the workpieces and contact states are shown in Figure 5.6. From this data it can be seen that none of the values came close to crossing over the decision boundaries (at -½ and ½) to produce an incorrect result. The distributions for left and right end contact for workpiece #1 were noticeably wider than for the other workpieces. At the same time the increased magnitude of the values helped to prevent incorrect decisions (as previously mentioned).

The 100% success rate in all these tests for sensor fusion indicates that the decision boundaries and the NC threshold, T were properly selected. However, if the FMS and SGFs are considered individually, there is an argument for changing T. The average estimated standard deviations for X1 and X2 under no contact were 6.3 and 7.1, respectively. As these are much larger than T, the probability of detecting no contact as contact was very low and did not occur in any of the tests. However, a contact state was incorrectly identified as no contact in 23% of the FMS and SGFs tests. If T was moved closer to the NC $\sigma$ values, this percentage could be decreased without greatly affecting the probability of incorrectly detecting no contact as contact.

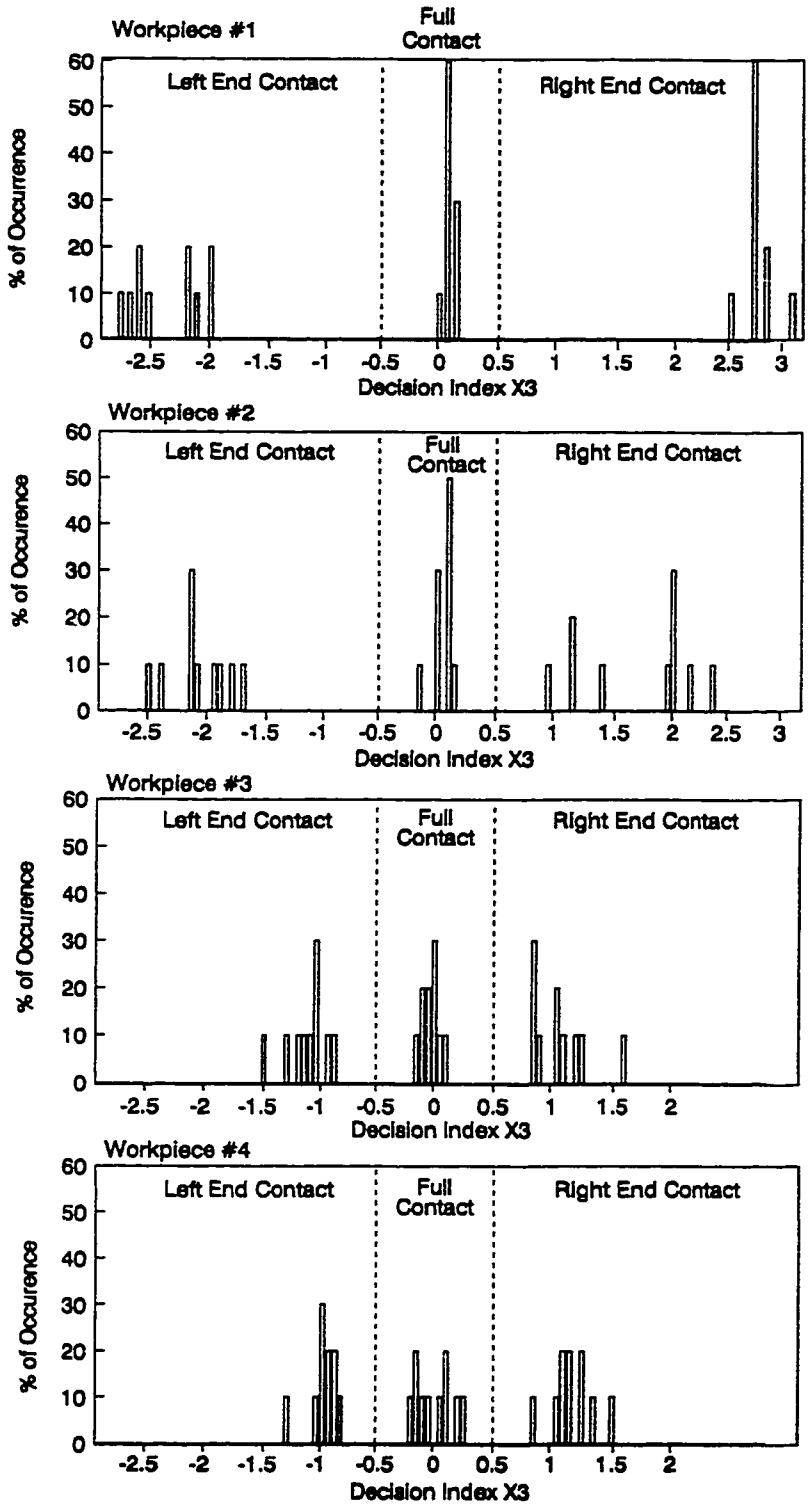


Figure 5.6 Frequency Distributions of X3 for All of the Contact Tests

## 5.6 CONTACT STATE MEASUREMENT FOR 3-D PARTS ASSEMBLY

Contact state measurement methods employing a Force/Moment Sensor (FMS) and Strain Gauge Fingers (SGFs) respectively, were developed in section 5.1 for 2-D sheet metal parts assembly. The main equations employed in the FMS and SGFs systems for handling 2-D parts are extended here to deal with the 3-D parts on hand. The scheme proposed here is applicable to any misalignment on the Pitch and Yaw angles in either of the two sheet metal parts. The initial position and orientation of two parts to be assembled is shown on the left of Figure 5.7.

The coordinate system of the FMS is shown in Figure 5.8, while the SGFs system is shown in Figure 5.9. For the FMS system, the normalized decision index, $X1_{FMS}$, for the measurement of left or right end contact is obtained as:

$$X1_{FMS} = \frac{M_y}{F_z \cdot D1} \qquad (5.19)$$

where $M_y$ is the moment along the y-axis, $F_z$ is the force along the z-axis, D1 is the horizontal distance from the centre of the FMS to the edge of the part. In order to extend the algorithm for the measurement of the top and bottom end contact, the normalized decision index, $X2_{FMS}$ is formed as:

$$X2_{FMS} = \frac{M_x}{F_z \cdot D2} \qquad (5.20)$$

where $M_x$ is the moment along the z-axis, D2 is the vertical distance from the centre of the FMS to the edge of the part. In the case of the SGF system, the strain gauge signals V1 to V4 respectively obtained from SGFs 1 to 4 are first combined according to the following

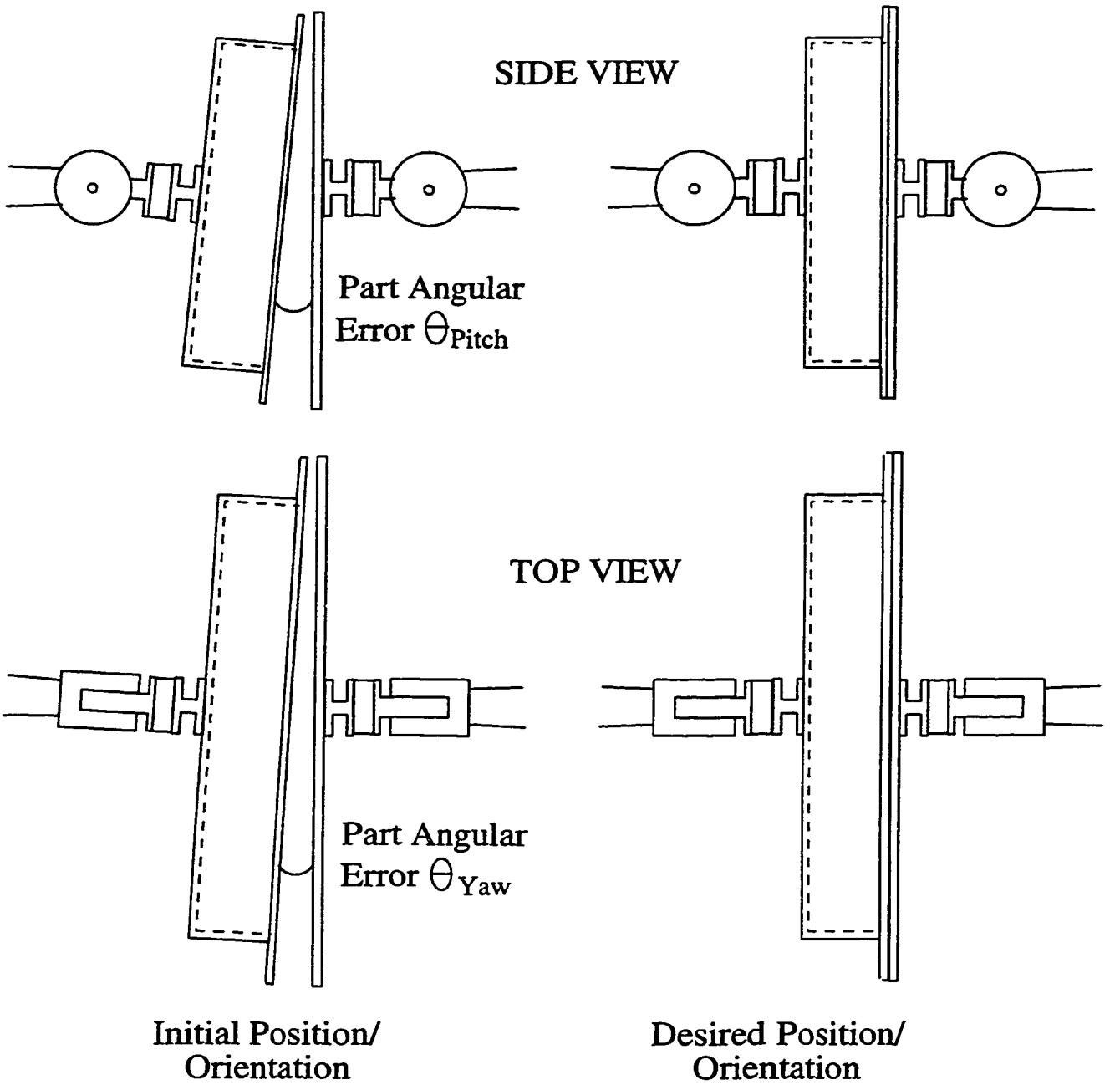


Figure 5.7 3-D Sheet Metal Part's Orientation Before and After Assembly

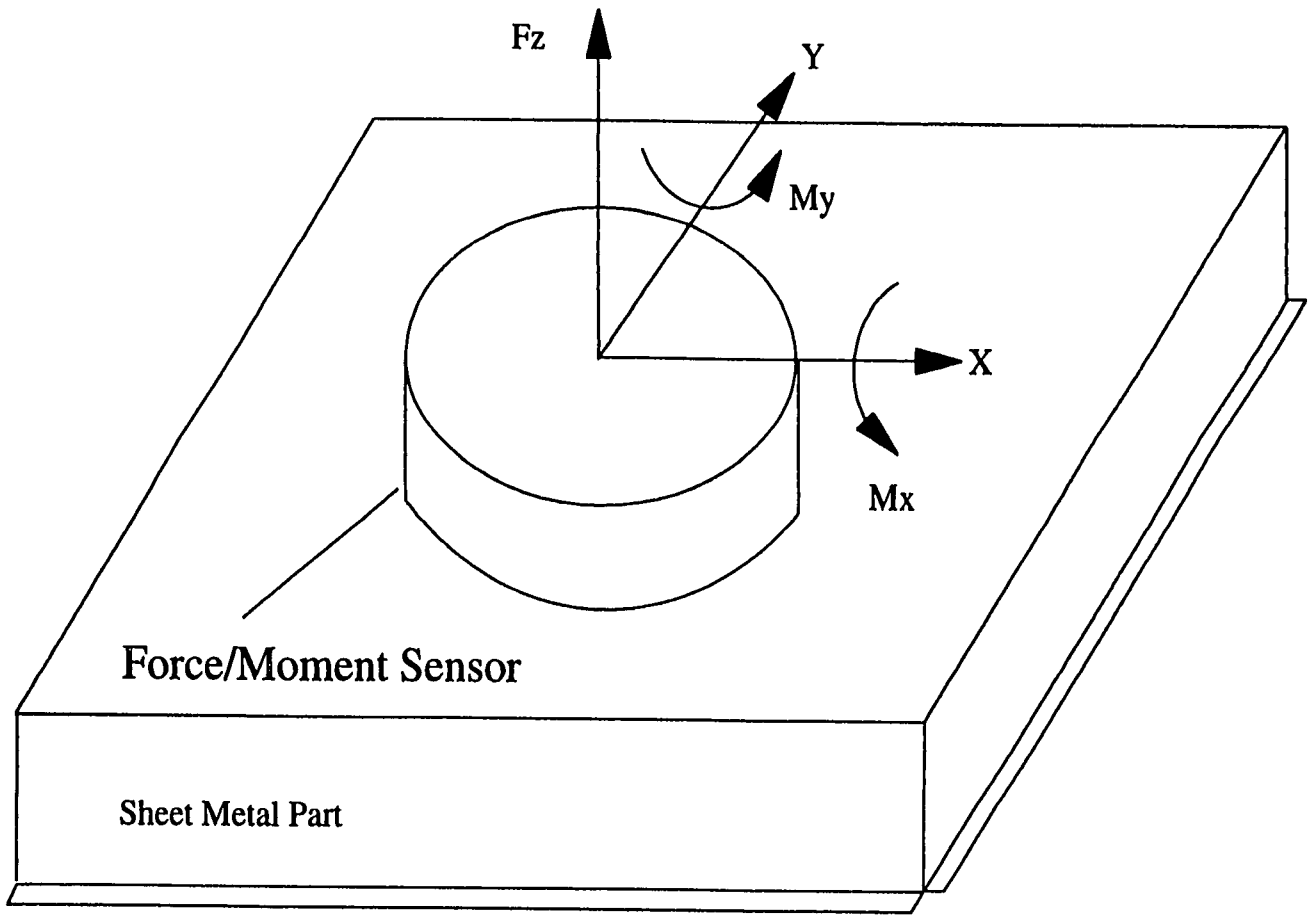


Figure 5.8 Force/Moment Sensor Coordinate System

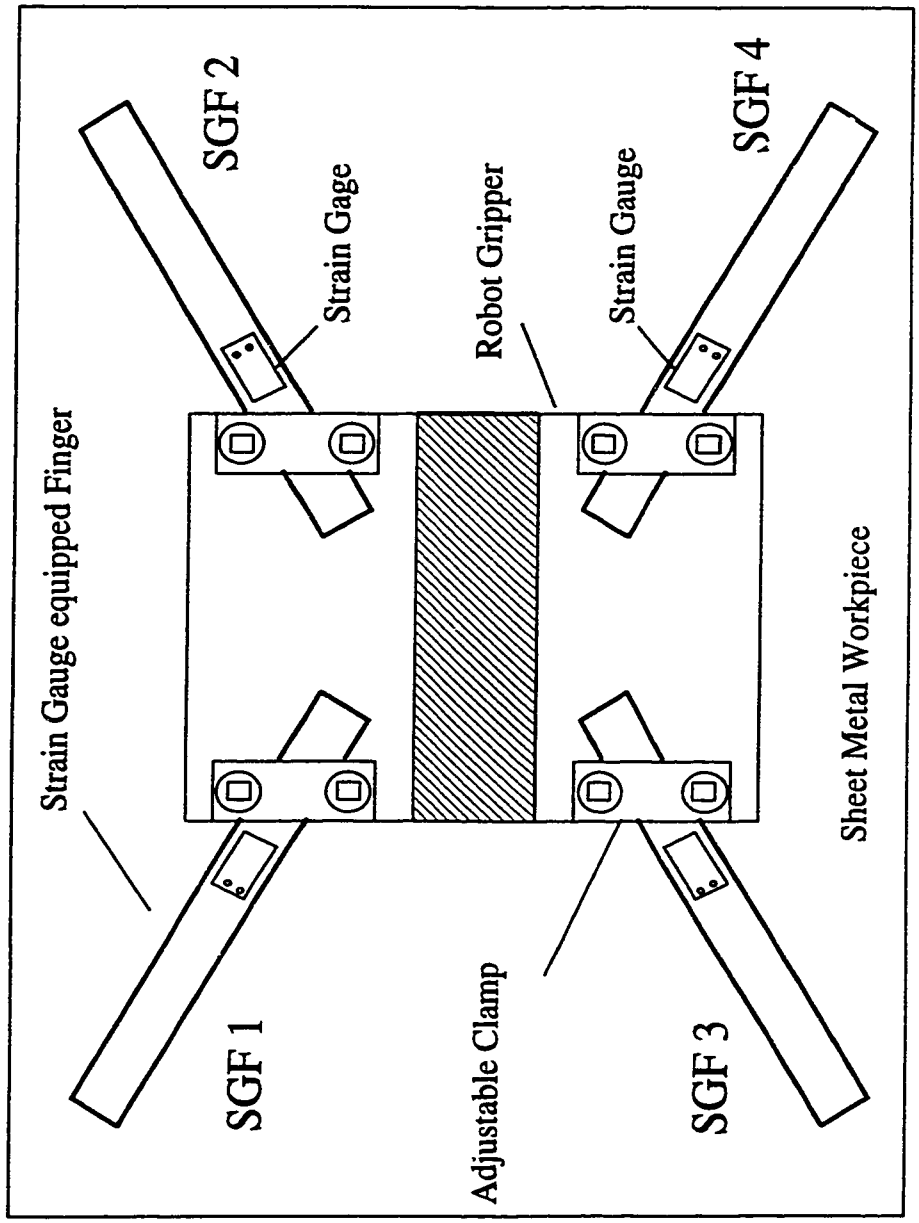


Figure 5.9 Strain Gauge-equipped Fingers System

formulas:

$$VL = V1 + V3 \qquad (5.21)$$

$$VR = V2 + V4 \qquad (5.22)$$

$$VB = V3 + V4 \qquad (5.23)$$

$$VT = V1 + V2 \qquad (5.24)$$

where VL, VR, VT and VB are the strain gauge voltage from the left, right, top and bottom end of the part, respectively. Then the normalized output for left and right hand contact, $X1_{SGF}$ is obtained as:

$$X1_{SGF} = \frac{VR - VL}{VR + VL} \qquad (5.25)$$

Similarly, the normalized output for top and bottom contact, $X2_{SGF}$ is obtained as:

$$X2_{SGF} = \frac{VT - VB}{VT + VB} \qquad (5.26)$$

Under ideal conditions, for both the FMS and SGFs, X1 should equal -1, 0 and 1 for left end, full and right end contact, respectively. Similarly, X2 should equal -1, 0 and 1 for bottom end, full and top end contact, respectively. X1 and X2 will vary between these limits for intermediate contact states.

For fusion of the FMS and SGF sensory information for the left and right contact, the decision indices $X1_{FMS}$ and $X1_{SGF}$ are combined to give the maximum likelihood estimate [34]:

$$X3_{LR} = \frac{\sigma_{1SGF}^{-2}}{\sigma_{1SGF}^{-2} + \sigma_{1FMS}^{-2}} \cdot X1_{SGF} + \frac{\sigma_{1FMS}^{-2}}{\sigma_{1SGF}^{-2} + \sigma_{1FMS}^{-2}} \cdot X1_{FMS} \quad (5.27)$$

where $X3_{LR}$ is the decision index for the left and right contact for the sensor fusion method, ${\sigma_1}^2_{SGF}$ is the estimated variance of $X1_{SGF}$ and ${\sigma_1}^2_{FMS}$ is the estimated variance of $X1_{FMS}$. Note that $X3_{LR}$ should also produce the desired values of -1, 0 and 1 for left end, full and right end contact, respectively. Similarly, for top and bottom contact:

$$X3_{TB} = \frac{\sigma_{2SGF}^{-2}}{\sigma_{2SGF}^{-2} + \sigma_{2FMS}^{-2}} \cdot X2_{SGF} + \frac{\sigma_{2FMS}^{-2}}{\sigma_{2SGF}^{-2} + \sigma_{2FMS}^{-2}} \cdot X2_{FMS} \quad (5.28)$$

where $X3_{TB}$ is the decision index for the top and bottom contact for the sensor fusion method, ${\sigma_2}^2_{SGF}$ is the estimated variance of $X2_{SGF}$ and ${\sigma_2}^2_{FMS}$ is the estimated variance of $X2_{FMS}$. Again $X3_{TB}$ should also produce the desired values of -1, 0 and 1 for top end, full and bottom end contact, respectively.

## 5.7 CONCLUSIONS

Three contact state measurement algorithms for 2-D parts assembly were developed based on feedback signal coming from a FMS, SGFs and the fusion of the FMS and SGFs sensory information, respectively. Based on 160 tests performed using 2-D sheet metal parts

with four different stiffnesses, the performance of these algorithms was evaluated. It was found that the FMS was more effective with stiffer parts, while the SGFs were better suited for more flexible parts. The sensor fusion system maintained a 100% success rate in all tests, and surpassed the best individual performance of the FMS and SGFs. It is also shown that a trade-off exists between the measurement time and the measurement success rate.

The contact state measurement algorithms developed for 2-D parts were extended to allow the contact state of 3-D parts to be measured. In Chapter 6, the majority of the algorithms developed in this chapter are implemented for the control of contact state for 2-D and 3-D sheet metal parts.

# Chapter 6

# Control of the Contact State

## 6.1 INTRODUCTION

In this chapter, an Integral Contact Controller (ICC) [ 37 ] is developed to control the contact state between 2-D and 3-D sheet metal parts. The ICCs performance is tested experimentally. Furthermore, ICSM is combined with the ICC and comparisons are made.

## 6.2 CONTROL OBJECTIVE

The objective for the control of contact state for the 2-D case is to move one of the parts to a position and orientation, as shown on the right of Figure 6.1, in the minimum amount of time, such that the angular error, $\theta_2$ , becomes small enough to meet the +/- 0.1 mm alignment accuracy at the mating edge, as stated in section 3.2, and full contact is achieved along the lap joint formed between the parts. Similarly, the control objective for 3-D parts is to move one of the parts to a position and orientation, as shown on the right of Figure 5.7, in the minimum amount of time, such that the angular errors, $\theta_{Pitch}$ and $\theta_{Yaw}$, become small enough to meet the +/- 0.1 mm alignment accuracy required, and the part edges where welding will be performed are in full contact.

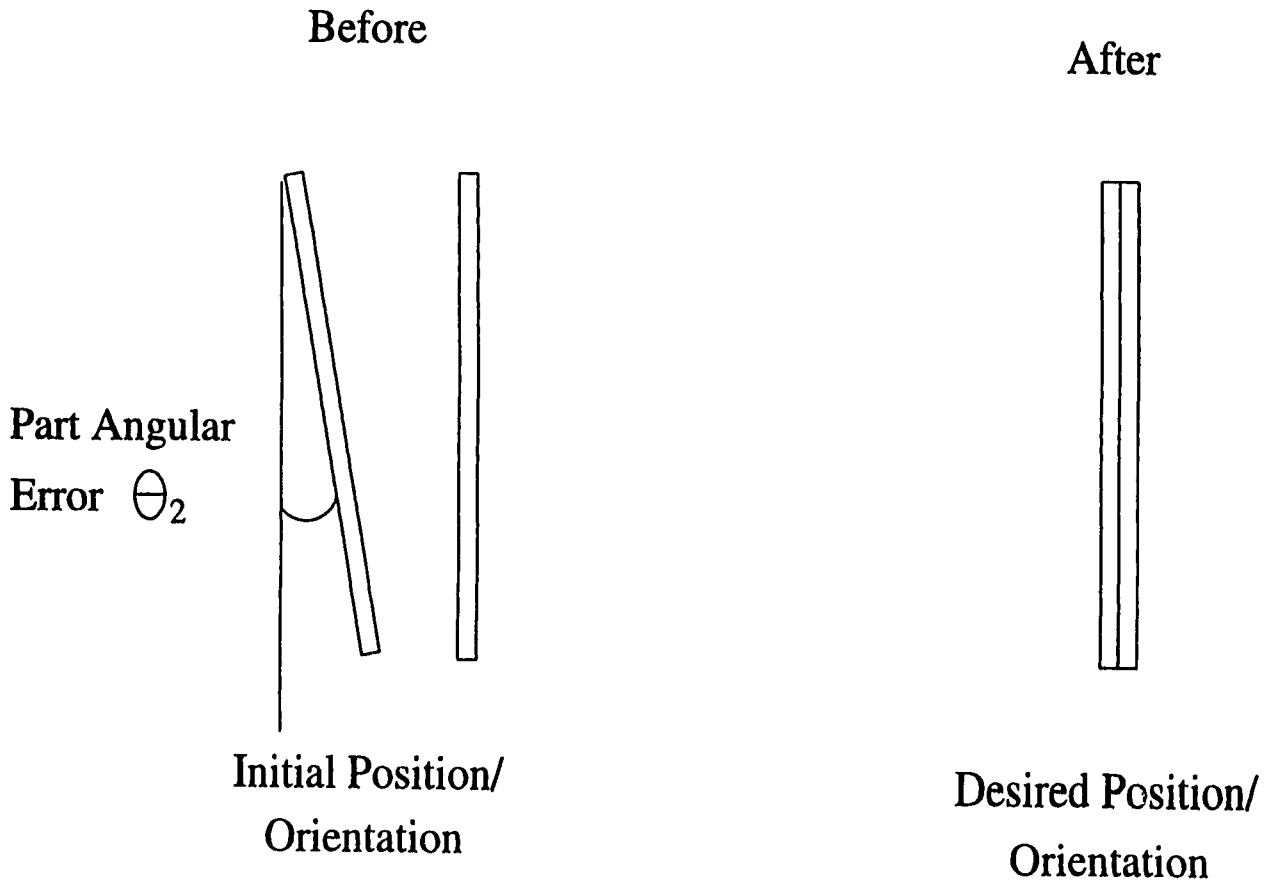


Figure 6.1 Top View of Two 2-D Sheet Metal Parts Before and After Assembly

## 6.3 THE INTEGRAL CONTACT CONTROL (ICC) ALGORITHM FOR 2-D PARTS

An integral controller was designed to eliminate the part's angular error using the fusion of the FMS and SGF sensory information as follows:

$$\Delta\theta_2 = K\cdot(X3^* - X3) \qquad (6.1)$$

where $\Delta\theta_2$ is the change in part orientation angle with respect to the point of contact, K is the controller gain, X3 is the decision index for the sensor fusion method, X3* is the setpoint value for X3. Since it is desired to get full contact between the parts to be assembled, X3* is set to be zero. Therefore the control equation becomes:

$$\Delta\theta_2 = -K \cdot X3 \qquad (6.2)$$

or after rearranging:

$$\theta_2 = \frac{-K \cdot X3}{\Delta} \qquad (6.3)$$

The Integral Contact Control (ICC) algorithm starts with taking measurements from the FMS and SGFs sensors. To determine whether the initial contact is achieved, the following two criteria are used:

$$S_m > Th1, \quad m = 1,2,3,4 \qquad (6.4)$$

and

$$\sigma_n \leq T, \quad n = 1,2 \qquad (6.5)$$

where $S_m$ are the sensor readings of $F_y$, $M_z$ and the two SGFs. Th1 is a threshold value to distinguish the signal due to noise from the signal due to contact. Th1 was set at 0.1 Volts. $\sigma_1$ and $\sigma_2$ are the estimated standard deviation of the FMS and SGF signals, respectively. T was set at 1/6 as suggested in section 5.3.

If initial contact is not detected, the robot will move the part 1 mm towards the other part until initial contact is detected. Once initial contact is detected, the contact state decision index X3 is calculated using the fusion of the FMS and SGFs signal. To prevent oscillations near full contact due to measurement noise, X3 was mapped according to:

$$X3 = 0, \quad -0.15 \leq X3 \leq 0.15 \qquad (6.6)$$

If X3 is not mapped into 0, then the integral control law (6.3) is used to calculate the necessary angular rotation to correct the angular error. The gain K was manually tuned to 0.58. When X3 = 0, the controller is shut off.

### 6.3.1 Experimental Verification of ICC with 2-D Parts

The GMF robot used for the contact state measurement experiments was used here to test the ICC. A six-degree-of-freedom $JR^3$ force/moment sensor was attached between the robot wrist and the gripper. Two SGFs were attached to the robot gripper, as shown previously in Figure 3.1. A 0.69 mm thick steel sheet (workpiece #2 from Table 5.1) and a 1.88 mm thick steel sheet (workpiece #4 from Table 5.1) were employed in the experiments. A third flat sheet metal part was mounted rigidly on a work table as if it were held by another robot during assembly. Since the control of contact is intended to come from one of the

robots only, this setup does not affect the generality of the result. Two dial gauges mounted on the work table were used to measure the deflection of the stationary sheet at the two ends of the contact edge. This provided external verification of the experimental results. If full contact is achieved between two parts, the deflection at the two ends of the contact edge should be the same.

The block diagram of the ICC implemented for the 2-D parts contact state control experiments is shown in Figure 6.2. The GMF robot employed for the experiment was controlled by a Delta Tau PMAC control board. The robot's joint position was controlled at 2260 Hz through encoder feedback. The contact state information was measured by both the SGFs and FMS. The SGFs signal was first amplified then filtered by a low pass filter at 10 Hz to prevent aliasing. The FMS signal was sampled at 95 Hz by the JR3 signal processor, which had a 16 Hz low pass filter installed. The processed sensor information was then sampled and converted by the Delta Tau ACC-28 A/D board at 18 kHz. The sampled sensor information was used to compute the contact state decision index, X3, for the sensor fusion method using the procedure from Chapter 5. After performing the mapping based on (6.6), the ICC control algorithm was then used to calculate the required control action to modify the contact state. The computation of X3, the mapping based on (6.6) and the ICC control were all implemented in a Delta Tau motion control program. The program is listed in Appendix C. An average velocity of 8 deg/s was chosen, and a maximum output of 1 degree per control cycle was allowed for safety reasons. This gave the ICC controller a maximum output rate of 8 times per second i.e. 8 Hz. However, some computational effort was required to update the monitor screen to inform the user about the current contact before the control

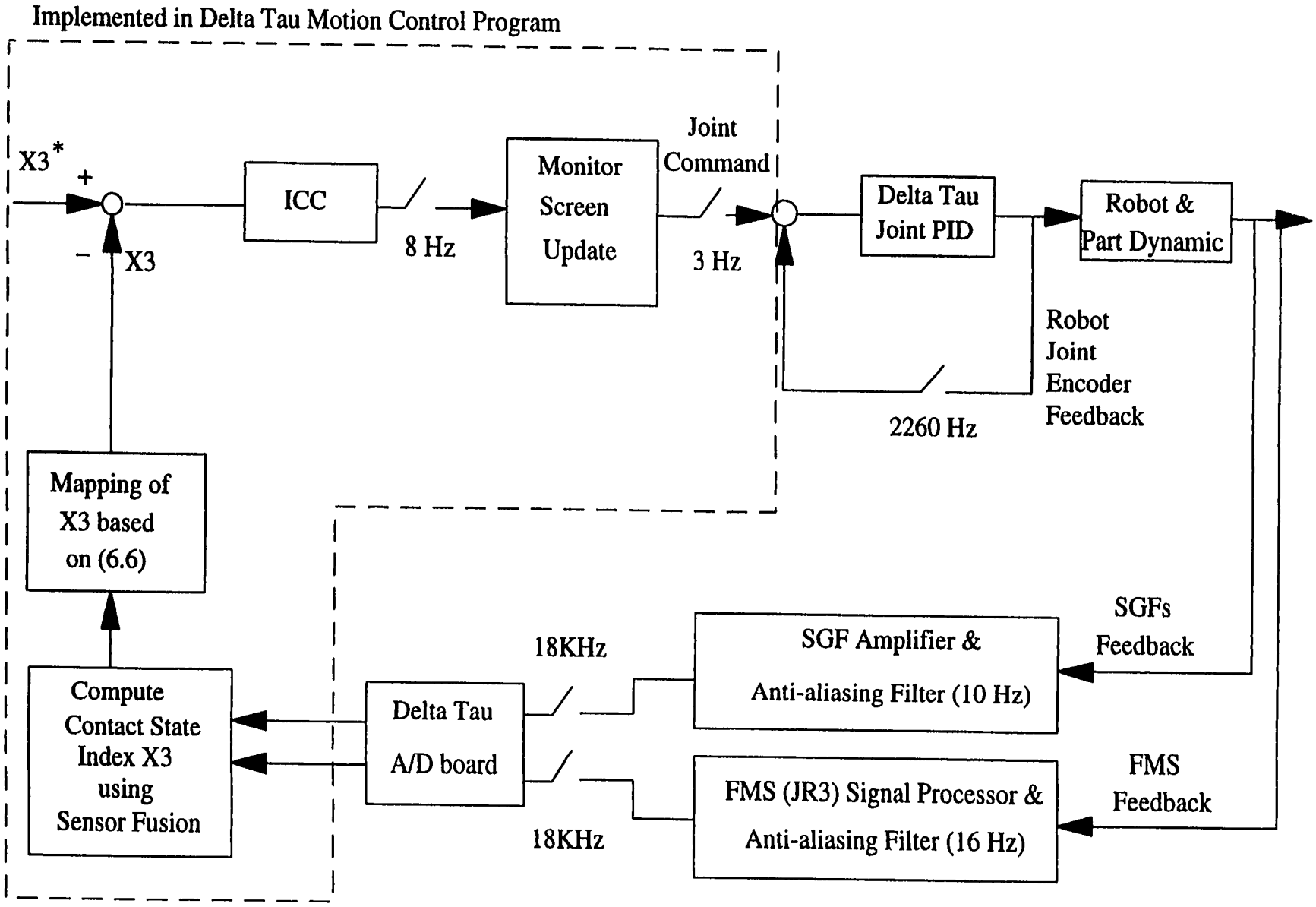


Figure 6.2 Block Diagram of the ICC Implementation for the Contact State Control Experiment for 2-D Parts

signal was sent to the joint. Therefore, the final ICC control command update rate was limited to 3 Hz.

#### 6.3.1.1 Experimental Procedure for ICC with 2-D Parts

The sheet metal part was held tightly by the robot gripper at the centre of its top edge, as shown in Figure 3.1. The robot positioned the part in front of the table mounted part, leaving about a 4 mm gap between them to act as a positioning error. The robot then rotated the part for an angle $\theta_2$ to generate an angular error between the parts. After the rotation, the shortest distance between the two parts was about 2 mm. The robot then moved the part using the ICC algorithm with the fusion of the FMS and SGF sensory information until full contact was achieved.

#### 6.3.1.2 Experimental Results for ICC with 2-D Parts

Angular errors of +0.5 and -0.5 degrees were tested five times each with the 0.69 mm and 1.88 mm thick sheet metal parts, respectively. Typical angular error versus time graphs for handling the two sheets are shown in Figures 6.3 and 6.4, respectively. In all of the tests, it took less than two seconds to correct the angular error to within 0.025° accuracy, and the difference between the dial gauge readings at the two ends of the contact edge was within 0.05 mm. This alignment accuracy was two times better than the required accuracy of +/- 0.1 mm.

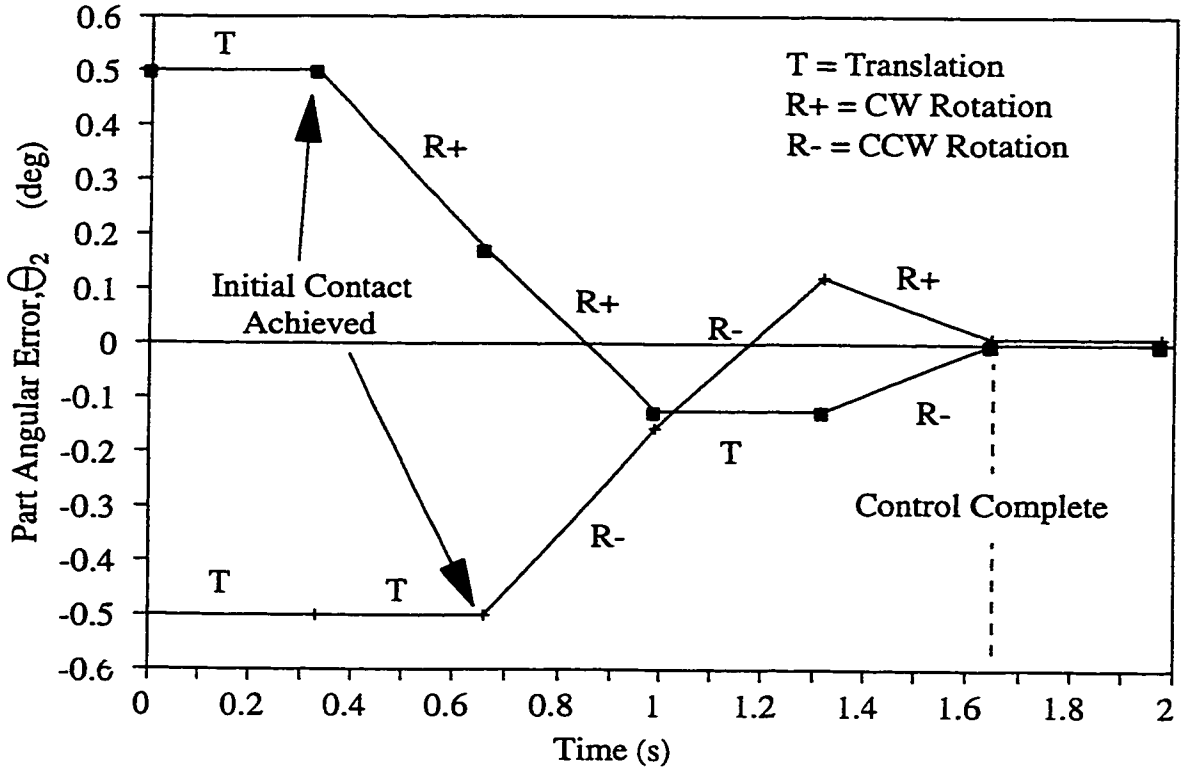


Figure 6.3 Angular Error Versus Time Graph for the Thin (0.69mm) Part (2-D Parts Experiment using Sensor Fusion)

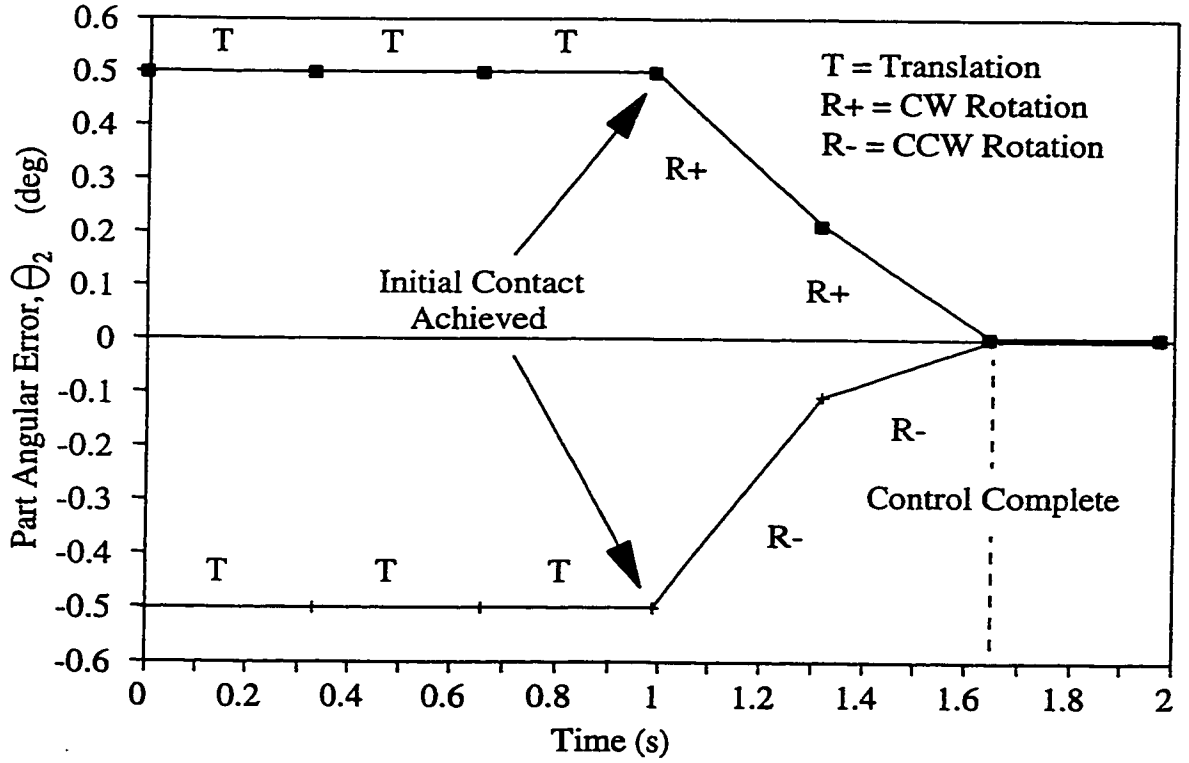


Figure 6.4 Angular Error Versus Time Graph for the Thick (1.88mm) Part (2-D Parts Experiment using Sensor Fusion)

## 6.4 THE ICC ALGORITHM FOR 3-D PARTS

For the control of contact state for 3-D parts assembly, the sensor fusion algorithm requires at least the readings of $F_z$ , $M_x$ , $M_y$ from the FMS and the reading from four SGFs. Therefore altogether seven A/D channels are required. Due to limitation in the number of A/D channels available, only four sensor readings could be fed into the controller simultaneously. The integral controller developed previously for 2-D parts using sensor fusion is modified as follows to use either the FMS or the SGFs to measure the contact state:

$$\Delta\theta_{Yaw} = K\cdot( X1^{*} - X1 ) \qquad (6.7)$$

and

$$\Delta\theta_{Pitch} = K\cdot( X2^{*} - X2 ) \qquad (6.8)$$

where $\Delta\theta_{Yaw}$ is the change in the part's Yaw angle with respect to the point of contact, $\Delta\theta_{Pitch}$ is the change in the part's Pitch angle with respect to the point of contact, K is the controller gain, X1 is the decision index for left and right contact obtained using the FMS or the SGFs, X1* is the setpoint value for X1, X2 is the decision index for top and bottom contact obtained using the FMS or the SGFs, and X2* is the setpoint value for X2. Since it is desired to get full contact between the parts to be assembled, both X1* and X2* are set to be zero. Therefore the control equations become:

$$\Delta\theta_{Yaw} = -K \cdot X1 \qquad (6.9)$$

and

$$\Delta\theta_{Pitch} = -K \cdot X2 \qquad (6.10)$$

or after rearranging:

$$\theta_{Yaw} = \frac{-K \cdot X1}{\Delta} \qquad (6.11)$$

and

$$\theta_{Pitch} = \frac{-K \cdot X2}{\Delta} \qquad (6.12)$$

Similar to the ICC algorithm for 2-D parts, the ICC algorithm for 3-D parts starts with taking measurements from either the FMS or the SGFs. To determine whether the initial contact is achieved, the following two criteria are used:

$$S_m > Th1, \quad m = 1,2,3,4 \qquad (6.13)$$

and

$$\sigma_n \leq T, \quad n = 1,2 \qquad (6.14)$$

where $S_m$ are the sensor readings of $F_z$, $M_x$, $M_y$ or the four SGFs. Th1 is a threshold value to distinguish the signal due to noise from the signal due to contact. Th1 was set at 0.1 Volts. $\sigma_1$ and $\sigma_2$ are the estimated standard deviation of the FMS and SGF signals, respectively. T

was set at 1/6 as suggested in section 5.3.

Again, if initial contact is not detected, the robot will move the part 1 mm towards the other part until initial contact is detected. Once initial contact is detected, the contact state decision indices X1 and X2 will be calculated using either the FMS alone or the SGFs alone. To prevent oscillations near full contact due to measurement noise, X1 and X2 were mapped according to:

$$X1 = 0, \quad -0.15 \leq X1 \leq 0.15 \tag{6.15}$$

and

$$X2 = 0, \quad -0.15 \leq X2 \leq 0.15 \tag{6.16}$$

If either X1 or X2 is not mapped into 0, then the integral control law (6.11) or (6.12) is used to calculate the necessary rotation in Yaw or Pitch angle to correct the angular error. The gain K was manually tuned to 0.15 for both X1 and X2. When X1 and X2 = 0, the controller is shut off.

### 6.4.1 Experimental Verification of ICC with 3-D Parts

The GMF robot and the 3-D part used for the vibration control experiments were used here to test the ICC. A six-degree-of-freedom JR$^3$ force/moment sensor was attached between the robot wrist and the gripper. A 560 x 460 x 1.88 mm flat sheet metal part was held rigidly by a PUMA 760 robot to be assembled with the 3-D part. Since the control of contact is intended to come from one of the robots only, the PUMA robot was kept stationary

throughout the whole assembly process. The experimental setup employed is shown in Figure 6.5.

The block diagram of the ICC implemented for the 3-D parts was basically the same as the one shown in Figure 6.2 for the 2-D case; except that either the FMS or the SGFs was used and the final effective joint command update rate was 4.3 Hz instead of 3 Hz. This increase in control command rate was achieved by reducing the amount of information printed on the monitor screen before each joint command was sent to the Delta Tau controller. The program listings for the implementation of ICC using FMS and SGFs are given in Appendices D and E, respectively.

#### 6.4.1.1 Experimental Procedure for ICC with 3-D Parts

The 3-D sheet metal part was held tightly by the GMF robot gripper at the centre. The robot positioned the part in front of the stationary part held by the PUMA robot leaving about a 6 mm gap between them to act as a positioning error. The robot then rotated the part for a Pitch angle of 0.5° and Yaw angle of 0.5° to generate angular errors between the parts, as shown in Figure 5.7. After the rotations, the shortest distance between the two parts was about 2 mm. The robot then moved the part using the ICC algorithm until full contact was achieved.

#### 6.4.1.2 Experimental Results for ICC with 3-D Parts

Tests were repeated five times using the FMS system and the SGFs system, respectively. Typical angular error versus time graphs for assembling the two sheet metal

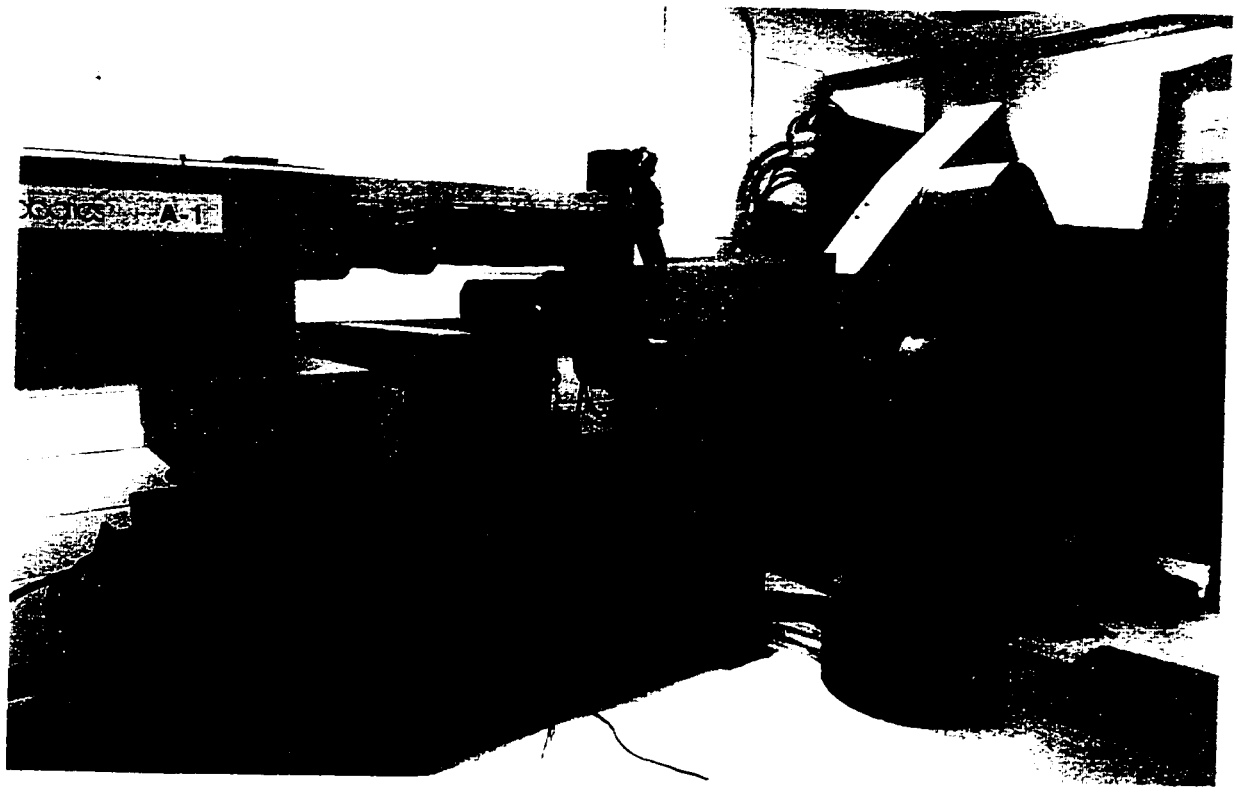

Figure 6.5 Experimental Setup for the Contact State Control Tests for 3-D Parts

parts using the two sensor systems are shown in Figures 6.6 and 6.7, respectively. In all of the tests, when the FMS system was in use, it took less than 2.4 seconds to correct the angular error to within 0.05° accuracy. When the SGFs system was employed, in all of the tests, it took less than 3.6 seconds to achieved the same degree of accuracy. With a 0.05° angular accuracy, in order to achieve the required +/- 0.1 mm accuracy at the mating edge, assuming that the part is held at the center, the length and width of the part are limited to 230 mm. The sheet metal part used in the experiment was too large for the system to handle to achieve the required accuracy.

The fact that it took longer for the SGF system than for the FMS system to correct the errors shows that the part handled by the GMF robot was relatively rigid; therefore, when in contact, it generated higher force but less deflection. As a result, when the same gain value was used in the controllers, the effective gain for the FMS system was higher than that of the SGF system. The higher gain made the FMS system detect the initial contact in 4 translations as opposed to 6 for the SGFs system, and respond more rapidly to the angular errors.

It is expected that if there is no need to update the contact state information on the monitor screen, the effective control action update rate could be increased from 3 Hz to 8 Hz, and the cycle time required could be reduced by almost three times. As mentioned before, this 8 Hz control action update rate was determined by the average velocity of the robot, which was set at 8 deg/s for the revolute joints and 8 mm/s for the prismatic joints. This average velocity was selected to give the robot a fast response, yet be slow enough to not to excite the sheet metal parts vibration too much. In the next section, a method is investigated to see whether the feedrate of the robot could be increased without exciting the vibration of

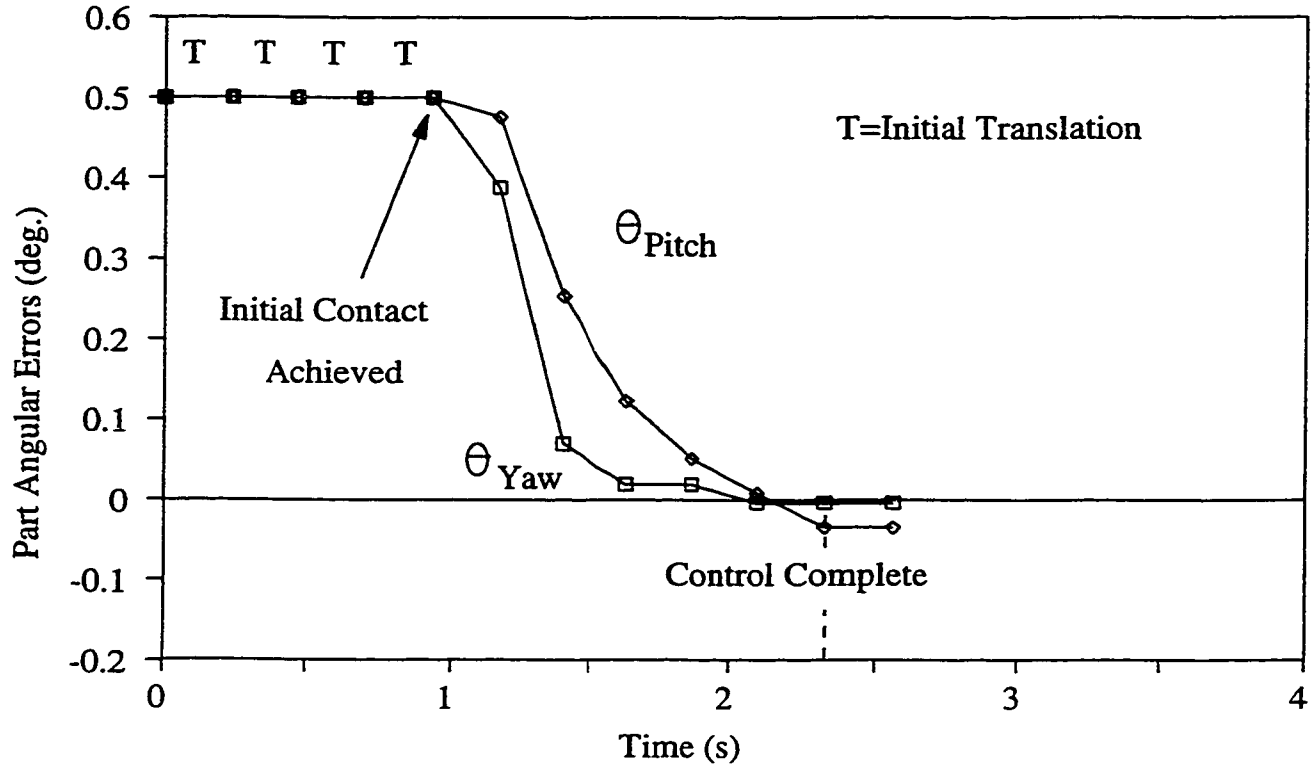


Figure 6.6 Angular Error Vs. Time When Using FMS in 3-D Parts Experiment

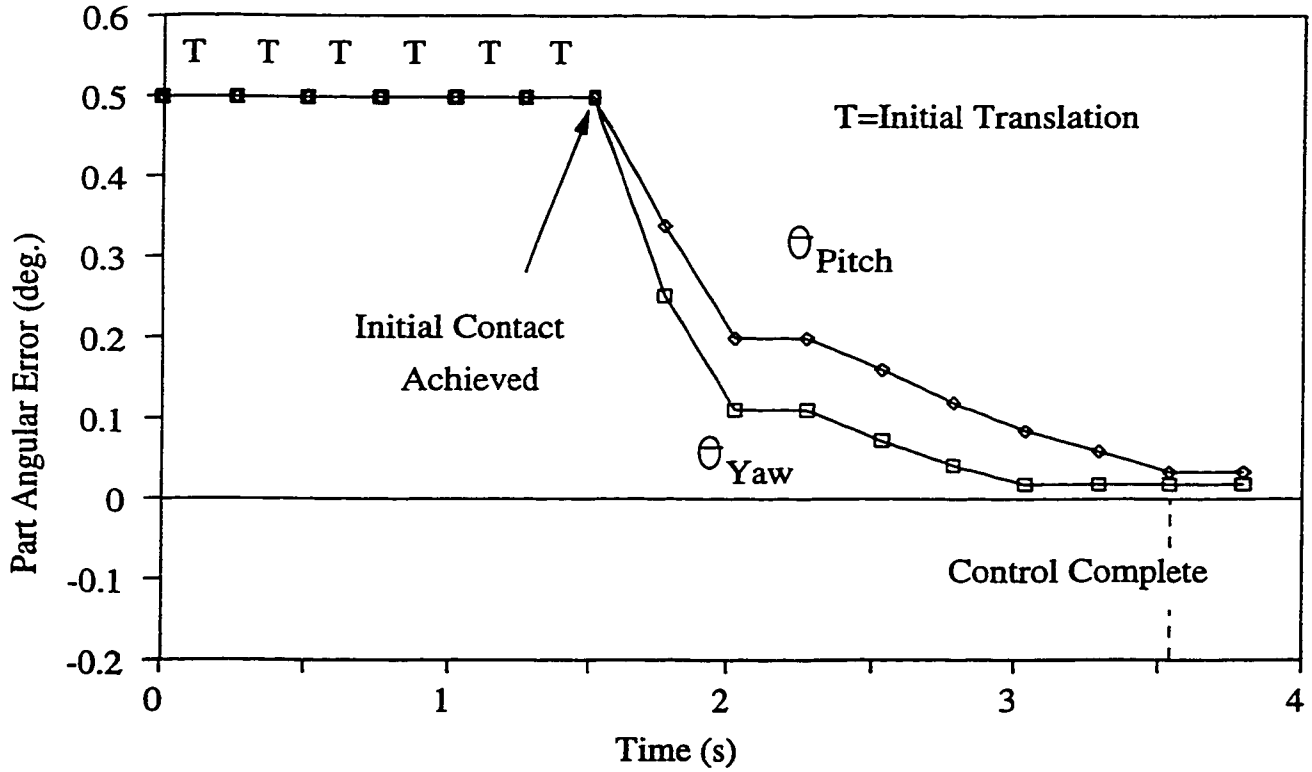


Figure 6.7 Angular Error Vs. Time When Using SGFs in 3-D Parts Experiment

sheet metal parts.

## 6.5 THE APPLICATION OF INPUT COMMAND SHAPING METHOD IN CONTACT STATE CONTROL EXPERIMENTS

To improve production rate, it is desired to speed up the contact state control process during sheet metal parts assembly. One way to reduce the time required to control the contact state is to increase the robot motion's acceleration and/or velocity. However, when this is done, it is much easier to excite the vibration of the part being handled. The Input Command Shaping Method (ICSM) [ 28 ] was shown in Chapter 4 to be very effective in suppressing vibration when sheet metal parts are being handled by robots. Therefore, the ICSM was combined with the ICC in an effort to achieve a faster response in the contact state control experiments. The block diagram of the use of ICSM with ICC is shown in Figure 6.8.

During the contact state control experiments, when no contact was detected between the parts, the controller would command the robot to move Joint 3 forward for 1 mm to bring the parts closer until an initial contact is detected. The ICSM is used to try to speed up this motion without affecting ICC's performance. The following tests were performed using exactly the same setup and procedure described in section 6.4.1 to investigate the effectiveness of the use of ICSM in the contact state control experiments with 3-D sheet metal parts.

(i) Moving joint 3 forward by 1 mm at an average velocity of 8 mm/s with no ICSM applied.

(ii) Moving joint 3 forward by 1 mm at an average velocity of 8 mm/s with ICSM

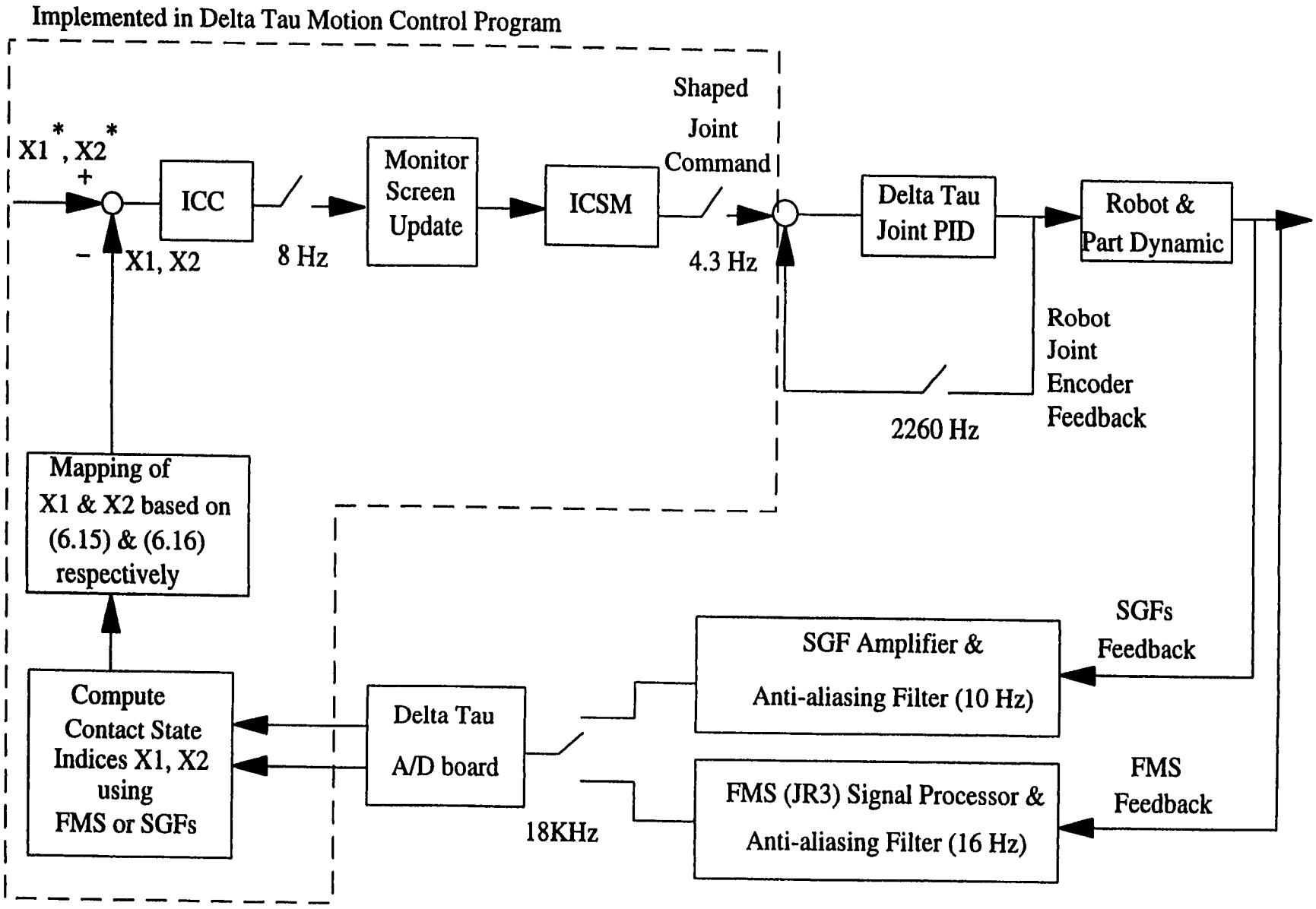


Figure 6.8 Block Diagram of the Implementation of ICSM with ICC for the Contact State Control Experiment for 3-D Parts

applied to suppress the first mode of vibration.

(iii) Moving joint 3 forward by 1 mm at an average velocity of 8 mm/s with ICSM applied to suppress the second mode of vibration.

(iv) Moving joint 3 forward by 1 mm at an average velocity of 5 mm/s with no ICSM applied.

(v) Moving joint 3 forward by 1 mm at an average velocity of 5 mm/s with ICSM applied to suppress the first two modes of vibration.

(vi) Moving joint 3 forward by 1 mm at an average velocity of 5 mm/s with no ICSM applied. Motion repeated 5 times with contact state measurement performed in between motions.

(vii) Moving joint 3 forward by 1 mm at an average velocity of 5 mm/s with ICSM applied to suppress the first two modes of vibration. Motion repeated 5 times with contact state measurement performed in between motions.

### 6.5.1 Experimental Results with ICSM in Contact State Control

Table 6.1 summarizes the average peak-to-peak vibration amplitude obtained from all of the seven test motions. The average amplitude values were calculated using the SGF 1 reading obtained in the first 3 seconds immediately after each motion started.

Typical vibration versus time plots obtained from tests (i), (ii) and (iii) are shown in Figures 6.9, 6.10 and 6.11, respectively. No significant difference was observed when either the FMS or the SGFs were employed for the contact state detection. As discussed before in

| Test Motion | Average Peak-to-peak Vibration Amplitude (mm) | Remarks |
|---|---|---|
| i | 1.54 | Average Vel. = 8 mm/s<br>No ICSM |
| ii | 1.34 | Average Vel. = 8 mm/s<br>ICSM to control first mode |
| iii | 0.75 | Average Vel. = 8 mm/s<br>ICSM to control second mode |
| iv | 0.38 | Average Vel. = 5 mm/s<br>No ICSM |
| v | 0.38 | Average Vel. = 5 mm/s<br>ICSM to control first and second modes |
| vi | 1.01 | Average Vel. = 5 mm/s<br>No ICSM,<br>move 1 mm at a time for 5 mm |
| vii | 2.4 | Average Vel. = 5 mm/s<br>ICSM to control 1st and 2nd modes, move 1 mm at a time for 5 mm |

Table 6.1 Summary of Average Peak-to-peak Vibration Amplitude from the Test Motions

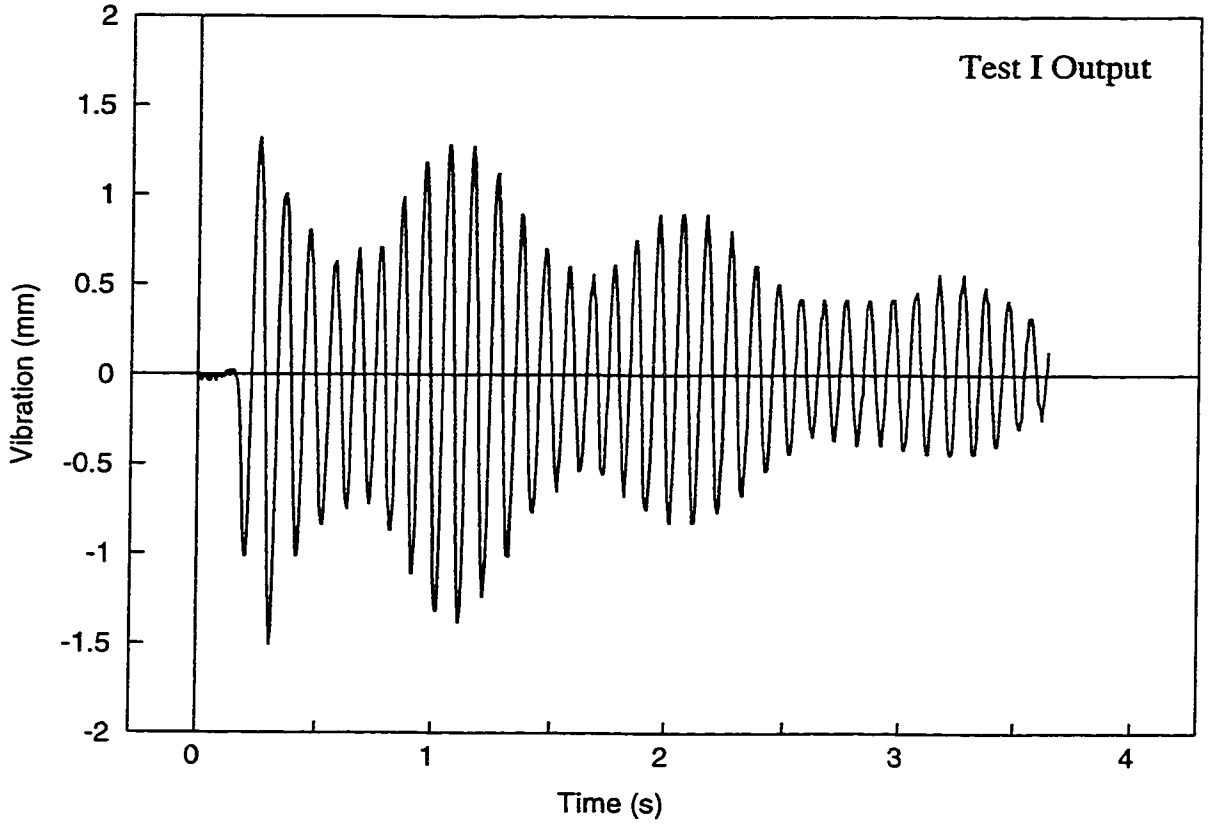


Figure 6.9 Real Time Test Result from Moving Joint 3 by 1 mm
(average velocity = 8 mm/s)
(with no ICSM applied)

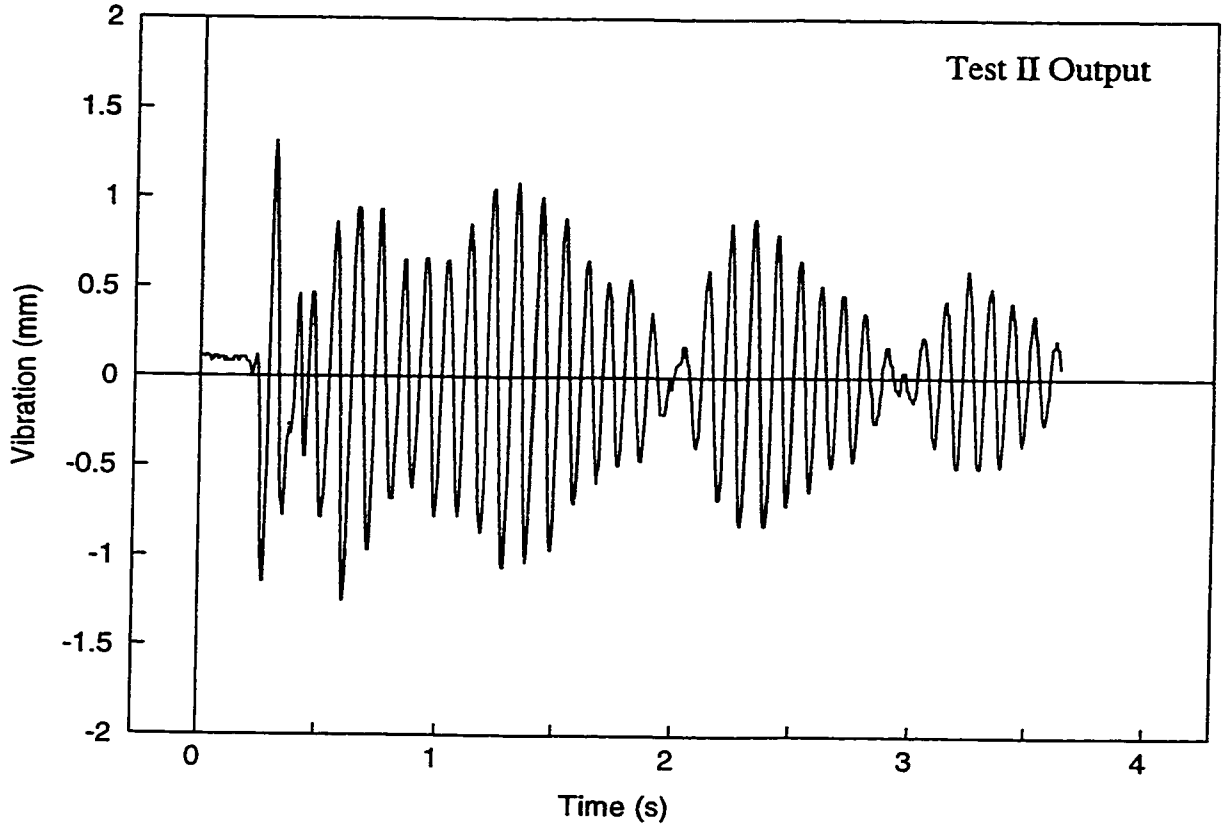


Figure 6.10 Real Time Test Result from Moving Joint 3 by 1 mm
(average velocity = 8 mm/s)
(with first mode of vibration controlled by ICSM)

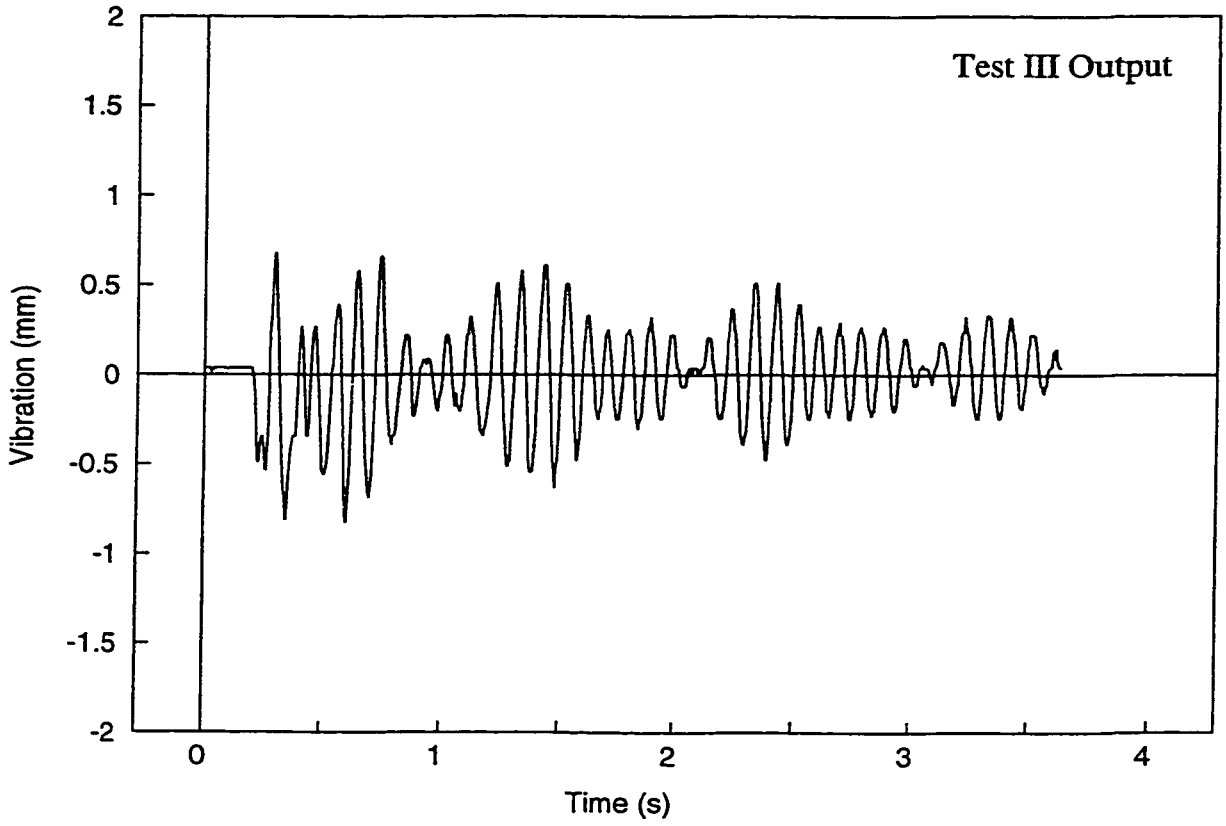


Figure 6.11 Real Time Test Result from Moving Joint 3 by 1 mm
(average velocity = 8 mm/s)
(with second mode of vibration controlled by ICSM)

chapter 4, since the ICSM will create a delay in the input command trajectory, in order to keep the average velocity after the shaping at 8 mm/s, an original input function with higher velocity was used for tests (ii) and (iii). It is clear from these three figures and the average vibration amplitudes shown in Table 6.1 that the ICSM was effective in controlling the vibration of the parts. Although it is expected that suppressing the first mode should reduce the vibration more, it could be due to modelling error that it is more effective in reducing the vibration when the second mode is suppressed.

Since it was determined in Chapter 4 that it is more effective to suppress both the first and second mode of vibration, the next set of tests were performed to investigate the effect of using ICSM to suppress the first two modes of vibration. The first problem encountered in suppressing two modes of vibration was the large time delay created. Using the same original input function employed in the last set of tests, when shaping was applied to suppress the first two modes, the average velocity was reduced from 8 mm/s to 5 mm/s. This represents a 37.5% reduction in speed. In order to make a fair assessment of the effectiveness of the control method, the same velocity was used on the tests with no ICSM applied. Typical vibration versus time plots obtained from tests (iv) and (v) are shown in Figures 6.12 and 6.13, respectively. Comparing these two figures, and the identical vibration amplitude listed in Table 6.1 obtained from test (iv) and (v), one can see that the effect of ICSM is minimal. From Table 6.1, it can be seen that in test (iv), probably because of the low robot speed, the average vibration amplitude was only 0.38 mm even with no ICSM implemented. Since the ICSM algorithm only controlled the first two modes of vibration, the residual vibration from vibration modes that are not controlled is relatively large when the original vibration

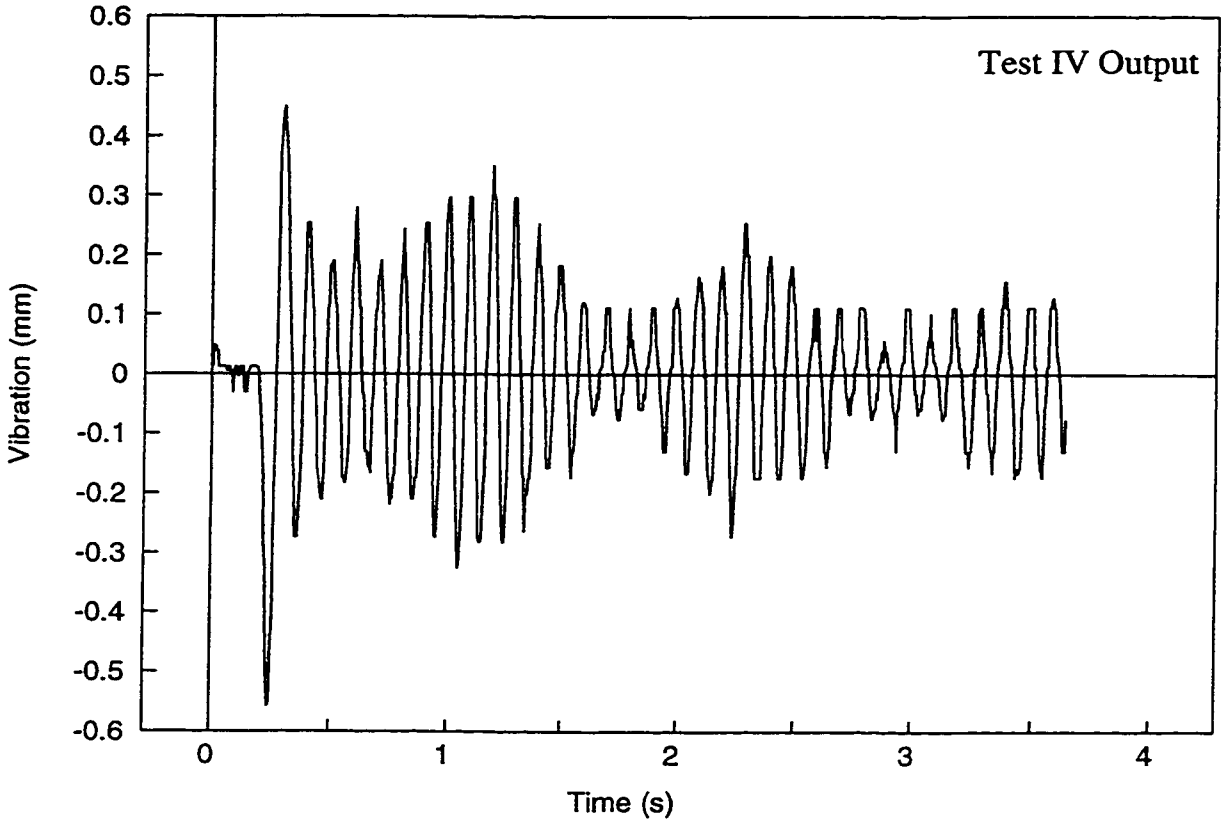


Figure 6.12 Real Time Test Result from Moving Joint 3 by 1 mm

(average velocity = 5 mm/s)

(with no ICSM applied)

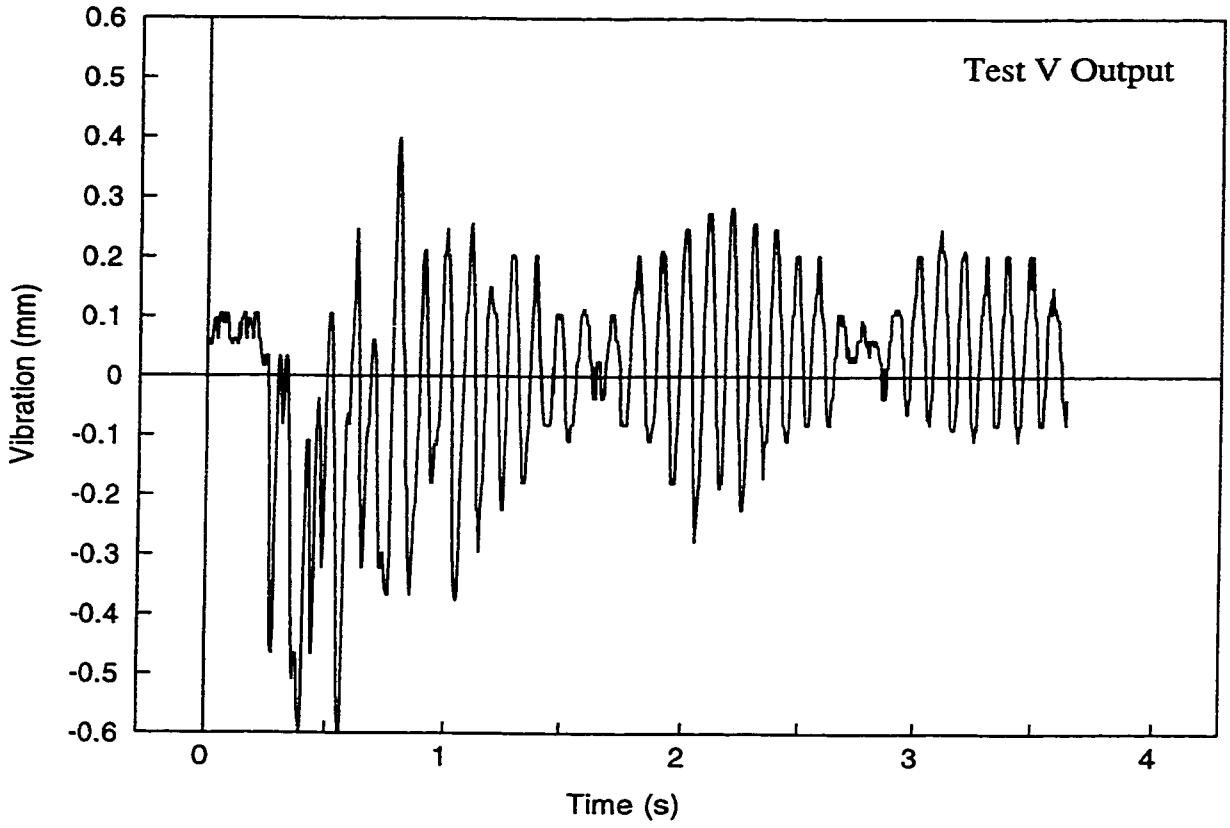


Figure 6.13 Real Time Test Result from Moving Joint 3 by 1 mm

(average velocity = 5 mm/s)

(with first 2 modes of vibration controlled by ICSM)

amplitude is small. Also, when the original vibration amplitude is small, modelling error could become relatively significant. This could have adversely affected the ICSM as well.

Tests (vi) and (vii) demonstrated a very common situation when the two parts to be assembled are 5 mm apart, and it is necessary to move one of the parts 1 mm towards the other part. Then a measurement of the contact state is taken, and a decision has to be made before another move is started. These tests assumed that it was necessary to move forward 1 mm at a time for 5 times. Typical results from these tests are shown in Figures 6.14 and 6.15. The average vibration amplitude obtained with no ICSM and with ICSM controlling the first two modes was 1.01 mm and 2.4 mm, respectively. The ICSM actually made the vibration worse. This result reveals one problem in applying the ICSM in contact control experiments. One assumption that the ICSM algorithm made is that the shaped input command begins with the system sitting at a fixed position. However, since only the first two modes of vibration are controlled and because of modelling error, not all the vibrations are eliminated at the end of the move. Therefore, if ICSM is implemented continuously in a series of small motions, it is likely that the input command intended to cancel vibration in the present move would amplify the residual vibration from the preceding moves. This explains the results observed in the experiments.

## 6.6 CONCLUSIONS

In this chapter an Integral Contact Controller (ICC) was developed and implemented to control the contact state between 2-D and 3-D parts. The ICC's performance was tested experimentally using the fusion of the FMS and SGF sensory information on 2-D sheet metal

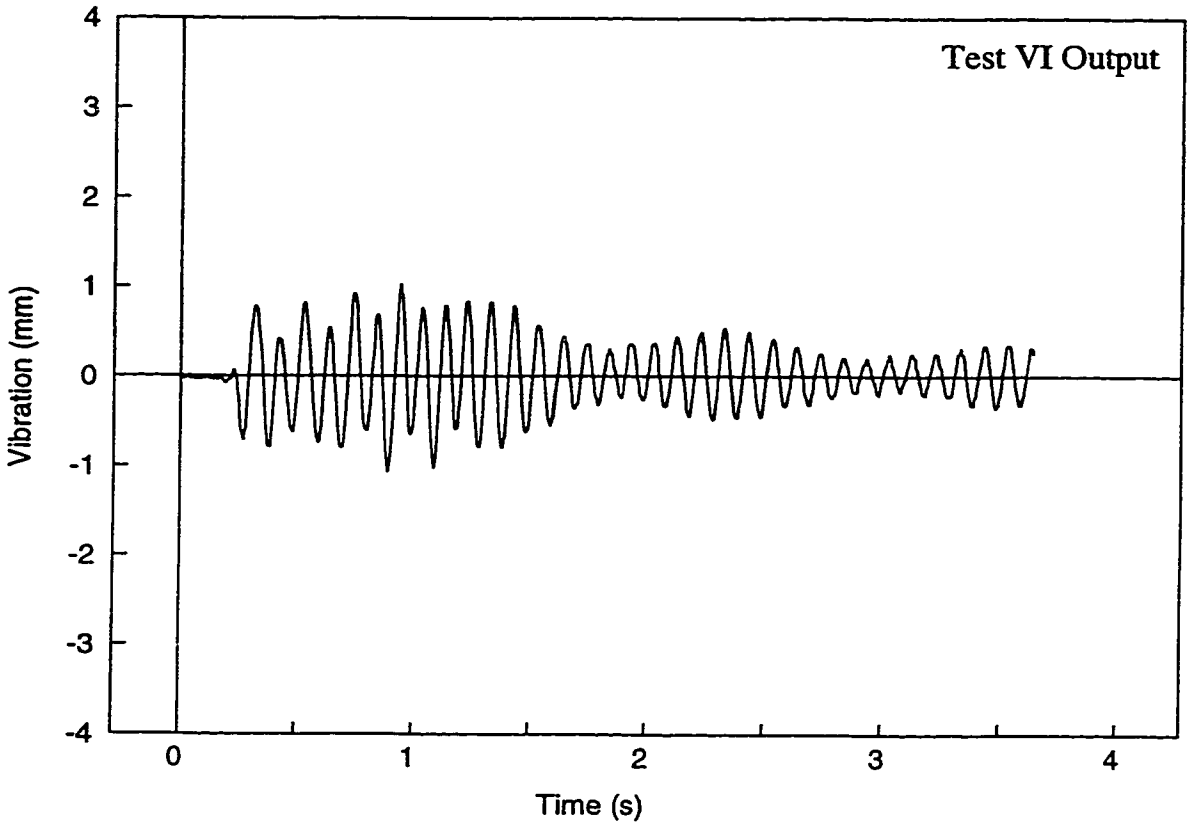


Figure 6.14 Real Time Test Result from Moving Joint 3 one mm at a Time for 5 Times

(average velocity = 5 mm/s)

(with no ICSM applied)

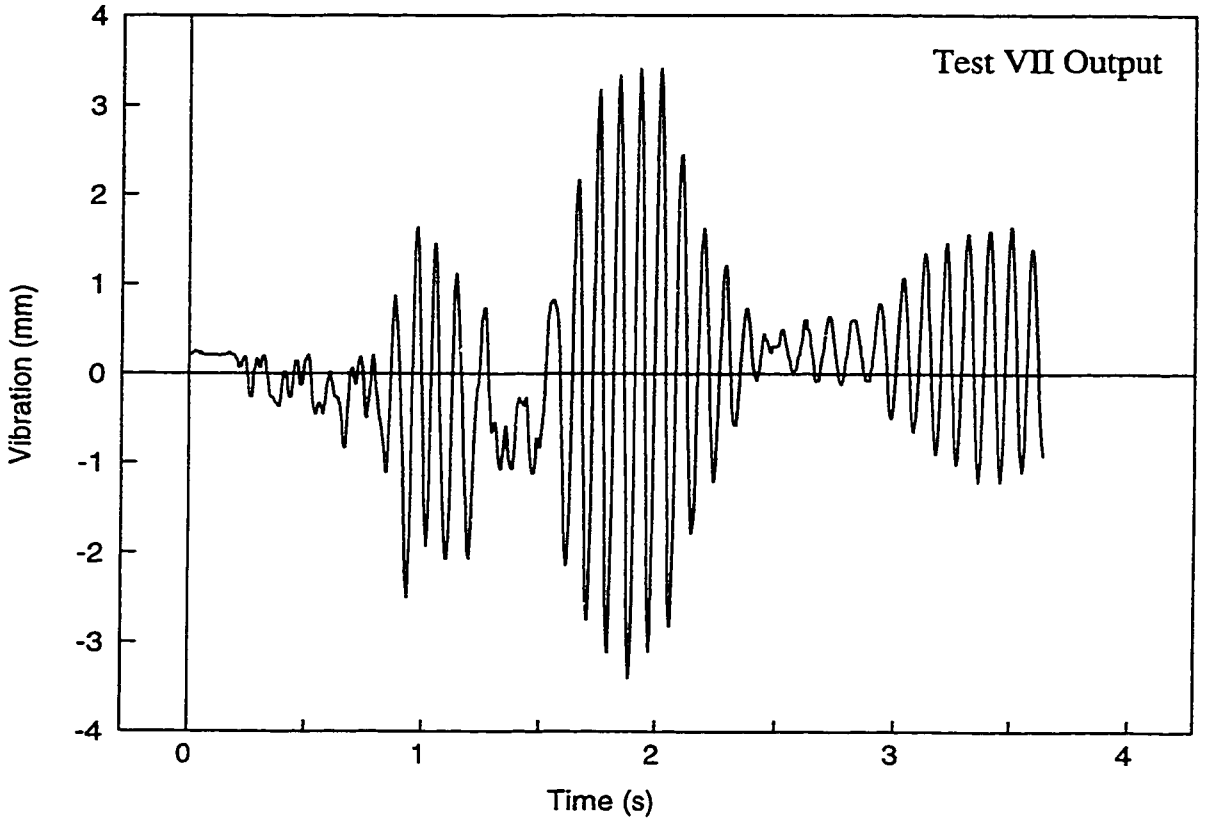


Figure 6.15 Real Time Test Result from Moving Joint 3 one mm at a Time for 5 Times

(average velocity = 5 mm/s)

(with first 2 modes of vibration controlled by ICSM)

parts. In all of the tests, it took less than two seconds to correct an angular error of 0.5° to within 0.025° accuracy. With this angular accuracy, the alignment accuracy at the part's mating edge was 0.05 mm. This was two times better than the +/- 0.1 mm accuracy required. The ICC was also tested experimentally using 3-D sheet metal parts. Due to a limitation in the availability of hardware, the tests could only be performed with either the FMS or the SGFs (and not with sensor fusion of the two). An angular error of 0.5° in the Pitch angle and 0.5° in the Yaw angle between the parts was used. In all of the tests when the FMS system was in use, it took less than 2.4 seconds to correct the angular error to within 0.05° accuracy. With this angular accuracy, in order to meet the required alignment accuracy of +/- 0.1mm, the part length and width are limited to 230 mm. When the SGFs system was employed, in all of the tests, it took less than 3.6 seconds to achieve the same degree of accuracy.

In an effort to achieve a faster response in the contact state control experiments, the ICSM was combined with the ICC. Although the ICSM was shown in Chapter 4 to be very effective in suppressing vibrations in large motion, it was shown to be not effective when applied continuously in a series of small motions. The input command intended to cancel vibrations in the present move would amplify the residual vibration from the preceding moves. The vibration amplitude was 58 % higher with ICSM implemented.

# Chapter 7

# Conclusions and Major Contributions

## 7.1 INTRODUCTION

This thesis dealt with two control problems encountered in Robotic Fixtureless Assembly of sheet metal parts. They are the control of vibration when handling the sheet metal parts and the control of the contact state between the parts during assembly. Both 2-D parts and 3-D parts were considered when the two problems were addressed.

## 7.2 CONCLUSIONS

(1) An effective and practical sensing device was required to measure both the vibration and contact state of flexible sheet metal parts for RFA. Strain gauges were found to be very effective in detecting deflection of a flexible payload; however, bonding a strain gauge permanently onto a sheet metal part is not feasible. A novel sensing device, termed SGF, was developed. The SGF met all the design criteria and constraints for RFA, and it allowed the measurement of both the vibration and contact state of flexible parts. A SGF has a typical

resolution of 0.4 V per mm of part edge displacement.

(2) A LEC algorithm was developed and implemented successfully with SGFs to control the vibration of sheet metal parts during RFA. The performance of this algorithm was studied based on vibration control experiments using 2-D and 3-D parts. Experimental results demonstrated that LEC could effectively reduce the resulting vibration of the parts when they were handled at high speed by a robot. The vibration amplitude was reduced by up to 45% in 2-D parts and 71% in 3-D parts.

(3) The effectiveness of ICSM in controlling vibration in sheet metal parts was examined. The 3-impulse ICSM was studied in computer simulations to control the vibration of a sheet metal part by suppressing the first mode, the second mode and both the first and second mode of vibration, respectively. The ICSM performed best when both the first and second modes were suppressed. The performance of ICSM was then examined experimentally. It was found to be very effective in suppressing the sheet metal parts' vibration when moving at high speed in large motions. The vibration amplitude was reduced by up to 78%. However, a time delay was introduced into the input command trajectory by the ICSM algorithm.

(4) Three contact state detection algorithms were developed based on feedback signal coming from a Force/Moment Sensor (FMS), SGFs and the fusion of the FMS and SGFs

information, respectively. Based on 160 tests performed using 2-D sheet metal parts with four different stiffnesses, the performance of these algorithms was evaluated. It was found that the FMS was more effective with stiffer parts, while the SGFs were better suited for more flexible parts. The sensor fusion system maintained a 100% success rate in all tests, and surpassed the best individual performance of the FMS and SGFs. It is also shown that a trade-off exists between the detection time and the detection success rate.

(5) The contact state measurement algorithms developed for 2-D parts were extended to allow the contact state of 3-D parts to be measured.

(6) An ICC was developed and implemented to control the contact state between 2-D and 3-D parts. The ICC's performance was tested experimentally using the fusion of the FMS and SGF sensory information on 2-D sheet metal parts. In all of the tests, it took less than two seconds to correct an angular error of 0.5° to within 0.025° accuracy. With this angular accuracy, the alignment accuracy at the mating edge of the part was 0.05 mm, which was two times better than the +/- 0.1 mm accuracy required.

(7) The ICC was also tested experimentally using 3-D sheet metal parts. Due to a limitation in the availability of hardware, the tests were performed with either the FMS or the SGFs. An angular error of 0.5° in the Pitch angle and 0.5° in the Yaw angle between the parts was used. In all of the tests when the FMS system was in use, it took less than 2.4

seconds to correct the angular error to within 0.05° accuracy. With this angular accuracy, in order to meet the +/- 0.1 mm alignment accuracy at the mating edge, the part length and width are limited to 230 mm. When the SGFs system was employed, in all of the tests it took less than 3.6 seconds to achieved the same degree of accuracy.

(8) In an effort to achieve a faster response in the contact state control experiments, ICSM was combined with ICC. Although ICSM was shown in Chapter 4 to be very effective in suppressing vibration in large motion, it was shown to be not effective when applied continuously in a series of small motions. The input command intended to cancel vibration in the present move would be affected by the residual vibration from the preceding moves. The vibration amplitude was 58 % higher with ICSM implemented.

## 7.3 MAJOR CONTRIBUTIONS OF THIS THESIS

- A Novel Strain Gauge-equipped Finger (SGF) sensor was developed. The measurement of vibration of sheet metal parts in an automotive assembly plant was previously considered to be "not feasible" [ 24 ]. The SGF not only makes this feasible, it also allows the contact state between two sheet metal parts to be measured. As a further benefit, the measurements are done with a relatively inexpensive sensor without direct attachment of the sensor on to the parts.
- A sensor fusion system employing a Force/Moment Sensor (FMS) and SGFs was developed. It allows the contact state between sheet metal parts with a range of

thicknesses/flexibility to be measured effectively. Previous contact state measurement systems were limited to rigid parts only.

- A novel Learning Extremum Controller (LEC) was shown to effectively control the vibration of a flexible payload when carried by a robot. Unlike the majority of vibration control algorithms previously developed, this method may be applied with any industrial robot.
- An Integral Contact Controller (ICC) was proven to be an effective way to control the contact states between 2-D and 3-D sheet metal parts.
- The Input Command Shaping Method was applied to the problem of vibration control when a flexible payload is carried by a robot. The method's benefits and limitations were investigated. To the author's knowledge this is the first time ICSM has been applied to this problem.
- The application of the vibration control and contact state control methods developed in this thesis is not limited to sheet metal parts. They can be applied to parts made of other materials.
- Four research papers have been published from the work of this thesis. The published papers are:

[1] Bone, G.M. and Yuen, K.M., "Technologies for Flexible Fixturing and Higher Speed Part Handling and Automated Automotive Sheet Metal Assembly", Accepted for the *1998 ASME International Mechanical Engineering Congress and Exposition, Anaheim, CA.*

[2] Yuen, K.M. and Bone, G.M., "Control of Robotic Fixtureless Assembly." *13th Symposium on Engineering Application of Mechanics, CSME Forum*, 1996, p.213-

220.

[3] Yuen, K.M. and Bone, G.M., "Robotic Assembly of Flexible Sheet Metal Parts", *IEEE International Conference on Robotics and Automation*, Vol.2, 1996, p.1511-1516.

[4] Yuen, K.M. and Bone, G.M., "Multisensor-Based Detection of Contact State for Automated Sheet Metal Assembly", *Manufacturing Science and Engineering*, MED-Vol.2-2, ASME, 1995, p.1131-1144.

## 7.4 RECOMMENDATIONS FOR FUTURE WORK

1. Due to a hardware limitation, the ICC was unable to be tested with 3-D parts using the fusion of the FMS and SGFs sensory information. This should be done in the future when the hardware is available.
2. If a SGF is mounted onto an actively controlled gripper, the SGF can be actively repositioned based on signal strength.
3. Four SGFs were used for the rectangular 3-D sheet metal part in this thesis. For sheet metal parts of more complicated shape, an algorithm would be required to optimize the number of SGFs and their placement locations.
4. The contact state measurement algorithms developed in this thesis are applicable to 3-D sheet metal parts with angular error in the Pitch and Yaw angles only. Further development is required to allow the error in the roll joint to be detected.

# References


[1] Majda, Rick, Telephone Interview, April 12, 1994, Office Manager, Bramelea Assembly Plant, Chrysler Canada.

[2] Kurz, K., et al., "Developing a Flexible Automated fixturing Device",Mechanical Engineering, Vol.116, No.7, 1994, p.59-63.

[3] Naitoh, T., et al., "The Development of Intelligent Body Assembly System", 24th Int. Symp. on Ind. Robots, 1993, p.129-136.

[4] VanVarseveld, R.B.,"Development of a Multi-degree of Freedom Robotic Gripper for Robotic Fixtureless Assembly", Master's Thesis, McMaster University, 1997.

[5] Kotnik, P. T., Yurkovich, S. and Ozguner, U.," Acceleration Feedback for Control of a Flexible Manipulator Arm. Journal of Robotic Systems, 5(3), 1988, p.181-196.

[6] Suehiro, T. and Takase, K.,"Representation and Control of Motion in Contact and Its Application to Assembly Tasks, Robotic Research: the 5th Int. Symp., The MIT Press, 1990, p.367-374

[7] Hastings, G.G. and Book, W.J.," Verification of a linear dynamic model for flexible robotic manipulators," Proc. IEEE Inter. Conf. On Rob. & Auto. 1986, p.1024 - 1029.

[8] Jain, S. and Khorrami, F., "Vibration Suppression of Unknown Flexible Payloads Using a Wrist Mounted Force/Torque Sensor for Remote Manipulator Systems", Proc. IEEE Inter. Conf. On Rob. & Auto. 1994, p.2119-2124.

[9] Zheng, Y.F., Pei R. and Chen, C., "Strategies for Automatic Assembly of Deformable Objects", Proc. IEEE Inter. Conf. On Rob. & Auto. 1991, p.2598-2603.

[10] Chen, C. and Zheng, Y.F., "Deformation Identification and Estimation of One-Dimensional Objects by Using Vision Sensors", Proc. IEEE Inter. Conf. On Rob. & Auto. 1991, p.2306-2311.

[11] Ueno, N. And Kaneko, M., "Dynamic Active Antenna- A Principle of Dynamic Sensing", Proc. IEEE Inter. Conf. On Rob. & Auto. 1994, p.1784-1790.

[12] Wasfy, Tamer., "Modelling Contact/Impact of Flexible Manipulators with a Fixed Rigid Surface", Proc. IEEE Inter. Conf. On Rob. & Auto. 1995, p.621-626.

[13] Mills, J.K. and Ing, G.L., "Robotic Fixtureless Assembly of Sheet Metal Parts Using Dynamic Finite Element Models: Modelling and Simulation", Proc. IEEE Inter. Conf. On Rob. & Auto. 1995, p.2530-2536.

[14] Kosuge et. al.,"Manipulation of a Flexible Object by Dual Manipulators", Proc. IEEE Inter. Conf. On Rob. & Auto. 1995, p.318-323.

[15] Nguyen, W. & Mills, K.,"Multi-Robot Control for Flexible Fixtureless Assembly of Flexible Sheet Metal Parts", Proc. IEEE Inter. Conf. On Rob. & Auto. 1996, p.2340-2345.

[16] Tzes, A. and Yurkovich, S., "An Adaptive Input Shaping Control Scheme for Vibration Suppression in Slewing Flexible Structures", IEEE Trans. on Control Sys. Tech., Vol.1, No.2, June, 1993, p.114-121.

[17] Khorrami, F. and Jain, S., "Experimental Results on an Inner/Outer Loop Controller for a Two-Link Flexible Manipulator", IEEE Int. Conf. Rob. and Auto., Vol.1, 1992, p.742-747.

[18] Habib, M.S. and Radcliffe, C.J., "Active Parametric Damping of Distributed Parameter Beam Transverse Vibration", J. Dyn. Syst. Meas. Control, Trans ASME, 1991, p.295-299.

[19] Ashley, H., "On Passive Damping Mechanisms in Large Space Structures," J. Spacecraft and Rockets, Vol.21, No.5. , 1984, p.448-455.

[20] Chen, M.Z. and Zheng, Y.F., "Vibration-Free Handling of Deformable Beams by Robot End-Effectors,"J. Rob. Sys. Vol.12, No.5, 1995, p.331-347.

[21] Hirai, S. and Iwata, K., "Recognition of Contact State Based on Geometric Model", IEEE Int. Conf. Rob. and Auto., 1992, p.1507-1512.

[22] Kitaagaki, K., et al., "Methods to Detect Contact State by Force Sensing in an Edge Mating Task", IEEE Int. Conf. Rob. and Auto., Vol.2, 1993, p.701-706.

[23] Mills, J.K., "Multi-Manipulator Control for Fixtureless Assembly of Elastically Deformable Parts", ASME Japan/USA Symp. on Flex. Auto., 1992, p.1565-1572.

[24] Nguyen, W. and Mills, J.K., "Multi-Robot Control for Flexible Fixtureless Assembly of Flexible Sheet Metal Auto Body Parts', IEEE Int. Conf. Rob. and Auto., Vol.3, 1996, p.2340-2345.

[25] G.M. Bone,"Development of an Automated Robotic Edge Deburring System", Ph.D. Thesis, McMaster University, 1993.

[26] M.W. Spong & M. Vidyasagar,"Robot Dynamics and Control",John Wiley & Sons, New York, 1989.

[27] S. Yu,"Dynamics and Control of a Two Link Flexible Planar Manipulator", Ph.D. Thesis, McMaster University, 1994.

[28] Singer, N.C. and Seering, W.P., "Preshaping Command Inputs to Reduce System Vibration,"J. Dyn. Syst. Meas. Control, Trans ASME, Vol.112, No.1, March 1990, pp.76- 82.

[29] Hillsly, K.L. and Yurkovich, S., "Vibration Control of a Two-Link Flexible Robot Arm" IEEE Int. Conf. Rob. and Auto., 1991, p.2121-2126.

[30] Yuen, K.M. and Bone, G.M., "Robotic Assembly of Flexible Sheet Metal Parts", IEEE Int. Conf. Rob. and Auto., Vol.2, 1996, p.1511-1516.

[31] Astrom, K.J. and Wittenmark, B.,"Adaptive Control", Addison-Wesley Publishing Company, New York, 1989.

[32] Singer, N.C. and Seering, W.P.,, "Experimental Verification of Command Shaping Methods for Controlling Residual Vibration in Flexible Robots,' American Control Conference, San Diego, California, May 1990, p.1738-1744.

[33] Desai, R. S. and Volz, R. A., "Identification and Verification of Termination Conditions in Fine Motion in Presence of Sensor errors and Geometric Uncertainties", IEEE Int. Conf. Robotics and Automation, 1989, p.800-807.

[34] Durrant-Whyte, H. F., "Sensor Models and Multisensor Integration", The International Journal of Robotics Research, Vol.7, No.6, December 1988, p.97-113.

[35] Sethi, P., "Defining Precision in a Control System", Machine Design, April 1976, p.80-84.

[36] Yuen, K.M. and Bone, G.M., "Multisensor-Based Detection of Contact State for Automated Sheet Metal Assembly", Manufacturing Science and Engineering, MED-Vol.2-2, ASME, 1995, p.1131-1144.

[37] Yuen, K.M. and Bone, G.M., "Control of Robotic Fixtureless Assembly." 13th Symposium on Engineering Application of Mechanics, CSME Forum, 1996, p.213-220.

[38] PMAC Software Reference for Firmware Version 1.16, Delta Tau Data Systems, Northridge, CA, August 1996, p.7-60.

[39] Moallem, M., Khorasani, K & Patel, R.V., "An Integral Manifold Approach for Tip Position Tracking of Flexible Multi-Link Manipulators", *IEEE Transactions on Robotics & Automation*, vol. 13, no. 6, 1997, p.823-837.

[40] Geniele, H., Patel, R.V., & Khorasani, K., " End-point Control of a Flexible-link Manipulator: Theory and Experiment", *IEEE Transactions on Control Systems Technology*, vol.5, 1997, p.556-570.

# Appendix A

# Listing of MATLAB Programs for ICSM Simulations

```
% MATLAB Simulation Program 1
% Singer and Seering Input Command Shaping Method
% For suppression of 1 vibration mode only

% Perform ARX model identification using 744 data points
% input = robot joint command (mm for Joint 3)
% output = response from four Strain Gauge Fingers (SGFs) in mm

u = input;          % unshaped input
y1 = outpSGF1;  % response measured by SGFs
y2 = outpSGF2;
y3 = outpSGF3;
y4 = outpSGF4;

% Simulation time scale in seconds

timeScale = 0.004454 ;

z = [y1, y2, y3, y4, u];

nn=[   30 30 30 30 30 2
       30 30 30 30 30 2
       30 30 30 30 30 2
       30 30 30 30 30 2 ];

th3 = arx(z,nn);
```

```
[A3, B3, C3, D3] = th2ss(th3);


% Plot simulated response

y = dlsim(A3, B3, C3, D3, u);

t = 1:1:744;
plot(t, y1, 'y-', t, y(:, 1), 'g--')
xlabel('Time (s)')
ylabel('Vibration (mm)')
title(' Joint 3 Modelling, 10 mm Input ')

% Implement ICSM

A = A3;
B = B3;
C = C3;
D = D3;

T = 0.004454;

% Determine natural frequency and damping factor

[M, Wn, zi] = ddamp(A, T);

% Use the following to suppress Joint 3 first mode
zi1 = zi(1)
Wn1 = Wn(1)

% Use the following to suppress Joint 3 second mode
% zi1 = zi(3)
% Wn1 = Wn(3)

dt = pi / (Wn1 * sqrt(1 - zi1 * zi1));
k = exp(-zi1 * pi / sqrt(1 - zi1 * zi1));

q = round(dt / T) - 1;

D1 = 1 + 2 * k + k * k;
```

```
p1 = 1 / D1;
p2 = 2 * k / D1;
p3 = k * k / D1;

x1 = p1 * u;
x2 = p2 * u;
x3 = p3 * u;

z1 = zeros(1, q);
z1 = rot90(z1);
z2 = zeros(1, 2 * q);
z2 = rot90(z2);

k1 = [z1; x2];
k2 = [z2; x3];

x = x1 + k1(1:744) + k2(1:744);

% Plot simulated output with and without ICSM
ya = dlsim(A, B, C, D, u);
yb = dlsim(A, B, C, D, x);

t = 1:1:744;
t = t * T;

plot(t, ya(:, 1), 'y-', t, yb(:, 1), 'g--')
xlabel('Time (s)')
ylabel('Vibration (mm)')
title(' Joint 3, 10 mm Input, first mode suppressed ')


%---------- END OF PROGRAM ----------
```

```
% MATLAB Simulation Program 2
% Singer and Seering Input Command Shaping Method
% For suppression of 2 vibration modes

T = 0.004454; % Simulation time scale in seconds

% Determine natural frequencies and damping factors

[M, Wn, zi] = ddamp(A, T);

zi1 = zi(1);
Wn1 = Wn(1);

zi2 = zi(3);
Wn2 = Wn(3);

dt1 = pi / (Wn1 * sqrt(1-zi1 * zi1));
k1 = exp(-zi1 * pi / sqrt(1-zi1 * zi1));
q1 = round(dt1 / T) - 1;
D1 = 1 + 2 * k1 + k1*k1;
p11 = 1 / D1 ;
p21 = 2 * k1 / D1 ;
p31 = k1 * k1 / D1 ;

dt2 = pi / (Wn2 * sqrt(1 - zi12 * zi2));
k2 = exp(-zi2 * pi / sqrt(1 - zi2 * zi2));
q2 = round(dt2 / T) - 1;
D2 = 1 + 2 * k2 + k2 * k2;
p12 = 1 / D2 ;
p22 = 2 * k2 / D2 ;
p32 = k2 * k2 / D2 ;

z2 = zeros(1, q1);
z2 = rot90(z2);
z3 = zeros(1, q2);
z3 = rot90(z3);
z4 = zeros(1, 2*q1);
z4 = rot90(z4);
z5 = zeros(1, q1+q2);
z5 = rot90(z5);
z6 = zeros(1, 2*q2);
z6 = rot90(z6);
```

```
z7 = zeros(1, 2*q1+q2 );
z7 = rot90(z7);
z8 = zeros(1, 2*q2+q1 );
z8 = rot90(z8);
z9 = zeros(1, 2 * (q1 + q2) );
z9 = rot90(z9);

'The impulses should be applied at the following control periods:'
1
q1 + 1
q2 + 1
2 * q1 + 1
q1 + q2 + 1
2 * q2 + 1
2 * q1 + q2 + 1
2 * q2 + q1 + 1
2 * (q1 + q2) + 1


% Construct shaped input

j1 = p11 * p12 * u;
j2 = p21 * p12 * u;
j3 = p11 * p22 * u;
j4 = p31 * p12 * u;
j5 = p21 * p22 * u;
j6 = p11 * p32 * u;
j7 = p31 * p22 * u;
j8 = p21 * p32 * u;
j9 = p31 * p32 * u;


j2 = [z2; j2];
j3 = [z3; j3];
j4 = [z4; j4];
j5 = [z5; j5];
j6 = [z6; j6];
j7 = [z7; j7];
j8 = [z8; j8];
j9 = [z9; j9];
```

```
% The shaped input is :

x4 = j1 + j2(1:744) + j3(1:744) + j4(1:744) + j5(1:744)
     + j6(1:744) + j7(1:744) + j8(1:744) + j9(1:744);

% Compute response from original input

ya = dlsim(A3, B3, C3, D3, u);

% Compute response from shaped input

yb = dlsim(A3, B3, C3, D3, x4);

t = 1:1:744;
t = t * T;

plot(t, ya(: , 1), 'y-', t, yb(: , 1), 'g--')
xlabel('Time (s)')
ylabel('Vibration (mm)')
title(' Joint 3, 10 mm Input, first and second modes suppressed ')

%---------- END OF PROGRAM ----------
```

# Appendix B

# Listing of PMAC Motion Control Program to Implement ICSM for 3-D Parts

```
; Delta Tau PMAC Motion Control Program to move Joint 4 for 20 deg.
; Using PVT mode to implement ICSM

CLOSE OPEN PROG 44 CLEAR
CMD"I3=3"
INC
;

PVT 35
U 0.000539:0.0815
PVT 9
U 0.0008607:0.1467
PVT 22
U 0.0053:0.4311
PVT 44
U 0.0019:0.5255
PVT 9
U 0.0051:0.7485
PVT 9
0.0073:1.0396
PVT 22
U 0.0318:2.1125
PVT 4
U 0.0094:2.3938
PVT 9
```

```
U 0.0227:3.0108
PVT 9
U 0.0284:3.7436
PVT 22
U 0.1029:6.0709
PVT 4
U 0.027:6.6166
PVT 18
U 0.1336:9.0699
PVT 27
U 0.2902:13.5038
PVT 18
U 0.2626:16.8572
PVT 44
U 0.9338:26.1597
U 1.3604:35.8829
U 1.7853:44.9785
U 2.1533:51.9295
U 2.3908:54.9686
U 2.4298:53.1624
U 2.2588:47.0738
U 1.9296:38.4056
U 1.5181:28.7366
U 1.0868:19.2161
U 0.6832:10.9314
U 0.3568:4.8999
U 0.1418:1.5541
U 0.0378:0.2709
U 0.005:0.0024
U 0.00001138:0
CLOSE

;---------- END OF PROGRAM ----------
```

# Appendix C

# Listing of PMAC Motion Control Program to Implement ICC for 2-D Parts using Sensor Fusion

```
CLOSE
; ------------------------------------------------------------------------------
; Delta Tau PMAC Motion Control Program 505 for
; 2-D Sheet Metal Parts Contact Contol using Intrgral Contact Control (ICC)
; with sensor fusion of FMS and SGFs.
;------------------------------------------------------------------------------
; This program controls the motion of the GMF joints 3 and 4 based on the
; Force/Moment Sensor (FMS) and Strain Gauge equipped Fingers (SGFs) reading
; to achieve a full contact between 2 sheet metals.
;------------------------------------------------------------------------------
; A/D signals are 10 V maxmium
; A/D   channel 1 : left  SGF
;       channel 2 : right SGF
;       channel 3 : Fy  ( 10 lbs per V )
;       channel 4 : Mz  ( 40 in-lbs per V )
;
; sample all 4 ADC channels continuously
; Note that ACC-28A is plugged into port JS2 so channels 5-8 are being used
; M1005->Y:$C016,8,16,S
; M1006->Y:$C017,8,16,S
; M1007->Y:$C01E,8,16,S
; M1008->Y:$C01F,8,16,S
;
;
```

```
; see p. 3-96 of the DELTA TAU manuel for the array setup lines used below

M60->L:$1000 ; Pointer to p0, L stands for long word floating point
M61->Y:$BC3C,0,12 ; Address of the pointer
M62->L:$1000 ;
M63->Y:$BC3E,0,12
M64->L:$1000 ;
M65->Y:$BC40,0,12
M66->L:$1000 ;
M67->Y:$BC42,0,12
M68->L:$1000 ;
M69->Y:$BC44,0,12
M70->L:$1000 ;
M71->Y:$BC46,0,12
; Pointer for saving X3, U(), and C()
M72->L:$1000
M73->Y:$BC48,0,12

CLOSE OPEN PROG 505 CLEAR
CMD "i3=3"
LINEAR       ; Linear interpolation
FRAX(U,C)
F60
TS 50
INC          ; Incremental mode
P500=10      ; Number of samples per average
P501=0       ; Counter
P502=1.0     ; Forward motion step size ( mm )
P503=0       ; Total distance moved
P504=0.1     ; Rotational motion step size ( degrees )
P505=0             ; Total rotation
P506=0       ; flag for contact establishment
P507=100     ; max. number of control cycles
P508=0       ; Magnitude of total rotation
P509=0.3214 ;  forward motion after each rotation
P510=0       ; QUIT flag
P511 = 0
P512 = 0
P513 = 0
P514 = 0
P515 = 0   ; contact test 1 flag
P516 = 0   ; contact test 2 flag
```

```
P517 = 0   ; backup motion after initial contact
P520=0.6   ; CONTROLLER GAIN

; Initialize arrays to zero

WHILE (P501 < 20)
  M73=P501+600
  M72=0
  M73=P501+620
  M72=0
  M73=P501+640
  M72=0
  M73=P501+660
  M72=0
  P501 = P501 + 1
ENDWHILE

P501 = 0

;-------------------------------------------------------------
;                          Main Program:
;-------------------------------------------------------------

WHILE(P501<P507 AND P503 < 6 AND P508 < 2 AND P510 = 0)
 ; limit total number of control cycles, forward motion and rotation
GOSUB 100        ; Read Sensors

; No contact test 1: If variances of X1 AND X2 too big

IF (P424 > 0.0278 AND P425 > 0.0278)
   P515 = 0
ELSE
   P515 = 1
ENDIF

; No contact test 2: If sensor signals too small

IF (P511 < 0.1 AND P512 < 0.1 AND P513 < 0.1 AND P514 < 0.1)
   P516 = 0
ELSE
   P516 = 1
ENDIF
```

```
P517=0
IF (P515 = 0  OR P516 = 0) ; If either test failed
;if X1 and X2 variance very large OR sensor reading very small -> no contact
  SEND "N"              ; NO contact. Moving forward by 1 mm
  C(P502)           ; Forward motion
  P503=P503+P502    ; Sum forward motion (mm)
  P506 = 0          ; set no contact flag
ELSE
  IF (P506 = 0)
    P517=-P502*0.75;  Used to back up by -P502/2
    P506 = 1            ; Contact achieved, set flag to 1
    SEND "I"  ;  Initial contact achieved.
  ENDIF
ENDIF

IF (P426 !> -0.15 AND P506 = 1 )      ; if left end contact
    SEND"L"             ; LEFT end contact. Rotating CCW
    P504=-P520*P426 ; Compute rotation adjustment based on X3 and gain
    IF(P504>1) P504=1           ; Limit to 1
    P509=3.214*P504+P517; adding backup: P517 here
    U(P504) C(P509)     ; forward motion accompany each rotation
    P505=P505+P504      ; Sum rotation (deg)
    P503=P503+P509  ; Sum forward move
    P517 = 0          ; reset backup after initial contact
ENDIF

IF (P426 !< 0.15 AND P506 = 1)       ; if right end contact
    SEND "R"            ; RIGHT end contact. Rotating CW
    P504=-P520*P426 ; Compute rotation adjustment based on X3 and gain
    IF(P504<-1) P504=-1 ; Limit to -1
    P509=-3.214*P504+P517; note sign change
    U(P504) C(P509)     ; forward motion accompany each rotation
    P505=P505+P504      ; Sum rotation (deg)
    P503=P503+P509  ; Sum forward move
    P517 = 0          ; reset backup after initial contact
ENDIF

IF (P426 > -0.15 AND P426 < 0.15 AND P506 = 1) ; if full contact
    C(P517)
    SEND "FULL contact achieved !!!"
    P510 = 1        ; set flag to quit
ENDIF
```

```
P501=P501+1          ; Increment counter
P508=ABS(P505)

; Store X3
M73=P501+600
M72=P426

; Store Rotation
M73=P501+620
M72=P505

; Store Forward Move
M73=P501+640
M72=P503

; Store Time
M73=P501+650
M72=M0*I10*.001/8388608
ENDWHILE

;---------- output results ----------
;
SEND "Sensor Readings: Left G, Right G, Fx, Mz"
CMD "P406"
CMD "P407"
CMD "P408"
CMD "P409"
SEND "Variances: X1 (FMS), X2 (SGF)"
CMD "P425"
CMD "P424"
SEND "RESULTS: X1 (FMS), X2 (SGF), X3 (FINAL) = "
CMD "P411"
CMD "P410"
CMD "P426"
SEND "Total Forward Movement (mm) ="
CMD "P503"
SEND "Total Rotation (deg) = "
CMD "P505"
SEND "Total # of moves taken"
CMD "P501"
```

```
;-------------------------------------------------------------
;                Subroutine to read sensors
;-------------------------------------------------------------
N100
;SEND "Sampling all 4 channels now."
; Using p1 to p300 as arrays ( arrays have been set up at the beginning )
P401=1
P406=0
P407=0
P408=0
P409=0
P410=0
P411=0

WHILE (P401 !> P500);loop through 10 times at 1 ms each or = 100 Hz sampling
 M61 = P401
 M60 = M1005/3276.8-P402  ; channel 1 : left SGF
 M63 = P401+50
 M62 = M1006/3276.8-P403  ; channel 2 : right SGF
 M65 = P401+100
 M64 = M1007/3276.8-P404  ; channel 3 : Fy
 M67 = P401+150
 M66 = M1008/3276.8-P405  ; channel 4 : Mz

; Calculate X2 = M68 (SGFs)
 M69 = P401+200
 M68 = (M62-M60)/(M60+M62)

; Calculate X1 = M70 (FMS)
 M71 = P401+250
 M70 = -M66/M64*40/70

;--------- Initially a delay was set here to achieve desired sampling rate;
; DELAY 0                ; (ms)
;--------- however, we discovered that if delay = 0, motion will be much smoother

 P401=P401+1
 P406=P406+M60
 P407=P407+M62
 P408=P408+M64
 P409=P409+M66
 P410=P410+M68
```

```
  P411=P411+M70
;  CMD "P401"
ENDWHILE ;(P401 !> P500)

; Calculate Mean values
P406=P406/P500 ;strain gauge 1
P407=P407/P500 ;strain gauge 2
P408=P408/P500 ;Force
P409=P409/P500 ;Moment
P410=P410/P500 ;X2 (Normalized combined reading for strain gauges 1 & 2)
P411=P411/P500 ;X1 (Normalized combined reading for force and moment)

P511 = ABS(P406)
P512 = ABS(P407)
P513 = ABS(P408)
P514 = ABS(P409)

; Calculate variances
P401=1
P420=0
P421=0
P422=0
P423=0
P424=0
P425=0

WHILE(P401!>P500)
  P420 = P420+(P(P401)-P406)*(P(P401)-P406)
  P421 = P421+(P(P401+50)-P407)*(P(P401+50)-P407)
  P422 = P422+(P(P401+100)-P408)*(P(P401+100)-P408)
  P423 = P423+(P(P401+150)-P409)*(P(P401+150)-P409)
  P424 = P424+(P(P401+200)-P410)*(P(P401+200)-P410)
  P425 = P425+(P(P401+250)-P411)*(P(P401+250)-P411)
  P401 = P401+1
ENDWHILE

P420 = P420/P500
P421 = P421/P500
P422 = P422/P500
P423 = P423/P500
P424 = P424/P500
P425 = P425/P500
```

```
;Calculate final decision X3 = P426
P426 = (P425*P410+P424*P411)/(P424+P425)
RETURN

CLOSE

;---------- END OF PROGRAM ----------
```

# Appendix D

# Listing of PMAC Motion Control Program to Implement ICC for 3-D Parts using FMS

```
CLOSE
;-------------------------------------------------------------------------
; Delta Tau PMAC Motion Control Program for
; 3-D Sheet Metal Parts Contact Contol with ICC.
;-------------------------------------------------------------------------
; This program controls the motion of the GMF joints 3 and 4 based on the
; Force/Moment Sensor (FMS) readings
; to achieve a full contact between 2 sheet metals.
;-------------------------------------------------------------------------
; A/D channel 1 : for Fy
; A/D channel 2 : for Mx
; A/D channel 3 : for Mz
;
; sample all 4 ADC channels continuously
; Note that ACC-28A is plugged into port JS2 so channels 5-8 are being used
; M1005->Y:$C016,8,16,S
; M1006->Y:$C017,8,16,S
; M1007->Y:$C01E,8,16,S
; M1008->Y:$C01F,8,16,S
;
; see p. 3-96 of the DELTA TAU manuel for the array setup lines used below

M60->L:$1000 ; Pointer to p0, L stands for long word floating point
M61->Y:$BC3C,0,12 ; Address of the pointer
```

```
M62->L:$1000 ;
M63->Y:$BC3E,0,12
M64->L:$1000 ;
M65->Y:$BC40,0,12
M66->L:$1000 ;
M67->Y:$BC42,0,12
M68->L:$1000 ;
M69->Y:$BC44,0,12
M70->L:$1000 ;
M71->Y:$BC46,0,12
; Pointer for saving X3, U(), and C()
M72->L:$1000
M73->Y:$BC48,0,12

CLOSE OPEN PROG 505 CLEAR
CMD "i3=3"
LINEAR        ; Linear interpolation
FRAX(U,V,C)

F15.0              ; Feedrate
TS 50      ; S-curve acceleration time

INC        ; Incremental mode
P500=10     ; Number of samples per average
P501=0             ; Counter
P502=1.0    ; Forward motion step size ( mm )
P503=0             ; Total distance moved
P504=0.1    ; Rotational motion step size ( degrees )
P505=0             ; Total rotation
P506=0      ; flag for contact establishment
P507=100    ; max. number of control cycles
P508=0      ; Magnitude of total rotation
P509=0      ; forward motion accompaning each rotation (0.1 deg.) in U
P510=0      ; QUIT flag
P511 = 0
P512 = 0
P513 = 0
P514 = 0
P515 = 0   ; contact test 1 flag
P516 = 0   ; contact test 2 flag
P517 = 0   ; backup motion after initial contact
P520 = 0.15 ; CONTROLLER GAIN for U
```

```
P530 = 0.15 ; CONTROLLER GAIN for V
P525=0
P528=0
P531=0
P532=0
P533=0
P534=0
P535=0

; sample all 3 channels now to obtain sensor offsets
WHILE (P531 < 50)
  P402 = M1005/3276.8
  P403 = M1006/3276.8
  P404 = M1007/3276.8

  P532 = P532 + P402
  P533 = P533 + P403
  P534 = P534 + P404
  P531 = P531 + 1
ENDWHILE
P402 = P532/50
P403 = P533/50
P404 = P534/50

CMD "P402"
CMD "P403"
CMD "P404"

; Initialize arrays to zero

WHILE (P501 < 20)
  M73=P501+600
  M72=0
  M73=P501+620
  M72=0
  M73=P501+640
  M72=0
  M73=P501+660
  M72=0
  P501 = P501 + 1
ENDWHILE
```

```
P501 = 0
;-------------------------------------------------------
;                        Main Program:
;-------------------------------------------------------

WHILE(P501<P507 AND P503 < 15 AND P508 < 2 AND P528 <2 AND P510 = 0)
 ; limit total number of control cycles   :P501
 ;                       forward motion   :P503
 ;                       rotation U()     :P508
 ;                       and rotation V() :P528
GOSUB 100       ; Read Sensors

;--------"No contact" test 1: See if variances of X1 AND X2 are too big

 IF (P424 > 0.0278 AND P425 > 0.0278)
   P515 = 0
 ELSE
   P515 = 1
 ENDIF

;----------"No contact" test 2: See if sensor signals are too small

 IF (P511 < 0.05 AND P512 < 0.05 AND P513 < 0.05)
   P516 = 0
 ELSE
   P516 = 1
 ENDIF

P517=0
IF (P515 = 0  OR P516 = 0) ; If either test failed -> no contact
 SEND "N"             ; NO contact. Moving forward by 1 mm
 C(P502)          ; Forward motion
 P503=P503+P502    ; Sum forward motion (mm)
 P506 = 0          ; set no contact flag
ELSE              ; else contact achieved
 IF (P506 = 0)
  P517=-P502*0.75;  back up by -P502/2 or -P502*0.75
  P506 = 1          ; Contact achieved, set flag to 1
  SEND "I"  ;  Initial contact achieved.
 ENDIF
ENDIF
```

```
IF (P506 = 1)          ; if contact achieved

;----- reset all motion inputs to zero

P504=0
P509=0
P527=0
P529=0

IF (P410 !> -0.15)     ; if left end contact
   SEND "L"            ; LEFT end contact. Rotating CCW
   P504=P520*P410      ; Compute rotation adjustment based on X1 and gain
   IF(P504<-1) P504=-1 ; Limit rotation to -1 degree
   P509=-4.88*P504; +P517 ; forward = 4.71 mm/deg. adding backup P517 here
ENDIF

IF (P410 !< 0.15)      ; if right end contact
   SEND "R"            ; RIGHT end contact. Rotating CW in U()
   P504=P520*P410      ; Compute rotation adjustment based on X1 and gain
   IF(P504>1) P504=1           ; Limit control action to 1 degree
   P509=4.88*P504; +P517 ; forward = 4.71 mm/deg. adding backup P517 here
ENDIF

IF (P411 !> -0.15)     ; if bottom end contact
   SEND "B"            ; Bottom end contact. Rotating CW in V()
   P524=-P530*P411     ; Compute rotation adjustment based on X2 and gain
   IF(P524>1) P524=1           ; Limit control action to 1 degree
   P529=3.99*P524; +P517 ; forward = 3.84 mm/deg. adding backup P517 here as well
ENDIF

IF (P411 !< 0.15)      ; if top end contact
   SEND "T"            ; TOP end contact. Rotating CCW in V()
   P524=-P530*P411     ; Compute rotation adjustment based on X2 and gain
   IF(P524<-1) P524=-1 ; Limit to -1
   P529=-3.99*P524; +P517; forward : note sign change
ENDIF

IF (P410>-0.15 AND P410<0.15 AND P411>-0.15 AND P411<0.15) ; if full contact
   C(P517)
   SEND "FULL contact achieved !!!"
   P510 = 1            ; set flag to quit
   P509 = 0            ; no forward motion
```

```
   P529 = 0
ENDIF

   P527 = P509+P529    ; total forward motion has to perform
   U(P504) V(P524) C(P527)    ; forward motion accompaning each rotation

   P505=P505+P504      ; Sum rotation (deg) in U()
   P525=P525+P524      ; Sum rotation (deg) in V()

P503=P503+P527    ; Sum forward motion
P517 = 0          ; reset backup after initial contact
ENDIF ; P506 = 1

P501=P501+1           ; Increment counter
P508=ABS(P505)        ; Total rotation controlled for safety
P528=ABS(P525)

; Store Rotation U()
M73=P501+600
M72=P505

; Store Rotation V()
M73=P501+620
M72=P525

; Store Forward Move
M73=P501+640
M72=P503

; Store Time
M73=P501+660
M72=M0*I10*.001/8388608
ENDWHILE

;---------- output results ----------
;
SEND "Sensor Readings: Fy, Mx, Mz"
CMD "P406"
CMD "P407"
CMD "P408"
; CMD "P409"
SEND "Variances: X1 (Left or Right), X2 (Top or Bottom)"
```

```
CMD "P424"
CMD "P425"
SEND "RESULTS: X1, X2 = "
CMD "P410"
CMD "P411"
SEND "Total Forward Movement (mm) ="
CMD "P503"
SEND "Total U() Rotation (deg) ="
CMD "P505"
SEND "Total V() Rotation (deg) ="
CMD "P525"
SEND "Total # of moves taken"
CMD "P501"

;-----------------------------------------------------------------
;                Subroutine to read sensors
;-----------------------------------------------------------------
N100
;SEND "Sampling all 3 channels now."
; Using p1 to p300 as arrays ( arrays have been set up at the beginning )
P401=1
P406=0
P407=0
P408=0
P409=0
P410=0
P411=0

WHILE (P401 !> P500);loop through 10 times at 1 ms each or = 100 Hz sampling
 M61 = P401
 M60 = M1005/3276.8-P402  ; channel 1 : Fy
 M63 = P401+50
 M62 = M1006/3276.8-P403  ; channel 2 : Mx
 M65 = P401+100
 M64 = M1007/3276.8-P404  ; channel 3 : Mz

 ; correct for the moment created by the angle bracket
 M62 = M62 - M60*2/4   ; moment arm = 2 " , scaling factor F->M is 4

; Calculate X1 = M68 (contact along horizontal axis, +ve for Right end contact)
 M69 = P401+200
 M68 = M64/M60*40/106.3 ; Mz : 40in.lbs/V, Fy : 10in.lbs/V
```

```
; Calculate X2 = M70 (contact along vertical axis, +ve for Top end contact)
  M71 = P401+250
  M70 = -M62/M60*40/80.66

;---------- Initially a delay was set here to achieve desired sampling rate;
;  DELAY 0                    ; (ms)
;---------- however, we discovered that if delay = 0, motion will be much smoother

  P401=P401+1
  P406=P406+M60 ;sum Fy readings
  P407=P407+M62 ;sum Mx readings
  P408=P408+M64 ;sum Mz readings

  P410=P410+M68 ;sum X1
  P411=P411+M70 ;sum X2
ENDWHILE ;(P401 !> P500)

;---------- Calculate Mean values

P406=P406/P500 ;Fy
P407=P407/P500 ;Mx
P408=P408/P500 ;Mz

P410=P410/P500 ;X1 (for Left or Right contact)
P411=P411/P500 ;X2 (for Top or Bottom contact)

P511 = ABS(P406) ; get absolute value of readings to test for contact
P512 = ABS(P407)
P513 = ABS(P408)

; Calculate variances
P401=1
P420=0
P421=0
P422=0

P424=0
P425=0

WHILE(P401!>P500)
  P420 = P420+(P(P401)-P406)*(P(P401)-P406)
  P421 = P421+(P(P401+50)-P407)*(P(P401+50)-P407)
```

```
  P422 = P422+(P(P401+100)-P408)*(P(P401+100)-P408)
;  P423 = P423+(P(P401+150)-P409)*(P(P401+150)-P409)
  P424 = P424+(P(P401+200)-P410)*(P(P401+200)-P410)
  P425 = P425+(P(P401+250)-P411)*(P(P401+250)-P411)
  P401 = P401+1
ENDWHILE

P420 = P420/P500 ; Fy variance
P421 = P421/P500 ; Mx variance
P422 = P422/P500 ; Mz variance

P424 = P424/P500 ; X1 variance
P425 = P425/P500 ; X2 variance
RETURN

CLOSE

;---------- END OF PROGRAM ----------
```

# Appendix E

# Listing of PMAC Motion Control Program to Implement ICC for 3-D Parts using SGFs

```
CLOSE
;-------------------------------------------------------------------------
; Delta Tau PMAC Motion Control Program for
; 3-D Sheet Metal Parts Contact Contol with ICC.
;-------------------------------------------------------------------------
; This program controls the motion of the GMF joints 3 and 4 based on the
; 4 Strain Gauge equipped Fingers' (SGFs) readings
; to achieve a full contact between 2 sheet metals.
;-------------------------------------------------------------------------
; A/D channels 1-4 : for SGFs 1-4 respectively
;
; Sample all 4 ADC channels continuously
; Note that ACC-28A is plugged into port JS2 so channels 5-8 are being used
; M1005->Y:$C016,8,16,S
; M1006->Y:$C017,8,16,S
; M1007->Y:$C01E,8,16,S
; M1008->Y:$C01F,8,16,S
;
; see p. 3-96 of the DELTA TAU manuel for the array setup lines used below

M60->L:$1000 ; Pointer to p0, L stands for long word floating point
M61->Y:$BC3C,0,12 ; Address of the pointer
M62->L:$1000 ;
M63->Y:$BC3E,0,12
```

```
M64->L:$1000 ;
M65->Y:$BC40,0,12
M66->L:$1000 ;
M67->Y:$BC42,0,12
M68->L:$1000 ;
M69->Y:$BC44,0,12
M70->L:$1000 ;
M71->Y:$BC46,0,12
; Pointer for saving X3, U(), and C()
M72->L:$1000
M73->Y:$BC48,0,12

CLOSE OPEN PROG 505 CLEAR
CMD "i3=3"
LINEAR       ; Linear interpolation
FRAX(U,V,C)

F15.0     ; feedrate
TS 50     ; S-Curve acceleration period

INC       ; Incremental mode
P500=10    ; Number of samples per average
P501=0          ; Counter
P502=1.0   ; Forward motion step size ( mm )
P503=0          ; Total distance moved
P504=0.1   ; Rotational motion step size ( degrees )
P505=0          ; Total rotation
P506=0     ; flag for contact establishment
P507=100   ; max. number of control cycles
P508=0     ; Magnitude of total rotation
P509=0     ; forward motion accompaning each rotation (0.1 deg.) in U
P510=0     ; QUIT flag
P511 = 0
P512 = 0
P513 = 0
P514 = 0
P515 = 0   ; contact test 1 flag
P516 = 0   ; contact test 2 flag
P517 = 0   ; backup motion after initial contact
P520 = 0.15 ; CONTROLLER GAIN for U
P530 = 0.15 ; CONTROLLER GAIN for V
P525=0
```

```
p528=0

P531=0
P532=0
P533=0
P534=0
P535=0

; sample all 3 channels now to obtain sensor offsets
WHILE (P531 < 50)
  P402 = M1005/3276.8
  P403 = M1006/3276.8
  P404 = M1007/3276.8
  P405 = M1008/3276.8

  P532 = P532 + P402
  P533 = P533 + P403
  P534 = P534 + P404
  P535 = P535 + P405

  P531 = P531 + 1
ENDWHILE
P402 = P532/50
P403 = P533/50
P404 = P534/50
P405 = P535/50
CMD "P402"
CMD "P403"
CMD "P404"
CMD "P405"

; Initialize arrays to zero

WHILE (P501 < 20)
  M73=P501+600
  M72=0
  M73=P501+620
  M72=0
  M73=P501+640
  M72=0
  M73=P501+660
  M72=0
```

```
  P501 = P501 + 1
ENDWHILE

P501 = 0

;-------------------------------------------------------------
;                          Main Program:
;-------------------------------------------------------------

WHILE(P501<P507 AND P503 < 10 AND P508 < 2 AND P528 <2 AND P510 = 0)
 ; limit total number of control cycles   :P501
 ;                        forward motion   :P503
 ;                        rotation U()     :P508
 ;                        and rotation V() :P528
GOSUB 100        ; Read Sensors

;--------"No contact" test 1: See if variances of X1 AND X2 are too big

 IF (P424 > 0.0278 AND P425 > 0.0278)
   P515 = 0
 ELSE
   P515 = 1
 ENDIF

;----------"No contact" test 2: See if sensor signals are too small

 IF (P511 < 0.05 AND P512 < 0.05 AND P513 < 0.05 AND P514 < 0.05)
   P516 = 0
 ELSE
   P516 = 1
 ENDIF

P517=0
IF (P515 = 0  OR P516 = 0) ; If either test failed -> no contact
 SEND "N"              ; NO contact. Moving forward by 1 mm
 C(P502)           ; Forward motion
 P503=P503+P502    ; Sum forward motion (mm)
 P506 = 0          ; set no contact flag
ELSE               ; else contact achieved
 IF (P506 = 0)
  P517=-P502*0.75;  back up by -P502/2 or -P502*0.75
  P506 = 1          ; Contact achieved, set flag to 1
```

```
   SEND "I"  ;  Initial contact achieved.
  ENDIF
 ENDIF

 IF (P506 = 1)          ; if contact achieved

 ;----- reset all motion inputs to zero

 P504=0
 P509=0
 P527=0
 P529=0

 IF (P410 !> -0.15)     ; if left end contact
    SEND "L"            ; LEFT end contact. Rotating CCW
    P504=P520*P410   ; Compute rotation adjustment based on X1 and gain
    IF(P504<-1) P504=-1 ; Limit rotation to -1 degree
    P509=-4.71*P504+P517 ; forward = 4.71 mm/deg. adding backup P517 here
 ENDIF

 IF (P410 !< 0.15)      ; if right end contact
    SEND "R"            ; RIGHT end contact. Rotating CW in U()
    P504=P520*P410   ; Compute rotation adjustment based on X1 and gain
    IF(P504>1) P504=1          ; Limit control action to 1 degree
    P509=4.71*P504+P517 ; forward = 4.71 mm/deg. adding backup P517 here
 ENDIF

 IF (P411 !> -0.15)     ; if bottom end contact
    SEND "B"            ; Bottom end contact. Rotating CW in V()
    P524=-P530*P411  ; Compute rotation adjustment based on X2 and gain
    IF(P524>1) P524=1          ; Limit control action to 1 degree
    P529=3.84*P524+P517 ; forward = 3.84 mm/deg. adding backup P517 here as well
 ENDIF

 IF (P411 !< 0.15)      ; if top end contact
    SEND "T"            ; TOP end contact. Rotating CCW in V()
    P524=-P530*P411  ; Compute rotation adjustment based on X2 and gain
    IF(P524<-1) P524=-1 ; Limit to -1
    P529=-3.84*P524+P517; note sign change
 ENDIF

 IF (P410>-0.15 AND P410<0.15 AND P411>-0.15 AND P411<0.15) ; if full contact
```

```
    C(P517)
    SEND "FULL contact achieved !!!"
    P510 = 1        ; set flag to quit
    P509 = 0        ; no forward motion
    P529 = 0
  ENDIF

    P527 = P509+P529    ; total forward motion has to perform
    U(P504) V(P524) C(P527)    ; forward motion accompaning each rotation

    P505=P505+P504      ; Sum rotation (deg) in U()
    P525=P525+P524      ; Sum rotation (deg) in V()

 P503=P503+P527     ; Sum forward motion
 P517 = 0           ; reset backup after initial contact
 ENDIF ; P506 = 1

 P501=P501+1            ; Increment counter
 P508=ABS(P505)         ; Total rotation controlled for safety
 P528=ABS(P525)

 ; Store Rotation U()
 M73=P501+600
 M72=P505

 ; Store Rotation V()
 M73=P501+620
 M72=P525

 ; Store Forward Move
 M73=P501+640
 M72=P503

 ; Store Time
 M73=P501+660
 M72=M0*I10*.001/8388608
 ENDWHILE

 ;---------- output results ----------
 ;
 SEND "Sensor Readings: SGFs 1, 2, 3 and 4"
 CMD "P406"
```

```
CMD "P407"
CMD "P408"
CMD "P409"
SEND "Variances: X1 (Left or Right), X2 (Top or Bottom)"
CMD "P424"
CMD "P425"
SEND "RESULTS: X1, X2 = "
CMD "P410"
CMD "P411"
SEND "Total Forward Movement (mm) ="
CMD "P503"
SEND "Total U() Rotation (deg) ="
CMD "P505"
SEND "Total V() Rotation (deg) ="
CMD "P525"
SEND "Total # of moves taken"
CMD "P501"

;-----------------------------------------------------------------
;                Subroutine to read sensors
;-----------------------------------------------------------------
N100
;SEND "Sampling all 4 channels now."
; Using p1 to p300 as arrays ( arrays have been set up at the beginning )
P401=1
P406=0
P407=0
P408=0
P409=0
P410=0
P411=0

WHILE (P401 !> P500);loop through 10 times at 1 ms each or = 100 Hz sampling
 M61 = P401
 M60 = M1005/3276.8-P402  ; channel 1 : SGF 1
 M63 = P401+50
 M62 = M1006/3276.8-P403  ; channel 2 : SGF 2
 M65 = P401+100
 M64 = M1007/3276.8-P404  ; channel 3 : SGF 3
 M67 = P401+150
 M66 = M1008/3276.8-P405  ; channel 4 : SGF 4
```

```
 ; Calculate VL' = SGF 1 + SGF 3
   P431 = -(M60 + M64)/2
 ; Calculate VR' = SGF 2 + SGF 4
   P432 = -(M62 + M66)/2
 ; Calculate VT' = SGF 1 + SGF 2
   P433 = -(M60 + M62)/2
 ; Calculate VB' = SGF 3 + SGF 4
   P434 = -(M64 + M66)/2

 ; Calculate X1 = M68 (contact along horizontal axis, +ve for Right end contact)
   M69 = P401+200
   M68 = (P432-P431)/(P432+P431)

 ; Calculate X2 = M70 (contact along vertical axis, +ve for Top end contact)
   M71 = P401+250
   M70 = (P433-P434)/(P433+P434)

 ;---------- Initially a delay was set here to achieve desired sampling rate;
 ;  DELAY 0                    ; (ms)
 ;---------- however, we discovered that if delay = 0, motion will be much smoother

   P401=P401+1
   P406=P406+M60 ;sum SGF 1 readings
   P407=P407+M62 ;sum SGF 2 readings
   P408=P408+M64 ;sum SGF 3 readings
   P409=P409+M66 ;sum SGF 4 readings
   P410=P410+M68 ;sum X1
   P411=P411+M70 ;sum X2
ENDWHILE ;(P401 !> P500)

;---------- Calculate Mean values

P406=P406/P500 ;SGF 1
P407=P407/P500 ;SGF 2
P408=P408/P500 ;SGF 3
P409=P409/P500 ;SGF 4

P410=P410/P500 ;X1 (for Left or Right contact)
P411=P411/P500 ;X2 (for Top or Bottom contact)

P511 = ABS(P406) ; get absolute value of readings for safety reason
P512 = ABS(P407)
```

```
P513 = ABS(P408)
P514 = ABS(P409)

; Calculate variances
P401=1
P420=0
P421=0
P422=0
P423=0
P424=0
P425=0

WHILE(P401!>P500)
  P420 = P420+(P(P401)-P406)*(P(P401)-P406)
  P421 = P421+(P(P401+50)-P407)*(P(P401+50)-P407)
  P422 = P422+(P(P401+100)-P408)*(P(P401+100)-P408)
  P423 = P423+(P(P401+150)-P409)*(P(P401+150)-P409)
  P424 = P424+(P(P401+200)-P410)*(P(P401+200)-P410)
  P425 = P425+(P(P401+250)-P411)*(P(P401+250)-P411)
  P401 = P401+1
ENDWHILE

P420 = P420/P500 ; SGF 1 variance
P421 = P421/P500 ; SGF 2 variance
P422 = P422/P500 ; SGF 3 variance
P423 = P423/P500 ; SGF 4 variance
P424 = P424/P500 ; X1 variance
P425 = P425/P500 ; X2 variance
RETURN

CLOSE

; ---------- END OF PROGRAM ----------
```